



Optimisation of static and dynamic DNA conditions for biosensing and antimicrobial applications

by

Renzo A. Fenati
BSc. (Forensic and Analytical Sciences)
(Honours)

Thesis
Submitted to Flinders University
for the degree of Doctor of Philosophy

College of Science and Engineering
18/06/2019

Contents

Table of contents	xii
List of figures	xxv
List of tables	xxxix
Declaration	xxxix
Acknowledgements	xxxix
Publications	xli
Conferences	xli
Abbreviations	xlii
Glossary	xlii
1 Introduction and literature review	1
1.1 Synopsis	1
1.2 Introduction	2

1.3	DNA structure	2
1.3.1	DNA double helix	5
1.3.2	Melting temperature (T_m) of DNA	8
1.3.2.1	Mismatches	11
1.4	DNA modification and detection	13
1.4.1	DNA modification	13
1.4.2	Oligodeoxynucleotide coupling and surface immobilisation	14
1.4.3	Fluorophores	14
1.4.4	Fluorescence quenching	15
1.4.4.1	Dynamic quenching	16
1.4.4.2	Static quenching	17
1.4.5	The effect of fluorophores on DNA stability	17
1.4.6	Intercalators	20
1.4.6.1	Ethidium bromide	21
1.5	Structural and dynamic DNA	23
1.5.1	DNA assembly/disassembly	23
1.5.2	DNA origami	23
1.5.3	Static structural DNA	24
1.5.3.1	Triple helix DNA	25
1.5.3.2	Hairpin loops	26

1.5.3.3	iMotif	26
1.5.3.4	G-quadruplex	26
1.5.3.5	Cation and polymeric stabilisation of G4 structures	30
1.5.3.6	Circular dichroism spectroscopy and polyacrylamide gel electrophoresis analysis of G4s.	30
1.5.3.7	Aptameric G4 structures	31
1.5.3.8	Systematic evolution of ligands by exponential enrichment and genetic algorithm	33
1.5.3.9	G4 interactions with organic molecules, proteins and co-factors	34
1.5.3.10	Peroxidase-mimicking activity of G4/hemin aptamer	36
1.5.3.11	Biosensors	37
1.6	Dynamic DNA	38
1.6.1	Toehold-mediated strand displacement	40
1.6.1.1	Random walk: DNA ‘zippering’	41
1.6.2	Toehold-mediated strand displacement reaction kinetics	42
1.6.2.1	Temperature	43
1.6.2.2	Toehold properties	43
1.6.2.3	Mismatches	46
1.6.2.4	Four-way-branch migration: Holliday junction	47
1.6.3	Solution vs surface-immobilised DNA strand displacement reactions	49

1.6.3.1	Solution based toehold-mediated strand displacement reactions	49
1.6.3.2	Surface-immobilised DNA strand displacement reactions . . .	53
1.6.3.3	2D surface DNA strand displacement reactions	53
1.6.3.4	3D surface immobilised DNA strand displacement reactions .	55
1.7	Strategies to combat biofilms using synthetic and natural polymers	58
1.7.1	Bacteria and biofilms	58
1.7.2	History of biofilms	59
1.7.3	Life cycle of biofilms	60
1.7.4	Chronic infection	61
1.7.5	Antimicrobials and antifouling	62
1.7.5.1	Antimicrobials	62
1.7.5.2	Antifouling surfaces	65
1.8	Summary	66
1.9	Chapter 1 References	68
2	Methods and materials	106
2.1	Synopsis	106
2.2	Materials	107
2.2.1	Chemicals and reagents	107
2.2.2	Oligodeoxynucleotides used for toehold-mediated strand displacement reactions	112

2.2.3	Oligodeoxynucleotides for genetic algorithm	112
2.2.4	Oligodeoxynucleotides used for enzyme treatment and surface immobilisation onto microplates and microbeads	113
2.2.5	Antimicrobial studies	114
2.2.5.1	Oligodeoxynucleotides sequences for G4 formation used for antimicrobial studies	114
2.2.5.2	Bacterial strains	114
2.3	Methods	115
2.3.1	Toehold-strand displacement analysis	115
2.3.1.1	PCR amplification of DNA containing one of four SNPs (SNP-A, SNP-T, SNP-G and SNP-C)	115
2.3.1.2	Preparation of toehold PCR products (TPPs)	115
2.3.1.3	Toehold-mediated strand displacement reactions	116
2.3.1.4	Toehold-mediated strand displacement reactions in the presence of ethidium bromide	116
2.3.2	Genetic algorithm for increased peroxidase-mimicking G4 aptamers	117
2.3.2.1	Folding of G4 structures	117
2.3.2.2	Circular dichroism	117
2.3.2.3	TMB assay	117
2.3.2.4	Michaelis-Menten kinetics	118

2.3.3	G4 T7 endonuclease I digestion and immobilisation of 2D and 3D surfaces	118
2.3.3.1	T7 endonuclease I digestion of G4	118
2.3.3.2	G4 surface immobilisation onto Corning® DNA-Bind 96-well plates 96-well plates	118
2.3.3.3	Wash procedure	119
2.3.4	TMB assay procedure	119
2.3.4.1	ABTS assay for surface immobilised G4 aptamers	119
2.3.4.2	Luminol assay for surface immobilised G4 aptamers	120
2.3.4.3	Surface immobilisation on magnetic beads	120
2.3.4.4	TMB assay for surface immobilised G4 aptamers	121
2.3.5	G4 antimicrobial studies	121
2.3.5.1	Antibiotic coupling to G4 structures	121
2.3.5.2	DNA precipitation	122
2.3.5.3	Bacterial cell preparation	122
2.3.5.4	Minimum inhibitory concentration (MIC)	123
2.3.5.5	Biofilm growth	123
2.3.5.6	Growth of biofilms on silicone coupons	124
2.3.5.7	Colony forming unit (CFU) assay	124
2.3.5.8	Crystal violet (CV) staining	125

2.4	Characterisation methods	125
2.4.1	UV/visible spectroscopy: Nanodrop 2000	125
2.4.2	Roto-Gene Q 6-plex: Real-time thermocycler	126
2.4.3	Electrophoresis	126
2.4.4	Confocal fluorescence scanning microscopy	128
2.5	Chapter 2 References	130
3	Investigation of the effect of ethidium bromide on toehold-mediated strand displacement	132
3.1	Synopsis	132
3.2	introduction and purpose	134
3.3	Results and discussion	137
3.3.1	ATTO 550 and ATTO 647N effect on PCR and toehold-mediated strand displacement trials	137
3.3.1.1	PCR amplification using ATTO 550 and ATTO 647N	137
3.3.1.2	Fabrication of the TPP-C with ATTO 550 and ATTO 647N and toehold-mediated strand displacement reaction	144
3.3.2	Toehold-mediated strand displacement of TPP-C, TPP-G, TPP-A and TPP-T using ATTO 647N	149
3.3.2.1	Amplification of all four SPP-C, SPP-G, SPP-A and SPP-T	150
3.3.2.2	Toehold-mediated strand displacement reaction with TPPs labelled with ATTO 647N	151

3.3.2.3	TPP–C, labelled with ATTO 647N, toehold-mediated strand displacement	153
3.3.2.4	TPP–G, labelled with ATTO 647N, toehold-mediated strand displacement	155
3.3.2.5	TPP–A, labelled with ATTO 647N, toehold-mediated strand displacement	157
3.3.2.6	TPP–T, labelled with ATTO 647N, toehold-mediated strand displacement	159
3.3.2.7	Using ATTO 647N for investigation of toehold-mediated strand displacement reaction	160
3.3.3	Toehold-mediated strand displacement with ethidium bromide	161
3.3.3.1	TPP–C, labelled with ATTO 647N, toehold-mediated strand displacement in the presence of ethidium bromide	162
3.3.3.2	TPP–G, labelled with ATTO 647N, toehold-mediated strand displacement in the presence of ethidium bromide	164
3.3.3.3	TPP–A, labelled with ATTO 647N, toehold-mediated strand displacement in the presence of ethidium bromide	165
3.3.3.4	TPP–T, labelled with ATTO 647N, toehold-mediated strand displacement in the presence of ethidium bromide	166
3.3.3.5	Effect of ethidium bromide on the toehold-mediated strand displacement reaction	167
3.4	Concluding remarks	168
3.5	Chapter 3 References	171

4	Enhancement and characterisation of peroxidase-mimicking activity by screening G-quadruplexes using a genetic algorithm	173
4.1	Synopsis	173
4.1.1	Introduction and purpose	175
4.1.2	Evolution of G4 ODN sequences using a genetic algorithm	178
4.1.2.1	Applications of G4/hemin aptamers with enhanced peroxidase-mimicking activity	180
4.2	G4/hemin aptamer enzyme kinetics	183
4.2.1	Optimisation of the first generation of G4/hemin aptamer's peroxidase-mimicking activity testing	184
4.3	Results and discussion	185
4.3.1	Development of first generation of the G4/hemin aptamers and optimisation of TMB assay	185
4.3.1.1	Sequence modification: Investigation of additional G residues in the G-tracts affect on the G4 aptamer peroxidase-mimicking activity	186
4.3.1.2	Investigation of deletions and T residue substitutions affects on the G4 aptamer peroxidase-mimicking activity	188
4.3.1.3	Optimisation of G4/hemin aptamer folding procedure	191
4.3.2	Investigation of pegylated-hemin effect on the G4 aptamer peroxidase-mimicking activity	192
4.3.3	Enhancement of peroxidase-mimicking activity using genetic algorithm	194

4.3.4	Characterisation of G4/hemin aptamer structures using polyacrylamide gel electrophoresis, circular dichroism and K ⁺ dependence studies . . .	197
4.3.4.1	PAGE analysis of G4/hemin structures	197
4.3.4.2	Circular dichroism	199
4.3.5	Potassium ion dependence of G4/hemin aptamer	200
4.3.6	Enzyme kinetics of G4 aptamers with peroxidase-mimicking activity .	202
4.4	Concluding remarks	205
4.5	Chapter 4 References	207
5	Immobilisation of G-quadruplexes onto 2D and 3D surfaces and T7 endonuclease I digestion for biosensing applications	211
5.1	Synopsis	211
5.2	Introduction and purpose	213
5.3	Results and discussion	216
5.3.1	Optimisation of T7 endonuclease I digestion	216
5.3.2	G4 resistance to T7 endonuclease I digestion	216
5.3.3	Optimisation of T7 endonuclease I of PM and SM solutions	220
5.3.4	Investigation of G4 aptamer immobilised on 2D surfaces	222
5.3.4.1	Comparison of three detection systems of G4 aptamer testing on 2D surfaces	223
5.3.5	TMB assay of the G4 aptamers immobilised on the 2D surface	224

5.3.5.1	Increasing the sensitivity of the TMB assay with PEG rate accelerators	226
5.3.5.2	Solution-based detection of cleaved G4 aptamers containing a PM or SM from 2D surfaces	229
5.3.6	Investigation of PM and SM immobilised on 3D surfaces	231
5.4	Concluding remarks	234
5.5	Chapter 5 References	237
6	Chapter 6: Investigation of G-quadruplex aptamers as possible antimicrobial agents against <i>S. aureus</i> and <i>S. epidermidis</i>	240
6.1	Synopsis	240
6.2	Introduction and purpose	241
6.3	Results and discussion	243
6.3.1	Coupling and purification of antibiotic coupled G4 aptamers	243
6.3.1.1	Purification of antibiotic coupled G4 aptamers	244
6.3.2	Testing of the peroxidase-mimicking activity and antimicrobial activity of OXG4 aptamers	245
6.3.2.1	TMB assay testing of OXG4 aptamer	246
6.3.2.2	Minimum inhibitory concentration	248
6.3.3	Impact of G4 aptamer, OXG4 and OX on biofilms	249
6.3.4	Impact of G4 aptamer and OX on biofilms with added hydrogen peroxide (0.5%)	256

6.4	Concluding remarks	259
6.5	Chapter 6 References	261
7	Conclusion	264
7.1	Synopsis	264
7.2	Concluding remarks and future work	265
7.3	Chapter 7 References	269
8	Appendix	271
A	Additional possible SPP	271
B	Displacement curves for TPP-C	272
C	Genetic algorithm generations with G4 ODN sequences and peroxidase-mimicking activity	273
D	Digestion of G4 aptamers with T7 endonuclease I (2.5 U)	276
E	16 h digestion of G4 aptamers with T7 endonuclease I (2.5 U)	277
F	Detection of surface immobilised G4 aptamers using luminol assay	278
G	Detection of surface immobilised G4 aptamers using ABTS assay	279
H	OxG4 and NH ₂ G4 gel electrophoresis results	280

List of Figures

1.1	Chemical structures of a DNA nucleotide, with a hydrogen at the 2' position (left, red), and RNA nt , with a hydroxide at the 2' position (right, blue) nts. . . .	3
1.2	Nucleotides linked through a phosphate (black) and ribose sugar (pink) to make ssDNA. Pyrimidines: thymine (yellow) and cytosine (red) and uracil (grey). Purines: adenine (blue), guanine (green).	4
1.3	DNA double helix showing the major and minor grooves.	6
1.4	Stick model of the three main types of DNA: A-form, B-form and Z-form (left to right)	7
1.5	Comparison of (a) dynamic and (b) static quenching.	16
1.6	UV melting profiles of probe: target duplexes. Solid line: unmodified probe. Dashed line: 5' BHQ2 probe with 3' Black Hole quencher. Dotted line: 5' Cy5 dye and Iowa 3' Black Red Quencher.	19
1.7	Literature examples of static (left) designed by Han <i>et al.</i> and dynamic DNA (right) designed by Marras <i>et al.</i>	24

1.8	Comparison of Watson-Crick (Canonical) and Hoogsteen (Non-canonical) base pairing.	25
1.9	(a) Structure of a G-tetrad made up of four guanines with stabilisation by a monovalent cation and (b) G-quadruplex made up of 4 ssDNA (black arrows) stabilised by a monovalent cation, where the arrows indicate 5' to 3' directionality.	27
1.10	Diverse types of G4s: (a) intermolecular parallel (tetramolecular), (b) intermolecular parallel (bimolecular), (c) intramolecular parallel (unimolecular), (d) intermolecular antiparallel, (e) intermolecular antiparallel (bimolecular) and (f) intramolecular antiparallel (unimolecular). Adapted from J. L. Huppert	29
1.11	Schematic for a G4 biosensor that relies on a cascade effect from DNAzymes. Adapted from Elbaz <i>et al.</i>	39
1.12	Example schematic of a logic gate that used toehold-mediated strand displacement, developed by Liu <i>et al.</i>	39
1.13	Schematic of the toehold-mediated strand displacement (a) DS (red) is added to a target strand (black) with a toehold domain and a hybridised shorter incumbent strand (blue), (b) DS nucleates with the target strands toehold, (c) the random walk 'zippering' process begins and (d) the shorter incumbent strand is displaced by the DS.	40
1.14	(a) Toehold-mediated strand exchange and (b) four-way branch migration with formation of Holliday junction.	41
1.15	Diagram of the target strand (black) with toehold region γ and target sequence β with hybridised incumbent strand (blue, β). The DS (red) contains complementary regions to the target strand ($\underline{\gamma}$ and $\underline{\beta}$).	44

1.16	Genot <i>et al.</i> describes the proposed mechanism for the remote toehold. The target strand, labeled with fluorophore (F) and quencher (Q), is displaced from the substrate (S) by an invading strand (I). The toehold and displacement domains on both the substrate and invading strands are separated by spacer domains. Docking of the substrate and invading strand by hybridization of the toehold domains is followed by an internal diffusion step, which is required to align the displacement domains and initiate the branch migration reaction by which the target strand is displaced from the substrate. Displacement is reported by quenching of fluorescence from the target.	46
1.17	Increasing time required for strand displacement reaction from (a) a perfect match, (b) a mismatch in the toehold and (c) a mismatch within 6 bps after the toehold region.	47
1.18	(a) Schematic for creating a toehold (i) and performing toehold-mediated strand displacement (ii) and (b) toehold-mediated strand displacement of Amel for both male and female DNA and the derivative of the melting curve.	52
1.19	Schematic of a DNA microarray, where each spot has a different sequence immobilised on the surface.	54
1.20	(a) Schematic representation of STR genotyping in a micro-array. First capture probes for all potential lengths of a STR are immobilised onto a surface in (i) and an unknown target STR is added and hybridises with all capture probes (II). 1st competing strand is added to displace any target STR that is too long for capture probe (iii) and (iv) and 2nd competing strand is added to displace any target STR that is too short for the capture probe (v) leaving only fully complementary target STR (vi). (b) An example of a micro-array that shows only 9 and 10 repeats remain after both 1st and 2nd competing strands are added. (c) Histogram of intensity of fluorescence of microarray.	56

1.21	Schematic of the capture of the ds-PCR products tagged with ss-ODN with following sequences selective release via toehold- mediated DNA strand displacement reaction. Domains a and a', and b and b' are self-complementary. . .	57
1.22	Schematic of the surface immobilised toehold-mediated strand displacement technique, designed by Yao <i>et al.</i>	58
1.23	Life cycle of biofilm: (a) layer conditioning, (b) reversible adhesion, (c) irreversible adhesion, (d) population growth and (e) final stage development. . . .	61
3.1	Schematic of toehold-mediated strand displacement. Step 1: A region of the template mitochondrial DNA (mtDNA, black) that contains the single nucleotide polymorphism (SNP, green) is amplified with PCR using the modified reverse (red) primer labelled with a fluorophore (F) and the forward primer (purple) which contains deoxy-uracils (dUs, orange) at the 5 th and 9 th position. This creates multiple copies of the SNP PCR product (SPP), a copy of the region of the template mtDNA, with the fluorophore (F) and dUs at the 5 th and 9 th position on the target strand (red) and incumbent strand (purple), respectively. Step 2: The toehold PCR product (TPP) is then formed by the digestion of the SPP of step 1 with uracil-DNA glycosylase (UDG) to remove the dUs which creates a short toehold on the incumbent strand (purple). Step 3: The displacing sequence (DS) (light blue) containing a quencher (Q) is added to the TPP in solution and nucleates with the toehold of the incumbent strand. Toehold-mediated strand displacement then proceeds as the DS hybridises, nucleating at the toehold, with the target strand of the TPP until the incumbent strand of the TPP is completely displaced into solution. Static quenching occurs when Q on the DS comes into contact with F on the target strand of TPP to form a dimer whereby fluorescence is quenched.	135

3.2	Agarose gel 4% (w/v) electrophoretograms of the SNP PCR products (SPPs) labelled with either the fluorophore (a) ATTO 550 or (b) ATTO 647N. For visualisation, the gel was stained with 1x SYBR® safe and viewed using a Gel Doc™ EZ. A DNA Ladder (Quick-Load® Purple 50 bp DNA ladder) was used as the reference.	138
3.3	Example of correct annealing and elongation of the mtDNA using the reverse primer (red) labelled with the fluorophore (F, red) to the strand of mtDNA that has already been amplified with forward primer (purple). Complementary Watson-Crick bps are indicated by . The SNP position is underlined.	140
3.4	Example of incorrect annealing and elongation using reverse primer (purple) labelled with the fluorophore (F, red) to the strand of mtDNA that has already been amplified with forward primer (purple), showing nearest neighbour stabilised Watson-Crick bonds (), complementary Watson-Crick bonds (:) and mismatches (●). The SNP position is underlined.	141
3.5	Diagram of how A and T form a complementary base pair (top) and how G and T form a mismatched base pair.	143
3.6	Toehold-mediated strand displacement kinetic curves (relative fluorescence unit (RFU) versus time) of the displacement reactions of the incumbent strand of TPP-C, when TPP-C is labelled with either the fluorophore ATTO 550 (black line) or ATTO 647N (red line), with DS(A). The fluorescence was measured on a Roto-Gene 6plex. Each set of data plotted is an average of 3 replicates. Every 20 data points was omitted for ease of viewing.	145

- 3.7 Schematic of toehold-mediated strand displacement of the non-specific SNP PCR product (SPP), the 55 bp TPP, produced using the reverse primer labelled with ATTO 550. Step 1: A region of the template mitochondrial DNA (mtDNA, black) that contains the single nucleotide polymorphism (SNP, green) is amplified with PCR using the modified reverse (red) primer labelled with a fluorophore (F) and the forward primer (purple) which contains deoxy-uracils (dUs, orange) at the 5th and 9th position. However due to non-specific hybridisation of the reverse primer this creates multiple copies of the non-specific SPP without the SNP present, but does create copies of the region of the template mtDNA, with the fluorophore (F) and dUs at the 5th and 9th position on the target strand (red) and incumbent strand (purple), respectively. Step 2: The toehold PCR product (TPP) is then formed by the digestion of the SPP of step 1 with uracil-DNA glycosylase (UDG) to remove the dUs which creates a short toehold on the incumbent strand (purple). Step 3: The displacing sequence (DS) (light blue) containing a quencher (Q) is added to the TPP in solution and nucleates with the toehold of the incumbent strand. Toehold-mediated strand displacement then proceeds as the DS hybridises, proceeding from the toehold, with the target strand of the TPP until the incumbent strand of the TPP is completely displaced into solution. For the non-specific SPP the DS strand forms a loop that allows for the toehold-mediated strand displacement to proceed. This still allows for the formation of a dsDNA that brings the quencher close enough to the fluorophore to allow for quenching. 147
- 3.8 Agarose gel 4% (w/v) electrophoretogram of the four SPPs possessing different nts, (a) SPP-C, (b) SPP-G, (c) SPP-A and (d) SPP-T, all labelled with the fluorophore ATTO 647N. For visualisation, the gel electrophoretogram was stained with 1x SYBR® safe and viewed using a Gel Doc™ EZ. A DNA ladder (Quick-Load® Purple 50 bp DNA Ladder) was used as the reference. . . . 150

3.9	(a) TPP–C, (b) TPP–G, (c) TPP–A and (d) TPP–T (labelled with ATTO 647N) with DS(A) (black), DS(T) (pink), DS(G) (blue) and DS(C) (green) containing BHQ-1. Each set of data plotted is an average of 3 replicates. Every 20 data points was omitted for ease of viewing and the red dashed lines are the fits obtained using OriginPro 9 software.	152
3.10	(a) TPP–C, (b) TPP–G, TPP–A and TPP–T (labelled with ATTO 647N) with DS(A) (black), DS(T) (pink), DS(G) (blue) and DS(C) (green) containing BHQ-1 and in the presence of ethidium bromide. Data plotted is an average of the results of 3 replicates. Every 20 data points was omitted for ease of viewing and the red dashed lines are the fits obtained using OriginPro 9 software.	162
4.1	General structure of an intramolecular G4 made up of the oligodeoxynucleotide (ODN) sequence: $5'—X_{l1}G_mX_{l1}G_mX_{l2}G_mX_{l3}G_mX_{l2}—3'$. Consisting of 3 (left, $m = 3$) or 4 (right, $m = 4$) stacked G-tetrads (blue) stabilised with a cation (red). The G4 is made up of 2 terminal regions (pink), 3 loop regions (green) and 4 G-tracts (black). Arrows indicate the direction of the backbone ($5'$ to $3'$).	176
4.2	Chemical structure of hemin, an iron containing iron (III) protoporphyrin IX.	177
4.3	General schematic of how a GA was performed in this chapter. Step 1: The n generation is divided into terminal (X_{l1} and X_{l2} , pink), loop (X_{l1} , X_{l2} and X_{l3} , green) and G regions (G_m , black). Step 2: The terminal ends, and loops are shuffled within their respective groups. Step 3: A single base mutation, insertion (red) or deletion (blank space) to produce Generation $n + 1$. Step 4: Generation $n + 1$ is tested for peroxidase-mimicking activity (see Section 4.2.1) and the sequences with the highest peroxidase-mimicking activity are put back into the GA as Generation n	179

4.4	The proposed general mechanism for the catalytic cycle of G4/hemin with peroxidase-mimicking activity adapted from Chang <i>et al.</i> ¹⁵ Initially, the hemin (red) replaces the Cl residue with a water residue. Then the hemin is able to complex with an already formed G4 (green). This complexation allows for the structure to acquire peroxidase-mimicking activity. The hemin reacts with a hydrogen peroxide, replacing the water with the hydrogen peroxide. Compound I and compound II are able to form depending on homocleavage or heterocleavage occurs, respectively. Compound I is the active component which is able to react with the substrate, TMB in this case and produces a blue coloured product. This reaction results in compound I becoming compound II. Compound II is able to be recycled back into the water containing hemin or G4/hemin.	181
4.5	VMD snapshots of the G-quadruplex DNA-hemin complex for (left) initial and (right) final conformation resulting from MD simulation, adapted from Nasab <i>et al.</i>	182
4.6	Proposed schematic for how an A nt plays a role in the heterolytic cleavage of hydrogen peroxide during peroxidase-mimicking of the G4/hemin aptamer, adapted from Li <i>et al.</i> ¹⁰	182
4.7	Chemical structure of polyethylene glycol-hemin (PEG-hemin).	185
4.8	Native PAGE 10-20% (v/v) electrophoretogram, stained with 1x SYBR® gold and viewed using a Safe Imager Blue-Light Transilluminator, of 7-01, 7-02, 5-04, 7-08, 4-02, 6-07, 7-04, 5-08, 7-06 and 6-08, EAD-2 and G ₃ A ₃ G4 aptamers (a) without hemin and (b) with hemin added. Both have Invitrogen 10 bp DNA Ladder DNA Ladder (L).	198
4.9	CD spectra of G4 aptamers: (a) 7-01, (b) 7-02, (c) 5-04, (e) EAD-2 and (d) G ₃ A ₃ with (red) and without (black) hemin.	201

4.10	Michaelis-Menten curves for hemin base line (green), G ₃ A ₃ (black), EAD-2 (pink), 7-01 (red), 7-02 (blue) and 5-04 (turquoise). Each line is an average of three curves and the red dotted line is the curve fit performed using OriginPro 9 applying software non-linear line fit function.	203
5.1	Proposed mechanism for the SNP biosensor that utilises an enzymatic digestion step and a G-quadruplex (G4) aptamer for single nucleotide polymorphism (SNP) detection. Step 1: Immobilisation of ODN that contains a G-rich (green), SNP (red) and capture region (black), onto the surface (yellow) of either a 2D or 3D surface. Step 2: Target ODN is captured to the surface immobilised capture region, forming either a perfect match (PM, blue) or single mismatch (SM, purple). Step 3: T7 endonuclease enzyme (multicoloured) is added to cleave the any mismatched DNA and release the G-rich ODN into solution. Step 4: The G-rich ODN in solution is removed and then both G-rich ODN in solution and on the surface are folded with the addition of 50 mM K ⁺ to form G4 aptamers. Step 5: Hemin is added and a TMB assay is performed to determine the presence of G4 aptamers in solution and those remaining on the surface. . .	215
5.2	Schematic of (a) perfect match (G4(G) 001 + G4(C) 002) and (b) single-mismatch (G4(G) 001 + G4(T) 003), showing the G-rich (green), SNP (red, underlined) and captured target strands (PM blue, SM purple).	217
5.3	PAGE ePage1 10-20% (v/v) electrophoretogram, stained with 1x SYBR® gold and viewed using a Safe Imager Blue-Light Transilluminator, of G4(G) 001 with G4(C) 002 (perfect match (PM)) and G4(G) 001 with G4(T) 003 (single-mismatch (SM)) solutions after formation of the G4 aptamers with respective target strands. A DNA Ladder (Invitrogen 10 bp DNA ladder) was used as the reference. Dotted lines are to guide the eye to the bands of interest.	218

5.4	PAGE ePage1 10-20% (v/v) electrophoretogram, stained with 1x SYBR® gold and viewed using a Safe Imager Blue-Light Transilluminator, of perfect match (PM) and single mismatch (SM) solutions after incubation with T7 endonuclease for 15 min. A DNA Ladder (Invitrogen 10 bp DNA ladder) was used as the reference.	220
5.5	PAGE ePage1 10-20% (v/v) electrophoretogram, stained with 1x SYBR® gold and viewed using a Safe Imager Blue-Light Transilluminator, of 16 h digestion with T7 endonuclease I (1 U) incubation with the PM and SM solutions with undigested controls. A DNA Ladder (L) (Invitrogen 10 bp DNA ladder) was used as the reference.	222
5.6	Average of 3 UV/vis spectra (absorbance (a.u) vs time (min)) of TMB assay for blank (no G4 aptamer, red) and immobilised G4 aptamer (black) on the surface of Corning® DNA-Bind® 96-well microplates. Averages were performed using OriginPro 9 average curve function.	224
5.7	Average of 3 UV/vis spectra (absorbance versus time (min)) of TMB assay for no aptamer blank (red) and immobilised G4 aptamer (black) on the surface of Corning® DNA-Bind® 96-well microplates with (a) no PEG control, (b) PEG 6000 5% (w/v), (c) PEG 6000 10% (w/v) and (d) PEG 8000 5% (w/v), determined using a TMB assay. Averages were performed using OriginPro 9 average curve function.	227
5.8	Average of 3 peroxidase-mimicking activity measurements of PM and SM G4 aptamers released into solution after 16 h digestion at 37 °C with T7 endonuclease I. Showing blank (no aptamer) (blue), perfect match (PM, red) and single mismatch (SM, black) after digestion. Averages were performed using OriginPro 9 average curve function.	230

5.9	Average of 3 peroxidase-mimicking activity measurements of G4 aptamers immobilised onto BeMag® silica iron core microbeads: blank (no G4 aptamer) undigested (red), blank (no G4 aptamer) digested (pink), PM undigested (black), PM digested (blue), SM undigested (green), and SM digested (orange). Averages were performed using OriginPro 9 average curve function.	233
6.1	The chemical structure of (a) fluoroquinolonic acid and (b) oxacillin. The carboxylic acid functional groups used for coupling with the G4 ODN are highlighted in red.	244
6.2	General scheme for the carbodiimide coupling reaction. The antibiotic with carboxylic acid functional group (red) reacts with 1-ethyl-3-(3-dimethylaminopropyl) carbodiimide hydrochloride (EDC) to form an intermediate that reacts with the amine-functionalised G4 aptamer (amine-functionalised, green).	244
6.3	Average of 3 UV/vis spectra (absorbance versus time (min)) of TMB assay for blank (no G4 aptamer, green), G4 aptamer (black), NH ₂ -G4 aptamer (pink), OXG4 aptamer (red) and OX (no G4 aptamer, blue). Averages were performed using OriginPro 9 average curve function.	246
6.4	Fluorescence confocal scanning microscope image of (a) <i>S. aureus</i> and (b) <i>S. epidermidis</i> biofilms grown on silicone coupons for 20 h and 24 h, respectively. Stained with LIVE/DEAD™ BacLight™ Bacterial Viability Kit.	251
6.5	Graph comparing the number of viable (a) <i>S. aureus</i> and (b) <i>S. epidermidis</i> cells (log ₁₀ CFU mL ⁻¹) after treatment with additives: blank (MHB only), G4 aptamer, G4/hemin aptamer, OXG4, OXG4/hemin aptamer, hemin and oxacillin (see Table 6.3).	253
6.6	Example of a possible G-wire structure that can form between one hemin and two G4 aptamers.	255

6.7	Bar graph comparing the 3 averages of viable <i>S. aureus</i> cells (\log_{10} CFU mL ⁻¹) after treatment with additives: blank (broth only), G4/hemin aptamer 2 μ M, 3 μ M, 4 μ M and 5 μ M (with hemin 8 μ M), hemin (8 μ M) and oxacillin (1 μ g mL ⁻¹) in the presence of 0.5% hydrogen peroxide (v/v).	257
A.1	Examples of three other possible non-specific primer hybridisation with the target strand. Showing that although there are other possible non-specific targets, there is no possible way for the GoTaq® Flexi polymerase to extend the primer during the PCR process	271
B.2	Toehold-mediated strand displacement kinetic curves (relative fluorescence unit (RFU) versus time) of the displacement reactions of the incumbent strand of the TPP-C, labelled with ATTO 550, with DS(A)(black), DS(T)(pink), DS(G)(blue) and DS(C) (green). Each set of data is an average of 3 replicates. Every 20 data points was omitted for ease of viewing and the red dashed lines are the fits obtained using OriginPro 9 software.	272
D.1	PAGE ePage1 10-20% (w/v) electrophoretogram, stained with 1x SYBR® gold and viewed using a Safe Imager Blue-Light Transilluminator, of 15, 30, 45, 75, 90, 105 and 120 min digestion with T7 endonuclease I (2.5 U) incubation with the PM and SM solutions. A DNA Ladder (L) (Invitrogen 10 bp DNA ladder) was used as the reference.	276
E.1	PAGE ePage1 10-20% (w/v) electrophoretogram, stained with 1x SYBR® gold and viewed using a Safe Imager Blue-Light Transilluminator, of 16 h digestion with T7 endonuclease I (2.5 U) incubation with the PM and SM solutions. A DNA Ladder (L) (Invitrogen 10 bp DNA ladder) was used as the reference. . .	277
G.1	Average of 3 UV/vis spectra (absorbance (a.u) versus time (min)) of ABTS assay for blank (no G4 aptamer) (red) and immobilised G4 aptamer (black). . .	279

H.1 Left: Agarose 4% (w/v, made according to Chapter 2, Section 2.4.3) electrophoretogram, stained with 1X SYBR® Green I and viewed using a Gel Doc, of NH₂G4 aptamer and OXG4 aptamer. A DNA Ladder (Quick-Load® Purple 50 bp DNA ladder) was used for reference. Right: PAGE 12% (v/v, made according to Chapter 2, Section 2.4.3) electrophoretogram, stained with 1X SYBR® Green I and viewed using a Gel Doc, of NH₂G4 aptamer and OXG4 aptamer. A DNA Ladder (20/100 Ladder Oligo length standards) was used for reference. Red dotted line is to guide the eye to the intermolecular structures. . 280

List of Tables

1.1	Calculated binding energy of different length toeholds and sequence adapted from Zhang and Winfree.	45
2.1	List of chemicals and reagents.	107
2.1	List of chemicals and reagents cont.	108
2.1	List of chemicals and reagents cont.	109
2.2	List of materials	110
2.3	List of buffers	111
2.4	Sequences and melting temperature of primers and displacing (DS) ODNs. All ODNs in this table were purchased from IDT DNA Technology (USA), made up to 100 μ M and stored at -20 °C.	112

2.5	Sequences and melting temperature of G4 ODN sequences that had the highest peroxidase-mimicking activity, EAD-2 and G ₃ A ₃ sequences. All ODNs in this table were purchased from Eurofins Scientific (Japan), made up to 100 μM and stored at 4 °C.	113
2.6	Sequences and melting temperature of G4 ODN sequences that had the highest peroxidase-mimicking activity, EAD-2 and G ₃ A ₃ . All ODNs in this table were purchased from Eurofins Scientific (Japan), made up to 100 μM and stored at 4 °C.	113
2.7	Sequences and melting temperature of ODNs used for antimicrobial studies, including sequences used for coupling with antibiotics (see Section 6.3.1). All ODNs in this table were purchased from IDT DNA (USA), made up to 100 μM and stored at 4 °C	114
2.8	Strains of non-biofilm and biofilm forming bacteria used to study the affects of G4 ODN in Chapter 6, Section 6.3.2.2. Stored at 4 °C on MHB agar plates. . .	114
2.9	Dye channel selection chart with all 6 excitation and 6 emission channels available on the Roto-Gene Q 6-plex.	127
3.1	The properties maximum excitation wavelength (λ_{ex}), maximum fluorescence emission wavelength (λ_{fl}), quantum yield (Φ), molar extinction coefficient (ϵ_{max}) and intensity of 6-FAM, ethidium bromide, ATTO 550, ATTO 647N and Black hole quencher 1 (BHQ-1).	137

3.2	The displacement rate (k_{DS}) and the kinetic discriminator ratio (R_k) of the toehold-mediated strand displacement reactions of all TPPs (labelled with ATTO 647N) when treated with DS(T), DS(A), DS(C), or DS(G), as determined from the kinetic curves presented in Fig. 3.9. Trimer sequences for TPPs and the different DSs, where the underlined X is the SNP position and can be any one of the nts (C, G, A and T). Included are the orders for the displacement rates for each TPP	154
3.3	The displacement rate (k_{DS}) and the kinetic discriminator ratio (R_k) of the toehold-mediated strand displacement reactions of all TPP (labelled with ATTO 647N) when treated with DS(T), DS(A), DS(C), or DS(G), in the absence and presence of ethidium bromide as determined from the kinetic curves presented in Fig. 3.9 and Fig. 3.10. Trimer sequences for TPP and the different DSs, where the underlined X is the SNP position and can be anyone of the nt (C, G, A and T). Included are the orders for the displacement rates	163
4.1	Name and sequences used to investigate the effects of G residues on the peroxidase-mimicking activity of the EAD-2 sequence divided into separate terminal (X_{t1} and X_{t2}), loop (X_{l1} , X_{l2} , X_{l3}) and G (G_m) regions.	186
4.2	Peroxidase-mimicking activity (V_0) calculated for the G4 aptamer sequences from Table 4.1.	187
4.3	Name and sequences used to investigate the effects of deletions and substitution of A residues with T residues on the peroxidase-mimicking activity of the Parent sequence divided into separate terminal (X_{t1} and X_{t2}), loop (X_{l1} , X_{l2} , X_{l3}) and G (G_m) regions.	189

4.4	Peroxidase-mimicking activity (V_0) calculated for the G4 aptamer sequences in Table 4.3 With the ranking of each sequence based on V_0 and the top 4 sequences (highest V_0) are underlined.	189
4.5	Peroxidase-mimicking activity (V_0) calculated for the G4 aptamer sequence from Table 4.1 and 4.3 with post- and pre-addition of hemin during the folding procedure.	192
4.6	Peroxidase-mimicking activity (V_0) calculated for the G4 aptamer sequence from Table 4.1 and 4.3 with PEG-hemin.	193
4.7	Top 20 ranked G4 ODN sequences with the highest V_0 values after 8 generations (including generation 1) of the GA with EAD-2 and G ₃ A ₃	195
4.8	Number of times loop sequences (X_{I1} , X_{I2} and X_{I3}) are repeated in the top 20 G4 aptamers (with the highest V_0).	196
4.9	Effect of K ⁺ ions on G4/hemin peroxidase-mimicking (V_0) activity.	200
4.10	The calculated V_{max} , K_m , and $k_{(cat)}$ for the top 3 G4/hemin aptamers (with the highest V_0), the original EAD-2 and G ₃ A ₃ derived from the Michaelis-Menten curves in Fig. 4.10	204
5.1	Peroxidase-mimicking activity (V_0) of G4 immobilised on the surface of the Corning® DNA-Bind® 96-well microplates compared to the blank (no G4 aptamer) calculated from Fig. 5.6.	224
5.2	Peroxidase-mimicking activity (V_0) of immobilised G4 aptamers in the presence of no PEG control, PEG 6000 5% (w/v), PEG 6000 10% (w/v) and PEG 8000 5% (w/v)calculated from the data in Fig. 5.7.	228

5.3	Peroxidase-mimicking activity (V_0) of blank (no aptamer), PM and SM after digestion calculated from Fig. 5.8.	230
5.4	Peroxidase-mimicking activity (V_0) of undigested and digested PM and SM beads calculated using Eq. 5.4 from Fig. 5.9	234
6.1	Sample names and Sequences of G4 ODNs utilised throughout this chapter. . .	242
6.2	Peroxidase-mimicking activity (V_0) of TMB assay for blank (no G4 aptamer, green), G4 aptamer (black), NH ₂ -G4 aptamer (pink), OXG4 aptamer (red) and OX (no G4 aptamer, blue) calculated from Fig. 6.3	247
6.3	List of samples incubated with biofilm for 2 h, showing concentration of G4 aptamer, hemin and OX in each sample.	252
6.4	The $\Delta\log_{10}$ CFU mL ⁻¹ and percentage reduction of number of viable <i>S. aureus</i> cells, compared to the blank (MHB), after treatment with additives: G4 aptamer, G4/hemin aptamer, OXG4 aptamer, OXG4/hemin aptamer, hemin and OX. Also shown is confidence intervals.	252
6.5	The $\Delta\log_{10}$ CFU mL ⁻¹ and percentage reduction of number of viable <i>S. epidermidis</i> cells, compared to the blank (MHB), after treatment with additives: G4 aptamer, G4/hemin aptamer, OXG4 aptamer, OXG4/hemin aptamer, hemin and OX. Also shown is confidence intervals.	256
6.6	The $\Delta\log_{10}$ CFU mL ⁻¹ and percentage reduction of number of viable cells, compared to the control, after treatment with 0.5% H ₂ O ₂ (v/v) additives: G4/hemin aptamer 2 μ M, 3 μ M, 4 μ M and 5 μ M (with hemin 8 μ M), hemin (8 μ M) and oxacillin (1 μ g mL ⁻¹). Included are confidence intervals.	258

C.1	Generations (Gen) generated utilising the genetic algorithm with peroxidase-mimicking activity (V_0). Including the original EAD-2 and G_3A_3 sequences. . .	273
C.1	Generations (Gen) generated utilising the genetic algorithm with peroxidase-mimicking activity (V_0). Including the original EAD-2 and G_3A_3 sequences continued.	274
C.1	Generations (Gen) generated utilising the genetic algorithm with peroxidase-mimicking activity (V_0). Including the original EAD-2 and G_3A_3 sequences continued.	275
F.1	Chemiluminescent signatures of blank (no G4 aptamer) and immobilised G4 aptamer wells.	278

Abstract

DNA is fast becoming a valuable tool for nanotechnology with its unmatched specificity, and the numerous structures that can be formed. This thesis will look at the interaction of static and dynamic DNA with organic molecules such as intercalators and co-factors.

Static DNA is structured DNA that does not change shape once self-assembled, while dynamic DNA can change conformation, or shape, when performing a reaction. By understanding how these two types of DNA interact with other molecules, this will allow for development of more sensitive biosensors and new applications for DNA nanotechnology. Chapter 1 provides a literature overview of DNA and its various structures and Chapter 2 describes the experimental techniques used in the thesis.

Chapter 3 investigates ways to control the rate and specificity of toehold-mediated strand displacement reactions. These reactions are classified as dynamic DNA processes whereby one single-stranded DNA (ssDNA) displacing sequence (DS) is able to nucleate with a target DNA sequence with a “toehold” double-stranded DNA (dsDNA) that contains two hybridised ssDNA of differing lengths. The DS nucleates at the toehold and then begins a random walk

process that displaces the shorter incumbent strand from the target DNA sequence base-by-base, forming hybridised dsDNA and releasing the incumbent DNA strand as ssDNA. This process is also known as three-way branch migration due to the involvement of only three ssDNA strands. The displacement reaction is measured by the decrease in fluorescence of a fluorophore on the target as it duplexes with the DS containing a quencher.

This technique has been found to be useful for genotyping of single nucleotide polymorphisms (SNPs) in short dsDNA sequences (<20 bp). Current three-way branch migration toehold-mediated strand displacement techniques are unable to discriminate between hybridised dsDNA that is perfectly matched (PM), or contains a single mismatch (SM) of base pairs (bp) between the two ssDNA strands when the target DNA sequence is 80 bp long. This can cause issues as it may not be applicable to for genotyping of real life DNA. Therefore, Chapter 3 investigates increasing the specificity of the toehold-mediated strand displacement process with DNA strands of 80 bp of length. Two fluorophores, ATTO 550 and ATTO 647N, were investigated for compatibility with the polymerase chain reaction (PCR) process as well as the toehold-mediated strand displacement reaction. The fluorophore ATTO 550 was found to produce non-specific PCR products and so was not used. The addition of ethidium bromide, as well as using the fluorophore ATTO 647N, on the target DNA containing a toehold resulted in an improvement in both the specificity and the rate of the toehold-mediated strand displacement when using DNA strands of 80 bp of length, especially for SMs that involved cytosine. Thus, making the technique applicable for genotyping using real life DNA.

In Chapter 4, the peroxidase mimicking activity of different DNA sequences capable of forming static DNA structures, known as G-quadruplexes (G4), that complex hemin (G4/hemin complexes) were assayed. The highest peroxidase mimicking activity was then determined. A G4 is made up of 1-4 strands of guanine-rich (G-rich) ssDNA sequences that form by stacking guanine-tetrads (G-tetrads) through stabilisation by a mono-cation. The

peroxidase-mimicking activity of G4/hemin complexes can catalyse the oxidation of 3,3',5,5'-tetramethylbenzidine (TMB) in the presence of H₂O₂ to produce a coloured product, and therefore has potential to be used in biosensor, which is discussed in Chapter 5. Enhancing the rate of the peroxidase mimicking activity of the G4/hemin complex can allow for more sensitive biosensors. Here, a genetic algorithm (GA) was utilised to screen DNA sequences that form G4/hemin complexes to provide an enhanced rate of peroxidase-mimicking activity. The GA produced 10 new DNA sequences that form G4 from two initial parent DNA sequences. The rate of the peroxidase-mimicking activity of the DNA sequences identified by the GA were then experimentally evaluated using the TMB assay. The DNA sequences that form G4/hemin complexes with an increased rate of peroxidase-mimicking activity were then used in the next round of GA to produce 10 new DNA sequences that form G4/hemin. This was repeated seven times until the rates of peroxidase-mimicking activity appeared to decline, resulting in a DNA sequence with G4/hemin complex showing a rate increase of approximately 5-fold of peroxidase-mimicking activity as compared to the original parent sequences.

At the same time as the screening of the G4/hemin complexes, in Chapter 5 the peroxidase-mimicking activity of surfaces modified with DNA containing G4/hemin complexes were investigated as a potential method to distinguish between hybridised perfectly matched (PM) DNA and SM DNA. This was accomplished by immobilising the DNA sequence G4(G)001T that formed a G4/hemin complex onto NHS-functionalised Corning® DNA-Bind 96-well microplates. After complexing the G4-containing DNA sequences in the wells with hemin, the G4-containing DNA sequences on the surfaces of the wells were hybridised with PM DNA or SM DNA sequences in separate wells. The wells were then digested with the enzyme T7 endonuclease I, which cuts hybridised SM DNA, but not PM DNA, and releases the G4/hemin complex from the well. Comparing the peroxidase-mimicking activity of the digested and undigested wells was used to distinguish if the hybridised DNA in the well was PM DNA, or SM DNA, and therefore if the DNA sequence added to the well was PM or contained a SM (relative

to the DNA sequence attached to the surface of the well). However, it was found that there was no measurable difference between the PM and SM hybridised DNA. Similar experiments were performed using magnetic silica iron core beads, modified with the same G4-containing DNA sequence used in the wells, however there was also no measurable difference in the peroxidase-mimicking activity of modified beads hybridised with either PM or SM hybridised DNA. This was thought to be due to steric hindrance preventing T7 endonuclease I from approaching the DNA on the surfaces, and therefore not being able to cut the hybridised SM DNA.

Finally, Chapter 6 investigates using G4/hemin complexes as a possible antimicrobial to combat biofilms. Biofilms are made up of bacteria that are protected by extracellular polymer substances, that make conventional antimicrobial treatments against planktonic bacteria (not encapsulated in a biofilm) ineffective, such as antibiotics or peroxide-based (e.g., 3% H₂O₂ solution) treatments. This can lead to the bacteria becoming resistant to the antimicrobial treatments over time. Here, a modified DNA sequence containing a G4/hemin complex (identified to have the fastest peroxidase-mimicking activity in Chapter 4) was coupled with an antibiotic and tested to determine if the peroxidase-mimicking activity was able to eradicate bacteria inside a biofilm. The G4 was functionalised with an amine on the 5' terminal end of the DNA sequence (NH₂-G4), and was also coupled to the antibiotics fluoroquinolonic acid (FQ) or oxacillin (OX), referred to as FQG4 and OXG4, respectively. However, only OXG4 was able to be purified in concentrations high enough for use in antimicrobial treatments. It was determined using a TMB assay and minimum inhibitory concentration (MIC) assay that the OXG4 retained both a high peroxidase-mimicking activity and antimicrobial effectiveness on planktonic *Staphylococcus aureus* (*S. aureus*). For the treatment of biofilms, it was found that the OXG4 was more effective than free oxacillin but did not completely eradicate all the bacteria in the biofilm (as determined using CFU assay).

Using the CFU assay, the DNA sequence that was determined to have the highest peroxidase-mimicking activity, complexed with hemin to form G4/hemin complex with no

modifications, was also incubated with biofilms and then treated with a 0.5% peroxide (v/v) solution and found to be able to decrease the number of bacteria present in the biofilm by 50%.

Declaration

I certify that this thesis does not incorporate without acknowledgment any material previously submitted for a degree or diploma in any university; and that to the best of my knowledge and belief it does not contain any material previously published or written by another person except where due reference is made in the text

Renzo A. Fenati

2018

Acknowledgements

I would firstly like to thank all those who have supervised me over the course of my Ph.D.; Claire Lenehan, Tomohiko Yamazaki and Katherine Locock. Most importantly I would like to thank my primary supervisor Amanda Ellis, who helped me to achieve everything these past 5 years. Without Amanda's constant support, help, and patience I would not have finished honours and in turn this Ph.D. I will forever be grateful for the opportunity to work with, and learn from, the Ellis group. Special thanks go to Dmitriy Khodakov who taught me many of the skills that I used throughout this Ph.D.

There are many colleagues from Flinders University that I would like to acknowledge. Ashley Connolly, Nianjia Seow and Nick Adamson. I feel privileged to have known, and formed relationships with, you all. I would also like to thank Michael Wilson and Connor Retallick for the many years of friendship and interesting conversations. As well as all my friends that I have made over the course of my Ph.D. I will always cherish the many years of memories.

My thanks also go out to Jonathan Sierke and Tristan Kilmartin for their invaluable help in editing my thesis and giving me advice that I will use in my future endeavours. Without these two I would have never been able to complete this thesis. I would also like to thank everyone at the Institute for Nanoscale Science and Technology and the National Institute of Material Sciences for the opportunity to study in Japan for six months. Additionally, I would like to acknowledge the Australian Government Research Training Program Scholarship and Flinders University for the Research Higher Degree Scholarship.

I would like to thank my Mother for the support during my Bachelor's, Honours and Ph.D. studies. Without her support I would have not had the opportunity to achieve all that I have over the past several years.

Finally, I could have never achieved any of this without the most loving and support-

ive person in my life, my fiancée Cassandra. She has been nothing but supportive for the past eight years and always picked me up whenever I was down. Thank you for being so understanding, especially when I moved to Japan for six months and the cats did not allow you to sleep until I returned.

Publications

Journal articles

Fenati, R. A.; Khodakov, D.; Ellis, A. V. Optimisation of DNA Hybridisation and Toehold Strand Displacement from Magnetic Bead Surfaces. *Int. J. Nanotechnol.* **2017**, 14 (1–6).

Fenati, R. A.; Connolly, A. R.; Ellis, A. V. Single Nucleotide Polymorphism Discrimination with and without an Ethidium Bromide Intercalator. *Anal. Chim. Acta.* **2017**, 954, 121–128.

Seow, N.; Fenati, R. A.; Connolly, A. R.; Ellis, A. V. Hi-Fidelity Discrimination of IsomiRs Using G-Quadruplex Gatekeepers. *PLoS One.* **2017**, 12 (11).

Shearer, C. J.; Yu, L. P.; Fenati, R.; Sibley, A. J.; Quinton, J. S.; Gibson, C. T.; Ellis, A. V.; Andersson, G. G.; Shapter, J. G. Adsorption and Desorption of Single-Stranded DNA from Single-Walled Carbon Nanotubes. *Chem. - An Asian J.* **2017**, 12 (13), 1625–1634.

Wilson, M. J.; Fenati, R. A.; Williams, E. G. L.; Ellis, A. V. Synthesis of a Deoxyguanosine Monophosphate Rich Propyl Methacrylate Oligomer. *New J. Chem.* **2018**, 42 (11), 8815–8822.

Conferences

Fenati, R. A.; Ellis, A. V. Invited speaker at CSIRO Chemistry Discussion session 2018 (Oral)

Fenati, R. A.; Qu, Y.; Locock, L.; Ellis, A. V. 26th Annual Conference of the Australasian Society for Biomaterials and Tissue Engineering 2018 - Impact Of Loaded G-quadruplexes On Bacteria (Poster)

Fenati, R. A.; Connolly, A. R.; Ellis, A. V. International Conference on Nanoscience and Nanotechnology (ICONN 2016) - Optimised single nucleotide polymorphism genotyping (Poster)

Fenati, R. A.; Connolly, A. R.; Ellis, A. V. Royal Australian Chemistry Institute R&D Topics 2016- Optimised single nucleotide polymorphism genotyping (Poster)

Fenati, R. A.; Khodakov, D.; Ellis, A. V. Royal Australian Chemical Institute (RACI) Congress

2014- Optimising DNA hybridisation and strand displacement from surfaces of magnetic beads
(Oral)

Book Chapter

Connolly, A.R., Seow, N., Fenati, R.A. and Ellis, A.V., *DNA Nanostructures: Static and Dynamic*. **2014**.

Chapter 1

Introduction and literature review

1.1. Synopsis

This chapter contains relevant background information on deoxyribonucleic acid (DNA) structures and reactions; in solution and immobilised on surfaces. Attention will be focused on one type of static DNA structure, namely G-quadruplex (G4) and one type of dynamic DNA reaction, namely toehold-mediated strand displacement. To understand how these structures and reactions occur it is vital to understand the dimensions and base specificity. Particular consideration will be given to the manipulation of DNA by controlling sequence, modifying bases and changing buffer conditions. This chapter will also discuss ways in which DNA sequences with desirable properties can be discovered. Important literature that currently exists and was used to develop the methods in this thesis will be discussed. This chapter will further discuss applications of using static and dynamic DNA, as well as potential future uses; such as sensitive biosensors or antimicrobial activity.

1.2. Introduction

Deoxyribonucleic acid (DNA) is a fundamental genetic biopolymer used as instructions by all living organisms on earth on how to grow, develop, and evolve. DNA encodes all the genetic information (i.e., proteins) that is used and passed on by all cells to continue the survival of a living organism. Discovering ways to identify and manipulate genetic code has been revolutionary in the fields of science, medicine and criminology. This fundamental unit of life has been used in numerous ways such as in molecular recognition, targets for therapeutics and genetic fingerprinting. This is all made possible due to the versatility and variety of DNA structures, which can be divided into two main categories: static and dynamic. This Chapter will highlight the current literature and discuss the different structural and dynamic features of DNA, including how to control it by changing sequence, temperature and environmental factors. A discussion on applications of DNA will also be provided, from using DNA in genotyping, biosensing and possible antimicrobial applications. However, it is first vital to understand the structural features and specificity of DNA.

1.3. DNA structure

There exists two nucleic acids that are a vital part of biological organisms: DNA and ribonucleic acid (RNA). Nucleic acids are made up of nucleotides (nts), which consist of three parts: a phosphate group, a pentose group and a nucleobase group (Fig. 1.1). DNA is distinguished from RNA by the presence of a hydrogen on the second carbon (or 2', Fig. 1.1, left (red)) of the pentose sugar of the nt forming a deoxyribose, whereas RNA contains a hydroxyl at the same point to make a ribose sugar of the nt (Fig. 1.1, right (blue)). The pentose sugar is a vital part of the nt that links the nucleobase to the phosphates, often referred to as the phosphate sugar backbone (Fig. 1.1).

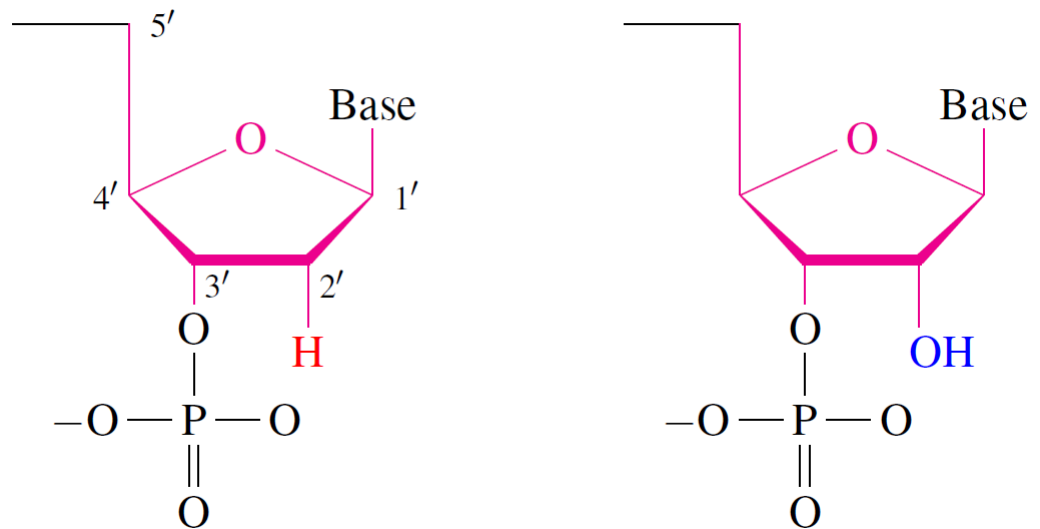


Figure 1.1: Chemical structures of a DNA nucleotide, with a hydrogen at the 2' position (left, red), and RNA nt , with a hydroxide at the 2' position (right, blue) nts.

The nucleobases are attached to the 1' position on the pentose sugar, that form the five possible nts; purines: adenine (A) and guanine (G) and pyrimidines: thymine (T) (for DNA only), uracil (U) (for RNA only) and cytosine (C) (Fig.1.2 , multicoloured). T (Fig. 1.2 yellow) is exclusive to DNA and U (Fig. 1.2, grey) is exclusive to RNA. Pyrimidines are aromatic heterocyclic organic compounds while purines are pyrimidines that have an extra imidazole attached. Single-stranded DNA (ssDNA) is formed by phosphodiester bonds between the 5' of one nt and 3' of another nt (Fig. 1.2). This sequential polymerisation of nts is what gives rise to DNA sequences that code for proteins.

DNA is vital for protein expression in cells and so it is important for it to preserve itself entirely. Therefore, ssDNA hybridises with a second (and in rare cases a third, see Section 1.5.3.1) ssDNA to become double-stranded DNA (dsDNA).¹ This is achieved by forming stable hydrogen bonds between the pyrimidines and purines, where A pairs with T and G pairs with C. Base pairing strength, and therefore stability of the whole dsDNA, is based on the number of hydrogen bonds formed as well as the number of hydrogen bonds between each base pair (bp).

A and T are able to form two hydrogen bonds and G and C form three hydrogen

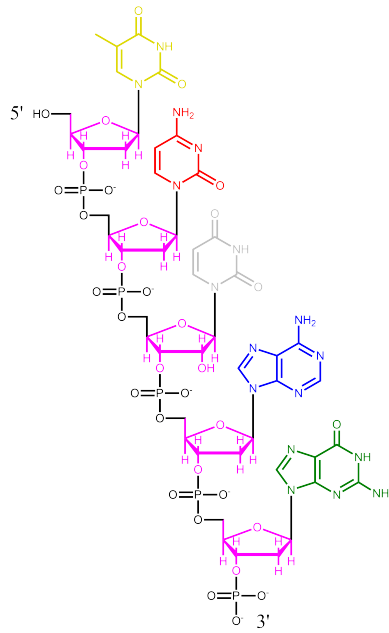


Figure 1.2: Nucleotides linked through a phosphate (black) and ribose sugar (pink) to make ssDNA. Pyrimidines: thymine (yellow) and cytosine (red) and uracil (grey). Purines: adenine (blue), guanine (green).

bonds, so G/C bps are therefore able to form more stable bonds than A/T bps. This is referred to as Watson-Crick base pairing and is regarded as the canonical base pairing. Stability of the dsDNA also comes from the stacking of the base pairs, where the π - π interactions from the cyclic ring systems stabilise the overall structure.²⁻⁴ Each base pair that stacks is on average able to stabilise the Gibb's free energy (ΔG°) of dsDNA by -7.92 ± 2.57 kcal/mol, this is referred to as the stabilising or binding energy of the DNA in literature.^{5,6} Frank-Kamenetskii *et al.*⁷ determined that the ΔG° was more dependent on the base stacking than the of the base pairs rather than the hydrogen bonds between each base pairs. They went on to add that the lose of base pairing can be compensated by hydrogen bonding with water molecules.

This information can be used to predict what DNA structures can be formed and the melting temperature (T_m), which is the temperature that half of all strands are in the single-stranded state.⁸ DNA hybridisation is classified as non-Arrhenius, this is due to the ΔG° being positive at lower temperatures ($<20^\circ\text{C}$) and negative at high temperatures (close to the T_m) ($>20^\circ\text{C}$).⁷ This results in slower hybridisation rates at lower temperatures than at higher temperatures

and as a result the rate limiting step is the nucleation between the two strands of DNA.⁹ However, above the T_m the hydrogen bonds are weakened to the point where the dsDNA is no longer stable and will dissociate. Section 1.3.2 will discuss how to predict the T_m of dsDNA.

DNA is described as having directionality based on the orientation of the sugar backbone structure, where the 5' terminus of one strand will hybridise to the 3' terminus of the other strand (see Fig. 1.2).¹ DsDNA must form between two complementary strands, where both strands have the correct nt sequence to form stable Watson-Crick base pairing, antiparallel strands (i.e., ssDNA running in the opposite direction) resulting in the twisted double helix structure. The conventional DNA notation is to write only the 5' to 3' (e.g., AGC), as the complementary 3' to 5' sequence can be deduced. However, if a mismatch occurs then the antiparallel sequence is indicated with a forward slash and the mismatch is underlined (e.g., AGC/TGG).¹⁰ Along with structure, the nt sequence may also dictate the rigidity of a dsDNA. dsDNA sequences with a persistence length < 150 base pairs are thought of as rigid rods, whereas longer sequences are more flexible.¹¹ An example of this is how genomic DNA is long enough to be able to be coiled, but still remain intact even under physical torsion strain.¹²

1.3.1. DNA double helix

DsDNA forms a unique double helix structure as a result of two single DNA strands hybridising and twisting around each other, forming a structure more stable than that of ssDNA.¹³⁻¹⁹ Hybridisation of dsDNA is far more energetically favourable than ssDNA and so dsDNA will self-assemble under the correct conditions (salt, pH and temperature). This propensity to self-assemble is so vital that even in the absence of complementary strands DNA will self-assemble into energetically favourable structures, see Section 1.5 for information on structures other than the double helix. DsDNA forms base pairs on the inside of the helix, whilst the phosphates make up the outer backbone, essentially protecting the base pairs from the environment. This is vital, as without this stability mutations would occur far more frequently.^{19,20} The double-stranded nature also allows for repair of mutations that have occurred based on the

complementary strand, this is known as proof reading. Overall the double helix has evolved to be stable and have a structure for binding proteins.^{21,22} An important aspect of the dsDNA is the groove formation.

The double helix forms two types of grooves, the major groove and the minor groove (Fig. 1.3).²³ Grooves are identified by the distance between the two ssDNA in the double helix. The major groove is where the two strands are farthest apart at $\sim 18 \text{ \AA}$, and the minor groove is where the two strands are closer together at $\sim 12 \text{ \AA}$. Major and minor grooves repeat every 34 \AA . These grooves are very important for biological purposes, such as protein binding,²¹ transcription²⁴ and replication.²⁵ Grooves are also targets of certain intercalating dyes (to be discussed later in Section 1.4.6) which allow for the identification and quantification of DNA.²⁶ The size of the grooves is completely dependent on the type of DNA formed.

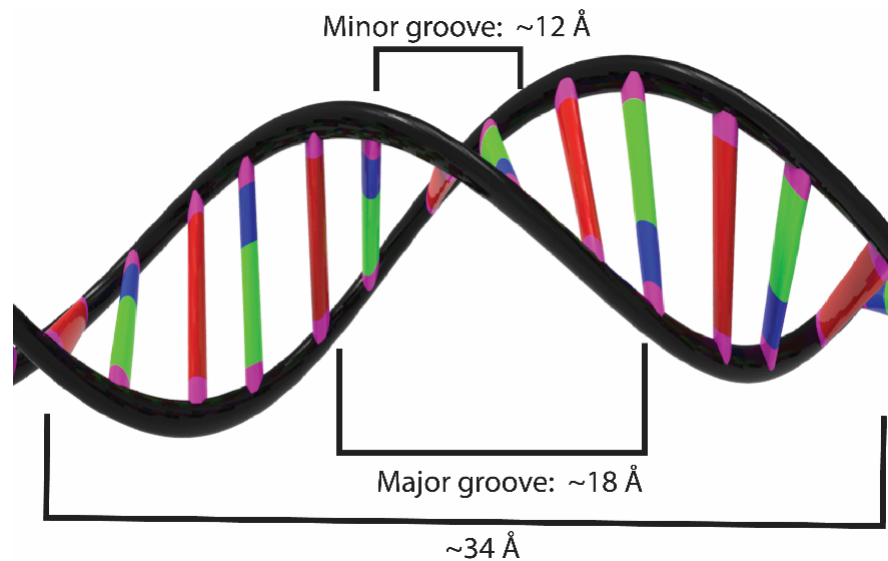


Figure 1.3: DNA double helix showing the major and minor grooves.⁵

There are three prominent forms of duplexed DNA, namely A-form (Fig. 1.4, left), B-form (Fig. 1.4, middle) and Z-form (Fig. 1.4, right). A-form DNA is formed under dry or low humidity conditions and was first published by Franklin *et al.*²⁶ in 1953. They discovered A-form by varying the amount of water available to DNA. A-form is described as having the following dimensions: diameter of 23 nm , 2.56 \AA between each bp, angle of rotation of 32.7

°/bp, a sugar pucker of 5.9 Å (C3'-endo conformation), and 11 bps per turn. The A-form has a condensed right-handed turn and due to the small sugar puckering distance, there is a negligible minor groove.²⁷

B-form is the classic right-handed form and is very similar to the A-form of DNA. The major differences of B-form DNA include: decreased diameter of 2.0 nm, increased distance between bp of 3.4 Å with 10.5 bp per twist rotating at 34.3 °/bp,²⁸ and a wider sugar pucker of 7.0 Å (C2'-endo/anti conformation).²⁹

The final Z-form is the most different of the three structures. Firstly, the two strands wrap around each other in a left-handed direction to produce a 'zig-zag' pattern in the backbone.³⁰ This type of DNA is primarily formed when the nt sequence alternates between purine and pyrimidine (e.g., GCGCGC),³¹ where the G have C3'-endo/syn conformation and the C is in the C2'-endo/anti conformation.³⁰

Figure removed due to copyright

Figure 1.4: Stick model of the three main types of DNA: A-form, B-form and Z-form (left to right).³²

The next section will discuss how to predict the T_m of a DNA structure and how it is

important to experimental design.

1.3.2. Melting temperature (T_m) of DNA

As mentioned previously the T_m is the point where half the strands of double-stranded and half are single-stranded. It is also described as the temperature at which dsDNA denatures and renatures. The T_m is determined by the bps that make up the strand and the environmental conditions (e.g., chaotropic agents, described later in this section). G/C base pairs contain 3 hydrogen bonds and stabilise the dsDNA more than A/T base pairs, so a higher G/C content results in a more stable DNA structure. There are several models that have been developed to predict the T_m of a DNA sequence, with early models simply considering the %G/C content that makes up the strand. Beginning with a simplistic Marmur-Doty equation.^{13,33} This method essentially calculates the T_m in 0.2 M Na⁺ using the following formula:

$$T_m = 69.3 + 0.41(G - C) \quad (1.1)$$

Where $G - C$ is the molar percentage of G residues + C residues in the DNA sequence. A modified Marmur-Doty equation has been used for T_m calculations of oligodeoxynucleotides (ODNs), which are short synthetic DNA sequences:

$$T_m = 2(A + T) + 4(G + C) - 7 \quad (1.2)$$

The most popular method for calculating the T_m is the nearest-neighbor (NN) model.^{13,34-37} Initially developed by Borer *et al.*³⁸⁻⁴⁰ and having been studied in further detail over the past half-century.^{13,34,41} The NN model has been described as the most accurate method, due to the calculation taking into account how base pairs interact with neighbouring base pairs.³⁶ Software that is available to calculate the T_m of DNA include nupack⁴² (nupac.org) and The mfold

Web Server⁴³ (<http://unafold.rna.albany.edu>).

SantaLucia *et al.*,³⁴ designed the most up-to-date *NN* model, that is able to be used for calculations of complementary DNA, mismatches (see Section 1.3.2.1) and dangling ends. They also expanded their model to take sodium concentration into consideration when determining the T_m . This has resulted in a model that only has an absolute deviation of 1.6 °C, compared to 6.8 °C from previous models. They used their *NN* model to determine that there was a trend of nearest-neighbour stabilities $GC > CG > GG > GA \approx GT \approx CA > CT > AA > AT > TA$ at 37 °C. This is to be expected, when considering the fact that G and C are able to form more stable hydrogen bonds than T or A. This work also showed that sequence, base stacking, and hydrogen bonding are important when determining the T_m . Understanding how base pairs interact with each other is vital for experimental design, it allows for fine tuning of experimental parameters like temperature control and buffer conditions. This model has been used most commonly for primer design for polymerase chain reaction (PCR) amplification, as understanding T_m is vital for successful amplification. The T_m of DNA is also dependent on factors other than bp and these are vital for understanding how DNA functions in different environments.

There are several ways in which dsDNA can dissociate to become ssDNA, also known as denaturation. Denaturation occurs when the hydrogen bonded base pairs are affected by conditions such as heat,¹⁵ physical strain¹⁷ or chemicals (salt concentration⁴⁴, pH⁴⁵ or chaotropics⁴⁶). The most common way to denature DNA is heating and this process is reversible (if the DNA is not destroyed). The reverse process being where DNA hybridises, also known as renaturation and refers to DNAs propensity to form structures spontaneously. For melting temperature studies of DNA it is very important that DNA is in a suitable buffer that contains the correct concentration of Na^+ and H^+ ions as the T_m is dependent on these factors.⁴⁷

Physical strain melting of DNA is far less commonly used and often only used to study mechanical strength of DNA. Orlandini *et al.*⁴⁸ developed a model of what effect physical

strain had on the T_m of DNA. Their simulations implied that indeed the more force applied to DNA the lower the T_m . Danilowicz *et al.*⁴⁹ used DNA tethered to a capillary tube at one end and a magnetic bead on the other to investigate DNA unzipping, which they termed force-induced melting. They found that not only did the DNA melt, but it went under several conformational changes to the structure. The unzipping of the double-strand was discontinuous as a function of time, replicating what occurs *in vitro* between DNA and proteins.⁵⁰ Physical force-induced melting of DNA is impractical and will not be used for this thesis. There are however less complex ways to denature DNA at room temperature.

Other ways to denature DNA in solution at room temperature (or below T_m) include using low salt concentration or chemicals called chaotropic agents. Low salt concentrations result in the negatively charged backbone repelling each other. Schildkraut and Lifson⁵¹ were one of the first to investigate this phenomenon, whereby they found that they could decrease the melting temperature of DNA by ~ 25 °C by simply decreasing the salt concentration (Na^+ or K^+) from 0.60 to 0.01 M. The opposite is also possible as a high salt concentration (4.5 M)⁴⁴ often favours renaturation of the DNA, increasing the T_m , by shielding the negatively charged phosphates on the backbone of the DNA. Lowering the salt concentration decreases the overall T_m due to the repulsive electrostatic forces on each strand.

Alkali conditions, such as 1M NaOH, can also cause DNA to denature due to the increased OH^- ions present decreasing the protons (deprotonation) available on the base pairs and therefore disrupting hydrogen bonding of DNA.⁴⁵ For RNA alkali conditions can be detrimental as it can cause breaking of phosphodiester bonds, effectively destroying the nucleic acid.⁵² Likewise, in acidic conditions DNA can also denature due to depurination, loss of purines forming an abasic site on the DNA, essentially destroying the DNA sequence.⁵³ In order to denature DNA without the need for changing salt concentration, and preserving the DNA, there are chaotropic agents.

Examples of chaotropic agents include cationic surfactants and high concentrations

of guanidinium salt (6 M)^{54,55} and urea (7 M).⁵⁶ Chaotropic agents can work by increasing the entropy of the system by interfering with intramolecular interactions, this can include effects such as repulsive forces between the two duplexed DNA strands. This has led to the development of protocols that use urea (7 M) to analyse and purify ssDNA.^{57,58}

Finally, there are a few chemicals that can help with the renaturation of DNA known as crowding agents but will be referred to as DNA hybridisation rate accelerators in this thesis (see Chapter 5.3.5.1).⁵⁹ Rate accelerators work by crowding the solution and excluding the DNA from the solution, due to excluded-volume effect. This is caused by the impermeability of the rate accelerators, essentially meaning there is less space for the DNA to occupy and so there is a higher probability of two ssDNA encountering and renaturing/hybridising. Amasino⁵⁸ was able to increase the rate at which DNA renatured by adding polyethylene glycol (PEG). PEG was a cheaper alternative to dextran sulphate, the most widely used rate accelerator at the time.^{60,61}

One final aspect that can affect the melting temperature is the formation of mismatches in the dsDNA. Mismatches are non-complementary base-pairing in DNA, which can have devastating effects on dsDNA. The next section will discuss the effect that mismatches can have on the T_m of dsDNA.

1.3.2.1. Mismatches

The longer the dsDNA sequence the more likely there will be the occurrence of mismatches. This is due to the stability associated with longer DNA strands as the more base pairing that is occurring is able to stabilise any mismatches that are present.⁶² In the typical Watson-Crick base paired dsDNA there are eight possible mismatches regardless of which strand each nt is present on. There are the four homo-mismatches: A●A, T●T, C●C and G●G; then the four hetero-mismatches: A●G, A●C, T●C, T●G (where the ● denotes mismatched base pairing). There have been studies that investigated the effect of mismatches on the T_m using the

NN model.^{10,63–69}

Some mismatches have been found to be detrimental to the stability of the dsDNA, while some have been found to be accommodated with no negative effects.^{70,71} Among the most destabilising mismatches are those involving a C residue, which is able to deform the sugar-phosphate backbone of the dsDNA.⁷² SantaLucia and Hicks³⁴ have studied how mismatches affect the stability of the DNA using the *NN* model. They found a trend of $G/C > A/T > G\bullet G > G\bullet T \geq G\bullet A > T\bullet T \geq A\bullet A > T\bullet C \geq A\bullet C \geq C\bullet C$ (where slash denotes complementary base pairing). They found the most and least stable mismatch had a ΔG_{37}° of -2.22 kcal/mol (GGC/CGC) and +2.66 kcal/mol (ACT/TCA), respectively (underlined denotes the mismatched base pair). Mismatches that involve G residues are the most stable, this is due to the incorporation of the mismatch into the backbone without any detrimental effects. On the other hand, mismatches that involved C residue were always destabilised.³⁴ It was also noted that these energies are accurate for any position, that were not the terminal or penultimate, in the dsDNA.

SantaLucia and Hicks³⁴ determined the effect of mismatches at the terminal or penultimate, using the *NN* model. They found that all mismatches at these positions were stabilising. This was attributed to the negligible effect on the backbone or helical structure of the DNA. In fact, if there was a mismatch present at the penultimate position and unhybridised terminal A/T, there was significant stabilisation ranging from -0.21 (AC/TC) to -1.23 (CG/GA) kcal/mol. If the mismatch and unhybridised A/T were at both ends the strand was stabilised by up to -2.5 kcal/mol.

Understanding where these mismatches occur is vital for genotyping techniques, as many rely on the formation of a mismatch being unfavourable and therefore preventing duplexing of the DNA. For more information on mismatches see Demidov *et al.*⁷³ Longer DNA strands are able to overcome negative effects of a single mismatch. Often genotyping techniques rely on a combination of heat and chemicals to allow for fast and accurate DNA analysis. The

next section will discuss how DNA can be modified and detected, and how these methods have allowed for more stringent DNA genotyping.

1.4. DNA modification and detection

This section will discuss ways that DNA can be detected quantified and modified. Synthetic DNA modification, fluorophore coupling and DNA detection using fluorescence spectroscopy will be discussed in detail.

1.4.1. DNA modification

Modification of DNA refers to the introduction of a new functionality to DNA, such as phosphorylation, methylation or amination. These modifications can occur anywhere along a strand of DNA including the middle and terminal ends (3' and 5') and this section will go into detail about how this is achieved.

Natural modifications include phosphorylation and methylation, often important for gene control in cells.^{74 75} There are a long list of non-natural synthetic DNA modifications, such as introduction of a fluorophore,⁷⁶ quencher,⁷⁷ linkers and modified bases.⁷⁸ Synthetic DNA can also allow for the inclusion of non-DNA nts. RNA can be inserted to allow for enzyme digestion, such as uracil-DNA glycosylase (see Section 1.6.3.1). DNA modification is widely used throughout research and companies (e.g., Integrated DNA Technologies, Inc) can synthesise ODNs (short DNA sequences of 5-200 nt) with modifications for relatively low cost.

The most prominent route for ODN synthesis and modification is to use phosphoramidite chemistry, due to its compatibility with solid phase support and automation.⁷⁹⁻⁸¹ This technique allows for sequential addition of nts, which allows for the introduction of a modified nt to be added at any time (as long as it is compatible with the technique). This is very useful for introducing fluorophores and quenchers at desired locations, but also for further post

modification of the synthesised ODNs. An important process is the coupling of an ODN with a desired molecule or immobilisation on a surface.

1.4.2. Oligodeoxynucleotide coupling and surface immobilisation

A prominent method for post modification of DNA is to couple DNA using carbodiimide cross linking chemistry.⁸² Carbodiimide compounds allow for cross linking of molecules with carboxylic acids (-COOH) and primary amine (-NH₂) functionalities. A nt containing either functionality can be introduced into the ODN using the phosphoramidite chemistry approach. Therefore, when deciding what functionality, the DNA should contain it is easier to look at what the ODN will be coupled with. 1-ethyl-3-(3-dimethylaminopropyl)carbodiimide hydrochloride (EDC) and *N,N'*-dicyclohexylcarbodiimide (DCC) are popular carbodiimides, the former allows for cross linking in acidic aqueous solutions and the latter for non-aqueous solutions.^{83,84} The coupling occurs through the activation of the carboxylic acid by reaction with the carbodiimide. This then allows for direct reaction with the primary amine. The final product is a secondary amide that contains none of the carbodiimide cross linker, making it a zero-length carboxyl-to-amine cross linker. *N*-hydroxysuccinimide (NHS) has been found to increase the yield of the EDC reaction and is often used for the immobilisation of ODNs to surfaces.⁸⁴ Many commercial products are available with pre-coupled NHS on the surface that allow for the immobilisation of amine functionalised ODNs in a one step process.⁸⁵ Coupling also allows for functionalisation of ODNs for PCR processes. Fluorophores can be introduced into longer DNA sequences that cannot be synthesised cheaply.

1.4.3. Fluorophores

Fluorophores are chromophores that contain cyclic ring structures. Fluorophores can be excited by a specific wavelength of light and then emit a different wavelength of light. These are very useful for detecting DNA as it allows for multiple fluorophores to be used at once.

Capillary electrophoresis with real time DNA sequencing using fluorophore detection has been used as early as 1989 by Hunkapiller *et al.*,⁸⁵ An example of this is for DNA fingerprinting where four different fluorophores are used to detect PCR products in the same solution. This is achieved by using capillary electrophoresis to separate PCR products based on size and then any size overlaps are separated based on the fluorophore attached.⁸⁶ Woolley and Mathies⁸⁷ were able to take this one step further by fabricating a microfabricated electrophoresis chip that allowed for high-speed, high-throughput DNA sequencing. However, a drawback to using fluorophores is the requirement that DNA be modified, or ODNs need to be synthesised with the fluorophores. An alternative to fluorophore attachment is to use intercalators that allow for DNA visualisation (see Section 1.4.6).

1.4.4. Fluorescence quenching

Fluorescence quenching is the process through which a fluorophore's intensity is decreased. This is usually done by the addition of a quenching molecule that is able to interact with the fluorophore. Quenching is very useful for studying DNA as it can be detected in sub μM quantities, and both quencher and fluorophore can easily be incorporated into DNA strands.⁸⁸ Usually the quenching effect is used to detect hybridisation or melting of DNA as the intensity increases or decreases depending on whether the DNA is double-stranded or single-stranded. The fluorophores are also compatible with processes such as PCR or enzyme digestions. Two main types of quenching exist with two different quenching mechanisms. The first is the more traditional type called dynamic quenching (Fig. 1.5 (a)), or more commonly known as Förster resonance electron transfer (FRET) The second type is static or contact quenching (Fig. 1.5 (b)), also known as Stern-Volmer quenching.⁸⁹ Both have their advantages and disadvantages, and often both can occur in a single reaction. The following sections discuss each in more detail.

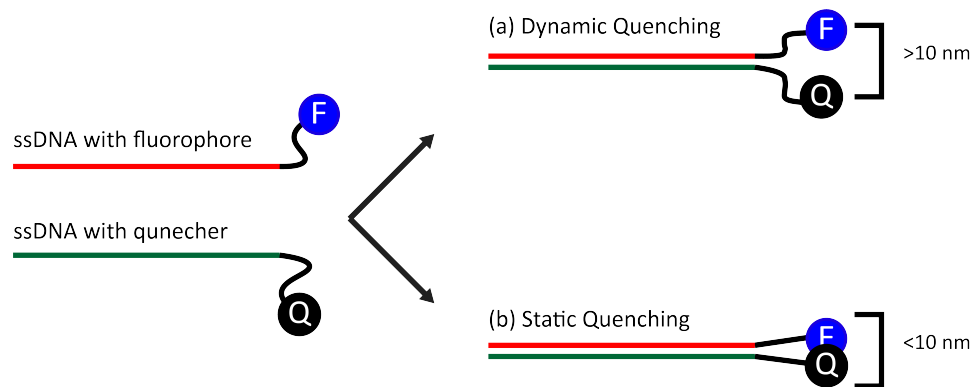


Figure 1.5: Comparison of (a) dynamic and (b) static quenching.

1.4.4.1. Dynamic quenching

Dynamic quenching (or FRET) is the most used and studied form of quenching. Dynamic refers to the fact that the quencher and fluorophore do not have to be locked in place through dimerisation for quenching to occur. The important aspect for dynamic quenching is the overlapping of the emission band of the donor (fluorophore) and the absorption band of the acceptor (quencher), with the efficiency of the quenching being reliant on the degree of overlapping of the bands.⁹⁰ The distance that FRET is effective is usually 20-100 Å, with a fall off of $1/R^6$.⁹¹ This distance can be typically calculated using the equation:

$$E_{FRET} = \frac{R_0^6}{R_0^6 + r^6} \quad (1.3)$$

Where E_{FRET} is the efficiency of energy transfer, R_0 is the Förster radius (50% transfer efficiency between donor/acceptor), and r is the radius between the donor/acceptor.⁹⁰

Examples of dynamic quenchers include, 5-carboxytetramethylrhodamine (TAMRA), carboxyfluorescein (FAM), carboxy-2',4,4',5,7,7'-hexachlorofluorescein (HEX) and 6-carboxy-2',4,7,7'-tetrachlorofluorescein (TET).

1.4.4.2. Static quenching

Static quenching, also known as contact or Stern-Volmer quenching, is very similar to dynamic quenching and often plays a part in it.⁸⁹ Where dynamic quenching can occur over a distance, static quenching refers to the formation of a dimer complex between the donor fluorophore and the acceptor quencher.⁷⁷ Hydrophobic interactions drive the dimerisation process and allow for the transfer of electrons and therefore prevents the fluorophore from emitting any light. Unlike dynamic quenching, that relies on the overlap of the emission band of the donor and the absorption band of the acceptor, static quenching occurs when the absorption bands of both donor and acceptor overlap. The intensity of the quenching effect does not rely on the amount of overlap. As a result, strong quenching can occur even if there is only a slight overlap of bands. Examples of static quenchers include Black hole quencher (BHQ) and 2,2',6,6'-tetramethyl-piperidine-*N*-oxyl (TEMPO).⁹¹

There is often a lot of overlap between static and dynamic quenchers as most quenchers undergo both forms of quenching, where quenching is reliant on which fluorophore quencher combination as well as the physical distance that separates the two.

1.4.5. The effect of fluorophores on DNA stability

DNA hybridisation is dependent on many factors such as temperature, T_m of the sequence, and whether there are stabilising and/or destabilising molecules in the environment. This section will mainly focus on how intercalators and fluorophores affect the stability of the DNA duplex. These affects include stabilisation and destabilisation and how the T_m is affected.

Bower *et al.*⁹² reported that dsDNA was stabilised when there were additional phosphates on the 5' terminal ends of the DNA, i.e., increased T_m . Whereas any on the 3' had negligible effects. They determined that addition of 5' phosphates stabilised dsDNA by about -0.5 to -0.6 kJ/mol. This has led to studies about whether or not fluorophores and quenchers

have effects on the T_m of DNA.

Morrison and Stols⁷⁶ found that the fluorophore-fluorophore and fluorophore-DNA interaction had a large effect on the stability of the hybridisation. This work was extended by Marras *et al.*⁷⁷ where it was found that it was possible to increase the T_m of a 20 bp duplex by 2-10 °C depending on the dye. In summary, it was found that the nature of the DNA stabilisation and destabilisation was dependent on the fluorophore and quencher used.

Moreira *et al.*⁹³ expanded on this by investigating the effects of additional dyes, quenchers and linkers. They first studied several fluorophores and quenchers (mentioned as modifiers) attached to DNA to determine the effect on the T_m , these include CY5, FAM and BHQ (which are relevant to this thesis). By looking at the melting profiles they found that several modifiers were able to increase (BHQ, Cy3 and Cy5), decrease (TAMRA and Texas Red) or have no effect (FAM and HEX) on the T_m of a DNA sequence. Fig. 1.6 shows how much more stable DNA containing a BHQ (Fig. 1.6, dashed line) or CY5 + BHQ (Fig. 1.6, dotted line) are compared to unmodified DNA (Fig. 1.6, solid line). Moreira *et al.*⁹³ found that the stability could be increased by 1.8 Kcal/mol, and even increased the T_m by up to 4.3 °C. They attributed this to the same effect that the addition of a 5' phosphate group has on the T_m of DNA. They then investigated the effect of linker length, such as amino C3, amino C6, hydroxy C3 and triethyleneglycol, between the DNA and fluorophore. They determined that the linker length had a small effect on the T_m of dsDNA. For dyes that were stabilising (Cy3) the addition of a C3 linker decreased the T_m from 71.7 °C to 71.1 °C (-0.6 °C) and adding a triethyleneglycol decreased the T_m from 71.7 °C to 70.7 °C (-1.0 °C). For destabilising dye FAM, the linker further exacerbated the destabilising effect with a decrease from 70.2 °C to 69.6 °C (-0.6 °C), which was 0.7 °C lower than the unmodified dsDNA. Therefore, it is important to take note of how far away the dye is from the DNA itself. Longer linkers seem to have negative effects on the T_m .

Mergny^{94,95} investigated how fluorophores affected DNA structures that were not a

Figure removed due to copyright

Figure 1.6: UV melting profiles of probe: target duplexes. Solid line: unmodified probe. Dashed line: 5' BHQ2 probe with 3' Black Hole quencher. Dotted line: 5' Cy5 dye and Iowa 3' Black Red Quencher.⁹³

double helix. They determined that fluorophores could destabilise structures other than double helices, with i-motifs and G4s (see Section 1.5.3.3 and 1.5.3.4 for detailed explanation) being destabilised by 1 to 11 °C. The affect that dyes, quenchers and linkers have on DNA is vital to consider when using DNA as a static structure or for a dynamic process. The next section will discuss in detail the diverse types of DNA structures and applications.

1.4.6. Intercalators

Intercalators have been used for many years to visualise and characterise DNA. For DNA visualisation intercalators are primarily used in agarose⁹⁶ or PAGE.⁹⁷ For DNA characterisation flow cytometry,⁹⁸ biochips⁹⁹ and PCR¹⁰⁰ applications have been used, in conjunction with intercalators. This has also allowed for the study of enzyme activity (DNase, telomerase, etc.),^{101–103} and they have potential to increase genotyping accuracy and reliability, a topic of this thesis.

Intercalators are heterocyclic molecules that are able to slip between the base pairs of dsDNA or interact with the negative charge on the backbone (dsDNA and ssDNA), resulting in a fluorescent product that can be used as a reporter dye for DNA analysis.^{104,105} Another effect that intercalators have, is to affect the structure and stability of DNA. This can be helpful for elucidating biological functions such as DNA synthesis,¹⁰⁶ gene transcription¹⁰⁷ and translation,¹⁰⁸ and also prevent tumour^{109–111} and viral¹¹² incidences. Intercalators have been used to study the mechanisms of enzymes such as helicase or translocase; both enzymes that affect the structure of DNA.^{113,114} The high affinity intercalators have for DNA can often have fatal effects on biological systems.¹¹⁵

The effect of an intercalator depends on the type of intercalator used. The two types are mono- and bis-intercalators, where a bis-intercalator is usually a homodimer of a mono-intercalator. Mono-intercalators, such as [(3,8-diamino-5-ethyl-6-phenyl phenanthridinium-bromide)] (ethidium bromide),^{103,116,117} acridine orange [3,6-bis(dimethyl)acridiniumchloride

hemi(zinc chloride salt)]¹¹⁰ and YO-PRO® are able to intercalate between two bps.^{118,119} Whereas the bis-intercalator contains two intercalating groups such as bis-ethidium bromide and YOYO®, which are able to intercalate between four bps.¹¹¹

Bis-intercalators have been looked at closely as possible anti-cancer drugs due to high biological activity. This thesis will only focus on ethidium bromide as a means of affecting the structure of DNA. Ethidium bromide effects are predominantly physical and affect the stability, shape and length of the DNA, allowing for hybridisation methods such as DNA origami and others to become more efficient and specific.^{102,109,111,120}

There have been several studies of how intercalators can cause strain on the DNA double helix.^{106,121,122} These studies have found that certain dyes that contain cyanine are able to lengthen DNA without affecting the rigidity.^{123–127} Ughetto *et al.*¹²⁸ and Wang *et al.*¹²⁹ found that the lengthening of the DNA can be as drastic as 3.9 Å – 6.8 Å, which is more than a single base pair adds (in B-form DNA). Gunther *et al.*,¹²⁵ determined that the intercalation of YOYO® was able to increase the length of DNA by almost double. Intercalators are limited to no more than one intercalator per two bps due to the neighbour exclusion principle.^{130,131} The use of an intercalator can be useful for using strain to affect the T_m of dsDNA.

The next section will focus on ethidium bromide as it is relevant to work done in this thesis and it is vital to understand the effects of it can have on DNA.

1.4.6.1. Ethidium bromide

Ethidium bromide is a very well-known and studied cationic intercalator, that has mainly been used as a reporter molecule for agarose gel electrophoresis. However, in recent years it has been studied for its structural effects on DNA.^{116,132–134} The main mode for intercalation of ethidium bromide is to insert itself between base pairs of dsDNA and become fluorescent like most other intercalators.¹³⁵ Therefore it is highly specific for dsDNA and not ssDNA. The intercalation is favoured due to the base stacking, or π -stacking, with the base pairs

and the electrostatic complementation. The positive charge on the ethidium bromide mediates an attractive electrostatic effect with the DNA.^{136–140} Nafisi *et al.*¹³² studied the stabilities of DNA when intercalated with three intercalators (acridine orange, methylene blue and ethidium bromide) and found ethidium bromide had the highest binding constant and the lowest dissociation equilibrium constant of $K_{EB} = 6.58 \times 10^4 \text{ M}^{-1}$ and $K_d = 15 \text{ }\mu\text{M}$, respectively. This was attributed to the greater accessibility of ethidium bromide to the DNA, compared to the other two investigated.

Large three-dimensional (3D) DNA structures, known as DNA origami (see Section 1.7) have a wide range of possible conformations. The only way to control the structure formed is by controlling the folding conditions. Ke *et al.*¹⁴¹ explored two methods that would allow finer control over the folding of the DNA origami structures. The first method was by adding in a single nucleotide that would allow for increased bending at points where there were crossovers, where DNA strands share a junction point and crossover, reducing static repulsion and increasing stability.^{142,143} The second method was the addition of an intercalator that was able to reduce the torsional strain caused by the added nucleotide. Greschner *et al.*¹²⁰ went on to explore ethidium bromide as a molecular chaperone to force a 3D DNA structure into the lowest energy conformation. They found that ethidium bromide was able to successfully influence the hybridisation of the DNA into the most stable conformation, a ninja star, as opposed to any other structure. This was noted to be due to the π -interactions of the aromatic stacking between the base pairs of the DNA as well as the expanding and unwinding of the double helix. They had found that the intercalation of the ethidium bromide prevented high energy structures from forming. The ethidium bromide was also easily removed and because of no additional folding steps the structures were not altered. This work showed that the intercalation of ethidium bromide, and possibly other intercalators, created high energy barriers when the DNA was folding, due to strain. This analysis was in line with other studies from Bjorndal *et al.*¹⁴⁴ who found that the T_m was affected by the presence of intercalators such as YO-PRO®.

1.5. Structural and dynamic DNA

DNA is primarily described in two ways: static and dynamic, with both being used in a variety of DNA applications. Static DNA is structural DNA that once assembled does not contain moving parts nor undergoes further change. Dynamic DNA often undergoes a structural change or reaction that results in a changed final product. These are not exclusive as there are many applications that use both types of DNA. This section we will discuss both types, with an emphasis on one example of each, G4s (static) and toehold-mediated strand displacement (dynamic).

1.5.1. DNA assembly/disassembly

The formation of DNA nanostructures can be controlled by the DNA sequence, environment and renaturation conditions. Researchers have taken advantage of DNA's ability to self-assemble and have engineered it to perform a range of tasks, such as molecular recognition,¹⁴⁵ structural assemblies¹⁴⁶ and DNA genotyping.^{147,148} Examples of DNA engineered to perform tasks include DNA aptamers (see Section 1.5.3.7), DNazymes and DNA origami (to be discussed in more detail in the following). SsDNA is difficult to study as it often prefers to form secondary structures to become more stable in the absence of a complementary strand, especially in longer sequences (~ 50 nt).¹⁴⁹ This section will discuss all structures of DNA that are not the double-helix as well as large 3D structures that can be assembled.

1.5.2. DNA origami

DNA origami will be briefly discussed as it is important to understand the how DNA structures are designed to form larger macrostructures. DNA origami consists of short single ODN staple strands, beginning at six and ranging to hundreds of nts, that hybridise to a larger ssDNA scaffold molecule (usually extracted from bacteriophages). The scaffold can range from

lengths of 700 – 7000 nts long to form a large nanostructure.^{147,150} Using specialised software, such as CADNANO®, it is possible to design a range of two-dimensional (2D) and 3D structures. Fig. 1.7 (left) shows a static half sphere, full sphere and oblong sphere designed by Han *et al.*¹⁵¹ and Fig 1.7 (right) shows a DNA origami device that mimics macroscopic machinery designed by Marras *et al.*¹⁵² DNA origami structures can be used in applications such drug delivery,¹⁵³ single molecule detection¹⁵⁴ and templates for nanoparticle (NP)¹⁵⁵ or proteins.¹⁵⁶ Functionality can be introduced into a DNA origami structure through incorporation of G4s, i-motifs and hairpins or through modification of the staple strands (see review¹⁵⁷). DNA origami structures that change shape or are able to perform dynamic functions will be discussed in Section 1.6.

Figure removed due to copyright

Figure 1.7: Literature examples of static (left) designed by Han *et al.*¹⁵¹ and dynamic DNA (right) designed by Marras *et al.*¹⁵².

1.5.3. Static structural DNA

Controlling and manipulating DNA on the nanoscale has led to advancements in DNA research that allow for researchers to design complex DNA systems. The most basic DNA structure is the double helix, mentioned earlier, however there exists several other possible non-canonical DNA structures. These structures are possible due to a combination of canonical Watson-Crick bonds and Hoogsteen bonds (non-canonical)(see Fig1.8). Hoogsteen bonds are an alternative base pairing that occur when the purine base is rotated 180° around

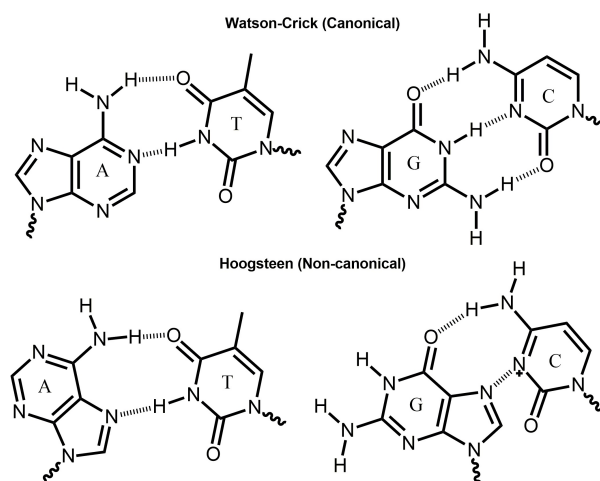


Figure 1.8: Comparison of Watson-Crick (Canonical) and Hoogsteen (Non-canonical) base pairing.

the glycosidic bond. This changes the binding conformation of the purine from an *anti* to a *syn* conformation.¹⁵⁸ The alternative structures include triple helices,¹⁵⁹ hairpin (also known as stem) loops,^{160,161} i-motifs and G4s.¹⁶² For this thesis G4s will be a main focus and so will be explained in more detail in Section 1.5.3.4 However, this section will briefly discuss several other possible structures, as it is vital for understanding how to control nucleic acids on a nanoscale.

1.5.3.1. Triple helix DNA

Triple helices, or triple helix DNA, occur when there are three strands of DNA that are bound together and require very specialised conditions in order to form. Whereby, a purine rich ssDNA hybridises to a dsDNA in the major groove through pyrimidine-purine-pyrimidine bonds.¹⁶³ In this case the dsDNA, with already formed Watson-Crick base pairs, hybridises through newly created Hoogsteen bonds with the third strand. This is made possible by the recognition of T to A/T pairs and protonated C⁺ to C/G pairs. The resulting triple helix was the basis for many of the first hypothesised structures of DNA before Watson and Crick.^{1,164,165} But, it wasn't until the late 80's that this structure was demonstrated, named the triple helix forming oligonucleotide.^{159,166} This structure has been implicated in gene regulation (i.e., c-

myc promotor).¹⁶⁷ When the triple helix is formed, the pyrimidine strand (5' → 3') is parallel to the purine (5' → 3') and anti-parallel to the already duplexed pyrimidine strand (3' → 5'). The C⁺ blocks Watson-Crick bonds from forming and stabilises the formation of Hoogsteen bonds by an electrostatic interaction.¹⁶⁸

1.5.3.2. Hairpin loops

Hairpin loops occur when nucleic acids have palindromic regions, where one single-stranded nucleic acid has undergone intra-strand hybridisation (also known as intramolecular).¹⁶⁹ A hairpin is made up of two parts, the stem and the loop. The stem contains the palindromic regions and the loop is made up of unpaired nts that link to the two palindromic sequences. The hybridised stem sections undergo conical Watson-Crick base pairing and form a double helix. Hairpins occur in many biological pathways such as DNA replication,¹⁷⁰ repair¹⁷¹ and transcription.¹⁷²

1.5.3.3. iMotif

i-Motifs are C-rich DNA sequences that are capable of forming an intramolecular structure, made up of intercalating hemi-protonated cytosine•cytosine⁺ base pairs (C•C⁺).^{173,174} The name refers the fact that the base pairing is intercalated. i-Motifs are formed under slightly acidic conditions and stabilised through three hydrogen bonds between each base pair.¹⁷⁵ This structure can consist of 1-4 strands and has been found to be naturally occurring in genomic DNA.^{176–178}

1.5.3.4. G-quadruplex

German chemist I. Bang¹⁷⁹ observed that high millimolar concentrations of guanylic acid formed a gel. It was later discovered through X-ray diffraction data that a tetrameric structure was assembled that gave aqueous solutions gel characteristics.¹⁸⁰ This same phenomenon

was observed in G-rich regions on DNA sequences that contained two or more runs of guanine mono-phosphate tracts (G-tract). One or more strands that have G-tracts can fold into a G4 structure through Hoogsteen bonds (non-canonical). This is achieved first by four guanine monophosphates (Gs) forming a square planar G-tetrad (Fig. 1.9 (a)). Fig. 1.9 (a) also shows how the G-tracts are stabilised by the presence of a cation (see Section 1.5.3.5). These G-tetrads are able to further stack with stabilisation from the monovalent cation (Fig. 1.9 (b), blue).

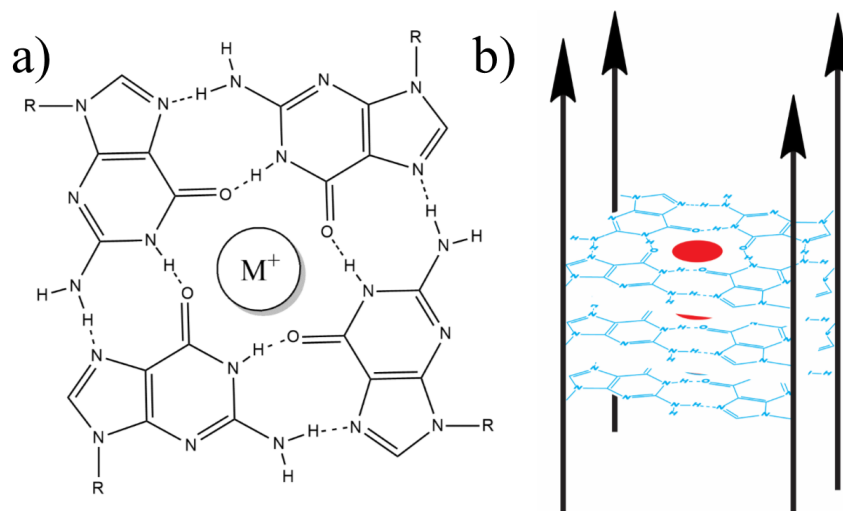


Figure 1.9: (a) Structure of a G-tetrad made up of four guanines with stabilisation by a monovalent cation and (b) G-quadruplex made up of 4 ssDNA (black arrows) stabilised by a monovalent cation, where the arrows indicate 5' to 3' directionality.

There are two types of G4 with two different structures that are possible from any G4 sequence. The first type is intramolecular, a G4 that is made up entirely by one strand of DNA, the second is intermolecular, a G4 made up of two or more strands of DNA. G4 structures are often determined using techniques such as single crystal diffraction,¹⁸¹ nuclear magnetic resonance(NMR) spectroscopy¹⁸², electrophoresis gel shift assay¹⁸³ and circular dichroism(CD).¹⁸⁴

There are three G4 orientations that are possible, these include parallel, antiparallel and hybrid of the two. Parallel is when all the directionality (5' to 3') of the nucleic acid runs in the same direction. Fig. 1.10 (a-c) illustrates how parallel intermolecular and intramolecular G4s are able to fold. The loop regions, regions of non-G residues that link the G-tracts (Fig.

1.10 green), are bent in a way that they laterally cross the G-trad and has been found more likely to form when in the presence of a co-factor, such as hemin (see Section 1.5.3.7).¹⁸⁴ Antiparallel is when all the directionality alternates between strands, often occurring in bimolecular G4s. Fig 1.10 (d-f) illustrates how antiparallel intermolecular and intramolecular G4s are able to fold. Unlike parallel, the loop regions do in fact form a loop on the top and bottom of the G-tetrads. If both parallel and antiparallel structures exist in the same solution it is regarded as a mixture and if a G4 contains 3 parallel and 1 antiparallel (or *vice versa*) this is described as a hybrid.¹⁸⁴ Wu *et al.*¹⁸⁵ showed that proteins, such as thioflavin T, were able to switch G4 structures between the two different hybrids (3 parallel + 1 antiparallel into 1 parallel + 3 antiparallel).

There is no way however to predict exactly what conformation a G-rich ODN will take. This is due to being possible for any one sequence to form one or both orientations (mixture) depending on the buffer conditions. Hazel *et al.*¹⁸⁶ used predicative modelling and NMR spectroscopy to determine rigidity of the loop regions. They found that short loop regions (≥ 2) restricted the flexibility of G4, and that although the sequence was important it played less of a role in flexibility. They also concluded that although some simulations were in agreement with NMR data, it was not possible to predict if the G4 was parallel or antiparallel.

An intramolecular G4 is made up of four distinct regions, that include the terminal ends (5' and 3'), loops and G-tracts. The loop regions, consisting of nts that are not G, are required to allow for the folding of the nucleic acid in onto itself. If the G4 does not contain 3 loop regions, and therefore 4 distinct G-tracts, then only an intermolecular G4 is possible. However, this does not mean that a sequence with 4 distinct G-tracts will exclusively form an intramolecular structure as both structures are possible.

Naturally occurring G4s have been of great interest to researchers as drug targets.¹⁸⁸⁻¹⁹⁶ Neidle *et al.*,¹⁹⁴ von Zglinicki *et al.*¹⁹¹ and Hurley *et al.*¹⁹⁶ have all tried to investigate ways of targeting these naturally occurring G4s, known as telomeres, using anti-cancer drugs. Telomeres found on the ends of chromosomes contain sequence repeats that have been discovered to

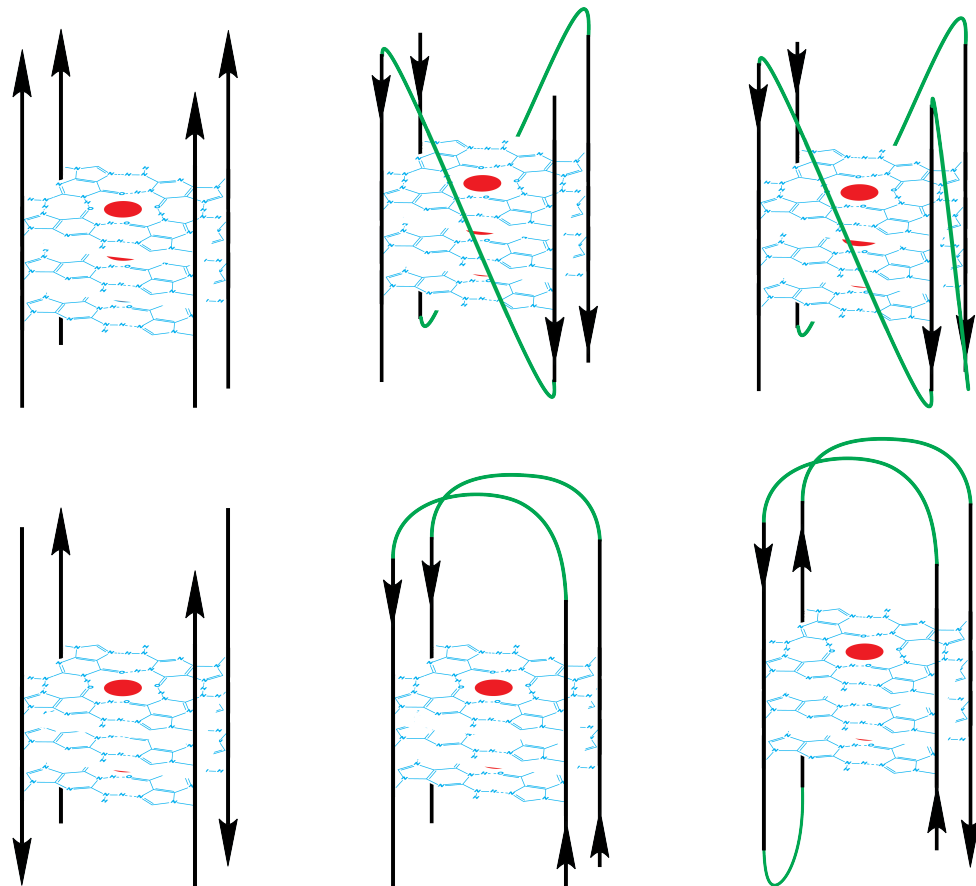


Figure 1.10: Diverse types of G4s: (a) intermolecular parallel (tetramolecular), (b) intermolecular parallel (bimolecular), (c) intramolecular parallel (unimolecular), (d) intermolecular antiparallel, (e) intermolecular antiparallel (bimolecular) and (f) intramolecular antiparallel (unimolecular). Adapted from J. L. Huppert¹⁸⁷

form G4s. These telomeric regions have been found to be highly preserved across all organisms, with vertebrates having the repeat TTAGGG and plants having TTTAGGG.¹⁹⁷ Naturally occurring G4s, outside of telomeres, have been found to control gene expression by affecting enzymes involved in DNA replication and transcription.¹⁹⁸ Piazza *et al.*¹⁹⁹ found that in genomic DNA the length of the loop regions were a way to help regulate gene diversity. There have been many G4 studies both, *in vitro* and *in vivo*, that look at why these structures are important. This thesis however will only focus on *in vitro* investigations.

1.5.3.5. Cation and polymeric stabilisation of G4 structures

G4s have been found to be more thermodynamically stable than dsDNA and as a result slower to unfold than DNA or RNA hairpins.²⁰⁰ It has been shown that G4s are stabilised by cations, usually monovalent, by complexing between the G-tetrads. The most common cations used are Group 1 metals with a stability order of $K^+ > Na^+ > Li^+$.^{201,202} The Li^+ ion was thought to destabilise G4s, however Bhattacharyya *et al.*²⁰³ determined that it neither stabilised nor destabilised G4s. But in fact, played a neutral role. This is helpful as Li^+ ions are often used as a control when studying the G4 structures. K^+ ions are by far the most used cation for G4 stabilisation by researchers, due to its strong electrostatic interaction and lower dehydration energy than other cations.^{182,204–208} Other stabilising agents used include quartet inducers, which do not stabilise but do encourage the G4 structure formation, such as polymers (PEG) or large heterocyclic structures.²⁰⁹ For destabilisation of G4s divalent cations such as Co^{2+} , Mn^{2+} and Mg^{2+} often used.²¹⁰ Blume *et al.*²¹¹ determined that the effect of divalent cations was similar to that of Li^+ ions, whereby the size of the van der Waals radii of the divalent cations is too small to sufficiently stabilise the G4. Co^{2+} , Mn^{2+} and Mg^{2+} ions have van der Waals radii of 1.64, 1.66 and 1.96 ρm , respectively, which is comparable to Li^+ which has a van der Waals radius of 2.32 ρm .²¹² They also noted that the divalent cations compete with K^+ ions and therefore destabilise already formed G4s. Once a G4 had been folded or unfolded it is important to determine the structure using well understood characterisation techniques. In this thesis CD spectroscopy and PAGE were employed and are discussed in more detail in the following section.

1.5.3.6. Circular dichroism spectroscopy and polyacrylamide gel electrophoresis analysis of G4s.

CD spectroscopy is often used to determine what type of structure(s) have formed based on the absorption of light and PAGE can be used to determine if the structures are inter-

or intra-molecular based on molecular mass of the structure. CD spectroscopy is used to study how chiral molecules interact with light. Most often used in biological studies of DNA and protein structures, which change conformation based on the environment (e.g., pH, heat and salt concentration).²¹³ CD is defined by how a chiral molecule absorbs left circularly polarised light (L-CPL) and right circularly polarised light (R-CPL) to different extents at different wavelengths. It is more specifically referred to as the difference between the amount of L-CPL and R-CPL as a function of wavelength.²¹⁴ This allows for the elucidation of simple and complex structures, and for this thesis, specifically which conformation the G4s exist in based on sequence alone. Hardin *et al.*²⁰¹ were some of the first researchers to investigate how telomeric DNA G4s folded in the presence of monovalent cations using CD. They found that the chiral environments of the bases were not the same once folded into a G4 structure, essentially determining that the structure was hairpin like. It has since been shown that it is possible to determine the structure of the G4 based on where positive and negative ellipticity peaks occur on a CD spectrum. Parallel G4 have a distinctive positive maximum *ca.* 264 nm and a negative minimum *ca.* 240 nm.¹⁸⁴ Whereas, antiparallel G4 have a distinctive positive maximum *ca.* 295 nm and a negative minimum *ca.* 260 nm.¹⁸⁴ A mixed, or hybrid, G4 will have peaks at 260 nm and 295 nm. Paramasivan *et al.*¹⁹⁷ used CD spectroscopy to investigate what affect the concentration of the stabilising cation had on the structure of the G4s. They determined that different salts (i.e., Na⁺ and K⁺) were able to induce different structures. Indicating that buffer conditions were important for experimental design. By changing which cations are present determines which G4 structures are formed (see Section 1.5.3.4). A substantial portion of the literature reviewed in this thesis used K⁺ ions as a G4 stabiliser. This thesis will be exclusively using K⁺ ions as a G4 stabiliser due to its availability and biological compatibility.

1.5.3.7. Aptameric G4 structures

Aptamers are a generic term used for 3D structures made up of single-stranded nucleic acid ligands that are able to recognise and complex target molecules. Aptamers can have

high selectivity, being able to distinguish different enantiomers or functional groups.²¹⁵ Aptamers can simply bind a target, but others can mimic enzymes (biological catalysts) and perform reactions. Aptameric G4s are able to recognise and bind target molecules specifically, and with high affinity. These targets can include ions, organic compounds and biologically relevant targets.²¹⁶⁻²¹⁸ Certain G4s are able to complex with co-factors to form DNAzymes, such as the peroxidase-mimicking structure (see Section 1.5.3.10).

The advantage that aptamers have over other biological ligands, such as antibodies (the gold standard biological ligand) is the reversible denature and renaturing that they can undergo without loss of function.²¹⁹ This makes them a viable replacement for common antibody techniques such as enzyme-linked immunosorbent assay (ELISA) (see Section 1.7.5).²¹⁹ It has been shown that there exist aptamers that have higher affinity for targets than antibody equivalents, such as the aptamer MT32 protein of Apple Stem Pitting Virus (ASPV) with an affinity of 54 nM compared to the antibody MT32 protein with an affinity of 290 nM.²²⁰ The aptamer MT32 also showed exceptional specificity, being able to distinguish the ASPV from other virus that often co-infect. This shows great promise for aptamers as an alternative to using antibodies. Aptamers are also showing great promise as an alternative to therapies due to being almost invisible to immune systems inside of a biological organism.²²¹ One of the first therapeutic aptamers was used to treat neovascular age-related macular degeneration, which was approved by the US Food and Drug administration in 2004.²²²

Discovering aptamers for these purposes can be extremely difficult as there is no way to know if a nucleic acid sequence is an aptamer for a target without *in vitro* testing and even then, it can take a large amount of testing to find sequences with high affinity for the target of interest. The next section will discuss two methods that are used to find aptamer sequences *in-vitro* and then optimise the aptamer *in silico*.

1.5.3.8. Systematic evolution of ligands by exponential enrichment and genetic algorithm

There are several ways developed that allow for the investigation and identification of aptamers that can recognise and bind proteins or small molecules. Some of the first ways of identifying G4 aptamers were computer simulation tools or immune-assays, however these have drawbacks that are not easy to overcome. Computer simulation tools require that a pattern for DNA-target recognition already be known and the immune-assay methods are limited to proteins that are well understood.^{223,224} This section describes two common techniques that can be used in combination for determining aptamer sequences with desirable traits, such as increased binding affinity or increased DNase activity.^{224,225} The first method is known as systematic evolution of ligands by exponential enrichment (SELEX) and the second is a genetic algorithm (GA). Both have been used in tandem to design G4 sequences that are able to bind to a specific target of interest.²¹⁵

SELEX is an *in vitro* selection method that is used to find sequences that can bind to a specific target.^{146,225,226} The first steps of SELEX are to synthesise a library of random ODN sequences, often taking sequences that are found in the genomes of organisms. The library used can consist of up to 10^{14} sequences, however for G4 aptamer discovery this library can be limited to sequences that are G-rich. The first step is to expose the target molecule of interest to the sequences to determine which have the best affinity. This is done by removing non-binding targets through affinity chromatography.²²⁴ PCR is then used to amplify all the sequences that are bound to the target molecule and this is then repeated multiple times with more and more stringent conditions until those sequences with the tightest binding affinity are identified. Once the aptamer sequences have been discovered and published they are then used to make up a large combinatorial aptamer library. Pfeiffer *et al.*²²⁷ recently took this one step further and developed a method that allowed for using SELEX to discover nucleobase-modified aptamers. Using click chemistry they were able to introduce new functionality into a ssDNA sequence and then used SELEX to determine binding affinity. This shows that SELEX is a robust process

that has a lot of potential use in biosensing applications.

A Genetic Algorithm GA is an *in – silico* technique that is used to mimic evolution. Whereby, new generations only retain characteristics that help for specific purposes, such as increased binding affinity of target molecules. GAs are often used to increase the binding affinity or activity of aptamers found using SELEX.²¹⁵ The purpose of this is to mirror the process of natural selection, where useful traits, or information, are passed down through generations. GAs are a multi-step process that, much like SELEX, is repeated several times. The first step is generating new sequences from known sequences with the desirable trait. These sequences are known as parent sequences. New sequences are then generated through a three step process, shuffle, mutation and synthesis.²¹⁵ Shuffling of the sequence is carried out by breaking G4 aptamer sequences up into groups: 2 terminal ends (5' and 3') and 3 separate loop regions that occur between the G-tracts. G-tract regions are the only regions to not change, the other 5 groups are shuffled within each group to produce a desired amount of new sequences. If starting from a small number of parent sequences (i.e., 2) there is a high probability to make the same sequence twice, particularly when trying to investigate many sequences at once (i.e., >10). Therefore, each sequence is then mutated at only one position (not in the G-tract region) and synthesised to be tested for the desired property.²¹⁵ Unlike SELEX, however, it is possible to retain regions of the sequence that are useful. For example, if a loop region that contains the sequence AAA is found to increase binding to target molecules there is a good chance that this region will be retained multiple times throughout the GA process. Ikebukuro *et al*,²²⁸ used a GA to improve a peptide that was able to inhibit trypsin. They then went on to use this in 2005 to design a GA that was able to improve G4 aptamers for thrombin inhibition. This thesis uses the modified GA by Ikebukuro's group.²²⁸

1.5.3.9. G4 interactions with organic molecules, proteins and co-factors

G4s have been found to interact with organic molecules in a variety of ways, ranging from increased reactivity to increased/decreased fluorescence. For example, G4s have been

shown to bind with fluorescent structures, such as *N*-methyl mesoporphyrin IX (NMM) and function by either turning on or off fluorescence.^{111,229,230} Lu *et al.*²³¹ found that benzothiazole-substituted benzofuroquinolinium dye could selectively bind to G4s, showing a remarkable enhancement of the fluorescence.

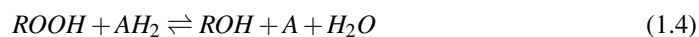
Certain proteins are capable of driving the folding of G4s such as Oxytricha, which allows for the stable formation of quartets,²³² and RAP1 (a small GTPase protein), which is capable of forcing G4s into parallel structures in the presence of K⁺ ions.²³³ Both proteins are classified as telomeric binding proteins. Certain proteins are able to recognise and cleave proximal to the G4, or resolve (unfold) its structure, all showing that G4s are important in natural DNA.²³⁴⁻²³⁸

Furthermore, it has been established that G4s have the ability to inhibit telomeric enzymes that extend DNA.²³⁹ Zahler *et al.*²⁴⁰ showed that the formation of telomeric G4s in the presence of K⁺ ions prevented linear telomere extension. Bryan *et al.*²⁴¹ investigated how G4s interacted with proteins to elucidate the roles that DNA structures played in gene regulation. They discovered that it was the intra-molecular G4s that inhibited telomerase from extending DNA. This was not observed when the G4s were inter-molecular. Therefore, when studying the interaction of G4s with proteins it is very important to understand what structures are present as heterogeneous mixtures of structures will result in different protein interactions.²⁴²

Another route of G4 research has been to identify G4 aptamers, where the DNA recognises the protein, for inhibiting or increasing enzyme activity. A very useful protein binding G4 has been the thrombin aptamer.^{243,244} The G4 thrombin aptamer has been found to inhibit the formation of fibrin clots, this is due to the fibrogen binding site recognising and tightly binding the loop regions of an antiparallel G4.²⁴⁵ On the other hand G4s have been found to increase the activity of co-factors such as porphyrins.^{162,184,246} This thesis will focus on one type of porphyrin, hemin, and its peroxidase-mimicking activity as it has been shown to have many possible applications for biosensors.²⁴⁷

1.5.3.10. Peroxidase-mimicking activity of G4/hemin aptamer

Peroxidases are a class of enzymes that can catalyse the oxidation of compounds. This is done at the expense of peroxide, according to the following scheme:



Hemin, the oxidised version of heme, is a co-factor of peroxidases and has been found to have very low peroxidase activity. The peroxidase activity of hemin is further hindered by the propensity to form dimers or trimers and the fact that oxidation of peroxide can destroy it. Sen *et al.*^{248,225} were the first to report a hemin (along with two other porphyrins) binding aptameric G4 sequence. They determined that the rate of peroxidase-mimicking activity was increased due to the G4s forming a DNAzyme, a DNA sequence with catalytic properties, or more specifically an apoenzyme (enzyme activated by binding cofactor). They also investigated if it was possible to increase the affinity of G4s through SELEX and found two sequences that were able to bind to hemin with sub-micromolar affinity.

Travasco *et al.*,²²⁵ Evans *et al.*²⁴⁹ and Dai *et al.*¹⁷² have gone on to report more G4 ODN sequences that have been found to have peroxidase-mimicking activity when complexed with hemin. The advantage of G4s taking on peroxidase-mimicking activity is that it is easier to detect using well established methods, such as enzyme-linked immunosorbent assay (ELISA). ELISA techniques are often used to detect the presence of horseradish peroxidase and therefore compatible with G4/hemin aptamer detection. Some examples of compounds used in ELISA include 3,3',5,5'-tetramethylbenzidine (TMB), 2,2'-azinobis(3-ethylbenzothiozoline)-6-sulfonic acid diammonium salt (ABTS) and luminol (referred to as substrates in this thesis). ABTS and TMB are colorimetric assays that produce a distinct colour and luminol is a chemiluminescent assay. However, strong binding does not necessarily correlate with increased peroxidase-mimicking activity.

Cheng *et al.*¹⁸⁴ investigated 19 G4 sequences, both naturally occurring and synthetic, to determine which sequences yielded the fastest peroxidase-mimicking activity using ABTS. They used CD to determine if the rate of peroxidase-mimicking activity was reliant on the structure of the G4 (parallel, antiparallel or hybrid/mixture). It was determined that parallel structures had an increased peroxidase-mimicking activity, when compared to the two other possibilities. This was attributed to the ability for the G4s to end-to-end stack more easily than other structures, as well as low steric hindrance from the loop regions.

Others have attempted to investigate how the peroxidase-mimicking activity of the G4/hemin aptamer is reliant on sequence of the G4. Chen *et al.*²⁵⁰ determined that A repeats inside of the loop regions were able to enhance the peroxidase-mimicking activity. Chang *et al.*²⁵¹ reported that when the G4 sequence was flanked by 3 C residues on either end there was an enhancement of peroxidase-mimicking activity. Stefan *et al.*²⁵² found that using nt supplements, such as adenine triphosphate(ATP), enhanced the peroxidase-mimicking activity. All this information is helpful for evaluating G4 sequences that are meant to have high peroxidase-mimicking activity, especially for designing biosensors.

1.5.3.11. Biosensors

The advantage of using DNA for biosensors is the range of different possible readouts in addition to being active in a wider range of temperatures, as opposed to conventional enzyme based biosensors (e.g., ELISA).²⁵³ Using G4 complexes allows for fluorescent,^{229,234} colorimetric,^{184,254} chemiluminescent^{255,256} and electrochemical²⁵⁷ readouts, which can be very useful when designing an assay. These assays have been used to detect G4s, DNA, metal ions, small molecules and proteins. Assays have also been developed for DNA genotyping such as single nucleotide polymorphisms (SNPs) and biomarkers. Willner *et al.*²⁵⁸ designed a chemiluminescent assay that was able to detect specific target DNA. They immobilised a DNA probe, that was complementary to the target, to a gold surface. The target DNA contained two regions, a complementary binding region and a G-rich sequence. Once bound the additions of

hemin, luminol and peroxide resulted in a chemiluminescent signal. They also used gold NPs to increase the sensitivity of the assay. Furthermore, the same group used a hairpin system that, once hybridised with the target, produced a colorimetric readout using ABTS, effectively reducing the need for the target to contain a G4 sequence and surface attachment.²⁵⁹ There have been a range of fluorometric assays developed that rely on the G4s complexing with a molecule that produces a fluorescent product. Xu *et al.*²⁵⁴ were able to develop a fluorescent biosensor using thioflavin T that could selectively bind to RNA G4s to produce a fluorescent product. Thioflavin T has also been used to detect G4 inducers such as thrombin, however the fluorescence was not detectable due to competition with the inducer.²⁶⁰ All these techniques have one thing in common: the G4 is used as a reporter molecule. This shows that G4s are versatile, robust and easily controlled under the correct conditions. All the publications described show great promise for not only using G4s as a biosensor component but also the compatibility with various other well-established methods. The next section will discuss using DNA to perform functions dynamically.

1.6. Dynamic DNA

Dynamic DNA is able to perform activities, such as logic gates, programmable motion origami mechanisms, and DNAzymes.^{261–263} Fig 1.11 is an example of a dynamic DNA technique that relies on the recognition of a DNA sequence which allows of the formation of a DNAzyme. Elbaz *et al.*²⁶⁴ designed a biosensor that relied on a cascade of DNAzymes that produce a G4 with peroxidase-mimicking activity (Fig. 1.11). Essentially, the system contained two ssDNA (Fig. 1.11, 2 and 3) that hybridised with a G-rich sequence (Fig. 1.11, 4 (blue)). Upon addition of a target DNA (Fig. 1.11, 1 (green)) a DNAzyme was created that could cleave the G-rich sequence into two separate reporter G4/hemin complexes. Wen *et al.*²⁶³ developed a similar system that could detect Pb(II), whereby the DNAzyme only cleaved when in the presence of Pb²⁺ ions. The advantage of this system was the recycling of the Pb²⁺ ions, as they were not used up in the reaction and so allowed for a continuous production of the G4s. This

Figure removed due to copyright

Figure 1.11: Schematic for a G4 biosensor that relies on a cascade effect from DNAzymes. Adapted from Elbaz *et al.*²⁶⁴

in turn increased the sensitivity of the biosensor. This same approach can be taken when using electro-chemistry to detect the presence of G4s. Wu *et al.*²⁵⁷ used a gold electrode to detect an electrocatalytic signal from the G4/hemin complex formation.

Another example of dynamic DNA is toehold-mediated strand displacement that is often used for genotyping and logic gates. Fig 1.12 is an example of a simple And Or (XOR) program using toehold-mediated strand displacement, developed by Liu *et al.*¹⁵⁵. The output (1 or 0) is completely dependent on the input and so it can be used to replicate large scale circuitry

Figure removed due to copyright

Figure 1.12: Example schematic of a logic gate that used toehold-mediated strand displacement, developed by Liu *et al.*¹⁵⁵. This scheme shows that a single dsDNA with toeholds is able to form 1 of 2 states depending on what displacement strands are present in solution. The reporter molecules used were gold nanoparticles (GNP) coupled to the DNA.

1.6.1. Toehold-mediated strand displacement

Toehold-mediated strand displacement is a dynamic DNA phenomenon where a reaction between a ssDNA molecule, referred to as a displacing sequence (DS), and a dsDNA molecule occurs.²⁶⁵ This process consists of a target strand (Fig. 1.13, black) hybridised to a shorter incumbent strand (Fig. 1.13, blue), that are semi-hybridised, and a DS (Fig. 1.13, red) which is complementary to the target (Fig. 1.13, black). The semi-hybridisation of the target strand with the shorter incumbent strand results in an overhang of nts referred to as a toehold (or toehold domain). The DS is able to nucleate with the toehold (Fig. 1.13 (b)) and begin to compete with the shorter strand in a random walk process, known as 'zippering' (Fig. 1.13 (c)). The overall process is referred to as branch migration' The reverse process is thermodynamically unfavourable and six orders of magnitude slower and so the result is a fully complementary dsDNA product.²⁶⁵

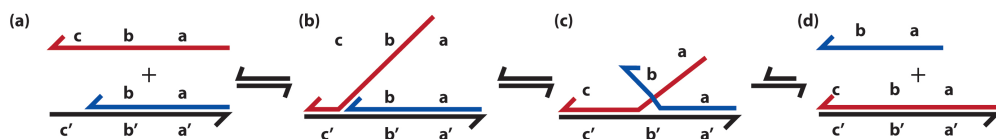


Figure 1.13: Schematic of the toehold-mediated strand displacement (a) DS (red) is added to a target strand (black) with a toehold domain and a hybridised shorter incumbent strand (blue), (b) DS nucleates with the target strands toehold, (c) the random walk 'zippering' process begins and (d) the shorter incumbent strand is displaced by the DS.

Another form of toehold mediated strand displacement is known as toehold-mediated strand exchange (Fig. 1.14 (a)). This is a process whereby after the displacement has taken place a second toehold region is created.⁶ This is very useful for techniques such as logic gates, as it allows for the system to become reversible and also allows for equilibrium to be a more prominent driving force on the reaction. These processes are also known as three-way branch migration due to the involvement of three strands, four-way branch migration is if four strands are involved. Four-way branch migration (to be expanded upon in Section 1.6.2.4) involves two dsDNA exchanging complementary strands, through the formation of a Holliday junction, to

form two new dsDNA products (Fig. 1.14 (b)).²⁶⁶

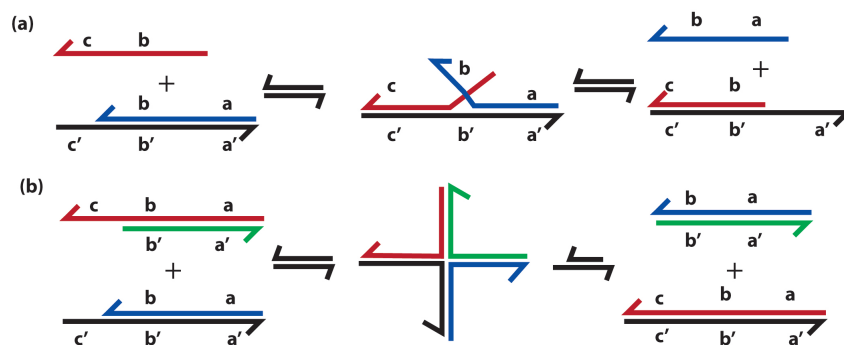


Figure 1.14: (a) Toehold-mediated strand exchange and (b) four-way branch migration with formation of Holliday junction.²⁶⁶

There are several conditions that must be considered when designing a strand displacement reaction and these will be discussed in further detail in the next sections.

1.6.1.1. Random walk: DNA ‘zippering’

The strand displacement process is described to have a random walk, this is due to the step-wise melting and hybridisation of base pairs in a random direction along a strand of DNA. This process is highly favourable and is used in nature by enzymes such as helicases (enzymes that are able to ‘unzip’ dsDNA)²⁶⁷ or transcriptases (mRNA transcription enzymes).²⁶⁸ For these enzymatic processes, energy is only needed at the beginning and relies completely on the random walk process to move across the DNA. The random part of the name refers simply to the one-dimensional (1D) nature where by it is just as likely to move forward as it is to move backwards (left or right) along the DNA strand.

There are various kinds of random walk processes that can occur on DNA, such as totally random walk (probability of moving left or right is 1/2), completely biased random walk process (probability of moving in one direction is 1) and general random walk.^{265,269} The general random walk is simply a model that considers the various conditions that DNA exists

in to determine which direction would (or would not) be favoured, as there are obstacles found on a DNA strand in nature such as DNA-bound proteins.²⁷⁰ This thesis will concentrate on the totally random walk process for toehold-mediated strand displacement, where the probability is 1/2. A probability of one half is argued to be because there are no proteins involved (*in vivo*) and two equal strands are competing to hybridise on a single target strand.^{265,271} The factors that affect this type of random walk process are mostly reliant on the sequence of the DNA strands. The only time the two strands are not equal is in the presence of mismatches, these change the thermodynamics to favour the reverse (incumbent strand displacing the DS). This can be further exacerbated in a Holliday junction during four-way branch migration process (see Section 1.14).

Landon *et al.*²⁶⁹ created a forward biased toehold-mediated strand displacement by placing nt spacer, ssDNA that linked two dsDNA sequences, inside of the path of the three-way branch migration. The nt runs helped the process by acting like new nucleation sites for the displacement process. The inclusion of inosine, a synthetic nt, into those regions also allowed for increased displacement rates.²⁶⁹ Overall, they found that with the inclusion of new nucleation sites the rate of displacement for a 1 nt toehold was increase by 7.5 orders of magnitude. There are however several factors that must be taken into consideration when performing a toehold-mediated strand displacement. Control over the kinetics can allow for more reliable and robust strand displacement reactions.

1.6.2. Toehold-mediated strand displacement reaction kinetics

The rate of strand displacement is not used to describe the rate at which each base pair is displaced during the branch migration, rather it is used to describe the net result of the random walk process once the reaction has reached completion. This is due to the methods used to detect the reaction, such as fluorescence or gel electrophoresis,²⁷² which can only be measured once the displacement reaction has been completed. The kinetics of the toehold-mediated strand displacement process is based on several environmental factors in addition to

the composition of the DNA strand. Factors include: temperature, salt concentration, toehold length and presence of mismatches, both in or after the toehold. All these factors must be considered when designing a successful strand displacement reaction.

1.6.2.1. Temperature

DNA hybridisation kinetics are highly reliant on the temperature of the environment the reaction takes place in, due to the non-Arrhenius nature of DNA hybridisation (see Section 1.3). The displacement rate tends to be faster the higher the temperature, much like with typical dsDNA hybridisation. The initial nucleation of the displacing sequence to the toehold domain on the target strand mimics the thermodynamics required for nucleation between two ssDNA. As mentioned previously DNA tends to hybridise best at temperatures that are above 20 °C, up until the T_m of the dsDNA. In order for successful nucleation, it must be stabilised by two or three base pairs. However, the number of base pairs required for nucleation increases with temperature.²⁶⁵ The displacement reaction is also possible if there is no toehold present; but is reliant on the fraying of the end base pairs.²⁷³ Fraying is the process whereby the ends of the DNA become unpaired and open up, although this is limited to one or two base pairs, and should not be confused for DNA zippering, which is the exchange of base pairs during displacement.²⁶⁵

1.6.2.2. Toehold properties

Zhang and Winfree⁶ found that the ΔG° was affected by the length of the toehold as well as the sequence. In particular, toehold domains that are primarily made up of strong binding nts (G/C) decreased the free energy of the system. This was due to the stronger hybridisation forces (i.e., three hydrogen bonds compared to two for A/T) and were classified as a strong binding site. Whereas A/T were not able to decrease the free energy to the same degree as the G/C for the same number of nts. These were classified as having a weak binding

site. Table 1.1 shows the calculated binding energies of different toehold lengths containing: a mixture of all nts (γ), strong binding nts (γ^s) and weak binding nts (γ^w). Table 1.1 also shows the stabilising energies of the incumbent strand based on length; the longer the strand the more stable the displacement process becomes. From this it was determined that the more G/C rich the toehold was, the stronger the binding of the DS to the target. As a result, this allows for the design of toehold domains that will favour the displacement of the incumbent strand. Fig. 1.15 shows a schematic of the corresponding regions of the target strand, incumbent strand and DS from Table 1.1. The target strand (black) consists of two regions, the toehold region (γ) and the target sequence (β). The incumbent strand (blue) consists only of a complementary sequence to target sequence (β). The DS contains both regions (γ and β) that are complementary to the target strand.



Figure 1.15: Diagram of the target strand (black) with toehold region γ and target sequence β with hybridised incumbent strand (blue, β). The DS (red) contains complementary regions to the target strand (γ and β)

Our group has previously reported on the effects of toehold length of 5 and 9 nts.²⁷¹ It was found that the displacement reaction kinetics increased as the number of nts increased. Looking at Table 1.1 it can be seen that a toehold region of 9 nt is ~ 2 times more stable than a toehold of 5. This is to be expected as the more nts used to nucleate the DS the more thermodynamically favourable the random walk process will be. For this thesis we continued to use the 9-nt long toehold for the mediation of the displacement process. Lastly the location of the toehold is very important, as it can increase or decrease the rate of displacement of the incumbent strand. Genot *et al.*²⁷⁴ used nt spacers after the toehold to try and control the displacement process. They used a remote toehold, which consisted of a spacer (Fig. 1.16, grey) that was inserted between the toehold domain (Fig. 1.16, blue) and a target domain (Fig.

Table 1.1: Calculated binding energy of different length toeholds and sequence adapted from Zhang and Winfree.⁶

Toehold length ^α	Binding energy (kcal/mol)	Toehold length ^α	Binding energy (kcal/mol)
γ^0	+1.9	γ_s^1	-1.1
γ^1	+0.2	γ_s^2	-3.2
γ^2	-1.7	γ_s^3	-5.0
γ^3	-3.0	γ_s^4	-8.0
γ^4	-4.7	γ_s^5	-10.3
γ^5	-6.9	γ_s^6	-12.1
γ^6	-8.3	γ_s^7	-15.1
γ^7	-9.2	γ_s^8	-17.3
γ^8	-11.9	γ_s^9	-19.2
γ^9	-12.9	γ_s^{10}	-21.2
γ^{10}	-14.8	γ_w^1	+0.2
γ^{15}	-21.8	γ_w^2	-0.8
β^0	+1.2	γ_w^3	-2.1
β^1	-0.6	γ_w^4	-3.8
β^2	-2.7	γ_w^5	-4.3
β^3	-4.5	γ_w^6	-5.3
β^4	-5.6	γ_w^7	-7.0
β^5	-6.7	γ_w^8	-7.5
β^6	-9.5	γ_w^9	-9.0
β^7	-10.2	γ_w^{10}	-8.9

^αSuperscript denotes number of nts in the toehold

1.16, pink). Spacers consisted of PEG, ssDNA or dsDNA and could be used to tune the rate of the displacement. They found that the remote toeholds were able to increase the relative rate of displacement. They also showed that more flexible spacers, such as the PEG or ssDNA, resulted in faster relative displacement rates.

Figure removed due to copyright

Figure 1.16: Genot *et al.*²⁷⁴ describes the proposed mechanism for the remote toehold. The target strand, labeled with fluorophore (F) and quencher (Q), is displaced from the substrate (S) by an invading strand (I). The toehold and displacement domains on both the substrate and invading strands are separated by spacer domains. Docking of the substrate and invading strand by hybridization of the toehold domains is followed by an internal diffusion step, which is required to align the displacement domains and initiate the branch migration reaction by which the target strand is displaced from the substrate. Displacement is reported by quenching of fluorescence from the target.

1.6.2.3. Mismatches

Although temperature may determine the maximum rate of the reaction, mismatches can have the largest impact when it comes to impeding the displacement reactions. Toehold-mediated strand displacement relies on the sequence specificity characteristics of DNA self-assembly.²⁶⁵ Kim and Broadwater²⁷⁵ and Zhang *et al.*²⁷⁶ have studied the effect of a mismatch occurring within the toehold region and have found that it was possible to completely impede the displacement process with mismatches of >2 bp. However, 1 mismatch can be stable enough to allow for the displacement to continue.^{275,277}

Kim and Broadwater²⁷⁵ designed a model that contained mismatches in a strand displacement reaction at different points along the DNA and found that a single mismatch could slow down the rate of displacement by orders of magnitude. It was found that if there was a mismatch formed within the first 4 nts of the toehold nucleation site that the time of displacement was increased from microseconds to minutes. However, if a mismatch formed >6 bps

after the toehold region the random walk process was completely impeded (Fig. 1.17). This shows that mismatches formed in the toehold region is more tolerated than a mismatch formed directly after the toehold-region. Fig. 1.17 shows the order of stability with perfect match being most stable, then a single mismatch in the toehold domain and finally a toehold within 6 bps after the toehold. This implied that the specificity of the displacement process was very important both in and around the toehold region and that if a mismatch was in the invading DS, after the toehold region, that there was a high kinetic barrier. Although it sounds counter intuitive this can be explained by the work of SantaLucia *et al.*³⁴ who had already determined that mismatches that were closer to the terminal ends of the DNA were found to be more stable than those further in.

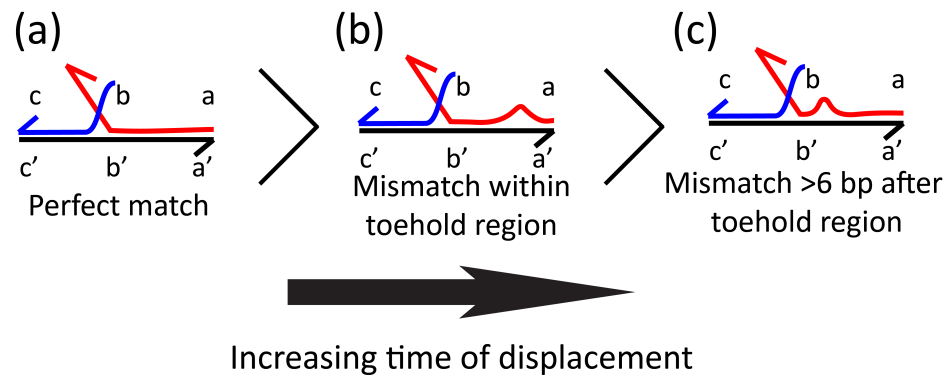


Figure 1.17: Increasing time required for strand displacement reaction from (a) a perfect match, (b) a mismatch in the toehold and (c) a mismatch within 6 bps after the toehold region.

1.6.2.4. Four-way-branch migration: Holliday junction

Four-way branch migration, as mentioned earlier, is a displacement process that involves two homologous dsDNA exchanging strands.^{266,278} This process occurs when the two homologous dsDNA both complementary toeholds (also referred to as tails, see Fig. 1.14). Once nucleated the strands form a four way intermediate, known as a Holliday junction, that essentially begins to exchange strands through the random walk process.²⁷⁸ High affinity, high selectivity, and robustness are vital to any, and all, hybridisation techniques. Three-way branch migration satisfies all three of these requirements, however SNP genotyping has been an issue

when it comes to high selectivity.^{271,277}

Single mismatches can form stable enough bonds to allow for strand displacement to occur, albeit it at a slower rate, as mentioned in the previous section. Panyutin and Hsieh²⁷⁸ studied four-way branch migration and how mismatches affected the rates. Although both three-way and four-way branch migration are spontaneous, four-way branch migration gave more control over the specificity but at the cost of the displacement rate.²⁷⁷ This is due to two base pairs being broken and formed at a time; as opposed to three-way where only one base pair is broken and formed. The extra base pairing involved requires higher energy to form and thus it is impossible for a mismatch to be sufficiently stabilised to allow for displacement to occur.

Khodakov *et al.*²⁷¹ discovered that once the length of the DNA was increased to 80 bp, considerably longer than any other toehold-mediated strand displacement experiments done previously, SNP was found to have very little effect on the displacement process. They also found that the only mismatch that was able to completely destabilise the strand displacement reaction was a mismatch that involved C residue. This is expected as cytosine is the weakest at forming mismatches and effectively hinders the process from going to completion.^{67,279} A four-way branch migration system was designed to allow for adequate discrimination of all four possible SNPs. This was achieved by introducing a protector strand onto the displacing sequence. A protector strand is a short sequence that is complementary to the displacing sequence at the region where the mismatch is liable to form. This resulted in a Holliday junction forming where the mismatch would occur. Mismatch discrimination power was improved; however, the implications were a slower rate of displacement.

There is one other factor that determines the rate of toehold-mediated displacement and that is whether the DNA is immobilised. Solution and immobilised DNA strand displacement reactions have been shown to have vastly different rates and applications and will be discussed in the next sections.

1.6.3. Solution vs surface-immobilised DNA strand displacement reactions

Toehold-mediated strand displacement is a very versatile process and can be performed in solution as well on surfaces. Solution based toehold-mediated strand displacement reactions have a clear advantage over surface-immobilised displacement reactions in terms of speed. In solution the DNA molecules have more chance to collide and react, however at the cost of spatial localisation. Multiplex displacement reactions in the same solution simultaneously requires equipment able to detect and separate multiple fluorophores. However, there is a limitation on the number of fluorophores that can be used in tandem, due to the requirement of discrete colours needed for accurate detection of each fluorophore.^{86,280} Fluorophores are most often used for solution based toehold-mediated strand displacement due to the relatively simple set up, DNA modification and compatibility with real-time thermocyclers. Colorimetric methods have also been developed where the reaction results in the formation of a G-quadruplex, however this completely eliminates the ability for multiplex reactions to be detected in a single solution.^{272,281}

Surface immobilised toehold-mediated strand displacement reactions allow for more varied set ups, 2D (micro-arrays and microfluidic devices) or 3D (microparticles and NP). This gives far more control over spatial localisation, however at the cost of speed due to the requirement of diffusion of the DS to the target, or vice versa.²⁸² Detection systems for surface bound DNA are more robust, as spatial control allows for multiple displacement reactions to occur on the same surface in isolated locations.²⁸³

1.6.3.1. Solution based toehold-mediated strand displacement reactions

In order to determine successful strand displacement in solution, often parallel detection systems such as fluorometric, colorimetric or gel electrophoresis are needed to determine completion of the reaction.^{86,281} Most detection systems use fluorescent methods such as FRET, whereby successful displacement is detected by an increase or decrease in fluorescence. The

following section will describe several methods that have used strand displacement reaction in solution and different detection methods of the reaction.

It has been shown that it is possible to perform genotyping on extracted DNA by toehold-mediated strand displacement, especially gender type DNA. Amelogenin (Amel) is the gender determining gene based on the length of the X and Y chromosomes in humans. The X chromosome has a 6 bp deletion, making it shorter in sequence when compared to the Y chromosome. Khodakov *et al.*²⁷¹ used toehold-mediated strand displacement to determine the length of the Amel. The toehold-mediated strand displacement reactions were performed using human DNA that had been amplified using PCR. The PCR process allowed for the introduction of a toehold after digestion with an enzyme. The forward primer was labelled with a fluorophore and the reverse contained deoxyuracil (dU) at position 5 (dU⁵), 9 (dU⁹) or both (dU^{5,9}) (Fig. 1.18 (a)(i)). After PCR was completed the PCR product was digested with the enzyme uracil-DNA glycosylase (UDG) which catalysed the release of uracil from the PCR product (Fig. 1.17 (a)(i)).

After the uracil had been removed, the shorter sequences (3, 4 or 7 bp) were no longer stable enough to stay hybridised and became ssDNA, leaving a toehold of 5 or 9 nts long. Fig. 1.18 (b)(ii) shows that once the toehold has successfully been created, the toehold-mediated strand displacement is able to proceed. The dU⁹ and dU⁵ were not as successful at displacement as the dU^{5,9} displacement. The dU⁵ toehold was only 5 nts long and therefore the nucleation of the displacement strand was not as stable as the dU⁹ toehold of 9 nts long. This is to be expected as a 9 nt toehold is almost twice as stable than a 5 nt long toehold (Table 1.1). The digestion of dU^{5,9} created two shorter protecting sequence with a low melting temperature of ($T_m < 10$ °C), much lower than that of the dU⁹ (45.3 °C) and therefore successfully dissociated at a lower temperature (30 °C). This in turn allowed for the toehold-mediated strand displacement to become more efficient at the 30 °C, which was the temperature the experiments were run at. This work also showed how selective the toehold mediated strand displacement process can be.

Although the X and Y Amel is only different by 6 nts, it was possible to displace all the X without affecting the Y, with only half the male sample being displaced. Another article published by this group showed that it was also possible to determine the gender by looking at the melting data alone. Fig. 1.18 (b)(ii) shows the fluorescence results that show it fluorescence is easily distinguishable between the X and Y chromosome based on the integrated fluorescence (dF/dT) vs temperature (°C) (Fig. 1.18 (b) (ii)). Male DNA can be clearly identified by the melting peaks only being half the size of the female toehold-PCR + Xi, which would have resulted in complete displacement.

Issues however did arise when trying to displace a sequence that had a singular mismatch such as a SNP. They attempted to genotype mitochondrial DNA using toehold-mediated strand displacement. It was found that they were able to distinguish between four different samples using a SNP-T displacing sequence that contained an A at the SNP position. However, with SNP-C (G at the SNP position) they were unable to distinguish between any of the samples. This is supported in literature that A•G and T•G cause minor disruption to the backbone of the dsDNA helix and therefore there is not enough energy difference to destabilise the displacement process.^{10,66}

Zhang *et al.*²⁸¹ designed a toehold-mediated strand exchange process that used G4s as a strand displacement facilitator. The formation of the G4 was amplified as more displacement reactions took place. This strand displacement facilitation was achieved by including a G-rich sequence, encoded for an ATP aptamer, on the ends of the incumbent strand which was partially hybridised to the target strand. Once ATP was added to the system the G4 folded and exposed more of the target strand, the incumbent strand was then the correct length to be completely displaced from the target strand. They were able to detect the displacement by using a FRET detection system. In the same work they also used the G4 system as a detection system and streptavidin, a protein with high affinity for biotin, as a strand displacement facilitator. In order to do this the G4 sequence was split between the target strand and the DS, so that only once the displacement reaction was completed the G4 formed. Once formed they used hemin

Figure removed due to copyright

Figure 1.18: (a) Schematic for creating a toehold (i) and performing toehold-mediated strand displacement (ii) and (b) toehold-mediated strand displacement of Amel for both male and female DNA and the integration of the melting curve.²⁷¹

and ABTS to detect the G4. In order to facilitate the strand displacement reaction, the incumbent strand was modified to contain a biotin molecule. Streptavidin was added to the solution and binds to the biotin on the strand. Once bound the incumbent strand/target duplex's T_m was lowered to below the DS/target duplex T_m . This shifted the strand displacement equilibrium to the completed reaction. Adding a second biotin shifted the equilibrium even further, as it affected the second toehold binding region.

Park *et al.*²⁷² created a toehold-mediated strand exchange technique that relied on a DNAzyme, that was activated in the presence of Cu^{2+} ions, to release the DS. Once the incumbent strand was displaced a G4 formed in the presence of hemin, which was detected with ABTS. Once the DS was released a second toehold region was created that allowed for a second DS to nucleate and displace the initial DS. The original DS could then go on to displace more incumbent strands. This is useful for signal amplification as it relies on a cascade effect to increase the concentration of G4s present.

1.6.3.2. Surface-immobilised DNA strand displacement reactions

Surface capturing of DNA is useful for screening subtle differences in genomic DNA and can be performed on 2D and 3D surfaces. These techniques can be used for highly efficient selection, separation and enrichment of DNA from a crude mixture. Examples of techniques that use 2D surface immobilised DNA are DNA microarrays. These can be used to detect mutations in DNA extracted from organisms.

1.6.3.3. 2D surface DNA strand displacement reactions

There are a variety of surfaces that DNA has been immobilised on, such as silica, silicon and gold to name a few. This section will discuss the diverse ways that toehold mediated strand displacement has been performed on surfaces 2D flat surfaces. Wang *et al.*²⁸⁴ immobilised DNA that contained a toehold onto a quartz crystal balance that was able to detect SNPs with great efficiency. This was achieved by having the target attached to the surface contain a hairpin loop, that could only be opened if the correct sequence successfully nucleated. Once open a second strand was able to hybridise with the now open hairpin loop and this was detectable by the quartz crystal balance. This method was sensitive down to 25 nM and could distinguish SNPs reliably.

Hwang *et al.*²⁸⁵ designed a system that relied on fluorescently tagged target DNA being grafted to graphene. This allowed for a two-fold identification of successful displacement reactions. When a successful displacement occurred, the fluorophore was activated when the quencher tagged incumbent strand was displaced, as well as a distinct change in a current-voltage (I-V) curve. However, these techniques were limited to a few samples at one time. Others have developed methods that can be used to detect a large variety of strand displacement reactions of surfaces by using microarrays. Microarrays are made up of many defined spots of immobilised ssDNA on a surface, that allow for the analysis of multiple DNA sequences.²⁸⁶ Fig 1.19 shows a typical schematic of a DNA microarray, with each spot containing a different

immobilised sequence. After immobilisation a solution containing many ssDNA sequences, tagged with a fluorophore to allow for identification, is washed over, and only complementary sequences will hybridise and be captured on the microarray. Upon identification it is possible to know the sequence of the DNA based on which spot fluoresces, this being useful for identification of a large amount of mutations or to resolve an individual's DNA in a complex mixture using one microarray. Using microarrays, SNPs have successfully been genotyped, however the process is slow and requires specialised equipment. As long as the sequences are unique enough, i.e., have a mutation (≥ 1 bp) such as an SNP, the DNA microarrays function appropriately.¹⁴⁸

Figure removed due to copyright

Figure 1.19: Schematic of a DNA microarray, where each spot has a different sequence immobilised on the surface.²⁸⁷

Issues arise when analysing regions of DNA that contain multiple repeats of the same sequence. Human identification, most often used in forensic cases, identify multiple known short tandem repeats (STRs) sequences. STRs are comprised of a short sequence being repeated multiple times, and the number of repeats is different between individuals. The main issue is

determining subtle differences such as comparing 9 to 10 repeats, due to the 9 repeats being able to bind strongly to a region containing 10 repeats, and *vice versa*, on the microarray. Kemp *et al.*²⁸⁸ used enzymes to digest any overhanging sequences after the hybridisation of the targets to capture probes, effectively removing any fluorescent probes from regions that contained capture probes smaller than the target, and only hybridised DNA was the probes that related to the exact length and higher of the STR. Issues arose from the lack of complete degradation of sequences where the probe was only one repeat smaller than the target. The complementary probe was found to only be 1.6 times brighter than the one repeat smaller probe. This method was only tested for synthetic DNA that did not contain the number of repeats found in real-life DNA and is yet to be tested using extracted DNA.

Pourmand *et al.*²⁸⁹ developed a microarray based on three-way branch migration that relied on repeated strand displacement to remove any DNA that was not 100% complementary in length. Fig. 1.20 shows the technique: (i) probes are immobilised on the surface of the microarray, (ii) the addition of the target for initial hybridisation, (iii) and (iv) add the first competing probe to remove strands longer than the capture probes, (v) addition of the second competing probe removes all targets shorter than the capture probe and (vi) only the complementary sized target remains hybridised to the surface. This showed promise as the length complementary probe was 2.8 times brighter than the probes that were longer and shorter than the capture probe. This system is more reliable for genotyping using real-life DNA. Fig. 1.20 (b) is an example of a microarray that shows that only the 9 and 10 repeats remain and Fig 1.20 (c) is the histogram representing the remaining fluorescence in the microarray, indicating that the samples were of 9 and 10 repeats in the STR.

1.6.3.4. 3D surface immobilised DNA strand displacement reactions

Microbeads or NPs are a 3D version of the surface immobilisation technique, that can be used in much a similar way as the microarrays. This thesis will focus on toehold-mediated strand displacement techniques used with microbeads.

Figure removed due to copyright

Figure 1.20: (a) Schematic representation of STR genotyping in a micro-array. First capture probes for all potential lengths of a STR are immobilised onto a surface in (i) and an unknown target STR is added and hybridises with all capture probes (II). 1st competing strand is added to displace any target STR that is too long for capture probe (iii) and (iv) and 2nd competing strand is added to displace any target STR that is too short for the capture probe (v) leaving only fully complementary target STR (vi). (b) An example of a micro-array that shows only 9 and 10 repeats remain after both 1st and 2nd competing strands are added. (c) Histogram of intensity of fluorescence of microarray.²⁸⁹

Khodakov *et al.*²⁹⁰ used microbeads (order of 1 μm) to capture and selectively release STRs based on a lock and key system. Fig. 1.21 shows the capture probes on the surface allowed for capture of PCR product, that contained a PEG linker with a target sequence. Once captured a toehold was created by the difference in length of the capture probe (24 nts) and the target sequence (18 nts). The toehold essentially now being “locked”, required the addition of a displacing sequence that was exactly complementary in sequence and length, the key, to displace the captured sequence. This meant that multiple sequences could be captured on the surface of the beads and have selective release of each unique sequence for analysis. This technique was improved upon later by the same group and used the rate accelerator PEG 6000 to increase the rate of displacement from the surfaces, overcoming the diffusion issue that is faced

Figure removed due to copyright

Figure 1.21: Schematic of the capture of the ds-PCR products tagged with ss-ODN with following sequences selective release via toehold-mediated DNA strand displacement reaction. Domains a and a', and b and b' are self-complementary.²⁹⁰

when performing displacement reactions from surfaces.²⁹¹

Yao *et al.*²⁶² designed a system that used nanoparticles (NPs) and strand displacement to genotype DNA (Fig. 1.22). Fig. 1.22 shows a gold nanoparticle (AuNP), referred to as AuNP-1, was modified to allow the attachment of linker protector complex, that contained the domains α and β . This could nucleate with a displacing sequence that contained a second AuNP-2, containing the domain α . Once the protector group was displaced, it then goes on to take place in a second displacement reaction. The second reaction involved dsDNA that contained a quencher/fluorophore system, so once the displacement reaction had taken place the fluorophore became fluorescent again and could be used to detect the kinetics of the reaction. Toehold-mediated strand displacement shows great promise as a genotyping tool. The issues that have to be overcome are the lack of sensitivity to SNPs. This thesis will discuss a possible route for this in Chapter 3.

All these techniques show that G4s and toehold-mediated strand displacement are

Figure removed due to copyright

Figure 1.22: Schematic of the surface immobilised toehold-mediated strand displacement technique, designed by Yao *et al.*²⁶²

useful techniques for genotyping and biosensing. However, this thesis will now discuss the impact that DNA may have as an antimicrobial. There is research that suggests that natural polymers are able to be used as antimicrobials and this thesis will now discuss those in more detail.

1.7. Strategies to combat biofilms using synthetic and natural polymers

This section will discuss a possible use of DNA as an antimicrobial, an unexplored alternative to common antimicrobials. The main target is biofilms, which are bacterial aggregates that have been found to cause a range of issues for the medical sector. Due to antibiotic resistance arising in bacteria there have been attempts to find alternatives that can target bacteria.

1.7.1. Bacteria and biofilms

Bacteria (and fungus) exist in two distinct states, planktonic (single cells free in solution) and sessile aggregates (biofilm).²⁹² Sessile aggregates are able to excrete a protective layer of mucilage that encapsulates cells onto the surface, known as a biofilm. Biofilms are

comprised mostly of DNA, proteins and polysaccharides, known as extracellular polymeric substance (EPS), which are excreted from cells.²⁹³ This allows for bacterial cells to proliferate and harbour persister cells, a small population of metabolically dormant cells that are able to survive antimicrobial treatment.²⁹⁴ Antimicrobial resistant cells can be dangerous when it comes to pathogenic microbial biofilms, causing chronic infection which can be difficult to identify and treat.²⁹⁵

1.7.2. History of biofilms

Biofilms have been known about in one way or another since 1684 when Leeuwenhoek described 'animal' in plaque, a sticky film, found on teeth, making it the first observation of microbial aggregates.²⁹⁶ It was not until 1933 that microbial aggregates were first imaged by micrograph.²⁹⁷ The first time biofilms were linked with infection was by HØiby and Olling in 1977 after they noticed 'bacterial clumps' in the lungs of patients with chronic cystic fibrosis.²⁹⁸ In 1981 biofilms were found to form even under high velocity fluid conditions, but only after the surface had been conditioned with EPS, which meant that EPS was vital for the formation of a permanent biofilm.²⁹⁹ In 1987 Costerton *et al.*³⁰⁰ described the bacteria in glycocalyx and how it allowed for pathogens to adhere to surfaces and persist. Costerton *et al.*³⁰¹ went on to describe biofilms as a structured community of bacterial cells enclosed in a self-produced polymeric matrix. Bigger³⁰² investigated the mechanism of penicillin treatment of bacteria and determined that there were cells that were not resistant but ultimately still survived treatment. These were termed persister cells. Persister cells are described as biologically dormant and do not divide.

Moyed *et al.*^{303–306} identified genes in *Escherichia coli* (*E. coli*) that were responsible for persister cells. For many years persister cells in biofilms had largely been ignored, until Lewis linked them to antimicrobial resistance in biofilms.^{307,308} In the last two decades it has been established that persister cells and biofilms form under physiological stress, in particular starvation. This has led to the increase of antibiotic resistance and often arises due to the

continued survival of the colonies after multiple antibiotic treatments.^{309,310} The next section will discuss how biofilms and persister cells have led to chronic infections that are extremely difficult to treat.

1.7.3. Life cycle of biofilms

The biofilm life cycle can be broken down into five distinct phases.³¹¹ The first phase is to condition the surface that will allow for the attachment of the bacteria and subsequent growth of the biofilm. This can be done either through adsorption of molecules from the environment or excretions from the microbes.^{292,312} An important aspect of the surface conditioning phase is to make these conditions favourable for cell adhesion. Some bacteria have been found to excrete DNA, as a method for conditioning the surface, through autolysis.^{313,314} DNA from those cells then coats the surface and allow for the second phase to begin. It has been seen that treatment of surfaces with DNase (enzyme that degrades DNA) can prevent the occurrence of biofilms.

The second phase is the reversible adhesion stage whereby the microbes absorb to the surface by physical forces or appendages (e.g., flagella). Flagella have been found to be mechanosensory and allow for bacteria to sense a surface and then attach.³¹⁵ Several factors influence whether or not the cells adhere to the surface these include available energy, orientation, temperature and pressure. Surface functionality can also influence adherence to the surface, and so researchers often try to make surfaces less favourable for bacterial adhesion. The forces that are involved with adhesion are van der Waals forces, steric interaction and electrostatic (double layer) interactions. These are referred to as Derjaguin, Verwey, Landau and Overbeek (DLVO) theory.³¹⁶ This theory is used to describe how all the forces, including hydrophobic and hydrophilic, balance to allow for the cells to physisorb (physically absorb) to the surface.

The third phase is the irreversible adhesion, where the cells are immobilised onto the surface, and is reliant on hydrophobic-hydrophilic interactions.³¹⁷ Bacteria are able to extend

flagella, or in some cases DNA, that allow them to overcome any unfavourable hydrophilic-hydrophobic interactions and condition the layer even after adhering to the surface. Afterwards the fourth phase begins, population growth, where adhered cells undergo binary fission to increase and spread population on the surface.³¹⁸ This is typically in a mushroom shape allowing for the passage of nutrients to bacteria that exist at the surface of the biofilm.³¹⁴ A lag phase is observed before an exponential growth phase that allows for rapid population growth. To allow for strong adhesion between the rapidly increasing cells polysaccharide polymers and divalent cations are used. The final stages of biofilm development is reached when the cell division rate is balanced by the cell death rate. Then the dead cells are released by the excretion of enzymes that break down the biofilm and release cells back into the environment. This phase also sees the cells released for colonisation of new surfaces.³¹⁹ Fig. 1.23 shows a simplified schematic of the five stages.

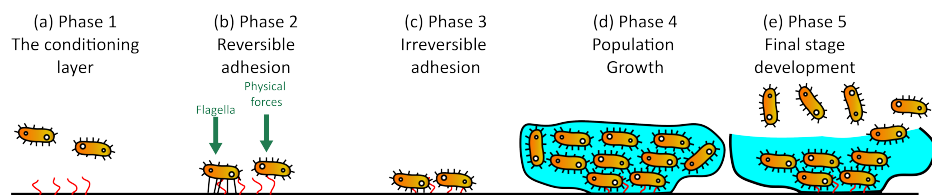


Figure 1.23: Life cycle of biofilm: (a) layer conditioning, (b) reversible adhesion, (c) irreversible adhesion, (d) population growth and (e) final stage development.

1.7.4. Chronic infection

Chronic infections have been linked to the persisting pathology of biofilms. However this connection has only been made recently.^{300,301,320,321} It has been determined that chronic infections do not occur when planktonic microbials are present, these are able to be eradicated by antimicrobial treatments fairly easily. Chronic infection only occur when biofilm forming colonies are present.³²¹ Chronic infections are characterised by slower progression compared to that of acute infections, ambiguous symptoms (inflammation and tissue damage), and are very difficult to treat with antibiotics. This can make it very difficult to research new treatments. Combating chronic infections inside of the body has been extremely difficult due to

the starvation response, whereby bacteria become more tolerant to antibiotics in the absence of a food source.³¹⁰ As the hosts defences (immune system) and proliferating bacteria consume all available nutrients the increased scarcity results in the activation of the starvation response. This can lead to a decrease in the effectiveness of antibiotics, having a further affect of increasing the likelihood of antibiotic resistant genes evolve. In biofilms, this is more likely to occur as it is difficult for nutrients to penetrate into the biofilm. It has been found that in particular beta-lactam antibiotics are unable to penetrate biofilms and require higher doses to be effective.³²² Therefore, the starvation response in conjunction with decreased antibiotic penetration can result in the emergence of antibiotic resistant bacteria. In turn this has the possibility to produce antibiotic resistant microbials, such as methicillin-resistant *Staphylococcus aureus* (*S. aureus*) (MRSA), known as super bugs and can cause severe problems such as bloodstream infections, pneumonia and surgical site infections.^{323,324}

1.7.5. Antimicrobials and antifouling

Biofilms are a major threat to patients who have undergone any type of surgery or insertion of a foreign medical device (catheters and pacemaker) as it is one of the major sources of chronic infection.^{295,325,326} There has been a great deal of research to try and reduce the prevalence of biofilms in these situations by trying to make more effective antimicrobials or antifouling surfaces. The next sections will discuss new antimicrobials and antifouling surfaces.

1.7.5.1. Antimicrobials

The most commonly known antimicrobials are antibiotics. Antibiotics, such as penicillin, have been used since the 1940's to treat and prevent bacterial infections.^{326,327} Antimicrobials can act in one of two ways: 1) kill any bacteria or 2) inhibit the growth, both of which are helpful in allowing the body's own immune system to eradicate bacterial infection.³²⁸⁻³³⁰ There have been many different classes of antibiotics designed and synthesised that allow for

treatment of almost all bacterial infections. Incorrect and overuse of antibiotics has led to the rise of antibiotic resistant bacteria. The World Health Organisation (WHO)³³¹ has reported that *E. coli*, *K. pneumoniae* (*K. pneumoniae*), *S. aureus*, and *Staphylococcus pneumoniae* (*S. pneumoniae*) are the most common to have antibiotic resistance. Some countries are reporting up to 82% of infections being antibiotic resistant as of 2018, an unprecedented percentage. Another issue that is cause for concern is that there are very few new antibiotic discoveries in recent years, an issue that could mean that one day antibiotics will become ineffective entirely.³³² Consequently, a new class of antibacterial agents must be developed, as there are very few antimicrobials currently that are compatible with treating *in vivo* infections.³³³ Antiseptics are a type of broad antimicrobial that kill bacteria and are most often used by applying (through cream or gel) to open wounds.³³⁴ General antiseptics include silver, hydrogen peroxide, povidone iodine, chlorohexidine and Dakin's solution (most effective against *S. aureus*).^{335,336} The main issue with these antiseptics is the damage to human tissue if not used correctly, for example hydrogen peroxide is more harmful to fibroblasts than bacteria and is not recommended for open wound treatment.³²⁰

Silver is one of the oldest antiseptics and has been used with varying success to treat bacterial infections. For centuries silver dressings (such as bandages) have been used to keep open wounds clean and has been found to have multiple pathways to kill bacteria. The multiple pathways reduce the chance of microbial resistance whilst being much less toxic to human tissue.³³⁷ Although useful there are several limitations. In order to prevent becoming toxic to humans the silver concentration must be controlled, the area of effect is limited to the area of a bandage and requires reapplication due to inactivation. This last limitation is an issue due to silver bandages being used commonly for treatment of burn wounds, which can become infected very quickly.^{338,339} However, like antibiotics, silver resistant bacteria have begun to emerge and making it far more difficult to treat open wounds.³⁴⁰

More recently, NPs have been shown to have antimicrobial effects that outpace other antiseptics or antibiotics, whilst being far less toxic to human cells. It is thought that due

to the high surface area of the NPs they can be used in lower concentrations to achieve the same results as other antimicrobials. Qi *et al.*³⁴¹ created chitosan with copper loaded NPs that showed antibacterial activity at sub- $\mu\text{g/mL}$ levels. Azam *et al.*³⁴² and Adams *et al.*³⁴³ investigated the antibacterial effect of gold and palladium NPs, respectively, and determined that the size of the NPs had to be the correct size to penetrate the cell wall of the bacteria. NPs have also been found to be useful when trying to prevent biofilm formation. De Faria *et al.*³⁴⁴ were able to prevent biofilm formation by exposing bacteria to graphene with biogenic silver NPs while Kalishwaralal *et al.*³³⁸ achieved the same using silver NPs.

Treating preformed biofilms has been far more difficult, often requiring complex NPs such as silver-gold bimetallic NPs to disrupt a biofilm. Mu *et al.*³⁴⁵ designed NPs that were loaded with the antibiotic gentamicin, which allowed for more effective eradication of already formed biofilms. The NPs were far more effective than gentamicin alone, showing promise for eliminating persister cells using already well-established antibiotics. From this it can be concluded that NPs can act as drug delivery vehicles, that transport antimicrobials across the biofilm. By encapsulating the antibiotics with the NPs there is less chance of being inhibited by enzymes or sticking to EPS. The local release also reduces the side effects to the host, in these cases humans. Polymer NPs have also been used as antimicrobials. Beyth *et al.*³⁴⁶ synthesised polyethylenimine NPs which showed bactericidal effects even when encapsulated in a biofilm. The NPs were found to be effective in both *in vivo* and *in vitro* with high biocompatibility.

There have also been attempts to use polymers to combat bacteria and biofilms. Lo-cock *et al.*,³⁴⁴ fabricated polymers that were efficient at removing biofilms by mimicking biological systems. They developed a system to remove biofilms, that were found to be biologically compatible, consisting of positively charged guanylated polymethacrylates. The same group further expanded this work to look at how changing the end groups of the polymers to see if there was a change in antimicrobial activity.³⁴⁷ They found that attaching a cyanovaleric acid and long lipophilic tail increased the antimicrobial potency against both bacteria and fungus. The polymers were even found to be effective against dual-resistant strains of bacteria, such as

vancomycin intermediate *S. aureus* (VISA). This shows that minor alterations to structure of antimicrobials can influence the antimicrobial activity.

Researchers have also explored using naturally occurring antimicrobials systems consisting of the synergetic relationship of peroxidase enzymes (e.g., lactoperoxidase or myeloperoxidase), hydrogenperoxide (H_2O_2), and thiocyanate ion (SCN^-)³⁴⁸ The resulting hypothiocyanite ion ($OSCN^-$) product has been shown to have antimicrobial activity. The production of the $OSCN^-$ is tolerated by the host cells but not invading bacterial cells.³⁴⁹ However, Klebanoff *et al.*³⁵⁰ determined that the components found in growth media often inhibited the antimicrobial activity by reacting with the ($OSCN^-$) before being able to reach bacterial cells, making it difficult to study in laboratory settings. The issue that faces all these techniques is toxicity to organisms being treated. As a result it would be preferred to prevent the occurrence of biofilms rather than to treat them once formed.

1.7.5.2. Antifouling surfaces

As the adage goes 'prevention is better than a cure' and researchers have attempted to prevent the formation of a biofilm rather than trying to eradicate the bacteria after a biofilm has formed. One approach has been to immobilise antibiotics to the surface however this still has the same limitations when dealing with antibiotic resistant bacterial strains.

Hickok and Shapiro³⁵¹ immobilised antibiotics onto surgical implants and found that it was able to decrease adhesion of bacteria, while still allowing for the adhesion of human osteoblastic cells. Another approach was to immobilise bactericidal polymers to a surface that killed any bacteria that came into contact with it.³⁵² The main issue with these surfaces is that once enough bacteria have been killed, the surfaces become inactive and the bacteria are eventually able to adhere and proliferate.

Others have used microtopographies on surfaces that either prevent the adhesion of bacteria to the surface or have bactericidal properties.³⁵³ These microtopographies prevent ad-

hesion of bacterial cells and are commonly used in nature by a variety of different macroorganisms. The most commonly cited is the lotus leaf, which create extreme hydrophobic interactions on the surface that prevent the bacteria from getting close enough to the surface to adhere (due to DLVO)³⁵⁴. Dickson *et al.*³⁵⁵ nanopatterned nanopillars of poly(methyl methacrylate) to both prevent the adherence of bacterial cells and also kill any bacteria that were able to adhere to the surfaces.

All these approaches have had very little success, with most surfaces becoming fouled eventually over time. This can be attributed to the first stage of the biofilm formation, where the bacteria condition the surface. Surfaces that kill bacteria by damaging the cell wall can help this process as bacteria often lyse themselves to condition the surface, essentially hiding the surface modifications.³¹¹ There are multitude of ways to combat bacterial biofilms, but none have yet tried to use DNA. In this thesis we explore the use of G4 aptamer peroxidase-mimicking activity to try eliminating bacterial growth inside of biofilms.

1.8. Summary

Chapter 1 has explored how DNA can be used as a tool for structural or analytical purposes. Dynamic DNA processes are crucial steps for more reliable genotyping and biocomputing, having already been implemented in DNA arrays and logic gates. Toehold-mediated strand displacement shows great promise in the fields of DNA genotyping. With the robustness and reliability being almost unmatched. This technique is possible in solution as well as on surfaces, which offers a variety of applications for this single process. The only issues faced with this technique are cheaper alternatives to fluorophores and increased speeds, especially on surfaces where it can take hours for complete displacement to occur. This thesis develops an improved toehold-mediated strand displacement genotyping technique by using different fluorophores and the intercalator ethidium bromide (Chapter 3).

There are many secondary structures, simple and complex, that can be formed by

DNA depending on length, sequence and environmental conditions. Understanding how these secondary structures form is key to designing successful experiments that rely on DNA structure formation. The most relevant structure for this thesis is the G4, which has many applications for biosensing. G4s show great promise as aptamers that could replace therapeutics and well-established reporter fluorophore systems. It is important to understand the dynamics of the peroxidase-mimicking activity as it will lead to the development and evolution of new sequences that have increased DNAzyme activity. These new sequences will make to cheaper, more robust alternative to the already established ELISA. The work in this thesis investigates G4 sequences with increased peroxidase-mimicking activity by using the GA established by Ikebukuro *et al.*,²¹⁵ as well as possible applications for G4s such as in biosensors or as antimicrobials (Chapters 4, 5 and 6).

1.9. Chapter 1 References

- [1] Watson, J.; Crick, F. Molecular structure of nucleic acids. *Nature*. **1953**, *171*, 737–8.
- [2] Manalo, M. N.; Pérez, L. M.; LiWang, A. Hydrogen-bonding and π - π base-stacking interactions are coupled in DNA, as suggested by calculated and experimental trans-hbond deuterium isotope shifts. *Journal of the American Chemical Society* **2007**, *129*, 11298–11299.
- [3] Yakovchuk, P.; Protozanova, E.; Frank-Kamenetskii, M. D. Base-stacking and base-pairing contributions into thermal stability of the DNA double helix. *Nucleic Acids Research* **2006**, *34*, 564–574.
- [4] Vologodskii, A. V.; Amirikyan, B. R.; Lyubchenko, Y. L.; Frank- Kamenetskii, M. D. Allowance for heterogeneous stacking in the DNA helix-coil transition theory. *Journal of Biomolecular Structure and Dynamics* **1984**, *2*, 131–148.
- [5] Ussery, D. W. *Encyclopedia of Life Sciences*; 2006.
- [6] Zhang, L.; Zhang, R. Y.; Zhu, Z. B.; Du, R.; Shen, W. F. The effect of sirolimus-eluting stent implantation on re- endothelialization: A comparative study with bare-metal stent implantation in rabbits. *Journal of Interventional Radiology* **2009**, *18*, 616–619.
- [7] Protozanova, E.; Yakovchuk, P.; Frank-Kamenetskii, M. D. Stacked-unstacked equilibrium at the nick site of DNA. *Journal of Molecular Biology* **2004**, *342*, 775–785.
- [8] Lesnik, E. A.; Freier, S. M. Relative Thermodynamic Stability of DNA, RNA, and DNA:RNA Hybrid Duplexes: Relationship with Base Composition and Structure. *Biochemistry* **1995**, *34*, 10807–10815.
- [9] Chen, C.; Wang, W.; Wang, Z.; Wei, F.; Zhao, X. S. Influence of secondary structure on

- kinetics and reaction mechanism of DNA hybridization. *Nucleic Acids Research* **2007**, *35*, 2875–2884.
- [10] Allawi, H. T.; SantaLucia, J. Nearest neighbor thermodynamic parameters for internal G.A mismatches in DNA. *Biochemistry* **1998**, *37*, 2170–2179.
- [11] Geggier, S.; Vologodskii, A. Sequence dependence of DNA bending rigidity. *Proceedings of the National Academy of Sciences* **2010**, *107*, 15421–15426.
- [12] Gilbert, N.; Allan, J. Supercoiling in DNA and chromatin. *Current Opinion in Genetics & Development* **2014**, *25*, 15–21.
- [13] Breslauer, K. J.; Frank, R.; Blöcker, H.; Marky, L. A. Predicting DNA duplex stability from the base sequence. *Proceedings of the National Academy of Sciences of the United States of America* **1986**, *83*, 3746–50.
- [14] Arnott, S.; Arnott, S. The sequence dependence of circular dichroism spectra of DNA duplexes. *Nucleic acids research* **1975**, *2*, 1493–502.
- [15] Crothers, D. M.; Zimm, B. H. Theory of the melting transition of synthetic polynucleotides: Evaluation of the stacking free energy. *Journal of Molecular Biology* **1964**, *9*, 1–9.
- [16] Wang, J. C.; Davidson, N. Thermodynamic and kinetic studies on the interconversion between the linear and circular forms of phage lambda DNA. *Journal of Molecular Biology* **1966**, *15*, 111–123.
- [17] Clausen-Schaumann, H.; Rief, M.; Tolksdorf, C.; Gaub, H. E. Mechanical Stability of Single DNA Molecules. *Biophysical Journal* **2000**, *78*, 1997–2007.
- [18] Lindahl, T. Instability and decay of the primary structure of DNA. *Nature* **1993**, *362*, 709–715.
- [19] Chan, K.; Sterling, J. F.; Roberts, S. A.; Bhagwat, A. S.; Resnick, M. A.; Gordenin, D. A.

- Base Damage within Single-Strand DNA Underlies In Vivo Hypermutability Induced by a Ubiquitous Environmental Agent. *PLoS Genetics* **2012**, 8, e1003149.
- [20] cheng Shen, J.; Rideout, W. M.; Jones, P. A. The rate of hydrolytic deamination of 5-methylcytosine in double-stranded DNA. *Nucleic Acids Research* **1994**, 22, 972–976.
- [21] Parikh, S. S.; Mol, C. D.; Tainer, J. A. Base excision repair enzyme family portrait: integrating the structure and chemistry of an entire DNA repair pathway. *Structure* **1997**, 5, 1543–1550.
- [22] Krokan, H. E.; Bjørås, M. Base excision repair. *Cold Spring Harbor Perspectives in Biology* **2013**, 5, 1–22.
- [23] Ahmad, H.; Wragg, A.; Cullen, W.; Wombwell, C.; Meijer, A. J. H. M.; Thomas, J. A. From Intercalation to Groove Binding: Switching the DNA-Binding Mode of Isostructural Transition-Metal Complexes. *Chemistry - A European Journal* **2014**, 20, 3089–3096.
- [24] Dervan, P. B.; Edelson, B. S. Recognition of the DNA minor groove by pyrrole-imidazole polyamides. *Current Opinion in Structural Biology* **2003**, 13, 284–299.
- [25] Dueber, E. L. C.; Corn, J. E.; Bell, S. D.; Berger, J. M. Replication Origin Recognition and Deformation by a Heterodimeric Archaeal Orc1 Complex. *Science* **2007**, 317, 1210 LP – 1213.
- [26] Franklin, R. E.; Gosling, R. G. The structure of sodium thymonucleate fibres. I. The influence of water content. *Acta Crystallographica* **1953**, 6, 673–677.
- [27] Williams, A. A.; Darwanto, A.; Theruvathu, J. A.; Burdzy, A.; Neidigh, J. W.; Sowers, L. C. Impact of Sugar Pucker on Base Pair and Mispair Stability. *Biochemistry* **2009**, 48, 11994–12004.
- [28] Potaman, V. N.; Sinden, R. R. CHAPTER 1 DNA: Alternative Conformations and Biology. *DNA Conformation and Transcription* **2005**, 1–16.

- [29] Berg JM.; Tymoczko JL; Stryer L., *Biochemistry. 5th edition. New York: W H Freeman;* .; 2002.
- [30] Doluca, O.; Withers, J. M.; Filichev, V. V. Molecular engineering of guanine-rich sequences: Z-DNA, DNA triplexes, and G-quadruplexes. *Chemical Reviews* **2013**, *113*, 3044–3083.
- [31] Chaires, J. B. THE JOURNAL OF BIOLOGICAL CHEMISTRY Allosteric Conversion of Z DNA to an Intercalated Right-handed Conformation by Daunomycin*. **1986**, *261*, 8899–8907.
- [32] Ghosh, A.; Bansal, M. A glossary of DNA structures from A to Z. *Acta Crystallographica - Section D Biological Crystallography* **2003**, *59*, 620–626.
- [33] Marmur, J.; Doty, P. Determination of the base composition of deoxyribonucleic acid from its thermal denaturation temperature. *Journal of Molecular Biology* **1962**, *5*, 109–118.
- [34] SantaLucia, J.; Hicks, D. The Thermodynamics of DNA Structural Motifs. *Annual Review of Biophysics and Biomolecular Structure* **2004**, *33*, 415–440.
- [35] SantaLucia, J.; Allawi, H. T.; Seneviratne, P. A. Improved nearest-neighbor parameters for predicting DNA duplex stability. *Biochemistry* **1996**, *35*, 3555–3562.
- [36] SantaLucia, J. A unified view of polymer, dumbbell, and oligonucleotide DNA nearest-neighbor thermodynamics. *Proceedings of the National Academy of Sciences of the United States of America* **1998**, *95*, 1460–5.
- [37] Carlos De Oliveira Guerra, J. ScienceDirect Thermodynamics of Denaturation Transition of DNA Duplex Oligomers in the Context of Nearest Neighbor Models: a short review. *Physics Procedia* **2015**, *68*, 37–42.
- [38] Borer, P. N.; Dengler, B.; Tinoco, I.; Uhlenbeck, O. C. Stability of ribonucleic acid double-stranded helices. *Journal of molecular biology* **1974**, *86*, 843–53.

- [39] Tinoco, I.; Borer, P. N.; Dengler, B.; Levin, M. D.; Uhlenbeck, O. C.; Crothers, D. M.; Bralla, J. Improved estimation of secondary structure in ribonucleic acids. *Nature: New biology* **1973**, *246*, 40–1.
- [40] Uhlenbeck, O. C.; Borer, P. N.; Dengler, B.; Tinoco, I. Stability of RNA hairpin loops: A6-Cm-U6. *Journal of Molecular Biology* **1973**, *73*, 483–496.
- [41] Gotoh, O.; Tagashira, Y. Stabilities of nearest-neighbor doublets in double-helical DNA determined by fitting calculated melting profiles to observed profiles. *Biopolymers* **1981**, *20*, 1033–1042.
- [42] Zadeh, J. N.; Steenberg, C. D.; Bois, J. S.; Wolfe, B. R.; Pierce, M. B.; Khan, A. R.; Dirks, R. M.; Pierce, N. A. Software News and Updates NUPACK: Analysis and Design of Nucleic Acid Systems. *J Comput Chem* **2011**, *32*, 170–173.
- [43] Zuker, M. Mfold web server for nucleic acid folding and hybridization prediction. *Nucleic acids research* **2003**, *31*, 3406–15.
- [44] Gruenwedel, D. W.; Hsu, C. H. Salt effects on the denaturation of DNA. *Biopolymers* **1969**, *7*, 557–70.
- [45] Uhlenhopp, E. L.; Krasna, A. I. Denaturation of DNA at pH 7.0 by acid and alkali. *Nature* **1969**, *223*, 1267–1269.
- [46] Schwinefus, J. J.; Engelsgerd, S.; Mangold, K.; Thompson, P. Urea Induced DNA Denaturation. *Biophysical Journal* **2013**, *104*, 425a.
- [47] Sigma-Aldrich, Melting Temperatures of Oligonucleotides — Sigma-Aldrich. 2017; <http://www.sigmaaldrich.com/technical-documents/articles/biology/oligos-melting-temp.html>.
- [48] Orlandini, E.; Bhattacharjee, S. M.; Marenduzzo, D.; Maritan, A.; Seno, F. Mechanical denaturation of DNA: Existence of a low-temperature denaturation. *Journal of Physics A: Mathematical and General* **2001**, *34*, L751–L758.

- [49] Danilowicz, C.; Coljee, V. W.; Bouzigues, C.; Lubensky, D. K.; Nelson, D. R.; Prentiss, M. DNA unzipped under a constant force exhibits multiple metastable intermediates. *Proceedings of the National Academy of Sciences* **2003**, *100*, 1694–1699.
- [50] Levens, D.; Benham, C. J. DNA stress and strain, in silico, in vitro and in vivo. *Physical Biology* **2011**, *8*.
- [51] Schildkraut, C.; Lifson, S. Dependence of the melting temperature of DNA on salt concentration. *Biopolymers* **1965**, *3*, 195–208.
- [52] MARKHAM, R.; SMITH, J. D. The structure of ribonucleic acid. I. Cyclic nucleotides produced by ribonuclease and by alkaline hydrolysis. *The Biochemical journal* **1952**, *52*, 552–7.
- [53] An, R.; Jia, Y.; Wan, B.; Zhang, Y.; Dong, P.; Li, J.; Liang, X. Non-Enzymatic Depurination of Nucleic Acids: Factors and Mechanisms. *PLoS ONE* **2014**, *9*, e115950.
- [54] Tao, S. C.; Lila, Y.; Liu, Y. H.; Ma, X. M.; Cheng, J. Room-temperature hybridization of target DNA with microarrays in concentrated solutions of guanidine thiocyanate. *BioTechniques* **2003**, *34*, 1260–1262.
- [55] Huang, P. C. Effect of guanidinium ion on DNA denaturation and renaturation. *Biochemical and Biophysical Research Communications* **1968**, *33*, 384–390.
- [56] Summer H, Grämer R, D. P. Denaturing Gel Electrophoresis of RNA and DNA Using Urea-Polyacrylamide Gels. *J Vis EXP* **2009**, *29*, 1485.
- [57] Hu, P. P.; Peng, L.; Zhen, S. J.; Chen, L. Q.; Xiao, S. J.; Huang, C. Z. Homochiral expression of proteins: A discussion on the natural chirality related to the origin of life. *Science China Chemistry* **2010**, *53*, 792–796.
- [58] Amasino, R. M. Acceleration of nucleic acid hybridization rate by polyethylene glycol. *Analytical Biochemistry* **1986**, *152*, 304–307.

- [59] Phillip, Y.; Sherman, E.; Haran, G.; Schreiber, G. Common crowding agents have only a small effect on protein-protein interactions. *Biophysical Journal* **2009**, *97*, 875–885.
- [60] Kessler, C. Enhancement of hybridization of nucleic acids by anionic polymers. *Proceedings of the National Academy of Sciences of the United States of America* **1984**, *748*.
- [61] Wetmur, J. G. Acceleration of DNA renaturation rates. *Biopolymers* **1975**, *14*, 2517–2524.
- [62] Hooyberghs, J.; Van Hummelen, P.; Carlon, E. The effects of mismatches on hybridization in DNA microarrays: Determination of nearest neighbor parameters. *Nucleic Acids Research* **2009**, *37*, e53.
- [63] Smith, S.; Vigilant, L.; Morin, P. A. The effects of sequence length and oligonucleotide mismatches on 5' exonuclease assay efficiency. *Nucleic acids research* **2002**, *30*, e111.
- [64] Li, Y.; Zont, G.; Wilson, W. D. NMR and molecular modeling evidence for a G-A mismatch base pair in a purine-rich DNA duplex. *Biochemistry* **1991**, *88*, 26–30.
- [65] Piao, X.; Sun, L.; Zhang, T.; Gan, Y.; Guan, Y. Effects of mismatches and insertions on discrimination accuracy of nucleic acid probes. *Acta Biochimica Polonica* **2008**, *55*, 713–720.
- [66] Allawi, H. T.; Santalucia, J. Thermodynamics and NMR of internal G.T mismatches in DNA. *Biochemistry* **1997**, *36*, 10581–10594.
- [67] Allawi, H. T.; SantaLucia, J. Nearest-neighbor thermodynamics of internal A.C mismatches in DNA: Sequence dependence and pH effects. *Biochemistry* **1998**, *37*, 9435–9444.
- [68] Allawi, H. T.; SantaLucia, J. Thermodynamics of internal C.T mismatches in DNA. *Nucleic Acids Research* **1998**, *26*, 2694–2701.

- [69] He, L.; Kierzek, R.; SantaLucia, J.; Walter, A. E.; Turner, D. H. Nearest-neighbor parameters for G.cntdot.U mismatches: 5'GU3'/3'UG5' is destabilizing in the contexts CGUG/GUGC, UGUA/AUGU, and AGUU/UUGA but stabilizing in GGUC/CUGG. *Biochemistry* **1991**, *30*, 11124–11132.
- [70] Johnson, S. J.; Beese, L. S. Structures of mismatch replication errors observed in a DNA polymerase. *Cell* **2004**, *116*, 803–816.
- [71] Skelly, J. V.; Edwards, K. J.; Jenkins, T. C.; Neidle, S. Crystal structure of an oligonucleotide duplex containing G.G base pairs: influence of mispairing on DNA backbone conformation. *Proceedings of the National Academy of Sciences* **1993**, *90*, 804–808.
- [72] Tikhomirova, A.; Beletskaya, I. V.; Chalikian, T. V. Stability of DNA duplexes containing GG, CC, AA, and TT mismatches. *Biochemistry* **2006**, *45*, 10563–10571.
- [73] Demidov, V. V.; Frank-Kamenetskii, M. D. Two sides of the coin: affinity and specificity of nucleic acid interactions. *Trends in Biochemical Sciences* **2004**, *29*, 62–71.
- [74] Camden, A. J.; Walsh, S. M.; Suk, S. H.; Silverman, S. K. DNA Oligonucleotide 3-Phosphorylation by a DNA Enzyme. *Biochemistry* **2016**, *55*, 2671–2676.
- [75] Liyanage, V.; Jarmasz, J.; Murugesan, N.; Del Bigio, M.; Rastegar, M.; Davie, J. DNA Modifications: Function and Applications in Normal and Disease States. *Biology* **2014**, *3*, 670–723.
- [76] Morrison, L. E.; Stols, L. M. Sensitive fluorescence-based thermodynamic and kinetic measurements of DNA hybridization in solution. *Biochemistry* **1993**, *32*, 3095–3104.
- [77] Marras, S. A. E. Efficiencies of fluorescence resonance energy transfer and contact-mediated quenching in oligonucleotide probes. *Nucleic Acids Research* **2002**, *30*, 122e–122.
- [78] Sowers, L. C.; Shaw, B. R.; Veigl, M. L.; David Sedwick, W. DNA base modification:

- Ionized base pairs and mutagenesis. *Mutation Research - Fundamental and Molecular Mechanisms of Mutagenesis* **1987**, *177*, 201–218.
- [79] Matteucci, M. D.; Caruthers, M. H. The synthesis of oligodeoxyrimidines on a polymer support. *Tetrahedron Letters* **1980**, *21*, 719–722.
- [80] Sinha, N. D.; Biernat, J.; Mcmanus, J.; Köster, H. Polymer support oligonucleotide synthesis XVIII.1.2: Use of β -cyanoethyl-N,N-dialkylamino-/N-morpholino phosphoramidite of deoxynucleosides for the synthesis of DNA fragments simplifying deprotection and isolation of the final product. *Nucleic Acids Research* **1984**, *12*, 4539–4557.
- [81] Stec, W. J.; Zon, G.; Egan, W.; Stec, B. Automated Solid-Phase Synthesis, Separation, and Stereochemistry of Phosphorothioate Analogues of Oligodeoxyribonucleotides. *Journal of the American Chemical Society* **1984**, *106*, 6077–6079.
- [82] Mikoz, M.; Lajczyk, M.; Kieziński, P. Recent developments in the carbodiimide chemistry. *Tetrahedron* **1981**, *37*, 233–284.
- [83] Manimala, J. C.; Anslyn, E. V. Solid-phase synthesis of guanidinium derivatives from thiourea and isothioureia functionalities. *European Journal of Organic Chemistry* **2002**, *2002*, 3909–3922.
- [84] Ghosh, S. S.; Musso, G. F. Covalent attachment of oligonucleotides to solid supports. *Nucleic Acids Research* **1987**, *15*, 5353–5372.
- [85] Hunkapiller, M. W.; Connell, C. R.; Mordan, W. J.; Lytle, J. D.; Bridgham, J. A. Real time scanning electrophoresis apparatus for DNA sequencing. **1989**,
- [86] van Daal, A. DNA profiling in forensic science and parentage testing. *Australasian biotechnology* **1994**, *4*, 92–96.
- [87] Woolley, A. T.; Mathies, R. A. Ultra-High-Speed DNA Sequencing Using Capillary Electrophoresis Chips. *Analytical Chemistry* **1995**, *67*, 3676–3680.

- [88] Juskowiak, B. Nucleic acid-based fluorescent probes and their analytical potential. *Analytical and Bioanalytical Chemistry* **2011**, *399*, 3157–3176.
- [89] Lytle, F. E.; Desilets, D. J.; Kissinger, P. T. Improved Method for Determination of Stern-Volmer Quenching Constants. *Analytical Chemistry* **1987**, *59*, 1244–1246.
- [90] Didenko, V. V. DNA Probes Using Fluorescence Resonance Energy Transfer (FRET): Designs and Applications. *BioTechniques* **2001**, *31*, 1106–1121.
- [91] Borissevitch, I. E. More about the inner filter effect: Corrections of Stern-Volmer fluorescence quenching constants are necessary at very low optical absorption of the quencher. *Journal of Luminescence* **1999**, *81*, 219–224.
- [92] Bower, M.; Summers, M. F.; Kell, B.; Hoskins, J.; Wilson, W. D. Synthesis and characterization of oligodeoxyribonucleotides containing terminal phosphates. NMR, UV spectroscopic and thermodynamic analysis of duplex formation of [d(PGGAATTCC)]₂, [d(GGAATTCCT)]₂ and [d(PGGAATTCCT)]₂. *Nucleic Acids Research* **1987**, *15*, 3531–3547.
- [93] Moreira, B. G.; You, Y.; Behlke, M. A.; Owczarzy, R. Effects of fluorescent dyes, quenchers, and dangling ends on DNA duplex stability. *Biochemical and Biophysical Research Communications* **2005**, *327*, 473–484.
- [94] Mergny, J. L. Fluorescence energy transfer as a probe for tetraplex formation: The imotif. *Biochemistry* **1999**, *38*, 1573–1581.
- [95] Mergny, J. L.; Maurizot, J. C. Fluorescence resonance energy transfer as a probe for G-quartet formation by a telomeric repeat. *ChemBioChem* **2001**, *2*, 124–132.
- [96] Sigmon, J.; Larcom, L. L. The effect of ethidium bromide on mobility of DNA fragments in agarose gel electrophoresis. *Electrophoresis* **1996**, *17*, 1524–1527.
- [97] McMaster, G. K.; Carmichael, G. G. Analysis of single- and double-stranded nucleic acids on polyacrylamide and agarose gels by using glyoxal and acridine orange. *Pro-*

ceedings of the National Academy of Sciences of the United States of America **1977**, *74*, 4835–4838.

- [98] Taylor, I. W.; Milthorpe, B. K. An evaluation of DNA fluorochromes, staining techniques, and analysis for flow cytometry. I. Unperturbed cell populations. *Journal of Histochemistry and Cytochemistry* **1980**, *28*, 1224–1232.
- [99] Ma, H.; Wallbank, R. W. R.; Chaji, R.; Li, J.; Suzuki, Y.; Jiggins, C.; Nathan, A. An impedance-based integrated biosensor for suspended DNA characterization. *Scientific Reports* **2013**, *3*, 2730.
- [100] Higuchi, R.; Dollinger, G.; Sean Walsh, P.; Griffith, R. Simultaneous amplification and detection of specific DNA sequences. *Bio/Technology* **1992**, *10*, 413–417.
- [101] Tavassoli, M.; Tavassoli, M. H.; Shall, S. Effect of DNA intercalators on poly(ADP-ribose) glycohydrolase activity. *Biochimica et Biophysica Acta (BBA) - Protein Structure and Molecular Enzymology* **1985**, *827*, 228–234.
- [102] Jain, N.; Francis, S.; Friedman, S. H. Inhibition of therapeutically important polymerases with high affinity bis-intercalators. *Bioorganic & medicinal chemistry letters* **2012**, *22*, 4844–8.
- [103] Zhu, J. D.; Sun, X. P.; Wang, F. The DNA intercalator, ethidium bromide, alters the pattern of DNase I hypersensitive sites of the beta A-globin gene in chicken erythrocytes. *Biochimica et biophysica acta* **1991**, *1089*, 158–66.
- [104] LERMAN, L. S. Structural considerations in the interaction of DNA and acridines. *Journal of molecular biology* **1961**, *3*, 18–30.
- [105] Glazer, A. N.; Rye, H. S. Stable dye–DNA intercalation complexes as reagents for high-sensitivity fluorescence detection. *Nature* **1992**, *359*, 859–861.
- [106] Biebricher, A. S.; Heller, I.; Roijmans, R. F.; Hoekstra, T. P.; Peterman, E. J.; Wuite, G. J.

The impact of DNA intercalators on DNA and DNA-processing enzymes elucidated through force-dependent binding kinetics. *Nature Communications* **2015**, *6*, 7304.

- [107] Welch, J. J.; Rauscher, F. J.; Beerman, T. A. Targeting DNA-binding drugs to sequence-specific transcription factor-DNA complexes. Differential effects of intercalating and minor groove binding drugs. *The Journal of biological chemistry* **1994**, *269*, 31051–8.
- [108] Toulmé, J. J.; Krisch, H. M.; Loreau, N.; Thuong, N. T.; Hélène, C. Specific inhibition of mRNA translation by complementary oligonucleotides covalently linked to intercalating agents. *Proceedings of the National Academy of Sciences of the United States of America* **1986**, *83*, 1227–31.
- [109] Wheate, N. J.; Brodie, C. R.; Collins, J. G.; Kemp, S.; Aldrich-Wright, J. R. DNA intercalators in cancer therapy: organic and inorganic drugs and their spectroscopic tools of analysis. *Mini reviews in medicinal chemistry* **2007**, *7*, 627–48.
- [110] Johnson, I. M.; Kumar, S. G. B.; Malathi, R. De-intercalation of Ethidium Bromide and Acridine Orange by Xanthine Derivatives and Their Modulatory Effect on Anticancer Agents: A study of DNA-directed Toxicity Enlightened by Time Correlated Single Photon Counting. *Journal of Biomolecular Structure and Dynamics* **2003**, *20*, 677–685.
- [111] Lin, S.; Gao, W.; Tian, Z. R.; Yang, C.; Lu, L. H.; Mergny, J. L.; Leung, C. H.; Ma, D. L. Luminescence switch-on detection of protein tyrosine kinase-7 using a G-quadruplex-selective probe. *Chemical Science* **2015**, *6*, 4284–4290.
- [112] Hess, G.; Arnold, W.; Möller, B.; Gahl, G. M.; Meyer zum Büschenfelde, K. H. Inhibition of hepatitis B virus specific DNA polymerase by intercalating agents. *Medical Microbiology and Immunology* **1980**, *168*, 25–34.
- [113] Bianco, P. R.; Brewer, L. R.; Corzett, M.; Balhorn, R.; Yeh, Y.; Kowalczykowski, S. C.; Baskin, R. J. Processive translocation and DNA unwinding by individual RecBCD enzyme molecules. *Nature* **2001**, *409*, 374–378.

- [114] Finkelstein, I. J.; Visnapuu, M.-L.; Greene, E. C. Single-molecule imaging reveals mechanisms of protein disruption by a DNA translocase. *Nature* **2010**, *468*, 983–987.
- [115] Paramanathan, T.; Vladescu, I.; McCauley, M. J.; Rouzina, I.; Williams, M. C. Force spectroscopy reveals the DNA structural dynamics that govern the slow binding of Actinomycin D. *Nucleic Acids Research* **2012**, *40*, 4925–4932.
- [116] Pohl, F. M.; Jovin, T. M.; Baehr, W.; Holbrook, J. J. Ethidium Bromide as a Cooperative Effector of a DNA Structure. *Proceedings of the National Academy of Sciences* **1972**, *69*, 3805–3809.
- [117] McMurray, C. T.; van Holde, K. E. Binding of ethidium bromide causes dissociation of the nucleosome core particle. *Proceedings of the National Academy of Sciences of the United States of America* **1986**, *83*, 8472–6.
- [118] Shearer, C. J.; Yu, L. P.; Fenati, R.; Sibley, A. J.; Quinton, J. S.; Gibson, C. T.; Ellis, A. V.; Andersson, G. G.; Shapter, J. G. Adsorption and Desorption of Single-Stranded DNA from Single-Walled Carbon Nanotubes. *Chemistry - An Asian Journal* **2017**, *12*, 1625–1634.
- [119] Benveniste, A. L.; Creeger, Y.; Fisher, G. W.; Ballou, B.; Waggoner, A. S.; Armitage, B. A. Fluorescent DNA nanotags: supramolecular fluorescent labels based on intercalating dye arrays assembled on nanostructured DNA templates. *Journal of the American Chemical Society* **2007**, *129*, 2025–34.
- [120] Greschner, A. A.; Bujold, K. E.; Sleiman, H. F. Intercalators as molecular chaperones in DNA self-assembly. *Journal of the American Chemical Society* **2013**, *135*, 11283–11288.
- [121] Hayashi, M.; Harada, Y. Direct observation of the reversible unwinding of a single DNA molecule caused by the intercalation of ethidium bromide. *Nucleic Acids Research* **2007**, *35*, e125.

- [122] Nojima, T.; Kondoh, Y.; Takenaka, S.; Ichihara, T.; Takagi, M.; Tashiro, H.; Matsumoto, K. Detection of DNA hybridization by use of a lanthanide fluorescent intercalator that specifically binds to double stranded DNA. *Nucleic Acids Research Supplement* 105–106.
- [123] Murade, C. U.; Subramaniam, V.; Otto, C.; Bennink, M. L. Interaction of oxazole yellow dyes with DNA studied with hybrid optical tweezers and fluorescence microscopy. *Biophysical Journal* **2009**, *97*, 835–843.
- [124] Paik, D. H.; Perkins, T. T. Dynamics and multiple stable binding modes of DNA intercalators revealed by single-molecule force spectroscopy. *Angewandte Chemie - International Edition* **2012**, *51*, 1811–1815.
- [125] Günther, K.; Mertig, M.; Seidel, R. Mechanical and structural properties of YOYO-1 complexed DNA. *Nucleic Acids Research* **2010**, *38*, 6526–6532.
- [126] Sischka, A.; Toensing, K.; Eckel, R.; Wilking, S. D.; Sewald, N.; Ros, R.; Anselmetti, D. Molecular mechanisms and kinetics between DNA and DNA binding ligands. *Biophysical Journal* **2005**, *88*, 404–411.
- [127] Rocha, M. S.; Ferreira, M. C.; Mesquita, O. N. Transition on the entropic elasticity of DNA induced by intercalating molecules. *Journal of Chemical Physics* **2007**, *127*, 105108.
- [128] Ughetto, G.; Wang, A. H.; Quigley, G. J.; van der Marel, G. A.; van Boom, J. H.; Rich, A. A comparison of the structure of echinomycin and triostin a complexed to a DNA fragment. *Nucleic Acids Research* **1985**, *13*, 2305–2323.
- [129] Wang, A. H.; Ughetto, G.; Quigley, G. J.; Rich, A. Interactions between an Anthracycline Antibiotic and DNA: Molecular Structure of Daunomycin Complexed to d(CpGpTpApCpG) at 1.2-Å Resolution. *Biochemistry* **1987**, *26*, 1152–1163.
- [130] Bond, P. J.; Langridge, R.; Jennette, K. W.; Lippard, S. J. X-ray fiber diffraction evidence

for neighbor exclusion binding of a platinum metallointercalation reagent to DNA. *Proceedings of the National Academy of Sciences of the United States of America* **1975**, *72*, 4825–4829.

- [131] Rao, S. N.; Kollman, P. a. Molecular mechanical simulations on double intercalation of 9-amino acridine into d(CGCGCGC) X d(GCGCGCG): analysis of the physical basis for the neighbor-exclusion principle. *Proceedings of the National Academy of Sciences* **1987**, *84*, 5735–5739.
- [132] Nafisi, S.; Saboury, A. A.; Keramat, N.; Neault, J. F.; Tajmir-Riahi, H. A. Stability and structural features of DNA intercalation with ethidium bromide, acridine orange and methylene blue. *Journal of Molecular Structure* **2007**, *827*, 35–43.
- [133] Tullius, T. D.; Lippard, S. J. Ethidium bromide changes the nuclease-sensitive DNA binding sites of the antitumor drug cis-diamminedichloroplatinum(II) (intercalator/exonuclease III/DNA sequence determination/combinational chemotherapy). *Biochemistry* **1982**, *79*, 3489–3492.
- [134] Afsar, T.; Trembley, J. H.; Salomon, C. E.; Razak, S.; Khan, M. R.; Ahmed, K. Growth inhibition and apoptosis in cancer cells induced by polyphenolic compounds of *Aca-cia hydaspica*: Involvement of multiple signal transduction pathways. *Scientific Reports* **2016**, *6*, 23077.
- [135] Olmsted, J.; Kearns, D. R. Mechanism of Ethidium Bromide Fluorescence Enhancement on Binding to Nucleic Acids. *Biochemistry* **1977**, *16*, 3647–3654.
- [136] Jain, S. C.; Sobell, H. M. Visualization of drug-nucleic acid interactions at atomic resolution. Vii. structure of an ethidium/dinucleoside monophosphate crystalline complex, ethidium: Uridylyl(3'-5')adenosine. *Journal of Biomolecular Structure and Dynamics* **1984**, *1*, 1161–1177.
- [137] Muravenko, O. V.; Amosova, A. V.; Samatadze, T. E.; Popov, K. V.; Poletaev, A. I.; Zelenin, A. V. 9-Aminoacridine: An efficient reagent to improve human and plant chro-

- mosome banding patterns and to standardize chromosome image analysis. *Cytometry* **2003**, *51A*, 52–57.
- [138] Hunter, C. A.; Lawson, K. R.; Perkins, J.; Urch, C. J. Aromatic interactions. *Journal of the Chemical Society, Perkin Transactions 2* **2001**, *0*, 651–669.
- [139] Šponer, J.; Leszczynski, J.; Hobza, P. Hydrogen bonding, stacking and cation binding of DNA bases. *Journal of Molecular Structure: THEOCHEM* **2001**, *573*, 43–53.
- [140] Bugs, M. R.; Cornelio, M. L. Analysis of the ethidium bromide bound to DNA by photoacoustic and FTIR spectroscopy. *Photochem Photobiol* **2001**, *74*, 512–520.
- [141] Ke, Y.; Bellot, G.; Voigt, N. V.; Fradkov, E.; Shih, W. M. Two design strategies for enhancement of multilayer-DNA-origami folding: Underwinding for specific intercalator rescue and staple-break positioning. *Chemical Science* **2012**, *3*, 2587–2597.
- [142] Hong, F.; Jiang, S.; Wang, T.; Liu, Y.; Yan, H. 3D Framework DNA Origami with Layered Crossovers. *Angewandte Chemie - International Edition* **2016**, *55*, 12832–12835.
- [143] Tsu-Ju, F.; Seeman, N. C. DNA Double-Crossover Molecules. *Biochemistry* **1993**, *32*, 3211–3220.
- [144] Bjorndal, M. T.; Fygenson, D. K. DNA melting in the presence of fluorescent intercalating oxazole yellow dyes measured with a gel-based assay. *Biopolymers* **2002**, *65*, 40–44.
- [145] Fujita, H.; Imaizumi, Y.; Kasahara, Y.; Kitadume, S.; Ozaki, H.; Kuwahara, M.; Sugimoto, N. Structural and affinity analyses of G-quadruplex DNA aptamers for camptothecin derivatives. *Pharmaceuticals* **2013**, *6*, 1082–1093.
- [146] Qian, L.; Wang, Y.; Zhang, Z.; Zhao, J.; Pan, D.; Zhang, Y.; Liu, Q.; Fan, C.; Hu, J.; He, L. Analogic China map constructed by DNA. *Chinese Science Bulletin* **2006**, *51*, 2973–2976.
- [147] Rungroj, N.; Nettuwakul, C.; Sudtachat, N.; Praditsap, O.; Sawasdee, N.; Sritipayawan, S.; Chuawattana, D.; Thai Yenchitsomanus, P. A whole genome SNP genotyp-

- ing by DNA microarray and candidate gene association study for kidney stone disease. *BMC Medical Genetics* **2014**, *15*, 50.
- [148] Kim S; Misra A., SNP Genotyping: Technologies and Biomedical Applications. *Annual Review of Biomedical Engineering* **2007**, *9*, 289–320.
- [149] Liang, X.; Kuhn, H.; Frank-Kamenetskii, M. D. Monitoring single-stranded DNA secondary structure formation by determining the topological state of DNA catenanes. *Biophysical journal* **2006**, *90*, 2877–89.
- [150] Praetorius, F.; Kick, B.; Behler, K. L.; Honemann, M. N.; Weuster-Botz, D.; Dietz, H. Biotechnological mass production of DNA origami. *Nature* **2017**, *552*, 84–87.
- [151] Han, D.; Pal, S.; Nangreave, J.; Deng, Z.; Liu, Y.; Yan, H. DNA origami with complex curvatures in three-dimensional space. *Science* **2011**, *332*, 342–346.
- [152] Marras, A. E.; Zhou, L.; Su, H.-J.; Castro, C. E. Programmable motion of DNA origami mechanisms. *Proceedings of the National Academy of Sciences* **2015**, *112*, 713–718.
- [153] Zhang, F. T.; Nie, J.; Zhang, D. W.; Chen, J. T.; Zhou, Y. L.; Zhang, X. X. Methylene blue as a G-quadruplex binding probe for label-free homogeneous electrochemical biosensing. *Analytical Chemistry* **2014**, *86*, 9489–9495.
- [154] Puchkova, A.; Vietz, C.; Pibiri, E.; Wünsch, B.; Sanz Paz, M.; Acuna, G. P.; Tinnefeld, P. DNA Origami Nanoantennas with over 5000-fold Fluorescence Enhancement and Single-Molecule Detection at 25 μm . *Nano Letters* **2015**, *15*, 8354–8359.
- [155] Liu, Y.; Dong, B.; Wu, Z.; Fang, W.; Zhou, G.; Shen, A.; Zhou, X.; Hu, J. Toehold-mediated DNA logic gates based on host-guest DNA-GNPs. *Chemical Communications* **2014**, *50*, 12026–12029.
- [156] Kuzyk, A.; Laitinen, K. T.; Törmä, P. DNA origami as a nanoscale template for protein assembly. *Nanotechnology* **2009**, *20*, 235305.

- [157] Wilner, O. I.; Willner, I. Functionalized DNA nanostructures. *Chemical Reviews* **2012**, *112*, 2528–2556.
- [158] Johnson, R. E.; Haracska, L.; Prakash, L.; Prakash, S. Role of Hoogsteen Edge Hydrogen Bonding at Template Purines in Nucleotide Incorporation by Human DNA Polymerase. *Molecular and Cellular Biology* **2006**, *26*, 6435–6441.
- [159] Jain, A.; Wang, G.; Vasquez, K. M. DNA triple helices: Biological consequences and therapeutic potential. *Biochimie* **2008**, *90*, 1117–1130.
- [160] Stiehl, O.; Weidner-Hertrampf, K.; Weiss, M. Kinetics of conformational fluctuations in DNA hairpin-loops in crowded fluids. *New Journal of Physics* **2013**, *15*, 8602–6.
- [161] Antao, V. P.; Tinoco, I. Thermodynamic parameters for loop formation in RNA and DNA hairpin tetraloops. *Nucleic Acids Research* **1992**, *20*, 819–824.
- [162] Siddiqui-Jain, A.; Grand, C. L.; Bearss, D. J.; Hurley, L. H. Direct evidence for a G-quadruplex in a promoter region and its targeting with a small molecule to repress c-MYC transcription. *Proceedings of the National Academy of Sciences of the United States of America* **2002**, *99*, 11593–8.
- [163] Van Dyke, M. W. Do DNA Triple Helices or Quadruplexes Have a Role in Transcription? *DNA Conformation and Transcription* **2005**, 105–126.
- [164] Pauling, L.; Corey, R. B. A Proposed Structure For The Nucleic Acids. *Proceedings of the National Academy of Sciences of the United States of America* **1953**, *39*, 84–97.
- [165] Akiyama, T.; Hogan, M. E. Structural analysis of dna bending induced by tethered triple helix forming oligonucleotides. *Biochemistry* **1997**, *36*, 2307–2315.
- [166] Nielsen, P. E. Design of sequence-specific DNA-binding ligands. *Chemistry - A European Journal* **1997**, *3*, 505–508.
- [167] POSTEL, E. H. Modulation of c-myc Transcription by Triple Helix Formation. *Annals of the New York Academy of Sciences* **1992**, *660*, 57–63.

- [168] Liu, K.; Miles, H. T.; Frazier, J.; Sasisekharan, V. A novel DNA duplex. A parallel-stranded DNA helix with Hoogsteen base pairing. *Biochemistry* **1993**, *32*, 11802–11809.
- [169] Bikard, D.; Loot, C.; Baharoglu, Z.; Mazel, D. Folded DNA in Action: Hairpin Formation and Biological Functions in Prokaryotes. *Microbiology and Molecular Biology Reviews* **2010**, *74*, 570–588.
- [170] Masai, H.; Arai, K. I. DnaA- and PriA-dependent primosomes: Two distinct replication complexes for replication of Escherichia coli chromosome. *Front Biosci* **1996**, *1*, d48–58.
- [171] Paull, T. T.; Gellert, M. The 3 to 5 exonuclease activity of Mre11 facilitates repair of DNA double-strand breaks. *Molecular Cell* **1998**, *1*, 969–979.
- [172] Dai, X.; Greizerstein, M. B.; Nadas-Chinni, K.; Rothman-Denes, L. B. Supercoil-induced extrusion of a regulatory DNA hairpin. *Pnas* **1997**, *94*, 2174–9.
- [173] Guéron, M.; Leroy, J.-L. The i-motif in nucleic acids. *Current Opinion in Structural Biology* **2000**, *10*, 326–331.
- [174] Zeraati, M.; Langley, D. B.; Schofield, P.; Moye, A. L.; Rouet, R.; Hughes, W. E.; Bryan, T. M.; Dinger, M. E.; Christ, D. I-motif DNA structures are formed in the nuclei of human cells. *Nature Chemistry* **2018**, *10*, 631–637.
- [175] Benabou, S.; Aviñó, A.; Eritja, R.; González, C.; Gargallo, R. Fundamental aspects of the nucleic acid i-motif structures. *RSC Advances* **2014**, *4*, 26956–26980.
- [176] Phan, A. T.; Guéron, M.; Leroy, J. L. The solution structure and internal motions of a fragment of the cytidine-rich strand of the human telomere. *Journal of Molecular Biology* **2000**, *299*, 123–144.
- [177] Louis Leroy, J.; Guéron, M.; Louis Mergny, J.; Hélène, C. Intramolecular folding of a fragment of the cytosine-rich strand of telomeric DNA into an I-motif. *Nucleic Acids Research* **1994**, *22*, 1600–1606.

- [178] Nonin-Lecomte, S.; Leroy, J. L. Structure of a C-rich strand fragment of the human centromeric satellite III: A pH-dependent intercalation topology. *Journal of Molecular Biology* **2001**, *309*, 491–506.
- [179] Bang, I. Untersuchungen über die Guanylsäure. *Biochemische Zeitschrift* **1910**, *26*, 293–311.
- [180] GELLERT, M.; LIPSETT, M. N.; DAVIES, D. R. Helix formation by guanylic acid. *Proceedings of the National Academy of Sciences of the United States of America* **1962**, *48*, 2013–8.
- [181] Campbell, N. H.; Parkinson, G. N. Crystallographic studies of quadruplex nucleic acids. *Methods* **2007**, *43*, 252–263.
- [182] Adrian, M.; Heddi, B.; Phan, A. T. NMR spectroscopy of G-quadruplexes. *Methods* **2012**, *57*, 11–24.
- [183] Moon, I. K.; Jarstfer, M. B. *G-Quadruplex DNA: Methods and Protocols*; 2010; Vol. 608; pp 51–63.
- [184] Cheng, X.; Liu, X.; Bing, T.; Cao, Z.; Shangguan, D. General peroxidase activity of G-quadruplex-hemin complexes and its application in ligand screening. *Biochemistry* **2009**, *48*, 7817–7823.
- [185] Wu, T.; Ye, M.; Mao, T.; Lin, F.; Hu, Y.; Gan, N.; Shao, Y. Human telomeric hybrid-2-over-hybrid-1 G-quadruplex targeting and a selective hypersaline-tolerant sensor using abasic site-engineered monomorphism. *Analytica Chimica Acta* **2017**, *964*, 161–169.
- [186] Hazel, P.; Parkinson, G. N.; Neidle, S. Predictive modelling of topology and loop variations in dimeric DNA quadruplex structures. *Nucleic Acids Research* **2006**, *34*, 2117–2127.
- [187] Huppert, J. L. Four-stranded nucleic acids: Structure, function and targeting of G-quadruplexes. *Chemical Society Reviews* **2008**, *37*, 1375–1384.

- [188] Chambers, V. S.; Marsico, G.; Boutell, J. M.; Di Antonio, M.; Smith, G. P.; Balasubramanian, S. High-throughput sequencing of DNA G-quadruplex structures in the human genome. *Nature Biotechnology* **2015**, *33*, 877–881.
- [189] Giancola, C.; Pagano, B. Energetics of ligand binding to G-quadruplexes. *Topics in Current Chemistry* **2013**, *330*, 211–242.
- [190] Callén, E.; Surrallés, J. Telomere dysfunction in genome instability syndromes. *Mutation Research/Reviews in Mutation Research* **2004**, *567*, 85–104.
- [191] von Zglinicki, T. Telomeres, telomerase and the cancer cell: an introduction. *Cancer letters* **2003**, *194*, 137–8.
- [192] Stampfer, M. R.; Yaswen, P. Human epithelial cell immortalization as a step in carcinogenesis. *Cancer letters* **2003**, *194*, 199–208.
- [193] Saretzki, G. Telomerase inhibition as cancer therapy. *Cancer letters* **2003**, *194*, 209–19.
- [194] Neidle, S.; Parkinson, G. Telomere maintenance as a target for anticancer drug discovery. *Nature Reviews Drug Discovery* **2002**, *1*, 383–393.
- [195] Gowan, S. M.; Harrison, J. R.; Patterson, L.; Valenti, M.; Read, M. A.; Neidle, S.; Kelland, L. R. A G-quadruplex-interactive potent small-molecule inhibitor of telomerase exhibiting in vitro and in vivo antitumor activity. *Molecular pharmacology* **2002**, *61*, 1154–62.
- [196] Hurley, L. H. DNA and its associated processes as targets for cancer therapy. *Nature Reviews Cancer* **2002**, *2*, 188–200.
- [197] Paramasivan, S.; Rujan, I.; Bolton, P. H. Circular dichroism of quadruplex DNAs: Applications to structure, cation effects and ligand binding. *Methods* **2007**, *43*, 324–331.
- [198] Hammond-Kosack, M. C.; Kilpatrick, M. W.; Docherty, K. The human insulin gene-linked polymorphic region adopts a G-quartet structure in chromatin assembled in vitro. *Journal of molecular endocrinology* **1993**, *10*, 121–6.

- [199] Piazza, A.; Adrian, M.; Samazan, F.; Heddi, B.; Hamon, F.; Serero, A.; Lopes, J.; Teulade-Fichou, M.-P.; Phan, A. T.; Nicolas, A. Short loop length and high thermal stability determine genomic instability induced by G-quadruplex-forming minisatellites. *The EMBO Journal* **2015**, *34*, 1718–1734.
- [200] Lane, A. N.; Chaires, J. B.; Gray, R. D.; Trent, J. O. Stability and kinetics of G-quadruplex structures. *Nucleic acids research* **2008**, *36*, 5482–5515.
- [201] Hardin, C. C.; Henderson, E.; Watson, T.; Prosser, J. K. Monovalent cation induced structural transitions in telomeric DNAs: G-DNA folding intermediates. *Biochemistry* **1991**, *30*, 4460–4472.
- [202] Venczel, E. A.; Sen, D. Parallel and antiparallel G-DNA structures from a complex telomeric sequence. *Biochemistry* **1993**, *32*, 6220–6228.
- [203] Bhattacharyya, D.; Mirihana Arachchilage, G.; Basu, S. Metal Cations in G-Quadruplex Folding and Stability. *Frontiers in chemistry* **2016**, *4*, 38.
- [204] Arnott, S.; Chandrasekaran, R.; Marttila, C. M. Structures for polyinosinic acid and polyguanylic acid. *The Biochemical journal* **1974**, *141*, 537–43.
- [205] Sundquist, W. I.; Klug, A. Telomeric DNA dimerizes by formation of guanine tetrads between hairpin loops. *Nature* **1989**, *342*, 825–829.
- [206] Kang, C.; Zhang, X.; Ratliff, R.; Moyzis, R.; Rich, A. Crystal structure of four-stranded Oxytricha telomeric DNA. *Nature* **1992**, *356*, 126–131.
- [207] Hud, N. V.; Smith, F. W.; Anet, F. A.; Feigon, J. The selectivity for K⁺ versus Na⁺ in DNA quadruplexes is dominated by relative free energies of hydration: A thermodynamic analysis by ¹H NMR. *Biochemistry* **1996**, *35*, 15383–15390.
- [208] Akhshi, P.; Mosey, N. J.; Wu, G. Free-energy landscapes of ion movement through a G-quadruplex DNA channel. *Angewandte Chemie - International Edition* **2012**, *51*, 2850–2854.

- [209] Sassano, M. F.; Schlesinger, A. P.; Jarstfer, M. B. Identification of G-Quadruplex Inducers Using a Simple, Inexpensive and Rapid High Throughput Assay, and Their Inhibition of Human Telomerase. *The open medicinal chemistry journal* **2012**, *6*, 20–8.
- [210] Hardin, C. C.; Perry, A. G.; White, K. Thermodynamic and kinetic characterization of the dissociation and assembly of quadruplex nucleic acids. 2000.
- [211] Blume, S. W.; Guarcello, V.; Zacharias, W.; Miller, D. M. Divalent transition metal cations counteract potassium-induced quadruplex assembly of oligo(dG) sequences. *Nucleic Acids Research* **1997**, *25*, 617–625.
- [212] Batsanov, S. Van der Waals Radii of Elements. *Inorganic Materials Translated from Neorganicheskie Materialy Original Russian Text* **2001**, *37*, 871–885.
- [213] Woody, R. W. *Circular Dichroism and the Conformational Analysis of Biomolecules*; Springer US: Boston, MA, 1996; pp 25–67.
- [214] Kelly, S. M.; Jess, T. J.; Price, N. C. How to study proteins by circular dichroism. *Biochimica et Biophysica Acta - Proteins and Proteomics* **2005**, *1751*, 119–139.
- [215] Ikebukuro, K.; Okumura, Y.; Sumikura, K.; Karube, I. A novel method of screening thrombin-inhibiting DNA aptamers using an evolution-mimicking algorithm. *Nucleic Acids Research* **2005**, *33*, 1–7.
- [216] Cao, Z.; Huang, C. C.; Tan, W. Nuclease resistance of telomere-like oligonucleotides monitored in live cells by fluorescence anisotropy imaging. *Analytical Chemistry* **2006**, *78*, 1478–1484.
- [217] Tuerk, C.; Gold, L. Systematic evolution of ligands by exponential enrichment: RNA ligands to bacteriophage T4 DNA polymerase. *Science* **1990**, *249*, 505–510.
- [218] Li, H.; Park, S. H.; Reif, J. H.; LaBean, T. H.; Yan, H. DNA-Templated Self-Assembly of Protein and Nanoparticle Linear Arrays. *Journal of the American Chemical Society* **2004**, *126*, 418–419.

- [219] Zhou, W.; Jimmy Huang, P. J.; Ding, J.; Liu, J. Aptamer-based biosensors for biomedical diagnostics. *Analyst* **2014**, *139*, 2627–2640.
- [220] Balogh, Z.; Lautner, G.; Bardóczy, V.; Komorowska, B.; Gyurcsányi, R. E.; Mészáros, T. Selection and versatile application of virus-specific aptamers. *The FASEB Journal* **2010**, *24*, 4187–4195.
- [221] Sundaram, P.; Kurniawan, H.; Byrne, M. E.; Wower, J. Therapeutic RNA aptamers in clinical trials. *European Journal of Pharmaceutical Sciences* **2013**, *48*, 259–271.
- [222] Apte, R. S. Pegaptanib sodium for the treatment of age-related macular degeneration. *Expert opinion on pharmacotherapy* **2008**, *9*, 499–508.
- [223] Sarai, A.; Kono, H. Protein-DNA Recognition Patterns and Predictions. *Annual Review of Biophysics and Biomolecular Structure* **2005**, *34*, 379–398.
- [224] Chai, C.; Xie, Z.; Grotewold, E. SELEX (systematic evolution of ligands by exponential enrichment), as a powerful tool for deciphering the protein-DNA interaction space. *Methods in Molecular Biology* **2011**, *754*, 249–258.
- [225] Travascio, P.; Li, Y.; Sen, D. DNA-enhanced peroxidase activity of a DNA aptamer-hemin complex. *Chemistry and Biology* **1998**, *5*, 505–517.
- [226] Einarson, O. J.; Sen, D. Self-biotinylation of DNA G-quadruplexes via intrinsic peroxidase activity. *Nucleic Acids Research* **2017**, *45*, 9813–9822.
- [227] Pfeiffer, F.; Tolle, F.; Rosenthal, M.; Brändle, G. M.; Ewers, J.; Mayer, G. Identification and characterization of nucleobase-modified aptamers by click-SELEX. *Nature Protocols* **2018**, *13*, 1153–1180.
- [228] Yokobayashi, Y.; Ikebukuro, K.; McNiven, S.; Karube, I. Directed evolution of trypsin inhibiting peptides using a genetic algorithm. *Journal of the Chemical Society - Perkin Transactions 1* **1996**, *0*, 2435–2437.

- [229] Qin, H.; Ren, J.; Wang, J.; Luedtke, N. W.; Wang, E. G-quadruplex-modulated fluorescence detection of potassium in the presence of a 3500-fold excess of sodium ions. *Analytical Chemistry* **2010**, *82*, 8356–8360.
- [230] Ren, J.; Qin, H.; Wang, J.; Luedtke, N. W.; Wang, E.; Wang, J. Label-free detection of nucleic acids by turn-on and turn-off G-quadruplex-mediated fluorescence. *Analytical and Bioanalytical Chemistry* **2011**, *399*, 2763–2770.
- [231] Lu, L.-M.; Zhang, X.-B.; Kong, R.-M.; Yang, B.; Tan, W. A Ligation-Triggered DNAzyme Cascade for Amplified Fluorescence Detection of Biological Small Molecules with Zero-Background Signal. *Journal of the American Chemical Society* **2011**, *133*, 11686–11691.
- [232] Fang, G.; Cech, T. R. The beta subunit of Oxytricha telomere-binding protein promotes G-quartet formation by telomeric DNA. *Cell* **1993**, *74*, 875–85.
- [233] Giraldo, R.; Rhodes, D. The yeast telomere-binding protein RAP1 binds to and promotes the formation of DNA quadruplexes in telomeric DNA. *The EMBO journal* **1994**, *13*, 2411–20.
- [234] Harrington, C.; Lan, Y.; Akman, S. A. The identification and characterization of a G4-DNA resolvase activity. *The Journal of biological chemistry* **1997**, *272*, 24631–6.
- [235] Baran, N.; Pucshansky, L.; Marco, Y.; Benjamin, S.; Manor, H. The SV40 large T-antigen helicase can unwind four stranded DNA structures linked by G-quartets. *Nucleic Acids Research* **1997**, *25*, 297–303.
- [236] Enokizono, Y.; Konishi, Y.; Nagata, K.; Ouhashi, K.; Uesugi, S.; Ishikawa, F.; Katahira, M. Structure of hnRNP D complexed with single-stranded telomere DNA and unfolding of the quadruplex by heterogeneous nuclear ribonucleoprotein D. *The Journal of biological chemistry* **2005**, *280*, 18862–70.
- [237] Sun, H.; Karow, J. K.; Hickson, I. D.; Maizels, N. The Bloom's syndrome helicase unwinds G4 DNA. *The Journal of biological chemistry* **1998**, *273*, 27587–92.

- [238] Sun, H.; Yabuki, A.; Maizels, N. A human nuclease specific for G4 DNA. *Proceedings of the National Academy of Sciences of the United States of America* **2001**, *98*, 12444–9.
- [239] Leonetti, C. Biological Activity of the G-Quadruplex Ligand RHPS4 (3,11-Difluoro-6,8,13-trimethyl-8H-quinolo[4,3,2-kl]acridinium methosulfate) Is Associated with Telomere Capping Alteration. *Molecular Pharmacology* **2004**, *66*, 1138–1146.
- [240] Zahler, A. M.; Williamson, J. R.; Cech, T. R.; Prescott, D. M. Inhibition of telomerase by G-quartet DNA structures. *Nature* **1991**, *350*, 718–720.
- [241] Bryan, T. M.; Jarstfer, M. B. Interrogation of G-quadruplex–protein interactions. *Methods* **2007**, *43*, 332–339.
- [242] Macaya, R. F.; Schultze, P.; Smith, F. W.; Roet, J. A.; Feigon, J. Thrombin-binding DNA aptamer forms a unimolecular quadruplex structure in solution. *Biochemistry* **1993**, *90*, 3745–3749.
- [243] Chhabra, R.; Sharma, J.; Ke, Y.; Liu, Y.; Rinker, S.; Lindsay, S.; Yan, H. Spatially addressable multiprotein nanoarrays templated by aptamer-tagged DNA nanoarchitectures. *Journal of the American Chemical Society* **2007**, *129*, 10304–10305.
- [244] Liu, Y.; Lin, C.; Li, H.; Yan, H. Aptamer-directed self-assembly of protein arrays on a DNA nanostructure. *Angewandte Chemie - International Edition* **2005**, *44*, 4333–4338.
- [245] McRae, E. K. S.; Booy, E. P.; Padilla-Meier, G. P.; McKenna, S. A. On Characterizing the Interactions between Proteins and Guanine Quadruplex Structures of Nucleic Acids. *Journal of nucleic acids* **2017**, *2017*, 9675348.
- [246] Chen, J.; Guo, Y.; Zhou, J.; Ju, H. The Effect of Adenine Repeats on G-quadruplex/hemin Peroxidase Mimicking DNAzyme Activity. *Chemistry - A European Journal* **2017**, *23*, 4210–4215.
- [247] Kosman, J.; Juskowiak, B. Peroxidase-mimicking DNAzymes for biosensing applications: A review. *Analytica Chimica Acta* **2011**, *707*, 7–17.

- [248] Li, Y.; Sen, D. Toward an efficient DNAzyme. *Biochemistry* **1997**, *36*, 5589–5599.
- [249] Evans, S. E.; Mendez, M. A.; Turner, K. B.; Keating, L. R.; Grimes, R. T.; Melchoir, S.; Szalai, V. A. End-stacking of copper cationic porphyrins on parallel-stranded guanine quadruplexes. *Journal of Biological Inorganic Chemistry* **2007**, *12*, 1235–1249.
- [250] Chen, J.; Zhang, J.; Guo, Y.; Li, J.; Fu, F.; Yang, H.-H.; Chen, G. An ultrasensitive electrochemical biosensor for detection of DNA species related to oral cancer based on nuclease-assisted target recycling and amplification of DNAzyme. *Chemical communications (Cambridge, England)* **2011**, *47*, 8004–6.
- [251] Chang, T.; Gong, H.; Ding, P.; Liu, X.; Li, W.; Bing, T.; Cao, Z.; Shanguan, D. Activity Enhancement of G-Quadruplex/Hemin DNAzyme by Flanking d(CCC). *Chemistry - A European Journal* **2016**, *22*, 4015–4021.
- [252] Stefan, L.; Denat, F.; Monchaud, D. Insights into how nucleotide supplements enhance the peroxidase-mimicking DNAzyme activity of the G-quadruplex/hemin system. *Nucleic Acids Research* **2012**, *40*, 8759–8772.
- [253] Nagraj, N.; Liu, J.; Sterling, S.; Wu, J.; Lu, Y. DNAzyme catalytic beacon sensors that resist temperature-dependent variations. *Chemical Communications* **2009**, 4103–4105.
- [254] Xu, S.; Li, Q.; Xiang, J.; Yang, Q.; Sun, H.; Guan, A.; Wang, L.; Liu, Y.; Yu, L.; Shi, Y.; Chen, H.; Tang, Y. Thioflavin T as an efficient fluorescence sensor for selective recognition of RNA G-quadruplexes. *Scientific Reports* **2016**, *6*, 24793.
- [255] Jiang, J.; He, Y.; Yu, X.; Zhao, J.; Cui, H. A homogeneous hemin/G-quadruplex DNAzyme based turn-on chemiluminescence aptasensor for interferon-gamma detection via in-situ assembly of luminol functionalized gold nanoparticles, deoxyribonucleic acid, interferon-gamma and hemin. *Analytica Chimica Acta* **2013**, *791*, 60–64.
- [256] Zou, P.; Liu, Y.; Wang, H.; Wu, J.; Zhu, F.; Wu, H. G-quadruplex DNAzyme-based chemiluminescence biosensing platform based on dual signal amplification for label-free and sensitive detection of protein. *Biosensors and Bioelectronics* **2016**, *79*, 29–33.

- [257] Wu, F.; Wu, Y.; Niu, Z.; Vollmer, F. Integrating a DNA Strand Displacement Reaction with a Whispering Gallery Mode Sensor for Label-Free Mercury (II) Ion Detection. **2016**,
- [258] Pavlov, V.; Xiao, Y.; Gill, R.; Dishon, A.; Kotler, M.; Willner, I. Amplified Chemiluminescence Surface Detection of DNA and Telomerase Activity Using Catalytic Nucleic Acid Labels. *Analytical Chemistry* **2004**, *76*, 2152–2156.
- [259] Xiao, Y.; Pavlov, V.; Niazov, T.; Dishon, A.; Kotler, M.; Willner, I. Catalytic beacons for the detection of DNA and telomerase activity. *Journal of the American Chemical Society* **2004**, *126*, 7430–7431.
- [260] Liu, X.; Hua, X.; Fan, Q.; Chao, J.; Su, S.; Huang, Y. Q.; Wang, L.; Huang, W. Thioflavin T as an Efficient G-Quadruplex Inducer for the Highly Sensitive Detection of Thrombin Using a New Förster Resonance Energy Transfer System. *ACS Applied Materials and Interfaces* **2015**, *7*, 16458–16465.
- [261] Li, W.; Yang, Y.; Yan, H.; Liu, Y. Three-Input Majority Logic Gate and Multiple Input Logic Circuit Based on DNA Strand Displacement.
- [262] Yao, D.; Song, T.; Sun, X.; Xiao, S.; Huang, F.; Liang, H. Integrating DNA-Strand-Displacement Circuitry with Self-Assembly of Spherical Nucleic Acids. *Journal of the American Chemical Society* **2015**, *137*, 14107–14113.
- [263] Wen, Y.; Wang, L.; Li, L.; Xu, L.; Liu, G. A sensitive and Label-Free Pb(II) fluorescence sensor based on a DNAzyme controlled G-Quadruplex/thioflavin T conformation. *Sensors (Switzerland)* **2016**, *16*.
- [264] Elbaz, J.; Moshe, M.; Shlyahovsky, B.; Willner, I. Cooperative multicomponent self-assembly of nucleic acid structures for the activation of DNAzyme cascades: A paradigm for DNA sensors and aptasensors. *Chemistry - A European Journal* **2009**, *15*, 3411–3418.
- [265] Srinivas, N.; Ouldrige, T. E.; Šulc, P.; Schaeffer, J. M.; Yurke, B.; Louis, A. A.; Doye, J.

- P. K.; Winfree, E. On the biophysics and kinetics of toehold-mediated DNA strand displacement. *Nucleic Acids Research* **2013**, *41*, 10641–10658.
- [266] Ouldridge, T. E.; Johnston, I. G.; Louis, A. A.; Doye, J. P. The self-assembly of DNA Holliday junctions studied with a minimal model. *Journal of Chemical Physics* **2009**, *130*.
- [267] Weinert, B. T.; Rio, D. C. DNA strand displacement, strand annealing and strand swapping by the *Drosophila* Bloom's syndrome helicase. *Nucleic Acids Research* **2007**, *35*, 1367–1376.
- [268] Whiting, S. H.; Champoux, J. J. Strand Displacement Synthesis Capability of Moloney Murine Leukemia Virus Reverse Transcriptase. *Journal of Virology* **1994**, *68*, 4747–4758.
- [269] Landon, P. B.; Lee, J.; Hwang, M. T.; Mo, A. H.; Zhang, C.; Neuberger, A.; Meckes, B.; Gutierrez, J. J.; Glinsky, G.; Lal, R. Energetically biased DNA motor containing a thermodynamically stable partial strand displacement state. *Langmuir* **2014**, *30*, 14073–14078.
- [270] Marcovitz, A.; Levy, Y. Obstacles may facilitate and direct DNA search by proteins. *Biophysical Journal* **2013**, *104*, 2042–2050.
- [271] Khodakov, D. A.; Khodakova, A. S.; Linacre, A.; Ellis, A. V. Toehold-Mediated Nonenzymatic DNA Strand Displacement As a Platform for DNA Genotyping. **2013**,
- [272] Park, Y.; Lee, C. Y.; Park, K. S.; Park, H. G. Enzyme-Free Colorimetric Detection of Cu²⁺ by Utilizing Target-Triggered DNAzymes and Toehold-Mediated DNA Strand Displacement Events. *Chemistry - A European Journal* **2017**, *23*, 17379–17383.
- [273] Baltierra-Jasso, L. E.; Morten, M. J.; Magennis, S. W. Sub-Ensemble Monitoring of DNA Strand Displacement Using Multiparameter Single-Molecule FRET. *ChemPhysChem* **2018**, *19*, 551–555.

- [274] Genot, A. J.; Zhang, D. Y.; Bath, J.; Turberfield, A. J. Remote toehold: A mechanism for flexible control of DNA hybridization kinetics. *Journal of the American Chemical Society* **2011**, *133*, 2177–2182.
- [275] Broadwater, D. W.; Kim, H. D. The Effect of Basepair Mismatch on DNA Strand Displacement. *Biophysical Journal* **2016**, *110*, 1476–1484.
- [276] Zhang, Q.; Jagannathan, L.; Subramanian, V. Label-free low-cost disposable DNA hybridization detection systems using organic TFTs. *Biosensors and Bioelectronics* **2010**, *25*, 972–977.
- [277] Khodakov, D. A.; Khodakova, A. S.; Huang, D. M.; Linacre, A.; Ellis, A. V. Protected DNA strand displacement for enhanced single nucleotide discrimination in double-stranded DNA. *Sci Rep* **2015**, *5*, 8721.
- [278] Panyutin, I. G.; Hsieh, P. Formation of a single base mismatch impedes spontaneous DNA branch migration. *Journal of Molecular Biology* **1993**, *230*, 413–424.
- [279] Rossetti, G.; Dans, P. D.; Gomez-Pinto, I.; Ivani, I.; Gonzalez, C.; Orozco, M. The structural impact of DNA mismatches. *Nucleic acids research* **2015**, *43*, 4309–21.
- [280] Tyagi, S.; Bratu, D. P.; Kramer, F. R. Multicolor molecular beacons for allele discrimination. *Nature Biotechnology* **1998**, *16*, 49–53.
- [281] Zhang, Z.; Birkedal, V.; Gothelf, K. V. Enzyme-free colorimetric detection systems based on the DNA strand displacement competition reaction. *New Journal of Physics* **2016**, *18*, 055002.
- [282] Dunn, K. E.; Trefzer, M. A.; Johnson, S.; Tyrrell, A. M. Investigating the dynamics of surface-immobilized DNA nanomachines. *Scientific Reports* **2016**, *6*, 29581.
- [283] Khodakov, D.; Thredgold, L.; Lenehan, C. E.; Andersson, G. G.; Kobus, H.; Ellis, A. V. DNA capture-probe based separation of double-stranded polymerase chain reaction am-

- plification products in poly(dimethylsiloxane) microfluidic channels. *Biomicrofluidics* **2012**, *6*, 26503.
- [284] Wang, D.; Tang, W.; Wu, X.; Wang, X.; Chen, G.; Chen, Q.; Li, N.; Liu, F. Highly selective detection of single-nucleotide polymorphisms using a quartz crystal microbalance biosensor based on the toehold-mediated strand displacement reaction. *Analytical Chemistry* **2012**, *84*, 7008–7014.
- [285] Hwang, M. T.; Landon, P. B.; Lee, J.; Choi, D.; Mo, A. H.; Glinsky, G.; Lal, R. Highly specific SNP detection using 2D graphene electronics and DNA strand displacement. *Proceedings of the National Academy of Sciences* **2016**, *113*, 7088–7093.
- [286] Schena, M.; Shalon, D.; Davis, R. W.; Brown, P. O. Quantitative monitoring of gene expression patterns with a complementary DNA microarray. *Science* **1995**, *270*, 467–470.
- [287] DNA Microarray. <http://learn.genetics.utah.edu/content/labs/microarray/>.
- [288] Kemp, J. T.; Davis, R. W.; White, R. L.; Wang, S. X.; Webb, C. D. A novel method for STR-based DNA profiling using microarrays. *J Forensic Sci* **2005**, *50*, 1109–1113.
- [289] Pourmand, N.; Caramuta, S.; Villablanca, A.; Mori, S.; Karhanek, M.; Wang, S. X.; Davis, R. W. Branch migration displacement assay with automated heuristic analysis for discrete DNA length measurement using DNA microarrays. *Proc Natl Acad Sci U S A* **2007**, *104*, 6146–6151.
- [290] Khodakov, D. A.; Khodakova, A. S.; Linacre, A.; Ellis, A. V. Sequence selective capture, release and analysis of DNA using a magnetic microbead-assisted toehold-mediated DNA strand displacement reaction. *The Analyst* **2014**, 3548–3551.
- [291] Fenati, R. A.; Connolly, A. R.; Ellis, A. V. Single nucleotide polymorphism discrimination with and without an ethidium bromide intercalator. *Analytica Chimica Acta* **2017**, *954*, 121–128.

- [292] Donlan, R. M. Biofilms: Microbial life on surfaces. *Emerging Infectious Diseases* **2002**, 8, 881–890.
- [293] Shim, S. E.; Yashin, V. V.; Isayev, A. I. Ultraschall-devulkanisation von silikonkautschukvulkanisat mit gefällter Kieselsäure. *Gummi, Fasern, Kunststoffe* **2002**, 55, 304–311.
- [294] Costerton, J. W.; Lewandowski, Z.; Caldwell, D. E.; Korber, D. R.; Lappin-Scott, H. M. Microbial Biofilms. *Annual Review of Microbiology* **1995**, 49, 711–745.
- [295] Deva, A. K.; Adams, W. P.; Vickery, K. The role of bacterial biofilms in device-associated infection. *Plastic and Reconstructive Surgery* **2013**, 132, 1319–1328.
- [296] Leeuwenhoek, A. Microscopical observations about animals in the scurf of the teeth. *Philos Trans.* **1684**, 14, 568–574.
- [297] Henrici, A. T. Studies of Freshwater Bacteria 1. A Direct microscopic technique. *Journal of bacteriology* **1933**, 25, 277.
- [298] HØiby, N.; Olling, S. Pseudomonas aeruginosa infection in cystic fibrosis. *APMIS* **1977**, 85, 107–114.
- [299] Costerton, J. W.; Irvin, R. T.; Cheng, K. J. The Bacterial Glycocalyx in Nature and Disease. *Annual Review of Microbiology* **1981**, 35, 299–324.
- [300] Costerton, J. W.; Cheng, K. J.; Geesey, G. G.; Ladd, T. I.; Nickel, J. C.; Dasgupta, M.; Marrie, T. J. Bacterial Biofilms in Nature and Disease. *Annual Review of Microbiology* **1987**, 41, 435–464.
- [301] Costerton, J. W.; Stewart, P. S.; Greenberg, E. P. Bacterial biofilms: A common cause of persistent infections. *Science* **1999**, 284, 1318–1322.
- [302] Bigger, J. Treatment of Staphylococcal Infections With Penicillin By Intermittent Sterilisation. *The Lancet* **1944**, 244, 497–500.

- [303] Moyed, H. S.; Bertrand, K. P. hipA, a newly recognized gene of Escherichia coli K-12 that affects frequency of persistence after inhibition of murein synthesis. *Journal of Bacteriology* **1983**, *155*, 768–775.
- [304] Moyed, H. S.; Broderick, S. H. Molecular cloning and expression of hipA, a gene of Escherichia coli K-12 that affects frequency of persistence after inhibition of murein synthesis. *Journal of Bacteriology* **1986**, *166*, 399–403.
- [305] Scherrer, R.; Moyed, H. S. Conditional impairment of cell division and altered lethality in hipA mutants of Escherichia coli K-12. *Journal of Bacteriology* **1988**, *170*, 3321–3326.
- [306] Black, D. S.; Irwin, B.; Moyed, H. S. Autoregulation of hip, an operon that affects lethality due to inhibition of peptidoglycan or DNA synthesis. *Journal of Bacteriology* **1994**, *176*, 4081–4091.
- [307] Lewis, K. Riddle of biofilm resistance. 2001; <http://www.ncbi.nlm.nih.gov/pubmed/11257008>
<http://www.pubmedcentral.nih.gov/articlerender.fcgi?artid=PMC90417>.
- [308] Lewis, K. Persister cells and the riddle of biofilm survival. *Biochemistry (Moscow)* **2005**, *70*, 267–274.
- [309] Høiby, N.; Bjarnsholt, T.; Givskov, M.; Molin, S.; Ciofu, O. Antibiotic resistance of bacterial biofilms. *International Journal of Antimicrobial Agents* **2010**, *35*, 322–332.
- [310] Nguyen, D.; Joshi-Datar, A.; Lepine, F.; Bauerle, E.; Olakanmi, O.; Beer, K.; McKay, G.; Siehnel, R.; Schafhauser, J.; Wang, Y.; Britigan, B. E.; Singh, P. K. Active starvation responses mediate antibiotic tolerance in biofilms and nutrient-limited bacteria. *Science* **2011**, *334*, 982–986.
- [311] Banerjee, P.; Singh, M.; Sharma, V. BIOFILM Formation: A Comprehensive Review. **2015**, *3*, 556–560.

- [312] Bayles, K. W. The biological role of death and lysis in biofilm development. *Nature Reviews Microbiology* **2007**, *5*, 721–726.
- [313] Sena-Vélez, M.; Redondo, C.; Graham, J. H.; Cubero, J. Presence of extracellular DNA during biofilm formation by *Xanthomonas citri* subsp. *citri* strains with different host range. *PLoS ONE* **2016**, *11*, e0156695.
- [314] Montanaro, L.; Poggi, A.; Visai, L.; Ravaioli, S.; Campoccia, D.; Speziale, P.; Arciola, C. R. Extracellular DNA in biofilms. *International Journal of Artificial Organs* **2011**, *34*, 824–831.
- [315] Belas, R. Biofilms, flagella, and mechanosensing of surfaces by bacteria. *Trends in Microbiology* **2014**, *22*, 517–527.
- [316] Hermansson, M. The DLVO theory in microbial adhesion. *Colloids and Surfaces B: Biointerfaces* **1999**, *14*, 105–119.
- [317] Liu, Y.; Yang, S.-F.; Li, Y.; Xu, H.; Qin, L.; Tay, J.-H. The influence of cell and substratum surface hydrophobicities on microbial attachment. *Journal of Biotechnology* **2004**, *110*, 251–256.
- [318] Costerton, Biofouling and biocorrosion in industrial water systems : proceedings of the . International Workshop on Industrial Biofouling and Biocorrosion,. 1990; p 297.
- [319] Li, W.; Li, Y.; Liu, Z.; Lin, B.; Yi, H.; Xu, F.; Nie, Z.; Yao, S. Insight into G-quadruplex-hemin DNAzyme/RNAzyme: Adjacent adenine as the intramolecular species for remarkable enhancement of enzymatic activity. *Nucleic Acids Research* **2016**, *44*, 7373–7384.
- [320] Ciofu, O.; Rojo-Moliner, E.; Macià, M. D.; Oliver, A. Antibiotic treatment of biofilm infections. *Apmis* **2017**, *125*, 304–319.
- [321] Wolcott, R. D.; Ehrlich, G. D. Biofilms and chronic infections. *JAMA - Journal of the American Medical Association* **2008**, *299*, 2682–2684.

- [322] Singh, R.; Ray, P.; Das, A.; Sharma, M. Penetration of antibiotics through Staphylococcus aureus and Staphylococcus epidermidis biofilms. *Journal of Antimicrobial Chemotherapy* **2010**, *65*, 1955–1958.
- [323] Smith, M. W.; Ghindilis, A. L.; Seoudi, I. A.; Smith, K.; Billharz, R.; Simon, H. M. A new restriction endonuclease-based method for highly-specific detection of DNA targets from methicillin-resistant staphylococcus aureus. *PLoS ONE* **2014**, *9*, e97826.
- [324] Dakheel, K. H.; Abdul Rahim, R.; Neela, V. K.; Al-Obaidi, J. R.; Hun, T. G.; Yusoff, K. Methicillin-Resistant Staphylococcus aureus Biofilms and Their Influence on Bacterial Adhesion and Cohesion. *BioMed Research International* **2016**, *2016*, 1–14.
- [325] Santos, A. P. A.; Watanabe, E.; de Andrade, D. Biofilm on artificial pacemaker: fiction or reality? *Arquivos brasileiros de cardiologia* **2011**, *97*, e113–20.
- [326] Stephen, C. R. First Use of Halothane in the United States. *Annals of Internal Medicine* **2008**, *149*, 135–136.
- [327] Kohanski, M. A.; Dwyer, D. J.; Collins, J. J. How antibiotics kill bacteria: From targets to networks. *Nature Reviews Microbiology* **2010**, *8*, 423–435.
- [328] Ezrow, L.; Saceanu, C.; Dabydeen, H. Range of antibacterial activity of antibiotics at subminimal inhibitory concentrations: The ratio of minimal inhibitory concentration to minimal antibiotic concentration. *Reviews of Infectious Diseases* **1979**, *1*, 821–824.
- [329] Kapoor, G.; Saigal, S.; Elongavan, A. Action and resistance mechanisms of antibiotics: A guide for clinicians. *Journal of Anaesthesiology Clinical Pharmacology* **2017**, *33*, 300.
- [330] Wise, R.; Piddock, L. The need for new antibiotics. *The Lancet* **2010**, *375*, 638.
- [331] WHO - World Health Organization, High levels of antibiotic resistance found worldwide, new data shows. *Media centre* **2018**, 1–7.
- [332] Rolain, J. M.; Abat, C.; Jimeno, M. T.; Fournier, P. E.; Raoult, D. Do we need new antibiotics? *Clinical Microbiology and Infection* **2016**, *22*, 408–415.

- [333] Martínková, N.; Nová, P.; Sablina, O. V.; Graphodatsky, A. S.; Zima, J. Karyotypic relationships of the Tatra vole (*Microtus tatricus*). *Folia Zoologica* **2004**, *53*, 279–284.
- [334] Mackow RC, Argy WP, Winchester JF, Rakowski TA, Fields PA, Rotellar C, S. G. Sclerosing encapsulating peritonitis in rats induced by long-term intraperitoneal administration of antiseptics. *The Journal of laboratory and clinical medicine* **1843**, *112*, 2 p. L., 86 p.
- [335] Doughty, D. A rational approach to the use of topical antiseptics. *Journal of Wound, Ostomy and Continence Nursing* **1994**, *21*, 224–231.
- [336] Clement, J. L.; Jarrett, P. S. Antibacterial Silver. *Metal-Based Drugs* **1994**, *1*, 467–482.
- [337] Tashi, T.; Vishal Gupta, N.; Mbuya, V. B. Silver nanoparticles: Synthesis, mechanism of antimicrobial action, characterization, medical applications, and toxicity effects. *Journal of Chemical and Pharmaceutical Research* **2016**, *8*, 526–537.
- [338] Kalishwaralal, K.; BarathManiKanth, S.; Pandian, S. R. K.; Deepak, V.; Gurunathan, S. Silver nanoparticles impede the biofilm formation by *Pseudomonas aeruginosa* and *Staphylococcus epidermidis*. *Colloids and Surfaces B: Biointerfaces* **2010**, *79*, 340–344.
- [339] Silver, S. Bacterial silver resistance: Molecular biology and uses and misuses of silver compounds. *FEMS Microbiology Reviews* **2003**, *27*, 341–353.
- [340] Qi, L.; Xu, Z.; Jiang, X.; Hu, C.; Zou, X. Preparation and antibacterial activity of chitosan nanoparticles. *Carbohydrate Research* **2004**, *339*, 2693–2700.
- [341] Qi, C.; Zhang, N.; Yan, J.; Liu, X.; Bing, T. RSC Advances Activity enhancement of G-quadruplex / hemin DNAzyme by spermine †. *RSC Adv.* **2014**, *4*, 1441–1448.
- [342] Azam, A.; Ahmed, F.; Arshi, N.; Chaman, M.; Naqvi, A. H. One step synthesis and characterization of gold nanoparticles and their antibacterial activities against *E. coli* (ATCC 25922 strain). *International Journal of Theoretical & Applied Sciences* **2009**, *1*, 1–4.

- [343] Adams, C. P.; Walker, K. A.; Obare, S. O.; Docherty, K. M. Size-dependent antimicrobial effects of novel palladium nanoparticles. *PLoS ONE* **2014**, *9*, e85981.
- [344] De Faria, A. F.; De Moraes, A. C. M.; Marcato, P. D.; Martinez, D. S. T.; Durán, N.; Filho, A. G. S.; Brandelli, A.; Alves, O. L. Eco-friendly decoration of graphene oxide with biogenic silver nanoparticles: Antibacterial and antibiofilm activity. *Journal of Nanoparticle Research* **2014**, *16*, 2110.
- [345] Mu, H.; Tang, J.; Liu, Q.; Sun, C.; Wang, T.; Duan, J. Potent Antibacterial Nanoparticles against Biofilm and Intracellular Bacteria. *Scientific Reports* **2016**, *6*, 5813–5822.
- [346] Beyth, N.; Yudovin-Farber, I.; Perez-Davidi, M.; Domb, A. J.; Weiss, E. I. Polyethyleneimine nanoparticles incorporated into resin composite cause cell death and trigger biofilm stress in vivo. *Proceedings of the National Academy of Sciences* **2010**, *107*, 22038–22043.
- [347] Locock, K. E. S.; Michl, T. D.; Valentin, J. D. P.; Vasilev, K.; Hayball, J. D.; Qu, Y.; Traven, A.; Griesser, H. J.; Meagher, L.; Haeussler, M. Guanylated polymethacrylates: A class of potent antimicrobial polymers with low hemolytic activity. *Biomacromolecules* **2013**, *14*, 4021–4031.
- [348] Tenovuo, J.; Pruitt, K. M.; Thomas, E. L. Peroxidase Antimicrobial System of Human Saliva: Hypothiocyanite Levels in Resting and Stimulated Saliva. *Journal of Dental Research* **1982**, *61*, 982–985.
- [349] Chandler, J. D.; Day, B. J. Thiocyanate: A potentially useful therapeutic agent with host defense and antioxidant properties. *Biochemical Pharmacology* **2012**, *84*, 1381–1387.
- [350] Klebanoff, S. J.; Clem, W. H.; Luebke, R. G. The peroxidase-thiocyanate-hydrogen peroxide antimicrobial system. *BBA - General Subjects* **1966**, *117*, 63–72.
- [351] Hickok, N. J.; Shapiro, I. M. Immobilized antibiotics to prevent orthopaedic implant infections. *Advanced Drug Delivery Reviews* **2012**, *64*, 1165–1176.

- [352] Green, J.-B. D.; Fulghum, T.; Nordhaus, M. a. Immobilized antimicrobial agents: a critical perspective. *Science against microbial pathogens: communicating current research and technological advances* **2011**, 84–98.
- [353] Decker, J. T.; Kirschner, C. M.; Long, C. J.; Finlay, J. A.; Callow, M. E.; Callow, J. A.; Brennan, A. B. Engineered antifouling microtopographies: An energetic model that predicts cell attachment. *Langmuir* **2013**, *29*, 13023–13030.
- [354] Damodaran, V. B.; Murthy, S. N. Bio-inspired strategies for designing antifouling biomaterials. *Biomaterials Research* **2016**, *20*, 18.
- [355] Dickson, M. N.; Liang, E. I.; Rodriguez, L. A.; Vollereaux, N.; Yee, A. F. Nanopatterned polymer surfaces with bactericidal properties. *Biointerphases* **2015**, *10*, 021010.

Chapter 2

Methods and materials

2.1. Synopsis

This chapter contains the information pertaining to the materials, reagents as well as experimental procedures and characterisation techniques used in Chapters 3, 4, 5 and 6. All relevant methods that are used throughout this thesis are described herein, with an explanation of characterisation methods.

2.2. Materials

2.2.1. Chemicals and reagents

All chemicals and reagents used in this thesis can be found in Table 2.1, with details of preparation and storage conditions.

Table 2.1: List of chemicals and reagents.

Name	Manufacturer	Additional information rate
Reverse Osmosis water (RO)	Not applicable	Prepared by filtering through a semi-permeable RO membrane (18.2 MΩcm)
Milli-Q water	Not applicable	Prepared by filtering through resin membrane filters to a resistivity of 18.6 MΩ cm
Dimethyl sulfoxide (DMSO)	Sigma-Aldrich, USA	Used as purchased
10,000X SYBR™ Safe	ThermoFisher Scientific, USA	Diluted in TAE-buffer to 1X
1-ethyl-3-(3-dimethylaminopropyl) carbodiimide	Sigma-Aldrich, USA	Used as purchased, stored at -20 °C
2-(4-morpholinyl) ethane sulfonic acid hydrate (MES)	Sigma-Aldrich, USA	Dissolved in Milli-Q water to make buffer (see Table 2.3)
2,2'-azino-bis(3-ethylbenzothiazoline-6-sulfonic acid) diammonium salt (ABTS)	Wako Pure Chemical Industries Ltd, USA	Dissolved in Milli-Q water to 10 mM
3,3',5,5'-tetramethylbenzidine (TMB)	Wako Pure Chemical Industries Ltd, USA	Dissolved in Milli-Q water to 400 μM
30% acrylamide/Bis solution	Bio-Rad Laboratories, USA	Used as purchased
4-(2-hydroxyethyl)-1-piperazineethanesulfonic acid (HEPES)	Wako Pure Chemical Industries Ltd, USA	Dissolved in Milli-Q water to 1 M
Agar powder	Sigma-Aldrich	Dissolved in RO water to make Mueller-Hinton agar (MHA) 1.5% (w/v) plates, autoclaved for 10 min at 121 °C, stored at 4 °C
Agarose powder	ThermoFisher Scientific, USA	Diluted in Tris-Acetic-EDTA TAE) buffer to 1X
Ammonium persulfate (APS)	Bio-Rad Laboratories	Dissolved in Milli-Q water to make 10% (w/v) solution

Table 2.1: List of chemicals and reagents cont.

Name	Manufacturer	Additional information rate
BacLight Dead/Live kit (SYTO® 9 and propidium)	ThermoFisher Scientific, USA	Dissolved in Milli-Q water, stored at 4 °C
Bovine serum albumin (BSA)	Sigma-Aldrich, USA	Used as purchased, stored at -20 °C
Crystal Violet 2% (w/v)	Sigma-Aldrich, USA	Used as purchased
Ethanolamine	Sigma-Aldrich, USA	Used as purchased
Ethidium bromide (10 mg/mL)	Sigma-Aldrich, USA	Diluted in TAE-buffer to 200 μM
Ethylene diaminetetraacetic acid (EDTA)	Sigma-Aldrich, USA	Dissolved in Milli-Q water to make buffers, pH adjusted using NaOH (1 M) or HCl (1 M) to pH 8.0
Exonuclease 1 (EXO 1)	New England Biolabs, USA	Followed recommended procedure, stored at -20 °C
Fluoroquinolonic acid	Promega, USA	Followed recommended procedure, stored at -20 °C
Glacial acetic acid	Sigma-Aldrich, USA	Dissolved in Milli-Q water to make buffers (see Table 2.3)
GoTaq® Flexi DNA polymerase	Promega, USA	Followed recommended procedure, stored at -20 °C
Hemin	Sigma-Aldrich, USA	Dissolved in DMSO, stored at 4 °C
Hydrogen peroxide 30% (v/v)	Sigma-Aldrich, USA	Diluted in Milli-Q water or buffer
Magnesium chloride	Sigma-Aldrich, USA	Dissolved in Milli-Q water to make buffer (see Table 2.3)
Mitochondrial DNA (mtDNA)	Not applicable	Extracted according to Khodakov <i>et al.</i> ¹
Mueller-Hinton Broth (MHB) (cation adjusted)	Sigma-Aldrich, USA	Dissolved in RO water, autoclaved for 10 min at 121 °C, stored at 4 °C
N,N,N',N'-tetramethylethylenediamine (TEMED)	Sigma-Aldrich, USA	Used as purchased
Oxacillin sodium, 95% salt	Qiagen, Germany	Followed recommended procedure
Pegylated-hemin (PEG-hemin)	National Institute of Material Science (NIMS), Japan	Dissolved in Milli-Q water, stored at 4 °C
Polyethylene glycol 6000 (PEG 6000)	APS Finechem, USA	Dissolved in Milli-Q water to make 10% (w/v) PEG 6000 solution

Table 2.1: List of chemicals and reagents cont.

Name	Manufacturer	Additional information rate
T7 Endonuclease I with NEB 2 buffer	New England Biolabs, USA	Followed recommended procedure, stored at 4 °C
TMB substrate solution	Sigma-Aldrich, USA	Used as purchased, stored at 4 °C
TRIS base	Sigma-Aldrich, USA	Dissolved in Milli-Q water to make buffers (see Table 2.2.3)
Uracil-DNA glycosylase (UDG)	New England Biolabs, USA	Followed recommended procedure, stored at 4 °C
<i>N,N,N',N'</i> -tetramethylethylenediamine (TEMED)	Sigma-Aldrich, USA	Used as purchased
TMB substrate solution	Sigma-Aldrich, USA	Used as purchased, stored at 4 °C
TRIS base	Sigma-Aldrich, USA	Dissolved in Milli-Q water to make buffers (see Table 2.2.3)
Uracil-DNA glycosylase (UDG)	New England Biolabs, USA	Followed recommended procedure, stored at 4 °C

Table 2.2: List of materials

Name	Manufacturer	Additional information rate
20/100 Ladder Oligo length standards	IDT DNA Technology, USA	Diluted according to manufacturer's instructions in TE buffer (see Table 2.3)
30 K Amicon® Ultra Centrifugal Filters	Millipore, Germany	Used as purchased
BcMag™, magnetic beads with <i>N</i> -hydroxysuccinimide (NHS) functionalised surface	Bioclone, USA	Used as purchased, stored at -20 °C
Corning® DNA-Bind 8X 12-wells	Corning Inc, USA	Used as purchased, stored at 4 °C
Costar® Multiple Well Cell Culture Plates: 12-well plate and 96-well plates, flat bottom	Corning Inc, USA	Used as purchased
e-PAGELmini gel 10-20%	ATTO, Japan	Used as purchased
Eppendorph tubes (0.5 - 2 mL)	Eppendorf, Germany	Used as purchased
PCR Tubes, 0.2 ml	QIAGEN, Netherlands	Used as purchased
Petri dishes	Corning Inc, USA	Used as purchased, used to make MHB agar (MHA) plates (see Table 2.1)
Silicone coupons	BioSurface Technologies Corporation, USA	Autoclaved and stored in aseptic conditions
Quick-Load® 50 bp ladder	New England Biolabds, USA	Diluted according to manufacturer's instructions in TE buffer (see Table 2.3)
SYBR® Green I and Gold	Thermo Fisher Scientific, USA	Used as purchased
Novex™ Hi-Density TBE Sample Buffer (5X)	Thermo Fisher Scientific, USA	Used as purchased

Table 2.3: List of buffers

Name	Reagents	Additional information rate
10X ABTS buffer	1.37 M NaCl, 100 mM Phosphate, 27 mM KCl	Dissolved in Milli-Q water, pH adjusted using NaOH (1 M) or HCl (1 M) to pH 6
BcMag™ coupling buffer	Potassium phosphate (10 mM), NaCl (0.15 M)	Used as purchased, pH 5.5
HEPES buffer	1 M HEPES	Dissolved in Milli-Q water, pH adjusted using NaOH (1 M) or HCl (1 M) to pH 9
Corning® DNA-Bind buffer (Corning Inc, USA)	Proprietary	Used as purchased, stored at 4 °C
MES buffer	2-(4-morpholinyl) ethane sulfonic acid hydrate (0.1 M)	Dissolved in Milli-Q water, pH adjusted using NaOH (1 M) or HCl (1 M) to pH 4.5
NEB 2 buffer (New England Biolabs)	Bis-Tris-propane-HCl (10 mM), MgCl ₂ (10 mM), dithiothreitol (1 mM)	Used as purchased, stored at -20 °C
Phosphate buffered saline (PBS)	137 mM NaCl, 10 mM Phosphate, 2.7 mM KCl	Dissolved in Milli-Q water, pH adjusted using NaOH (1 M) or HCl (1 M) to pH 7.5
Novex® Hi-Density TBE Sample Buffer	Thermo Fisher, USA	Used as purchased
Reaction buffer	TRIS base (10 mM), EDTA (1 mM), KCl (50 mM)	Dissolved in Milli-Q water, pH adjusted using NaOH (1 M) or HCl (1 M) to pH 4.5

2.2.2. Oligodeoxynucleotides used for toehold-mediated strand displacement reactions

The following are details about the primers and displacing oligodeoxynucleotide (ODN) sequences used for toehold-mediated strand displacement reactions in Chapter 3.

Table 2.4: Sequences and melting temperature of primers and displacing (DS) ODNs. All ODNs in this table were purchased from IDT DNA Technology (USA), made up to 100 μ M and stored at -20 $^{\circ}$ C.

ODN sequence ^a 5' \Rightarrow 3'		T_m $^{\circ}$ C
Forward primer- dU-4,9	CTAGdUG ₃ dUAG ₄ TG ₂ CT	68.0
Reverse primer- ATTO 647N	ATTO647N—ATGCT ₂ ACA ₂ GCA ₂ GTACAGCA ₂ T	64.1
DS(A)	CTAGTG ₃ TGAG ₄ TG ₂ CT ₃ G ₂ AGT ₂ GCAGT ₂ GAT GTGTGATAGT ₂ GA <u>A</u> G ₂ T ₂ GAT ₂ GCTGTACT ₂ GC T ₂ GTA ₂ GCAT	
DS(T)	CTAGTG ₃ TGAG ₄ TG ₂ CT ₃ G ₂ AGT ₂ GCAGT ₂ GAT GTGTGATAGT ₂ GAT <u>G</u> G ₂ T ₂ GAT ₂ GCTGTACT ₂ GC T ₂ GTA ₂ GCAT	
DS(G)	CTAGTG ₃ TGAG ₄ TG ₂ CT ₃ G ₂ AGT ₂ GCAGT ₂ GAT GTGTGATAGT ₂ GAG <u>G</u> G ₂ T ₂ GAT ₂ GCTGTACT ₂ GC T ₂ GTA ₂ GCAT	
DS(C)	CTAGTG ₃ TGAG ₄ TG ₂ CT ₃ G ₂ AGT ₂ GCAGT ₂ GAT GTGTGATAGT ₂ GAC <u>G</u> G ₂ T ₂ GAT ₂ GCTGTACT ₂ GC T ₂ GTA ₂ GCAT	

^aUnderlined is the complementary nucleotide to the single nucleotide polymorphism (SNP) in the toehold PCR product (TPP) (see Section 2.3.1 for preparation).

2.2.3. Oligodeoxynucleotides for genetic algorithm

The following describes the ODNs used in, and resulting from, a genetic algorithm for G4 screening as per Chapter 4.

Table 2.5: Sequences and melting temperature of G4 ODN sequences that had the highest peroxidase-mimicking activity, EAD-2 and G₃A₃ sequences. All ODNs in this table were purchased from Eurofins Scientific (Japan), made up to 100 μM and stored at 4 °C.

ODN sequence ^α 5' ⇒ 3'	T _m °C	
7-02	G ₃ A ₃ G ₃ CACG ₃ CG ₃	60.8
7-01	G ₃ TA ₃ G ₃ CACG ₃ TG ₃	55.5
5-04	G ₃ A ₃ G ₃ A ₃ CG ₃ CG ₃	56.8
G ₃ A ₃	(G ₃ A ₃) ₃ G ₃	53.4
EAD-2	CT(G ₃ A) ₃ G ₃	52.2

2.2.4. Oligodeoxynucleotides used for enzyme treatment and surface immobilisation onto microplates and microbeads

The following describes the ODNs used for G-quadruplex formation and testing their reactivity to T7 endonuclease I digestion, as described in Chapter 5, Section 5.3.2. This section describes the ODNs used to immobilise to both microplates and microbeads for determination of the peroxidase-mimicking activity, results shown in Chapter 5, Section 5.3.4 and 5.3.6.

Table 2.6: Sequences and melting temperature of G4 ODN sequences that had the highest peroxidase-mimicking activity, EAD-2 and G₃A₃. All ODNs in this table were purchased from Eurofins Scientific (Japan), made up to 100 μM and stored at 4 °C.

ODN sequence ^α 5' ⇒ 3'	T _m °C	
T7 endonuclease I digestion		
G4(G) 001	TAT ₂ G₃ T ₂ G₃ T ₂ G₃ T ₂ G₃ T ₂ GTCA ₂ CTACAGAC TATCA ₂ CT	67.3
G4(G) 002 ^α	AGT ₂ GATAGTC _γ TGTAGT ₂ GAC	47.3
G4(G) 003 ^α	AGT ₂ GATAGTT _γ TGTAGT ₂ GAC	45.7
Microplate and microbead immobilisation		
G4(G) 001	TAT ₂ G₃ T ₂ G₃ T ₂ G₃ T ₂ G₃ T ₂ GTCA ₂ CTACAGAC TATCA ₂ CTT ₂₀ -NH ₂	67.3
G4(G) 002 ^α	AGT ₂ GATAGTC _γ TGTAGT ₂ GAC	47.3
G4(G) 003 ^α	AGT ₂ GATAGTT _γ TGTAGT ₂ GAC	45.7

G4 structure forming sequences are labelled in bold.

The underlined nucleotide in the sequence results in either a perfect match (β) or single mismatch (γ) dsDNA.

^αIndicates the reverse complementary sequence for G4(G) 001 and G4(G) 001T from the 24th nt to the 47th nt.

2.2.5. Antimicrobial studies

2.2.5.1. Oligodeoxynucleotides sequences for G4 formation used for antimicrobial studies

The following shows the ODN sequences used to form G4 structures that were then used in antimicrobial studies as described in this Chapter 6, Section 6.3.3.

Table 2.7: Sequences and melting temperature of ODNs used for antimicrobial studies, including sequences used for coupling with antibiotics (see Section 6.3.1). All ODNs in this table were purchased from IDT DNA (USA), made up to 100 μ M and stored at 4 °C

ODN sequence ^a 5' \implies 3'	T _m °C	
G4	G₃A₃G₃CACG₃CG₃	60.8
NH ₂ G4	NH ₂ —ATGA ₂ T ₂ C ₂ G ₃ A ₃ G₃CACG₃CG₃ CACAC ₂ A—Cy3.5	70.9

G4 structure forming sequences are labelled in bold.

2.2.5.2. Bacterial strains

The following are the bacterial strains used in the antimicrobial studies of the G4 sequences (Section 2.2.5.1) in Chapter 6, Section 6.3.3.

Table 2.8: Strains of non-biofilm and biofilm forming bacteria used to study the affects of G4 ODN in Chapter 6, Section 6.3.2.2. Stored at 4 °C on MHB agar plates.

Strain	Notation	Additional information
<i>Staphylococcus aureus</i> (<i>S. aureus</i>)	ATCC 25923	Non-biofilm forming ²
<i>Staphylococcus aureus</i> (<i>S. aureus</i>)	ATCC 29213	Biofilm forming ³³
<i>Staphylococcus epidermidis</i> (<i>S. epidermidis</i>)	RP62A	Biofilm forming ⁴

2.3. Methods

2.3.1. Toehold-strand displacement analysis

2.3.1.1. PCR amplification of DNA containing one of four SNPs (SNP-A, SNP-T, SNP-G and SNP-C)

PCR was performed using 1X Gotaq® Flexi buffer with a final MgCl₂ concentration of 2.5 mM, 0.2 mM of each standard of deoxynucleic triphosphate (dATP, dTTP, dGTP and dCTP), 0.2 mM of both the forward and reverse primers (Table 2.4) and 5 μg of mtDNA (Table 2.1), isolated according to Khodakov *et al.*¹ The PCR amplification regime used was 95 °C for 15 s, 36 cycles of 94 °C for 15 s, 61 °C for 15 s, 72 °C for 25 s with a final elongation of 72 °C for 1 min.

2.3.1.2. Preparation of toehold PCR products (TPPs)

Directly after PCR was completed, EXO 1 (2.5 U) was added to the PCR tube and the mixture was mixed with a plastic pipette. The PCR mixture was then incubated at 37 °C for 30 min and then 80 °C for 20 min. UDG (2.5 U) was added to the PCR mixture and gently mixed with a plastic pipette. The PCR mixture was incubated at 36 °C for 15 min, 80 °C for 15 min and then cooled to room temperature. This resulted in the production of a 71 bp TPP with a 9 nt toehold overhang.

The PCR mixture is purified using Amicon Ultra 0.5 30K following the manufacturer recommendations and performing the final elution with 1X TEM buffer. Confirmation of PCR amplification was determined using 4% agar gel electrophoresis (see Section 2.4.3). Quantification of the eluted PCR TTP was carried out using a standard curve on a Roto-Gene Q 6-plex real time PCR thermocycler (Qiagen, Germany) (see Section 2.4.2).

2.3.1.3. Toehold-mediated strand displacement reactions

To achieve toe-hold mediated strand displacement, the 71 bp TPP with a 9-nt toehold overhang (2 pmol) was diluted with 1X TEM buffer to 0.15 μL , 15 μL was placed into four individual thin-walled PCR tubes (0.2 mL) and briefly centrifuged. The reaction was carried out with 5 times the concentration of DS over the TPP. DS (DS(A), DS(T), DS(G) and DS(C)) (see Table 2.4) were diluted to 10 pmol (1X TEM buffer) and then each DS was added to one of the lids of the four tubes. The tube lid was then carefully closed, and the tube placed into the thermocycler avoiding mixing of the DS and the TPP before the run protocol started. Acquisition of fluorescent signals was performed within the orange channel (see Section 2.4.2) at a gain of 6.67 within a time interval of 5 s between fluorescent reads. Normalisation of the raw fluorescence was carried out by dividing the signal values by the initial signal value.

2.3.1.4. Toehold-mediated strand displacement reactions in the presence of ethidium bromide

To determine the effect of an intercalating dye, ethidium bromide, on the reaction rate constant and specificity of the toehold-mediated strand displacement reactions, the displacement reactions were carried out as described in Section 2.3.1.3. with the following changes. 71 bp TPP with a 9-nt toehold overhang (2 pmol) and ethidium bromide were dissolved into 1X TEM buffer (15 μL) to a final concentration of 0.15 μL and 11.85 μM , respectively. The solutions were then incubated at a concentration 79X that of the DNA for 1 h prior to the displacement reaction. This ensured that all DNA intercalation sites were filled without a large excess of free ethidium bromide. Based on the TPP length (71 bp in the dsDNA + 9-nt in the toehold) there will be 79 potential sites for ethidium bromide molecules to intercalate in the DNA.

2.3.2. Genetic algorithm for increased peroxidase-mimicking G4 aptamers

2.3.2.1. Folding of G4 structures

The ODN concentrations were measured using a Nanodrop 2000 and then diluted down to 50 μM in a 1X TE buffer. The procedure for folding the G4 was as follows: Each G4 ODNs (50 μM , 4 μL) (see Table 2.5 and Appendix C) was diluted in Reaction buffer (32 μL) containing K^+ ions (50 mM, see Table 2.3). The solution was placed in a thermocycler and first heated to 95 $^{\circ}\text{C}$ then cooled to 30 $^{\circ}\text{C}$ over a 30 min time period. Once cooled, hemin (2 μL) or PEG-hemin (2 μL) was added to a concentration of 8 μM .

2.3.2.2. Circular dichroism

Circular dichroism (CD) was performed by first folding the G4 ODN according to Section 2.3.2.1. The folded G4 ODN solution was then diluted to 2 μM in 50 mM KCl + 10 mM Tris-HCl pH 8.0 buffer. Each sample was then placed in a J-1500 CD Spectrometer (JASCO, Tokyo, Japan) and spectra measured at 220 to 320 nm using a 1 mm path-length cuvette. The baseline of each spectrum was corrected for signal contributions by the buffer with and without the G4 aptamer.

2.3.2.3. TMB assay

In order to measure the peroxidase-mimicking activity of the G4 structures a TMB assay was performed. First a folded G4 solution (5 μM , 5 μL) was added to a 96-well plate. A TMB substrate solution (195 μL , containing H_2O_2 , see Table 2.3) was added to each well. The 96-well plate was then placed in a microplate reader and the absorbance measured at 652 nm every 30 s for 10 min. The results were then analysed using OriginPro 9.0 software applying linear fit function to determine slope of each curve.

2.3.2.4. Michaelis-Menten kinetics

In order to determine the kinetics of the peroxidase-mimicking reaction a Michaelis-Menten model was used.⁵ All G4 sequences (5 μ M) from Table 2.5 were folded as per Section 2.3.2.1 and added to a 96-well plate. To each sequence six different hydrogen peroxide (H_2O_2) concentrations in TMB (295 μ L, without H_2O_2) were added, namely 0, 0.5, 1.0, 2.0, 4.0 or 8.0 mM, carried out in triplicate. The 96-well plate was then placed in a microplate reader and the absorbance at 630 nm measured every 30 s for 10 min. The results were then analysed using OriginPro 9.0 software with a linear fit function to determine the slope of each curve. The slope of the linear fits were then used in the Michaelis-Menten equation (see Chapter 4, Eq. 4.1), to determine the maximum velocity (V_{max}) and Michaelis constant (K_m) of the G4 aptamers.⁵

2.3.3. G4 T7 endonuclease I digestion and immobilisation of 2D and 3D surfaces

2.3.3.1. T7 endonuclease I digestion of G4

Equimolar concentrations of the ODN G4(G) 001 (10 μ M) were added to either G4(C) 002 or G4(T) 003 (see Table 2.6) in a 0.5 mL PCR tube. 5X NEB 2 buffer was then added to make a 1X NEB 2 buffered solution (see Table 2.3). The ODN mixtures were heated to 95 °C and cooled to room temperature over a 30 min time period. T7 endonuclease I (2.5 U) was added and incubated at 37 °C for 1 h, 3 h or overnight, making sure the temperature was kept below 40 °C. The samples were then analysed using native 10-20% (v/v) polyacrylamide gel electrophoresis (PAGE).

2.3.3.2. G4 surface immobilisation onto Corning® DNA-Bind 96-well plates 96-well plates

In order to determine the peroxidase-mimicking activity of immobilised single-stranded G4 on a surface the following procedure was conducted.

For the immobilisation of the G4 sequences (Table 2.6) onto Corning® DNA-Bind 96-well plates (NHS-functionalised) the following procedure was followed: 1 μL of G4(G) 001T (amine-functionalised) ODN (100 μM) was added to 999 μL of immobilisation buffer (100 μL) (Table 2.3) and then 50 μL added to each of the 96-well plate. The wells were left at room temperature for 2 h. The immobilisation buffer was removed and ethanolamine (50 μL) was added and incubated for 10 min to ensure that no unreacted NHS was present on the surface.

2.3.3.3. Wash procedure

The wells were then washed with a 1X SSC wash buffer and with subsequent washes in 0.2X SSC wash buffer and then Milli-Q water. This was done to remove any physisorbed DNA.

2.3.4. TMB assay procedure

G4(G) 001T immobilisation success was then determined by measuring its peroxidase-mimicking activity by first adding 10% w/v hemin in Reaction buffer (5 μL) (Table 2.3) into the well and then adding TMB substrate solution (195 μL , containing H_2O_2 , see Table 2.1). The 96-well plate was then placed in a microplate reader and the absorbance measured at 559 nm every 30 s for 10 min. The results were then analysed using OriginPro 9.0 software applying linear fit function to determine the slope of each curve.

2.3.4.1. ABTS assay for surface immobilised G4 aptamers

In order to measure the peroxidase-mimicking activity of the G4 structures a TMB assay was performed. First a folded G4 solution (5 μM , 5 μL) was added to a 96-well plate. First immobilised G4 aptamers were folded by heating to 70 $^\circ\text{C}$ and cooling to room temperature. Hemin 10% (w/v) solution (5 μL) was added to the wells to form the immobilised G4/hemin

aptamers . A ABTS substrate solution (1 mM ABTS, 0.02% H₂O₂, 50 mM KCl and 1X ABTS buffer) was added to each well. The 96-well plate was then placed in a MTP-880 Lab (SF-6) Microplate reader and the absorbance measured at 414 nm every 30 s for 10 min. The results were then analysed using OriginPro 9.0 software linear fit function to determine slope of each curve.

2.3.4.2. Luminol assay for surface immobilised G4 aptamers

In order to measure the peroxidase-mimicking activity of the G4 structures a TMB assay was performed. First immobilised G4 aptamers were folded by heating to 70 °C and cooling to room temperature. Hemin 10% (w/v) solution (5 µL) was added to the wells to form the immobilised G4/hemin aptamers . 195 µL luminol substrate solution (25 µM HEPES, 20 mM KCl, 200 mM NaCl, 0.5 mM Luminol, 0.5% H₂O₂ and 30 mM Milli-Q water) was added to each well. Hydrogen peroxide 30% (v/v) was added to initiate the reaction and then the 96-well plate was then placed in a MTP-880 Lab (SF-6) Microplate reader and the chemiluminescent signal measured for 5 s. The ANOVA was determined using Microsoft Excel 2016.

2.3.4.3. Surface immobilisation on magnetic beads

To test the peroxidase-mimicking activity of G4 on 3D surfaces G4(G) 001T was immobilised onto NHS-modified magnetic beads (Table 2.2). The following procedure was followed: 10 mg of BeMagTM beads were weighed out, suspended in immobilisation buffer (Table 2.3) and vortexed for 30 s. Amine-modified DNA (100 µM, 10 µL) was added and placed in a thermomixer overnight at 50 °C. The beads were then washed with 1X SSC, 0.2X SSC and Milli-Q water (see Table 2.3). The beads were then stored at 4 °C in TE buffer (10 mg/mL) (Table 2.3). The peroxidase activity of the G4 coupled beads was then tested. Before use the G4 coupled beads were mixed. A 5 µL sample of the mixture was extracted and then placed in a 1 mL cuvette. The peroxidase-mimicking activity was determined by adding

10% (w/v) hemin in reaction buffer (5 μL) into the cuvette and then adding TMB substrate solution (195 μL , containing H_2O_2). The solution was mixed and then placed into a UV/Visible (UV/Vis) spectrophotometer (Varian Cary® 50 UV-Vis Spectrophotometer, Agilent, USA) and the absorbance measured at 559 nm. The results were then analysed using OriginPro 9.0 software linear fit function to determine the slope of each curve.

2.3.4.4. TMB assay for surface immobilised G4 aptamers

In order to measure the peroxidase-mimicking activity of the G4 structures a TMB assay was performed. First immobilised G4 aptamers were folded by heating to 70 °C and cooling to room temperature. A TMB substrate solution (195 μL , containing H_2O_2 , see Table 2.3) was added to each well. The 96-well plate was then placed in a MTP-880 Lab (SF-6) Microplate reader and the absorbance measured at 559 nm every 30 s for 10 min. The results were then analysed using OriginPro 9.0 software linear fit function to determine slope of each curve.

2.3.5. G4 antimicrobial studies

2.3.5.1. Antibiotic coupling to G4 structures

The antibiotics, fluoroquinolonic acid (FQ) or oxacillin (OX), were coupled to the sequence $\text{NH}_2\text{G4}$ (Table 2.7). This was achieved by coupling the carboxylic acid functional group on each antibiotic to the amine functional group on the $\text{NH}_2\text{G4}$ using EDC coupling. Briefly, $\text{NH}_2\text{G4}$ (100 μM , 5 μL) was added to excess antibiotic (45 μL) in 0.1 M MES buffer and vortexed for 60 s. EDC (20% (w/v), 50 μL) in 0.1 M MES buffer was added to the $\text{NH}_2\text{G4}$ antibiotic mixture and vortexed for a further 60 s. The mixture was incubated at 25 °C with alternating shaking for 30 s at 1400 rpm and 30 s of standing for 20 min using a thermomixer. The antibiotic attached ODN was labelled FQG4 and OXG4 after the attachment of fluoroquinolonic acid and oxacillin, respectively.

2.3.5.2. DNA precipitation

After the antibiotic coupling was performed the ODN solutions (FQG4 and OXG4) were precipitated out of solution using the ethanol precipitation method.⁶ In brief, ethanol that was 3 times the volume of the ODN solution was added and chilled to -20 °C overnight. The ODN solution was then centrifuged at 12.3 relative centrifugal force (RCF) for 5 min and the supernatant removed leaving behind a pellet. The pellet was washed with 80% ethanol (20% (v/v) water) and chilled to -20 °C for 2 h, centrifuged for 5 min at 12.3 RCF and the supernatant removed. The ODN pellet was re-suspended in 1X TE buffer (25 µL) (Table 2.3). The concentration of the re-suspended ODNs was determined using a standard curve carried out on a RotoGene Q 6-plex real time PCR thermocycler (Qiagen, Germany) (see Section 2.4.2). By determining the concentration of the DNA, assuming 100% attachment of the antibiotic to ODN, it was possible to determine the concentration of the antibiotic present on the DNA.

2.3.5.3. Bacterial cell preparation

Mueller-Hinton Agar (MHA) (Table 2.1) plates were prepared according to manufacturer's instructions by combining Mueller-Hinton broth (MHB) with agar (Table 2.1) and stored at 4 °C. Before use, the plates were left at room temperature for 10 min or until completely dry inside of a biosafety cabinet. A single colony of cells (*S. aureus* or *S. epidermidis*) was spread onto an MHA plate and grown for 24 h at 37 °C to obtain a fresh colony to be used for inoculation. A single colony from the MHA plate was inoculated into a fresh MHB (10 mL) and incubated at 37 °C for 24 h, with shaking at 75 rpm. After incubation the optical density at 600 nm (OD₆₀₀) and the number of cells was calculated (OD₆₀₀ of 1 is equal to 8×10^8 cells). The bacterial cells were then diluted to $\sim 8 \times 10^5$ in PBS buffer to make a cell suspension.

2.3.5.4. Minimum inhibitory concentration (MIC)

The minimum inhibitory concentration (MIC) was determined using the serial dilutions method. The antibiotics tested were methicillin derived oxacillin (OX) and the previously synthesised OXG4 aptamer (Section 2.3.5.1). OX was diluted from a stock solution (10240 $\mu\text{g}/\text{mL}$) to 8.0, 4.0, 2.0, 1.0, 0.5, 0.25 and 0.125 $\mu\text{g}/\text{mL}$. The OXG4 was diluted to 10.000, 5.000, 2.500, 1.250, 0.625 μM which is equivalent to 2.000, 1.000, 0.500, 0.250 and 0.125 $\mu\text{g}/\text{mL}$ of coupled antibiotic when diluted by a factor of 2. The OX and OXG4 aptamer serial dilutions (20 μL) were added to 96-well plates (ignoring the first column and row). A cell suspension (20 μL) was added to dilute the concentration of all samples by half. The 96-well plate was incubated at 37 °C for 20 h (*S. aureus* ATCC 25923). The plates were then removed, and visual inspection of the plates determined if there was successful growth of bacterial cells. Visual inspection was used to determine if any bacterial growth was successful.

2.3.5.5. Biofilm growth

Biofilm growth was determined through colony forming unit (CFU) assay, crystal violet (CV) staining and confocal fluorescence scanning microscopy (CFSM) of silicone coupons. Biofilms were grown by preparing a cell suspension in MHB (50 μL) (see Section 2.3.5.3) that was then added into 3X 96-well plates (ignoring the first column and row) and incubated at 37 °C for 90 min, shaking at 75 rpm. Afterwards the cell suspension was removed and MHB (1 mL) was replaced and the 96-well plates further incubated for 24 h at 37 °C, with shaking at 75 rpm. The 96-well plates were then washed with PBS solution to remove planktonic cells. One 96-well plate was used to determine the CFU of the biofilms (see Section 2.3.5.7). The two remaining 96-well plates were used for CV staining (see Section 2.3.5.8). These 96-well plates were dried upside down at 60 °C for 1 h prior to use.

2.3.5.6. Growth of biofilms on silicone coupons

At the same time, previously prepared sterilised silicone coupons that had been incubated in bovine serum albumin (BSA) overnight, then washed in PBS solution to remove excess BSA, were placed into a 12-well plate (ignoring the first column and row) with a cell suspension in MHB (1 mL) and incubated at 37 °C for 90 min, with shaking at 75 rpm. Afterwards the cell suspension was removed and the MHB (1 mL) was replaced. The plates were further incubated for 24 h at 37 °C, with shaking at 75 rpm. The silicone coupons are then removed and placed into PBS solution and vortexed for 5 min to remove any planktonic cells and then stained using BacLight Dead/Live kit for 40 min. The coupons were washed with PBS solution and analysed using a Confocal TCSPC fluorescence scanning microscope (CFSM, see Section 2.4.4) with a 100x objective. Blue and yellow excitation with SYTO® 9 and propidium emission filters were used to detect the staining.

2.3.5.7. Colony forming unit (CFU) assay

The drop plate method was used to evaluate the CFU.⁷ Briefly, PBS solution (50 µL) was added to each well that contained a biofilm. Then the biofilm was scratched off using a plastic pipette tip. This was performed 3 times for each well to ensure all the biofilm was removed. The PBS solution with scratched off biofilm from each well was placed in separate Eppendorf tubes and vortexed for 2 min and sonicated for 10 min to break apart the biofilm. Each sample was diluted 10-fold eight times. 10 µL of each dilution for each sample was dropped onto a horizontal MHA plate and the plate was lifted vertically to allow for the drop to run down the plate. The plates were incubated at 37 °C for 20 h. All the spots on each plate were counted, 1 spot was equivalent to 1 CFU, and multiplied by the dilution factor.

2.3.5.8. Crystal violet (CV) staining

The 96-well plates from Section 2.3.5.5 that had been dried upside down at 60 °C for 1 h were used here. Each well within the plate that contained a biofilm was filled with 2% (w/v) crystal violet (100 μ L), making sure to add to the wall and not directly to the surface of the well. The 96-well plate was left at room temperature for 30 min. The crystal violet solution was washed off several times to ensure excess crystal violet was removed. Ethanol (95% (v/v), 200 μ L) was added and incubated for 10 min at room temperature. The ethanol supernatant was then transferred to a new 96-well plate and the OD₆₀₀ measured.

2.4. Characterisation methods

2.4.1. UV/visible spectroscopy: Nanodrop 2000

All ODN concentrations were calculated using UV/vis spectroscopy on a Nanodrop 2000 instrument. Nucleotides have a maximum absorbance peak at 260 nm (A_{260}) and so absorbance at this wavelength can be used to evaluate the DNA.⁸ However, it is important to measure absorbance from 230 nm to 320 nm to determine concentration, purity and the T_m of DNA in a solution. A_{320} is used to measure the turbidity of the solution. At an ODN concentration of 50 μ g/mL with a 1 cm path length the $A_{260} = 1$. Therefore, the concentration is determined by using the following Eq. 2.1:

$$\text{Concentration} \left(\frac{\mu\text{g}}{\text{mL}} \right) = (A_{260} - A_{320}) \times \text{dilutionfactor} \times 33 \frac{\mu\text{g}}{\text{mL}} \quad (2.1)$$

Any molecules, such as proteins, that interfere with the A_{260} value can be quantified using the A_{280} . This is due to aromatic compounds in proteins having an absorbance peak at A_{280} . By using the following Eq. 2.2, the purity of the DNA is quantifiable:

$$\text{DNApurity} = \frac{A_{260} - A_{320}}{A_{280} - A_{320}} \quad (2.2)$$

A DNA purity of 1.7-2.0 is regarded as good-quality DNA, whereas lower values indicate contamination of the DNA solution. To see any other contaminants that are not proteins, such as chaotropic salts or other organic compounds, the measurement at 230 nm is used.⁸ Nanodrop UV-Vis instruments are most often used for this type of analysis as they allow for quantification of DNA at low volumes (2 μL). All synthetic ODN used throughout this thesis was had a purity of ≥ 1.8 .

2.4.2. Roto-Gene Q 6-plex: Real-time thermocycler

All modified, TPP and antibiotic coupled, ODN concentrations and toehold-mediated strand displacement reactions were quantified using a Roto-Gene Q 6-plex. The Roto-Gene Q 6-plex is a real-time PCR (RT-PCR) instrument equipped with 6 excitation and 6 emission channels for fluorescence spectroscopy measurements (see Table 2.9). The software provided with the instrument was used for analysis of data. To determine the concentration of all fluorophore-modified ODNs containing fluorophores a standard curve was generated using the software provided. The standard curve was made up of 0, 0.063, 0.125, 0.250, 0.500, 1.000 μM of fluorophore-modified ODN.

2.4.3. Electrophoresis

Gel electrophoresis is a chromatography method that is used to separate nucleic acids (DNA or RNA) based on nt or bp length.^{9,10} The phosphate-sugar backbone has a single charge per nucleotide, so the charge to weight ratio is 1. However, in native nucleic acid electrophoresis methods there are several factors that can affect the how the nucleic acid strands travel through the gel. Secondary structures such as hair pin loops, G4s and motifs can change the cross-

Table 2.9: Dye channel selection chart with all 6 excitation and 6 emission channels available on the Roto-Gene Q 6-plex.

Channel	Source nm	Detector nm	Compatible dyes
Green	470	510	FAM, SYBR Green1, Fluorescein, Alex Fluor 488
Yellow	530	555	JOE, VIC, HEX, TET, CAL Fluor Gold 540, Yakima Yellow
Orange	585	610	ROX, CAL Fluor Red 610, Cy3.5, Texas Red, Alexa Fluor 568
Red	625	660	Cy5, Quasar 670, Alexa FLuor 633
Crimson	680	710 hp	Quasar705, Alexa Fluor 680
High resolution melt	460	510	SYTO 9, EVAGreen

sectional area of the nucleic acid strand and increase or decrease the rate at which the strand travels through the gel.¹¹ After Gels are primarily made up of agarose or polyacrylamide and form semi-solid porous structures that allow for the diffusion of nucleic acids when a charge is applied. The addition of known ODN weight standards (a ladder) allows for the determination of the nucleic acid length.

For agarose gel electrophoresis the following procedure was followed: a agarose gel 4% (w/v) was prepared by dissolving agar powder in 1X TAE buffer and heating until powder was completely dissolved. 1X SYBR® safe was added to the agar solution and then poured into a mould and cooled for 30 min. Once solidified the agar gel was placed in a Bio-Rad mini electrophoresis tank (Bio-Rad Laboratories, USA) containing 1X TAE buffer. TPP (3 µL) was added to Go Flexi® buffer containing dye (3 µL) and then added to a well in the gel. Electrophoresis was performed at 100 V for 30 min and the gels were imaged on a Gel Doc® (Bio-Rad laboratories, USA).

For the native 10-20% PAGE, that were made in house the following procedure was followed: A separation gel was prepared by mixing 30% (w/v) acrylamide/bis solution (19:1) (3.2 mL), 5X TAE buffer (2.4 mL), 10% (w/v) APS (200 µL) and then made up to 12 mL with

Milli-Q water. TEMED (10 μL) was then added and mixed and this facilitated polymerisation. The mixture (6 mL) was then quickly added to Mini-Protean® gel cassette sandwiches ($\sim \frac{3}{4}$ filled) to allow for the PAGE gel to polymerise. Next a stacking gel was prepared by mixing 30% (w/v) acrylamide/bis solution (19:1) (1.6 mL), 5X TAE buffer (2.4 mL), 10% (w/v) APS (200 μL) and then made up to 12 mL with Milli-Q water. TEMED (10 μL) was then added to begin polymerisation. The stacking gel mixture was then added on top of the separation PAGE gel and Mini-Protean® combs (10 well, 1.0 mm, 44 μL) were inserted. Once the stacking PAGE gel had polymerised the combs were removed.

Once polymerised the gels were inserted into a Mini-Protean® buffer tank (Bio-Rad laboratories, USA) containing 1X TAE buffer. ODN samples (10 μM , 2 μL) were added to Novex Hi-density loading dye (40 μL), Milli-Q water (158 μL) and 5 μL added to each well. PAGE was run at 80 V for 65 min and stained with either SYBR® gold or SYBR Green II.

All gels were viewed using a Gel Doc® using the appropriate viewing plate. The ODN length was determined by using a standard curve extrapolated from the ladder by plotting the known ODN lengths against distance travelled in the gels using Excel software. Gel electrophoresis was used to determine if the PCR was successful and the molecularity of G4s.⁹ For G4 structures if the calculated length was twice, three or four times the actual length of the ODN, then the structure was determined to be intermolecular.

2.4.4. Confocal fluorescence scanning microscopy

All silicone coupon samples with biofilms were analysed using Confocal fluorescence scanning microscopy (CFSM). CFSM is a technique that allows for sample 3D reconstruction.¹² CFSM allows for an image to be viewed not only in the X and Y co-ordinates but also the Z. This is achieved by passing a laser beam through a light source aperture that is focused by an objective. The laser excites any fluorophores that are present in the sample. Light that is emitted by the fluorophores is reflected by a semi-mirror away from the light source and toward

a detector. To reach the detector, the light must first pass through a pin hole objective that only allows the central plane of light through. Emission filters are then used to filter out light that is not the colour of the fluorophores emitted light. Finally, the light reaches a photo-multiplier detector. An image is then built up by scanning the surface of the sample pixel-by-pixel in a raster fashion.

2.5. Chapter 2 References

- [1] Khodakov, D. A.; Khodakova, A. S.; Huang, D. M.; Linacre, A.; Ellis, A. V. Protected DNA strand displacement for enhanced single nucleotide discrimination in double-stranded DNA. *Sci Rep* **2015**, *5*, 8721.
- [2] Singh, R.; Ray, P.; Das, A.; Sharma, M. Penetration of antibiotics through *Staphylococcus aureus* and *Staphylococcus epidermidis* biofilms. *Journal of Antimicrobial Chemotherapy* **2010**, *65*, 1955–1958.
- [3] Mottola, C.; Matias, C. S.; Mendes, J. J.; Melo-Cristino, J.; Tavares, L.; Cavaco-Silva, P.; Oliveira, M. Susceptibility patterns of *Staphylococcus aureus* biofilms in diabetic foot infections. *BMC Microbiology* **2016**, *16*, 119.
- [4] Polonio, R. E.; Mermel, L. A.; Paquette, G. E.; Sperry, J. F. Eradication of biofilm-forming *Staphylococcus epidermidis* (RP62A) by a combination of sodium salicylate and vancomycin. *Antimicrobial Agents and Chemotherapy* **2001**, *45*, 3262–3266.
- [5] Wu, Z.-K.; Zhou, D.-M.; Wu, Z.; Chu, X.; Yu, R.-Q.; Jiang, J.-H. Single-base mismatch discrimination by T7 exonuclease with target cyclic amplification detection. *Chem. Commun.* **2015**, *51*, 2954–2956.
- [6] Shapiro, D. J. Quantitative ethanol precipitation of nanogram quantities of DNA and RNA. *Analytical Biochemistry* **1981**, *110*, 229–231.
- [7] Ruban, A. V.; Korzhavyi, P. A.; Johansson, B. First-principles theory of magnetically driven anomalous ordering in bcc Fe-Cr alloys. *Physical Review B - Condensed Matter and Materials Physics* **2008**, *77*, 179–83.
- [8] Desjardins, P. R.; Conklin, D. S. Microvolume quantitation of nucleic acids. *Current Protocols in Molecular Biology* **2011**,

- [9] Moon, I. K.; Jarstfer, M. B. *G-Quadruplex DNA: Methods and Protocols*; 2010; Vol. 608; pp 51–63.
- [10] Sigmon, J.; Larcom, L. L. The effect of ethidium bromide on mobility of DNA fragments in agarose gel electrophoresis. *Electrophoresis* **1996**, *17*, 1524–1527.
- [11] Summer H, Grämer R, D. P. Denaturing Gel Electrophoresis of RNA and DNA Using Urea-Polyacrylamide Gels. *J Vis EXP* **2009**, *29*, 1485.
- [12] BRAKENHOFF, G. J.; VOORT, H. T. M. V. D.; SPRONSEN, E. A. V.; NANNINGA, N. Three-Dimensional Imaging by Confocal Scanning Fluorescence Microscopy. *Annals of the New York Academy of Sciences* **1986**, *483*, 405–415.

Chapter 3

Investigation of the effect of ethidium bromide on toehold-mediated strand displacement

3.1. Synopsis

This Chapter details the investigation of the effect of the DNA intercalator ethidium bromide on the toehold-mediated strand displacement reaction for improved genotyping of single nucleotide polymorphisms (SNPs). In order to achieve this a modified method described by Khodakov et al.¹ was used, as set out in Chapter 2, Section 2.3.1.1 to 2.3.1.4. First, a polymerase chain reaction (PCR) was performed using mitochondrial DNA (mtDNA), which contained one of the four possible SNPs (adenine (A), thymine (T), guanine (G) or cytosine (C)), using modified primers. These modified primers included: a forward primer modified with a fluorophore, used for detection of the PCR product, and a reverse primer modified with deoxy-uracil (dU), which allowed for the fabrication of a toehold for toehold-mediated strand displacement reactions in the presence of a displacing sequence. After purification of the PCR product displacing sequences (complementary strands of deoxy-nucleic acid (DNA)), containing

a dark quencher, were added to the purified PCR product and the fluorescence quenching measured to determine the SNP identity. The fluorophore, 6-fluorescein (6-FAM), used in previous literature,¹ could not be used in this study as it has overlapping excitation wavelengths to that of the intercalating ethidium bromide to be studied. Therefore, the fluorophores ATTO 550 and ATTO 647 were evaluated.

*Sections 3.3.2.2 and 3.3.3 of this chapter have been published in Fenati, R. A.; Connolly, A. R.; Ellis, A. V. Single nucleotide polymorphism discrimination with and without an ethidium bromide intercalator. Anal. Chim. Acta. **2017**, 954, 121–128.*

3.2. introduction and purpose

Genotyping of DNA is used to determine subtle differences in the genome of living organisms. SNPs are examples of these minute differences where a single base change in a DNA sequence can occur in at least 1% of a population. These single base changes come about due to mutations occurring in an individual's genome, or passed down from parents. The detection of SNPs is therefore useful for medical diagnostics as they can be used as biomarkers for genetic diseases.² This Chapter uses toehold-mediated strand displacement reactions in order to identify SNPs in real-life DNA samples that are often used for evolutionary studies.³ In this work the hyper variable region 1 (HV1) of mitochondrial DNA (mtDNA), that is known to contain an SNP, was amplified using PCR and genotyped using the toehold-mediated strand displacement reaction. The HV1 region of mtDNA is routinely used for forensic and evolutionary studies, and so makes an excellent example of how toehold-mediated strand displacement reactions can be used for analysis of real-life DNA.⁴ The mtDNA used in this Chapter was the same as prepared by Khodakov *et al.*¹ and all verification data can be found in their manuscript. This mtDNA was used in this thesis to evaluate the efficacy of ethidium bromide on toehold-mediated strand displacement reactions. A schematic of the full method of toehold-mediated strand displacement reactions is shown in Fig. 3.1.

In brief, a forward primer (purple) containing deoxy-uracils (dUs) (orange boxes) and a reverse primer (red) labelled with a fluorophore (F) were used to amplify a region of mtDNA (Fig. 3.1, Step 1). PCR was performed to synthesise a double-stranded DNA (dsDNA) SNP PCR product (so-called SPP, Fig. 3.1, Step 1). This SPP contained the dUs at the 5th and 9th position on the incumbent strand (purple) and was labelled with a fluorophore on the target strand (red). A toehold PCR product (TPP) was then generated by digesting the SPP with the enzymes exonuclease 1 (EXO 1) and uracil-DNA glycosylase (UDG) (Fig. 3.1, Step 2). The digestion of the two dUs in the incumbent strand allow for a toehold to be created of 9-nucleotides (nts) long. To perform the toehold-mediated strand displacement reaction a

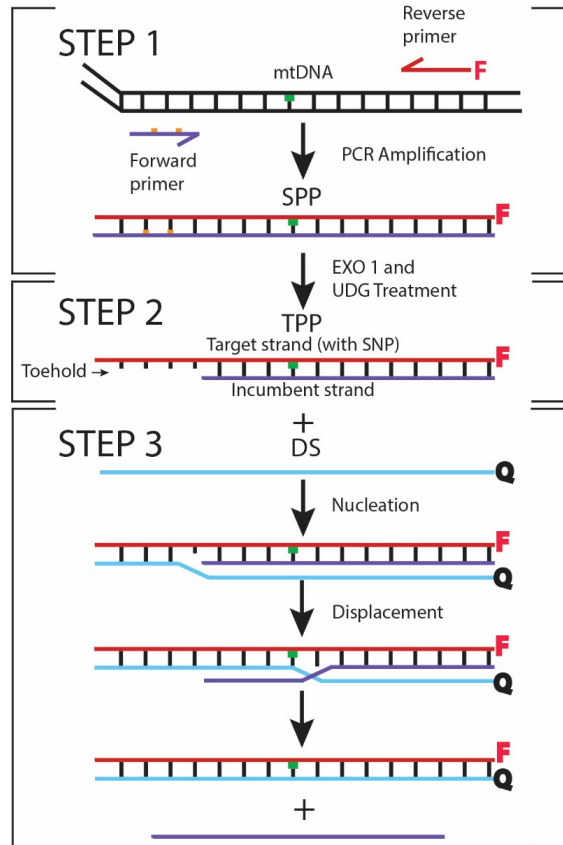


Figure 3.1: Schematic of toehold-mediated strand displacement. Step 1: A region of the template mitochondrial DNA (mtDNA, black) that contains the single nucleotide polymorphism (SNP, green) is amplified with PCR using the modified reverse (red) primer labelled with a fluorophore (F) and the forward primer (purple) which contains deoxy-uracils (dUs, orange) at the 5th and 9th position. This creates multiple copies of the SNP PCR product (SPP), a copy of the region of the template mtDNA, with the fluorophore (F) and dUs at the 5th and 9th position on the target strand (red) and incumbent strand (purple), respectively. Step 2: The toehold PCR product (TPP) is then formed by the digestion of the SPP of step 1 with uracil-DNA glycosylase (UDG) to remove the dUs which creates a short toehold on the incumbent strand (purple). Step 3: The displacing sequence (DS) (light blue) containing a quencher (Q) is added to the TPP in solution and nucleates with the toehold of the incumbent strand. Toehold-mediated strand displacement then proceeds as the DS hybridises, nucleating at the toehold, with the target strand of the TPP until the incumbent strand of the TPP is completely displaced into solution. Static quenching occurs when Q on the DS comes into contact with F on the target strand of TPP to form a dimer whereby fluorescence is quenched.

displacing sequence (DS) (Fig. 3.1, Step 3 light blue) that was labelled with a quencher was hybridised to the target strand (red) of the TPP thus displacing the incumbent (purple) strand of the TPP (see Chapter 1, Section 1.6.1 for more detail).

The rate of strand displacement can be determined by monitoring the decrease in fluorescence of the fluorophore with a fluorometer, on the target strand, as it becomes quenched by the dark quencher on the DS. This chapter investigates ways to increase specificity of toehold-mediated strand displacement reactions, described by Khodakov *et al.*¹ for the purpose of SNP genotyping (see Chapter 1, Section 1.6.3 for more details) using ethidium bromide. The addition of ethidium bromide forms a high energy barrier that leads to the formation of DNA structures with the lowest possible energy. In other words, only the lowest energy base pairs (bps) will form (canonical Watson-Crick base pairs, see Chapter 1, Section 1.3) and, in this case, prevent high energy base pairs forming such as mismatches (non-canonical Watson-Crick base pairs). This should help to decrease the likelihood of mismatches forming during the toehold-mediated strand displacement reaction. In previous work, the fluorophore 6-FAM was chosen because it was possible to be detected using the Roto-Gene 6plex real-time PCR (RT-PCR) device.¹ However, due to the overlapping of excitation wavelengths (and to some degree the emission wavelengths) of 6-FAM and ethidium bromide would lead to difficulties in the fluorescence measurement (Table 3.1). Therefore two new fluorophores, ATTO 550 and ATTO 647N were investigated to determine which fluorophore would be more suitable for this study (Table 3.1).

The fluorophores ATTO 550 and ATTO 647N were chosen due to their high intensity, approximately 1.3 times brighter than 6-FAM, and lack of overlapping maximum absorbance wavelength (λ_{ex}) or maximum fluorescence emission wavelength (λ_{fl}) with ethidium bromide (Table 3.1). However, due to the fluorophores being slightly more hydrophobic (according to the manufacturer)⁷ than 6-FAM there may be slight differences with the PCR. These differences include different annealing temperatures for the fluorophore-labelled primers or the toehold-mediated strand displacement reaction, such as different quenching modes (contact vs Förster

Table 3.1: The properties maximum excitation wavelength (λ_{ex}), maximum fluorescence emission wavelength (λ_{fl}), quantum yield (Φ), molar extinction coefficient (ϵ_{max}) and intensity of 6-FAM, ethidium bromide, ATTO 550, ATTO 647N and Black hole quencher 1 (BHQ-1).

Fluorophore	λ_{ex} nm	λ_{fl} nm	Φ (%)	ϵ_{max} ($\text{cm}^{-1}\text{M}^{-1}$) ($\times 10^4$)	Intensity ($\times 10^4$)
6-FAM ⁵	495	520	95	7.50	7.13
ethidium bromide (low salt buffer) ⁶	482	616	15	5.68	0.09
ATTO 550 ⁷	554	576	80	12.00	9.60
ATTO 647N ⁷	646	664	65	15.00	9.75
BHQ-1 ⁸	480-580	-	-	34.00	-

resonance electron transfer (FRET), see Chapter 1 Section 1.4.4). This may result in a change in the the rate of the reaction as hydrophobic interactions may drive the reaction to completion.⁹

3.3. Results and discussion

3.3.1. ATTO 550 and ATTO 647N effect on PCR and toehold-mediated strand displacement trials

This Section first discusses the results from the PCR of the SPP (see Fig. 3.1, Step 1) using the forward primer, containing the dU at the 5th and 9th position, and with two separate reverse primers, one labelled with ATTO 550 and one labelled with ATTO 647N. The procedures for these experiments can be found in Chapter 2, Section 2.3.1.1.

3.3.1.1. PCR amplification using ATTO 550 and ATTO 647N

The PCR process is outlined in Fig. 3.1, Step 1, whereby the forward and reverse primers amplify a region of the template mtDNA. These primers were designed to amplify a single region of 80 bps.¹ The PCR process was performed using GoTaq Flexi ® DNA polymerase protocol due to its ability to amplify DNA using primers that contain non-canonical nt residues, such as the dU in the forward primer.

MtDNA containing a C at the SNP position was used to evaluate the two new fluorophores. After PCR of the mtDNA the resulting SPPs labelled with either ATTO 550 or ATTO 647N, were analysed using an agarose gel 4% (w/v) in gel electrophoresis as shown in Fig. 3.2. Here after the resulting SPP will be referred to as SPP-C, where the C indicates the nt (cytosine) at the SNP position on the SPP. The second part of this section will discuss the fabrication of the toehold PCR product C (hereafter referred to as TPP-C) using the SPP-C, where the C indicates the nt at the SNP position.

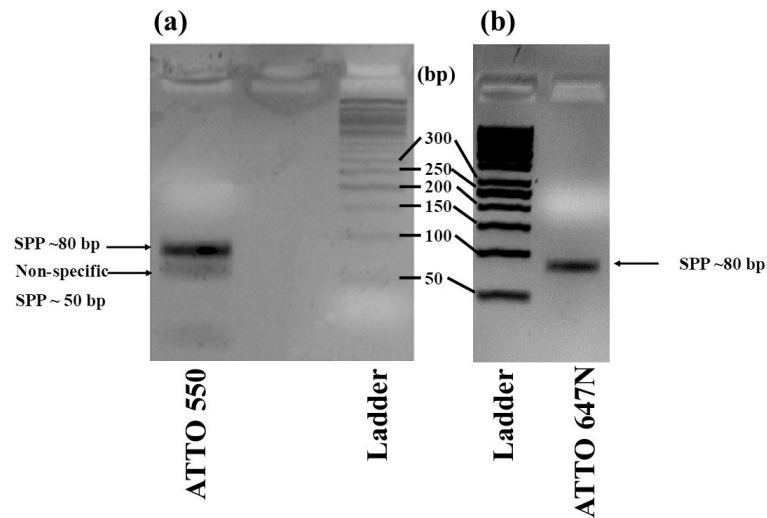


Figure 3.2: Agarose gel 4% (w/v) electrophoretograms of the SNP PCR products (SPPs) labelled with either the fluorophore (a) ATTO 550 or (b) ATTO 647N. For visualisation, the gel was stained with 1x SYBR® safe and viewed using a Gel Doc™ EZ. A DNA Ladder (Quick-Load® Purple 50 bp DNA ladder) was used as the reference.

Fig. 3.2 (a) shows that the gel electropherogram of the SPP labelled with the fluorophore ATTO 550 shows two bands. The first band at the top was calculated to have the expected length of ~80 bp (corresponding to the desired SPP labelled with ATTO 550) while the bottom band had a calculated length of ~55 bp. This secondary band was due to non-specific PCR amplification of the target mtDNA resulting in an undesired non-specific PCR product. Non-specific PCR products occur when the PCR procedure is not optimised for the primers being used. To understand why non-specific PCR products can be produced, first it must be understood how the PCR process can be performed successfully (i.e., only the desired target region is amplified).

Several steps must be followed for successful amplification of the target mtDNA. The first step is the denaturing of the double stranded mtDNA by heating to 95 °C, as dsDNA of any length will become single-stranded DNA (ssDNA) at that temperature. The next step is the annealing step, whereby the temperature is lowered to allow for the hybridisation of the forward and reverse primers. Primers (both forward and reverse primers) are known sequences of oligodeoxynucleotides (ODNs) that are able to hybridise next to the target region on the mtDNA, one primer is used for each strand in the original double stranded mtDNA (that now exists as two complementary ssDNA). The temperature of the annealing step is often just below (3-5 °C) of the melting temperature (T_m) of the primers hybridised to the DNA (if the temperature of the annealing step is above the T_m of the hybridised primers, the primers will denature). The final step is the elongation step that extends the now hybridised primers to make a complementary strand to the target. All these steps are repeated to create multiple copies of the same region of DNA, hence it is referred to as amplification of the target mtDNA.

The formation of secondary structures during amplification is explained in the following. Fig. 3.3 shows the reverse primer (red) labelled with the fluorophore (F, red) hybridising with the correct binding site on a target strand that has already been amplified using the reverse primer (purple). The reverse primer in this case will amplify the target strand that contains the SNP of interest. In Fig. 3.3 the SNP position is underlined and contains the G residue, as it is the complementary to the C SNP of interest. Due to the nature of DNA energetically favouring being as dsDNA it is possible for the primers to anneal to a random binding site on the target DNA. However, the more complementary the primer is to the binding site the more stable the dsDNA formed. Correct hybridisation of the primers occurs if the temperature of the annealing step is low enough to allow the primer to hybridise with the target region (temperature of the annealing step is below the T_m of the hybridised primer), but high enough to prevent incorrect hybridisation (non-complementary hybridisation) of the primer to the DNA. This prevents any non-specific amplification of the target strand of DNA that would result in a non-specific SPP. Once the primer has hybridised to the correct binding site and after the elongation step the target

region is successfully amplified.

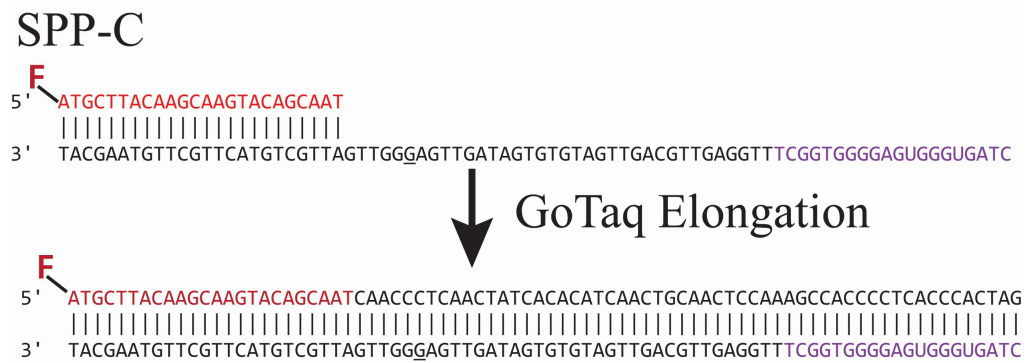


Figure 3.3: Example of correct annealing and elongation of the mtDNA using the reverse primer (red) labelled with the fluorophore (F, red) to the strand of mtDNA that has already been amplified with forward primer (purple). Complementary Watson-Crick bps are indicated by |. The SNP position is underlined.

During PCR it is possible for primers to form incorrect hybrids with the target DNA. In this case, the primer hybridises to the target strand even though the sequence of the primer is not fully complementary to the sequence of that particular section of the target strand, which after the elongation step yields a non-specific SPP.

Non-specific PCR amplification can occur due to a number of different factors (i.e., high magnesium concentration, incorrect temperature used for the annealing step), but for this case in particular it is thought that the temperature used for the annealing step is not correctly optimised to only allow the fully complementary hybridisation of the primer to the target strand to occur when the primer is labelled with ATTO 550. This could occur due to the presence of ATTO 550 stabilising hybridisation of the primer to the target strand, increasing the stability (and therefore the T_m) of incorrect hybrids of the primer and the target strand enough that the annealing temperature is no longer high enough to denature these incorrect hybrids. This leads to non-specific SPPs forming after the elongation step.

If the temperature of the annealing step is too high then the primers are not able to anneal to the target DNA, however if too low then non-specific hybridisation can occur.^{10,11} If the mismatches are not able to prevent extension of the primer a non-specific PCR product

is created. Fig. 3.4 shows an example of non-specific annealing and extension of the forward primer (red) labelled with the fluorophore (F, red).

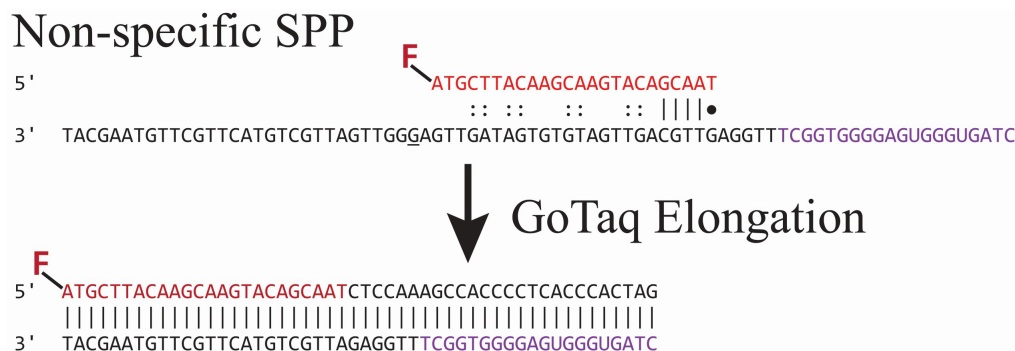


Figure 3.4: Example of incorrect annealing and elongation using reverse primer (purple) labelled with the fluorophore (F, red) to the strand of mtDNA that has already been amplified with forward primer (purple), showing nearest neighbour stabilised Watson-Crick bonds (|), complementary Watson-Crick bonds (:), and mismatches (●). The SNP position is underlined.

For the amplification of the mtDNA the temperature of the annealing step was set below the T_m of both primers, in this case it was set to 61 °C (see Chapter 2, Section 3, Table 2.4). The appearance of the non-specific SPP in Fig 3.2 (a) shows that the ATTO 550 may be increasing the T_m of the reverse primer above the calculated 64.1 °C. Thereby, decreasing the binding energy barrier and stabilising the formation of mismatches, such as those that can be seen in the non-specific SPP in Fig. 3.4.

In this particular case it would result in a non-specific SPP product that is 50 bp in length and contains the fluorophore and the dU required for the toehold fabrication. This could be attributed to several factors, such as the fluorophore being moderately hydrophobic or increased stabilisation through base stacking of the fluorophore with nucleotides on the target strand. However, due to the structure of ATTO 550 not being published this would require further study that is outside the scope of this project.

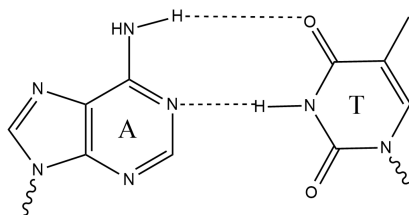
Oligo Analyzer (Integrated DNA, USA) shows that there are many possible regions where the primers could have hybridised along the target.¹² Fig. 3.4 shows the most likely region, that would result in a non-specific PCR product of ~55 bp (more non-specific binding

regions can be found in Appendix A for comparison). This is the most likely product seen for two main reasons.

The first is the amount of complementary Watson-Crick bonds present. There are four that are nearest-neighbour stabilised (high stability Watson-Crick bonds (|) in Fig. 3.4), that is, two bp have a neighbour either side to provide stability. There are eight complementary Watson-Crick bonds that are complementary (Fig. 3.4) but are not stabilised by neighbouring bps. Under conventional PCR conditions (i.e., the fluorophore does not add stability) the temperature used for the annealing step should prevent the primer hybridising in the incorrect region. However, it appears that the ATTO 550 is able to stabilise this product enough to allow for the elongation step to go to completion resulting in the product of 50 bp. Once the 50 bp non-specific SPP has been created it will contain a region for both primers to hybridise and will be amplified in the same manner that the desired PCR product is being amplified, albeit resulting in a lower concentration.

The second reason this non-specific PCR product is likely being amplified is the formation of the T•G mismatch (the • denotes a mismatch and non-canonical Watson-Crick base pairing) seen in at the 3' end of the fluorophore labelled reverse primer (Fig. 3.4, red). As mentioned in Chapter 1 Section 1.3.2.1, T•G mismatches are as stable as the complementary A/T bp (where the / denotes canonical Watson-Crick base pairing). Fig 3.5 shows how T residue is able to form a stable bond with A or G residue. A/T base pairing requires the formation of two hydrogen bonds (Fig. 3.5, top). This creates a stable bp and so therefore when a T•G mismatch forms it is still able to form two stable hydrogen bonds (Fig. 3.5, bottom).^{13,14} The complementary bp and the mismatch would be stable enough to allow for primer hybridisation and then subsequent GoTaq polymerase elongation. All other non-specific hybridised primers either do not contain enough stable bonds or do not have 3' stabilised regions that would allow for the elongation to occur. Fig. 3.5 also reveals that the SNP position is no longer present in the SPP and hereafter will be referred to as the ~55 bp SPP (not the SPP-C).

Adenine to thymine base pairing (complementary)



Guanine to thymine base pairing (non-complementary)

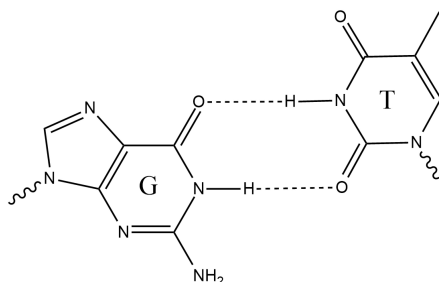


Figure 3.5: Diagram of how A and T form a complementary base pair (top) and how G and T form a mismatched base pair.

Several steps can be taken to optimise the PCR procedure to prevent the secondary non-specific PCR product, such as changing the temperature of the annealing step, magnesium concentration or redesign the primer. However, all these changes would require extra time to optimise. Removal of the secondary non-specific PCR product could result in loss of the desired SPP and so this was not undertaken. The crude SPP labelled with ATTO 550 (containing both ~80 bp and ~55 bp products) was used in toehold-mediated strand displacement reactions in the following section without further purification to ascertain whether the SPP (~55 bp) would interfere with the reactions. The analysis of the SPP labelled with ATTO 647N (Fig. 3.1 (b)) shows only one band at ~80 bp, corresponding to the desired SPP-C. In this case the resulting SPP was of high enough purity with no undesired secondary products. Therefore, the SPP labelled with ATTO 647N was used without any further purification.

3.3.1.2. Fabrication of the TPP-C with ATTO 550 and ATTO 647N and toehold-mediated strand displacement reaction

This section will discuss the fabrication of TPP-C (see Fig. 3.1, Step 2) labelled with either ATTO 550 or ATTO 647N, and subsequent use in toehold-mediated strand displacement reactions with different DSs (see Fig. 3.1, Step 3). TPP-C was produced by digestion of SPP-C, labelled with either ATTO 550 or ATTO 647N, with the enzyme EXO 1 to remove excess primers (forward and reverse) not incorporated into the SPP. This was followed by a digestion with the enzyme UDG to digest the dUs (at the 5th and 9th positions) to produce the 9-nt toehold on the incumbent strand of the SPP-C and create the toehold that allowed for the nucleation of the DS (Fig. 3.1, Step 2). The labelled TPP-C was then purified using 30 K Amicon® Ultra Centrifugal Filters. The procedure can be found in Chapter 2, Section 2.3.1.1, which resulted in a pink coloured product appearing due to concentration of the fluorophore containing TPP. The labelled TPP-C were then used in toehold-mediated strand displacement reactions without any further validation.

For the TPP-C solution, labelled with ATTO 550, there will be the expected TPP-Cs of two differing lengths (~55 bp, ~80 bp) observed in the SPP-C labelled with ATTO 550 by gel electrophoresis (Section 3.3.1.1).

All labelled TPP-Cs were then treated individually with one of four different DSs where each DS possessed a different nt at the SNP position on the DS strand, where the nt had the base A, T, G, or C, denoted as DS(A), DS(T), DS(G), DS(C), respectively. All of these DSs contain the quencher BHQ-1. The toehold-mediated strand displacement reaction was carried out according to the procedure set out in Chapter 2, Section 1.6.1 (Fig. 3.1, Step 3). The four different toehold-mediated strand displacement reactions of TPP-C (displacement of the incumbent strand of TPP-C with either DS(A), DS(T), DS(G), or DS(C)) were monitored by measuring the decrease in fluorescence of the reaction, as successful displacement of incumbent strand of the TPP-C by the DS puts the quencher on the DS close enough to the fluorophore on

the target strand of the TPP-C, quenching the fluorophore and decreasing the fluorescence.

Measuring the reduction of the fluorescence during the reaction therefore indicates whether the DS strand was successful in displacing the incumbent strand of the TPP-C. Addition of 5 times the concentration of DS to the TPP-C will result in a pseudo-first order kinetic curve if displacement is successful.¹

Fig. 3.6 shows an example toehold-mediated strand displacement kinetic curve for the displacement of the incumbent strand of TPP-C with DS(A), when the TPP-C is labelled with either ATTO 550 (black) or ATTO 647N (red). Appendix B shows ATTO 550 and Fig. 3.9 shows ATTO 647N labelled TPP-C displacement kinetic curves with each DS separately.

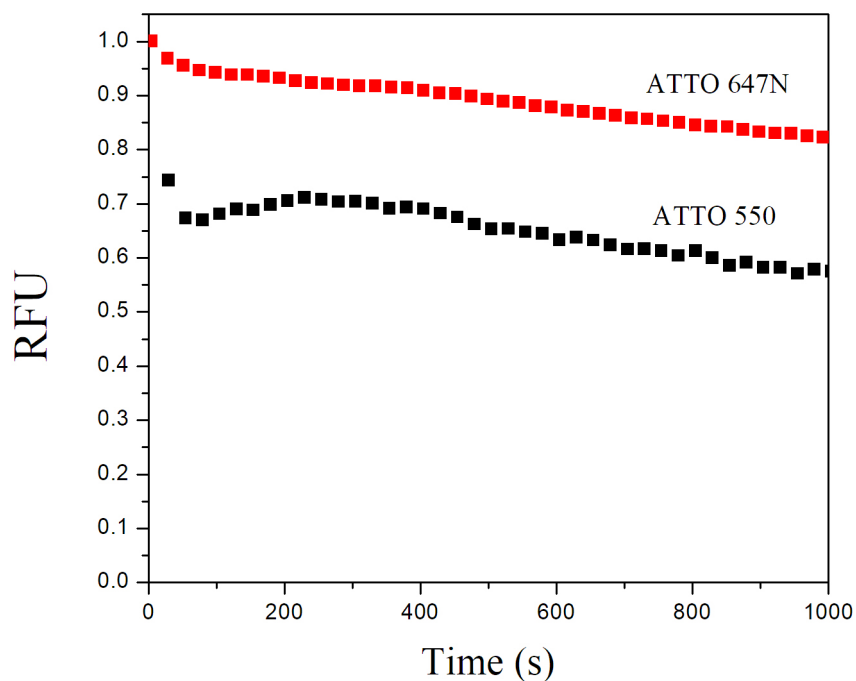


Figure 3.6: Toehold-mediated strand displacement kinetic curves (relative fluorescence unit (RFU) versus time) of the displacement reactions of the incumbent strand of TPP-C, when TPP-C is labelled with either the fluorophore ATTO 550 (black line) or ATTO 647N (red line), with DS(A). The fluorescence was measured on a Roto-Gene 6plex. Each set of data plotted is an average of 3 replicates. Every 20 data points was omitted for ease of viewing.

From Fig. 3.6 (black line) it can be seen that the displacement of TPP-C labelled with ATTO 550 has resulted in a decrease in fluorescence to 0.65 RFU in the first 50 s despite the presence of a A●C mismatch. There is then a further decrease of 0.1 RFU over the next 950 s. The decrease in fluorescence indicates that a fast toehold-mediated strand displacement has taken place. The ATTO 647N decreases by 0.1 relative fluorescence unit (RFU) over 1000 s, indicating a slow strand displacement reaction (Fig. 3.6 red line).

The C at the SNP position is thought to be too unstable to form a mismatch that is able to continue the random walk process of the strand displacement reaction (see Chapter 1, Section 1.6.1.1). However, it should be noted that the strand displacement reaction of the TPP-C labelled with ATTO 550 in Fig 3.6 was created from the SPP labelled with ATTO 550 solution from Fig. 3.2 without any isolation of the ~80 bp SPP. Therefore, the toehold-mediated strand displacement reaction involves both the ~55 bp TPP and ~80 bp TPP-C. Fig 3.7 demonstrates the full procedure of how the non-specific SPP is created, the TPP fabricated and the TPP undergoing successful toehold-mediated strand displacement

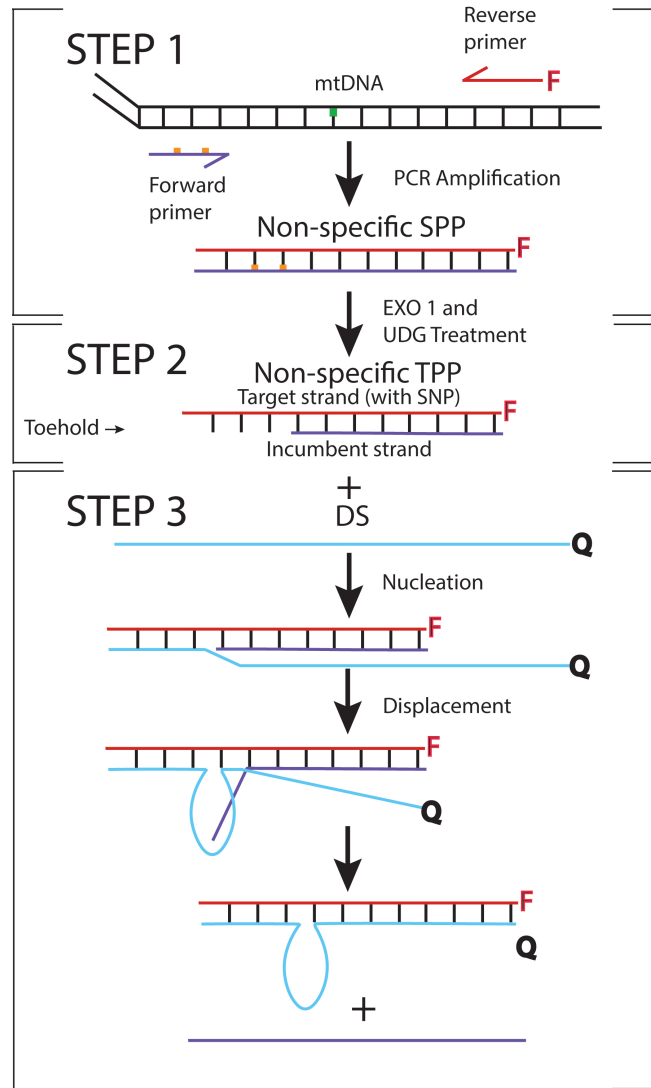


Figure 3.7: Schematic of toehold-mediated strand displacement of the non-specific SNP PCR product (SPP), the 55 bp TPP, produced using the reverse primer labelled with ATTO 550. Step 1: A region of the template mitochondrial DNA (mtDNA, black) that contains the single nucleotide polymorphism (SNP, green) is amplified with PCR using the modified reverse (red) primer labelled with a fluorophore (F) and the forward primer (purple) which contains deoxy-uracils (dUs, orange) at the 5th and 9th position. However due to non-specific hybridisation of the reverse primer this creates multiple copies of the non-specific SPP without the SNP present, but does create copies of the region of the template mtDNA, with the fluorophore (F) and dUs at the 5th and 9th position on the target strand (red) and incumbent strand (purple), respectively. Step 2: The toehold PCR product (TPP) is then formed by the digestion of the SPP of step 1 with uracil-DNA glycosylase (UDG) to remove the dUs which creates a short toehold on the incumbent strand (purple). Step 3: The displacing sequence (DS) (light blue) containing a quencher (Q) is added to the TPP in solution and nucleates with the toehold of the incumbent strand. Toehold-mediated strand displacement then proceeds as the DS hybridises, proceeding from the toehold, with the target strand of the TPP until the incumbent strand of the TPP is completely displaced into solution. For the non-specific SPP the DS strand forms a loop that allows for the toehold-mediated strand displacement to proceed. This still allows for the formation of a dsDNA that brings the quencher close enough to the fluorophore to allow for quenching.

The decrease to 0.65 RFU in the first 50 s (Fig. 3.6, black line) is most likely due to the toehold-mediated strand displacement of the incumbent strand from the ~ 55 bp TPP labelled with ATTO 550. The displacement is still able to take place due to the DS being ~ 30 bp longer than the non-specific TPP, allowing for the formation of a loop region (see Fig. 3.7 Step3). This due to ssDNA being flexible, see Chapter 1, Section 1.3.¹⁸ As stated previously, the ~ 55 bp TPP no longer contains the SNP (C residue in this case) and therefore there is no barrier to impede the strand displacement. This is thought to be the process as this is not seen in the displacement kinetic curve of the TPP-C labelled with ATTO 647N, which had no non-specific SPP.

The ~ 80 bp TPP-C labelled with ATTO 550, would account for the slower decrease of 0.1 RFU over the remaining 950 s. Due to the presence of the shorter ~ 55 bp TPP the reaction can no longer be deemed as a pseudo-first order reaction. From Fig 3.6 (red line) the displacement that takes place between the TPP-C labelled with ATTO 647N and DS(A) only decreases by 0.1 RFU in 1000 s. This result indicates that TPP-C labelled with ATTO 647N has better discrimination power than TPP-C labelled with ATTO 550 in the toehold-mediated strand displacement reaction. Therefore, further work investigating the toehold-mediated reaction was done using the reverse primer labelled with ATTO 647N for the remaining SNPs (A, T and G). Full analysis of the all TPP labelled with ATTO 647N will be discussed in the next section.

From Fig 3.6 (red line) we see that the displacement that takes place between the TPP-C labelled with ATTO 647N and DS(A) only reaches 0.9 RFU in the 1000 s. This indicates that although there is some toehold-mediated strand displacement taking place it is not to the same degree as the TPP-C labelled with ATTO 550. This result indicates that TPP-C labelled with ATTO 647N has better discrimination power than TPP-C labelled with ATTO 550 in the toehold-mediated strand displacement reaction. Therefore, further work investigating the toehold-mediated reaction was done using the reverse primer labelled with ATTO 647N for the remaining SNPs (A, T and G). Full analysis of the all TPP labelled with ATTO 647N will be

analysed in the next section.

From Fig 3.5 it can be determined that using the reverse primer labelled with ATTO 550 would only be viable if it was possible to either prevent the occurrence of the non-specific SPP or isolation of the correct ~80 bp SPP. For this project the use of ATTO 647N is satisfactory and so will be used for the remainder of this Chapter.

3.3.2. Toehold-mediated strand displacement of TPP-C, TPP-G, TPP-A and TPP-T using ATTO 647N

This section will now focus on the production of the SPP of all the four possible SNPs (SPP-C, SPP-G, SPP-A and SPP-T), the fabrication of the four TPPs (TPP-C, TPP-G, TPP-A and TPP-T) and then finally the toehold-mediated strand displacement of all the TPPs. It must be noted that the only difference between the four TPPs is the nt at the SNP position. This allows for accurate comparison of all the TPPs and will give insight into how each SNP will affect the toehold-mediated strand displacement process. The SNP is flanked by the same nt in all the strands and will be referred to as the “trimer sequence” as these are the only bps that play a role in the random walk process of the toehold-mediated strand displacement reaction. This is based on the nearest-neighbour interactions, whereby it is assumed that the only way for a bp to form is if the neighbour bp is first stable enough (see Chapter 1, Section 1.3.2 for further details).¹⁹ The trimer sequence of the target strand (see Fig.3.1, red) is TXC (3' to 5'), where X is any nt: C, G, A and T) and the complementary trimer sequence of the DS is AXG (5' to 3', where X is any nt: C, G, A and T). The DS is expressed in the 5' to 3' direction as the direction of the random walk starts at the 3' and ends at the 5' end of the target strand. Therefore, the first bp formed is a T/A bp which does not have as stable pairing as the closing bp, G/C. This will have an impact on the random walk process that will be discussed throughout this Chapter. Firstly, all four SPP must be created to allow for fabrication of the TPP and then subsequent toehold-mediated strand displacement reaction.

3.3.2.1. Amplification of all four SPP-C, SPP-G, SPP-A and SPP-T

As seen in Section 3.3.2 it was possible to amplify SPP-C using the primer labelled with ATTO 647N without any secondary non-specific SPP forming. For this section the remaining SPP were created using the same procedure, however different mtDNA were used. For SPP-G, SPP-A and SPP-T mtDNA containing G, A or T at the SNP position was used, respectively. All four SPPs were analysed using 4% (w/v) agarose gel electrophoresis, shown in Fig. 3.8.

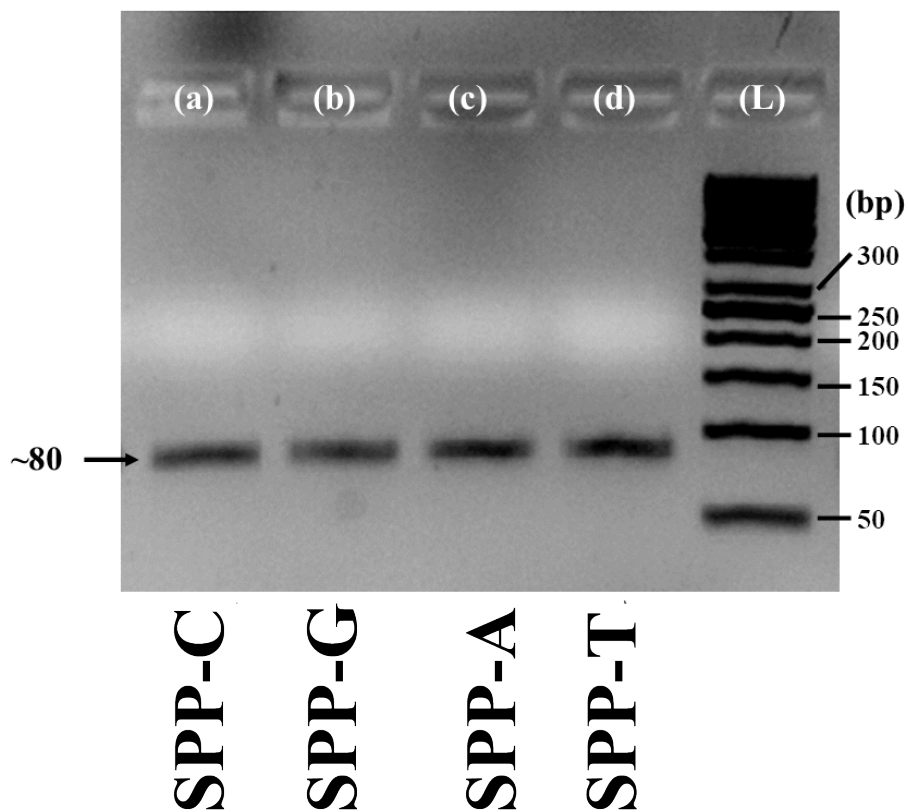


Figure 3.8: Agarose gel 4% (w/v) electrophoretogram of the four SPPs possessing different nts, (a) SPP-C, (b) SPP-G, (c) SPP-A and (d) SPP-T, all labelled with the fluorophore ATTO 647N. For visualisation, the gel electrophoretogram was stained with 1x SYBR® safe and viewed using a Gel Doc™ EZ. A DNA ladder (Quick-Load® Purple 50 bp DNA Ladder) was used as the reference.

Fig. 3.8 shows that all the PCR products, using the primer labelled with ATTO 647N, resulted in SPPs of identical lengths of approximately 80 bp. This is to be expected as the only

difference between each SPP is the nt at the SNP position. There are also no secondary bands observed, and this indicates that there is no further purification required before using in the fabrication of the toehold in the next Section.

3.3.2.2. Toehold-mediated strand displacement reaction with TPPs labelled with ATTO 647N

This section will discuss the fabrication of the TPPs (see Fig. 3.1, Step 2) when, labelled with ATTO 647N, and subsequent use in the toehold-mediated strand displacement reaction with different DSs (see Fig. 3.1, Step 3). TPP-C, TPP-G, TPP-A and TPP-T were produced from SPP-C, SPP-G, SPP-A and SPP-T. The TPPs were separately fabricated using the enzyme EXO 1 to remove excess primers (forward and reverse) not incorporated into the SPP. This was followed by a digestion with the enzyme UDG to digest the dUs (at the 5th and 9th positions) to produce the 9-nt toehold on the incumbent strand of the SPP-C and creating the toehold allows for DS to nucleate (Fig. 3.1, Step 2). TPPs were then separately purified using 30 K Amicon® Ultra Centrifugal Filters. The procedure for producing TPPs can be found in Chapter 2, Section 2.3.1.1. After purification the TPPs were used without any further validation.

Each TPP was treated in separate experiments with each of the four different DSs (DS(A), DS(T), DS(G), or DS(C)). All of these DSs contain the quencher BHQ-1. The toehold-mediated strand displacement reaction was carried out according to the procedure set out in Chapter 2, Section 2.3.1.3 (Fig. 3.1, Step 3). The four different toehold-mediated strand displacement reactions (displacement of the incumbent strand of each TPP with either DS(A), DS(T), DS(G), or DS(C)) were monitored by measuring the decrease in fluorescence of the reaction. Measuring the reduction of the fluorescence of the reaction, producing a toehold-mediated strand displacement curve, therefore indicates whether the DS strand was successful in displacing the incumbent strand of the specified TPP. Figure 3.9 shows the kinetic curves of the toehold-mediated strand displacement of (a) TPP-C, (b) TPP-G, TPP-A and TPP-T (la-

belled with ATTO 647N) with DS(A) (black), DS(T) (pink), DS(G) (blue) and DS(C) (green) containing BHQ-1. The line of best fit (Fig. 3.9, red dotted line) for the toehold-mediated strand displacement kinetic curves was calculated using the non-linear curve fitting function (see Eq. 3.1) in OriginPro 9 (Origin Corporation, USA).

Where F is the fluorescence intensity at time t , F_0 is the initial fluorescence intensity, F_1 is the intensity after reaction completion, k is the rate constant, $[DS]_0$ is the initial concentration of the displacing sequence, and t is the time in seconds.

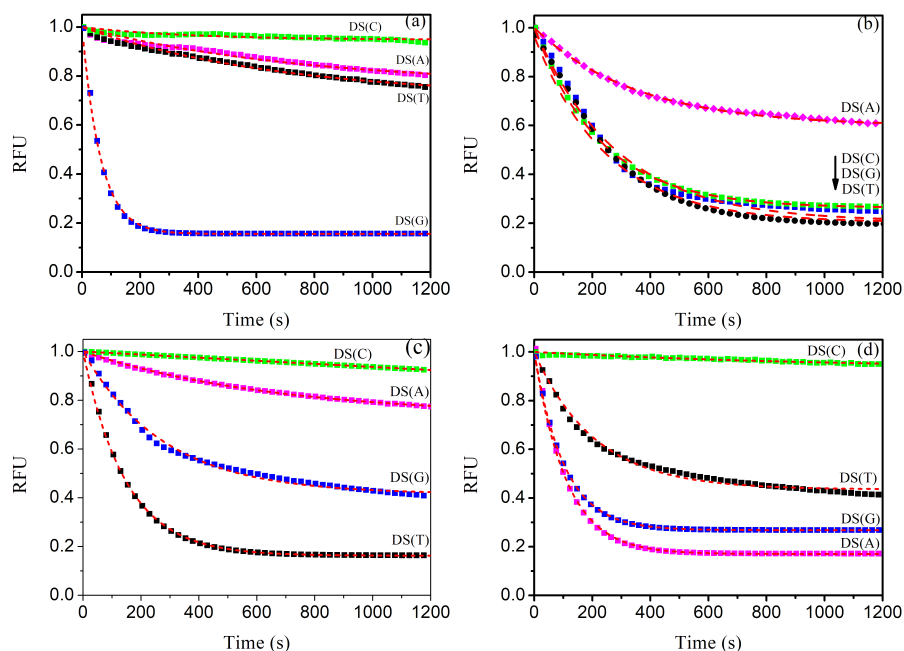


Figure 3.9: (a) TPP-C, (b) TPP-G, (c) TPP-A and (d) TPP-T (labelled with ATTO 647N) with DS(A) (black), DS(T) (pink), DS(G) (blue) and DS(C) (green) containing BHQ-1. Each set of data plotted is an average of 3 replicates. Every 20 data points was omitted for ease of viewing and the red dashed lines are the fits obtained using OriginPro 9 software.

All plots gave $R^2 \geq 0.95$. An excess of DS was used to make use of the pseudo first order kinetics equation described by Baker *et al.*²⁰

$$F = F_1 + (F_0 - F_1)e^{-kt[DS]_0} \quad (3.1)$$

The ratio between the reaction rate ($k_{complementary}$) and the reaction rate of non-complementary sequences ($k_{non-complementary}$) was then used as a kinetic discrimination ratio, R_k . (Eq. 3.2).

$$R_k = \frac{k_{complementary}}{k_{non-complementary}} \quad (3.2)$$

One-way ANOVA analysis was used to determine whether there was any significant difference between the averages (means) of the complementary and non-complementary displacements for each TPP, where $F < F_{crit}$ (a value that is corresponding to a 0.05% confidence interval (CI)). shows that the means of the means are not the same, implying discrimination. A CI of 95% and degrees of freedom of F(1,10) were computed for all results. If the p value was below $p = 0.05$ the F value was considered to be within the 95% CI and statistically significant. Table 3.2 shows the rate constants of displacement (denoted as k_{DS}) as well as the kinetic discriminator ratio (R_k) calculated from the kinetic curve in Fig. 3.9. The results for each TPP will be discussed in the following sections.

3.3.2.3. TPP-C, labelled with ATTO 647N, toehold-mediated strand displacement

The fastest displacement (<250 s) occurred when TPP-C was displaced with its complementary DS (DS(G)) and reached below 0.2 RFU (<80% displacement of incumbent strands) (Fig 3.9 (a), blue). All other toehold-mediated strand displacement reactions with non-complementary DS were far slower with only DS(T) reaching below 0.8 RFU ($\approx 20\%$ displacement of incumbent strands) in 1000 s (Fig 3.9 (a), pink). The rates for TPP-C with DS(T), DS(A), DS(C) and DS(G), as shown in Table 3.9, were $k_{DS} = 1946 (\pm 424) \text{ M}^{-1} \text{ s}^{-1}$, $k_{DS} = 947 (\pm 9) \text{ M}^{-1} \text{ s}^{-1}$, $k_{DS} = 1209 (\pm 99) \text{ M}^{-1} \text{ s}^{-1}$ and $k_{DS} = 9453 (\pm 114) \text{ M}^{-1} \text{ s}^{-1}$, respectively. The k_{DS} of the toehold-mediated strand displacement reaction of TPP-C follows the order of DS(A) < DS(C) < DS(T) << DS(G). The R_k values of the toehold-mediated strand displacement reactions of TPP-C with the different DSs indicate that the rate of reaction of TPP-C with

Table 3.2: The displacement rate (k_{DS}) and the kinetic discriminator ratio (R_k) of the toehold-mediated strand displacement reactions of all TPPs (labelled with ATTO 647N) when treated with DS(T), DS(A), DS(C), or DS(G), as determined from the kinetic curves presented in Fig. 3.9. Trimer sequences for TPPs and the different DSs, where the underlined X is the SNP position and can be any one of the nts (C, G, A and T). Included are the orders for the displacement rates for each TPP

TPP	DS	Displacement rate, k_{DS} , ($M^{-1} s^{-1}$), no ethidium bromide	Kinetic Discriminator, R_k , no ethidium bromide
$3' \Rightarrow 5'$	$5' \Rightarrow 3'$		
TPP-C(C)	DS(T): <u>T</u>	1946 (± 424)	4.9
	DS(A): <u>A</u>	947 (± 9)	10.3
	DS(C): <u>C</u>	1209 (± 99)	7.9
	DS(G): <u>G</u>	9453 (± 114)	1.0 (complementary)
Order of displacement rates:			
			DS(A) < DS(C) < DS(T) << DS(G)
TPP-G(G)	DS(T): <u>T</u>	6511 (± 38)	1.9
	DS(A): <u>A</u>	4222 (± 29)	1.3
	DS(C): <u>C</u>	5551 (± 47)	1.0 (complementary)
	DS(G): <u>G</u>	5986 (± 27)	1.1
Order of displacement rates:			
			DS(A) < DS(G) < DS(C) < DS(T)
TPP-A A	DS(T): <u>T</u>	6282 (± 41)	1.0 (complementary)
	DS(A): <u>A</u>	2360 (± 18)	2.7
	DS(C): <u>C</u>	1157 (± 18)	5.4
	DS(G): <u>G</u>	4642 (± 42)	1.4
Order of displacement rates:			
			DS(C) < DS(A) < DS(G) < DS(T)
TPP-T T	DS(T): <u>T</u>	4861 (± 136)	1.7
	DS(A): <u>A</u>	8069 (± 63)	1.0 (complementary)
	DS(C): <u>C</u>	446 (± 38)	18.1
	DS(G): <u>G</u>	7010 (± 41)	1.2
Order of displacement rates:			
			DS(C) << DS(T) < DS(G) << DS(A)

complementary DS (DS(G)) was 4.9 times faster than the rate of the reaction of TPP-C with the fastest non-complementary DS (DS(T)) (Table 3.2). This result is not unexpected, as any mismatches that involve the C nt (in this case the SNP on the target strand of TPP-C is a C residue) are the weakest of all the possible mismatches and decrease the rate of displacement due to the inability to form proper base stacking as well as the deformation of the phosphate backbone.^{4,5,8}

Table 3.2 also shows that the highest R_k value of the toehold-mediated strand displacement reactions of TPP-C was achieved when the SNP of the DS was an A nt (reaction with DS(A)), giving a $R_k = 10.1$. 5' bps play an important role in stabilising its nearest neighbour as it must first successfully form for the next bp to hybridise. In this case the closing group is an A/T, which is not as stable as G/C (see Chapter 1, Section 1.3.2). In this case the C mismatch that would form requires a stable neighbour in order to form a bp. Thus, in the case where the A/T is the closing group that forms a bp with low stability the mismatch in the displacement reaction is approximately 10 times slower to form than the complementary reaction. This gives the highest degree of discrimination.

The ANOVA for TPP-C was calculated to be $F(1,10) = 901$, $F_{crit} = 4.96$, $p = 3.93 \times 10^{-16}$. The ANOVA results, like Fig. 3.9 (a) and the R_k values (Table 3.2), show that TPP-C has excellent discrimination power as the F value is larger than the F_{crit} and that it is statically significant within the 95% CI.

3.3.2.4. TPP-G, labelled with ATTO 647N, toehold-mediated strand displacement

In the toehold-mediated strand displacement reaction of TPP-G labelled with the different DSs, discrimination was not achieved, as it is not possible to distinguish the complementary DS (in this case DS(C), Fig. 3.9 (green)) from non-complementary based on Fig. 3.9 (b).

The toehold-mediated strand displacement reactions with DS(T), DS(G) and DS(C)

all reach under 0.3 RFU (\approx 70% displacement of incumbent strands) by 1000 s (Fig. 3.9 (b), pink, black and green). DS(A), although slower, was still able to displace the incumbent strand and reach a RFU of 0.7 (\approx 30% displacement of incumbent strands) in 600 s (Fig. 3.9 (b), black). This is due to the stability of the G•A mismatch, much in the same way as the G•T mismatch (see Chapter 1, Section 1.3.2.1). The ANOVA analysis of the toehold-mediated strand displacement reactions of TPP–G with the different DSs indicates the reactions are indistinguishable from each other.

As shown in Table 3.2, the k_{DS} values of the toehold-mediated strand displacement reaction of TPP–G with DDS(T), DS(A), DS(C) and DS(G), where DS(C) is the complementary sequence, are $k_{DS} = 6511 (\pm 38) \text{ M}^{-1} \text{ s}^{-1}$, $k_{DS} = 4222 (\pm 29) \text{ M}^{-1} \text{ s}^{-1}$, $k_{DS} = 5551 (\pm 47) \text{ M}^{-1} \text{ s}^{-1}$ and $k_{DS} = 4986 (\pm 27) \text{ M}^{-1} \text{ s}^{-1}$, respectively (follows the order of DS(A) < DS(G) < DS(C) < DS(T)).

The rates of TPP–G with non-complementary DS(A) and DS(T) displacements are relatively high with $k_{DS} = 6511 (\pm 38) \text{ M}^{-1} \text{ s}^{-1}$ and $k_{DS} = 4222 (\pm 29) \text{ M}^{-1} \text{ s}^{-1}$, respectively, compared to the complementary rate of $k_{DS} = 4986 (\pm 27) \text{ M}^{-1} \text{ s}^{-1}$ (Table 3.2). For all other TPPs (Fig. 3.9 (a, c and d)) the DS(C) has the slowest displacement kinetic curve, often not reaching below 0.95 RFU, in the case of TPP–G the DS(C) is the complementary DS.

The k_{DS} observed for the toehold-mediated strand displacement reactions of TPP–G are high, regardless of the DS used. This is explained by the fact that mismatches formed between hybridised DNA strands that involve the G nt are stable enough that the displacement process occurs regardless of the nt pairs forming between the hybridised DNA strands. Allawi and SantaLucia^{19,21} and Tikhomirova *et al.*¹⁰ have described that the most stable mismatched pairings of nts occur between G•T, G•A, and G•G bps (where the • indicates non-canonical Watson-Crick base pairing). The TPP–G used in these displacement reactions possesses a G residue at the SNP position on the target strand, meaning that the DS used in the reaction will be forming a G mismatch. As any nt pairing between DNA strands involving a G nt is known to be

fairly stable,^{10,19,21} this leads to the k_{DS} of the toehold-mediated strand displacement reactions of TPP-G being relatively high regardless of the DS used. In regards to the TPP-G with DS(T) Table 3.2 shows that the rates are similar to that of the complementary TPP-A with DS(T), having rates of $k_{DS} = 6511 \text{ M}^{-1} \text{ s}^{-1}$ and $k_{DS} = 6282 \text{ M}^{-1} \text{ s}^{-1}$, respectively.

Interestingly, the toehold-mediated strand displacement reaction of TPP-G with DS(C) (the complementary DS) (TGC/ACG) is not the fastest, as would be expected. In fact, the highest k_{DS} is observed for the toehold-mediated strand displacement reaction of TPP-G with DS(T), which results in a G•T mismatch between the strands of DNA (TGC/ATG). The reason for this may be explained by the fact that a mismatch between a G residue and a T residue can be accommodated into the helical structure of DNA via changes in the sugar phosphate backbone.^{17,21,22} Subsequently, due to the formation of two hydrogen bonds it behaves similarly to a nt pairing of an A residue and a T residue match (TAC/ATG), which form two hydrogen bonds when hybridising. Fig. 3.5 shows how both A/T and G•T base pairs have two hydrogen bonds that allow for a stable formation of dsDNA, where the Watson-Crick edge of the G residue is able to form stable hydrogen bonds with the Hoogsteen edge of the T residue (see Chapter 1, Section 1.3.2.1 and 1.5.3 for more detailed explanation). Although Hoogsteen bonding is not as stable as Watson-Crick base pairing, the G residue is still able to form a base pair stable enough to allow for the displacement reaction to continue.

The ANOVA for TPP-G was $F(1,10) = 0.267$, $F_{\text{crit}} = 4.96$, $p = 0.616$. Not only is the F value far lower than the F_{crit} value, the p value is well above 0.05 (less than 95% CI). Therefore, it is not possible to distinguish the complementary from the non-complementary toehold-mediated strand displacement reactions.

3.3.2.5. TPP-A, labelled with ATTO 647N, toehold-mediated strand displacement

The results of the toehold-mediated strand displacement reaction of TPP-A with the different DSs indicates that that the toehold-mediated displacement reactions that involve non-

complementary DS(A) and DS(C) could be used accurately to discriminate TPP-A (Fig. 3.9 (c), pink and green). However, the DS(G) could not be used for the same accurate discrimination (Fig. 3.9 (c), blue). The complementary toehold-mediated strand displacement using DS(T) reached an RFU of ~ 0.8 ($\approx 20\%$ displacement of incumbent strands) in 1000 s (Fig 3.9 (c), pink). The toehold-mediated strand displacement reaction with DS(G) reached a RFU of ~ 0.5 ($\approx 50\%$ displacement of incumbent strands) in 600 s (Fig. 3.9 (c), blue). As expected the DS(C) underwent very little toehold-mediated strand displacement reaching only ~ 95 RFU in 1000 s (Fig. 3.9 (c), green).

Table 3.2 shows the k_{DS} values of the toehold-mediated strand displacement reaction of TPP-A with DS(T), DS(A), DS(C) and DS(G), where DS(T) is the complementary sequence to the target sequence of TPP-A, were $k_{DS} = 6282 (\pm 41) \text{ M}^{-1} \text{ s}^{-1}$, $k_{DS} = 2360 (\pm 18) \text{ M}^{-1} \text{ s}^{-1}$, $k_{DS} = 1157 (\pm 18) \text{ M}^{-1} \text{ s}^{-1}$ and $k_{DS} = 4642 (\pm 42) \text{ M}^{-1} \text{ s}^{-1}$, respectively. The rate of displacement of the incumbent strand follows the order of $\text{DS(C)} < \text{DS(A)} < \text{DS(G)} < \text{DS(T)}$.

The rate of displacement of the incumbent strand of TPP-A is fastest when the complementary DS (DS(T)) was used, and slower when the nt of the SNP of the DS used was mismatched to the SNP of the target strand of the TPP-A. The displacement reaction of the incumbent strand of TPP-A using DS(C) shows the slowest rate, due to C mismatches (when the nt mismatch between two DNA strands involves a C residue). C mismatches are known to result in the weakest interactions between DNA strands, and decrease, or prevent, strand displacement from occurring and therefore it is expected that they will have the lowest displacement rates.^{10,11,13}

This is also supported by the fact that the k_{DS} of the toehold-mediated strand displacement reaction of TPP-A with DS(T) (resulting in an A nt and a T nt match) is similar to the k_{DS} of the toehold-mediated strand displacement reaction of TPP-G with DS(T) (resulting in a G residue and a T residue mismatch), which are $k_{DS} = 6282 \text{ M}^{-1} \text{ s}^{-1}$ and $k_{DS} = 6511 \text{ M}^{-1} \text{ s}^{-1}$, respectively (Table 3.2).

The best discrimination between a DS with a non-complementary nt for the target strand of TPP-A was achieved when the non-complementary nt was a C nt, showing $R_k = 5.4$ (Table 3.2).

The ANOVA for TPP-A was $F(1,10) = 16.6$, $F_{crit} = 4.96$, $p = 0.002$. The ANOVA results show that it was possible to discriminate, with the F value being higher than the F_{crit} and this is statistically significant.

3.3.2.6. TPP-T, labelled with ATTO 647N, toehold-mediated strand displacement

The results of the toehold-mediated strand displacement of TPP-T with all four DS is similar to that when using TPP-A (Fig. 3.9 (d)). The complementary reaction with DS(A) reached <0.2 RFU in 250 s (Fig. 3.9 (d) black). However, the displacement reaction with DS(G) reached ~ 0.3 RFU in roughly the same time period of time (Fig. 3.9 (d), blue). DS(T) only reached ~ 0.5 RFU in 600 s (Fig. 3.9 (d), pink) and DS(C) showed a negligible RFU decrease (Fig. 3.9 (d), green).

As shown in Table 3.2, the k_{DS} values of the toehold-mediated strand displacement reaction of TPP-T with DS(T), DS(A), DS(C) and DS(G), where DS(A) was the complementary sequence, were $k_{DS} = 4861 (\pm 136) \text{ M}^{-1} \text{ s}^{-1}$, $k_{DS} = 8069 (\pm 63) \text{ M}^{-1} \text{ s}^{-1}$, $k_{DS} = 446 (\pm 38) \text{ M}^{-1} \text{ s}^{-1}$ and $k_{DS} = 7010 (\pm 41) \text{ M}^{-1} \text{ s}^{-1}$. The rate of the toehold-mediated strand displacement reaction follows the order of $DS(C) \ll DS(T) < DS(G) < DS(A)$, with increasing rate of displacement. The k_{DS} of the toehold-mediated strand displacement reactions of TPP-T with the complementary DS(A) was shown to be the fastest, while the rate using DS(C) was the slowest. This is because it results in a C nt mismatch between the target strand of the TPP-T and DS(C). Thus resulting in the highest R_k value ($R_k = 18.1$, Table 3.2), showing that the best discrimination from a non-complementary nt for the TPP-T was achieved when a C was present. This R_k value is higher than that observed for TPP-A with DS(C) ($R_k = 5.4$) and may be due to the fact that the base pairing is now a A nt to C nt mismatch (purine-pyrimidine) system rather than a T

nt to C nt (pyrimidine-pyrimidine) system.¹³

The ANOVA calculated was $F(1,10) = 5.255$, $F_{\text{crit}} = 4.96$, $p = 0.045$. Once again, the ANOVA results showed that it was possible to distinguish between the toe-hold mediated strand displacement reactions between TPP-T with complementary target strands to the DS used, as compared to when the TPP-T has a non-complementary target strand to the DS used in the reaction. The F value however is not much greater than the F_{crit} but is within the 95% CI. This concurs with Fig. 3.9 (d) as the only DS that makes discrimination difficult is DS(G). This is for the same reasons described in Section 3.3.2.5.

3.3.2.7. Using ATTO 647N for investigation of toehold-mediated strand displacement reaction

In both the toehold-mediated strand displacement reactions of TPP-A and TPP-T the complementary DS (TPP/DS) (i.e., TPP-A with DS(T) (TAC/ATG) and TPP-T with DS(A) (TTC/AAG)) were shown have the fastest rates, while the displacement rates with DS(C) for both TPP-A (TAC/ACG) and TPP-T (TTC/ACG) were the slowest. Allawi and Santa Lucia^{11,13} have found that TAC/ACG and TTC/ACG are amongst the most destabilising trimer sequences. This therefore results in slower rates of the toehold-mediated strand displacement reactions observed when using DS(C) with TPP-A or TPP-T (as compared to when using DS(A), DS(G), or DS(T)).

Overall it was found that the displacement rates for the TPPs with their complementary DSs follows the order of $\text{TPP-G} \leq \text{TPP-A} < \text{TPP-T} < \text{TPP-C}$. This indicates that when the SNP on the TPP is either a C nt or a T nt (a pyrimidine) the rate of displacement is higher than when the SNP on the TPP is an A residue or a G residue (a purine).

It can be concluded from Fig. 3.9 that it is possible to use the primers labelled with ATTO 647N to produce TPPs for investigating the effect of ethidium bromide on the toehold-mediated strand displacement reaction. There are no non-specific SPP formed that interfered

with the analysis (as occurred when using TPP-C labelled with ATTO 550) and ATTO 647N does not have any fluorescent interference from the ethidium bromide.

The next section will therefore discuss the investigation of the effect that ethidium bromide has on the toehold-mediated strand displacement reaction. Ethidium bromide intercalates by inserting itself between two bp in dsDNA (see Chapter 1, Section 1.4.6 for further details). This has been shown to stretch the DNA both in diameter and length.²³ Therefore, ethidium bromide should destabilise mismatches that may occur during the random walk process of the toehold-mediated strand displacement reaction and provide better discrimination.

3.3.3. Toehold-mediated strand displacement with ethidium bromide

In order to study the effects of the ethidium bromide on the toehold-mediated strand displacement reaction the procedure from Chapter 2, Section 2.3.1.4 was followed. In brief, each TPP (TPP-A, TPP-T, TPP-C and TPP-G) was treated with ethidium bromide first before being treated (in separate experiments) with each of the four different DSs (DS(A), DS(T), DS(C) and DS(G)) separately. All of these DSs contained the quencher BHQ-1. The concentration of the ethidium bromide was 79X that of the TPPs being studied, as there are 79 possible intercalation sites once the toehold on the target strand has nucleated with the DS. The concentration of the ethidium bromide was chosen to allow for maximum intercalation but to also keep the concentration low enough to not cause interference with the fluorophore detection (i.e., keep the solution colourless to allow transmission of light).

The four different toehold-mediated strand displacement reactions (displacement of the incumbent strand of each TPP with either DS(A), DS(T), DS(C) or DS(G)) were monitored by measuring the decrease in fluorescence of the fluorophore (ATTO 647N). Measuring the reduction of the fluorescence of the reaction therefore indicated whether the DS stand was successful in displacing the incumbent strand from the specified TPP

All the TPP toehold-mediated strand displacement reaction kinetic curves performed

in the presence of ethidium bromide are shown in Fig. 3.10. As with the previous sections all curve fitting for the kinetic curves was performed using Equation 3.1 and all kinetic discrimination ratios, R_k , were calculated using Equation 3.2.

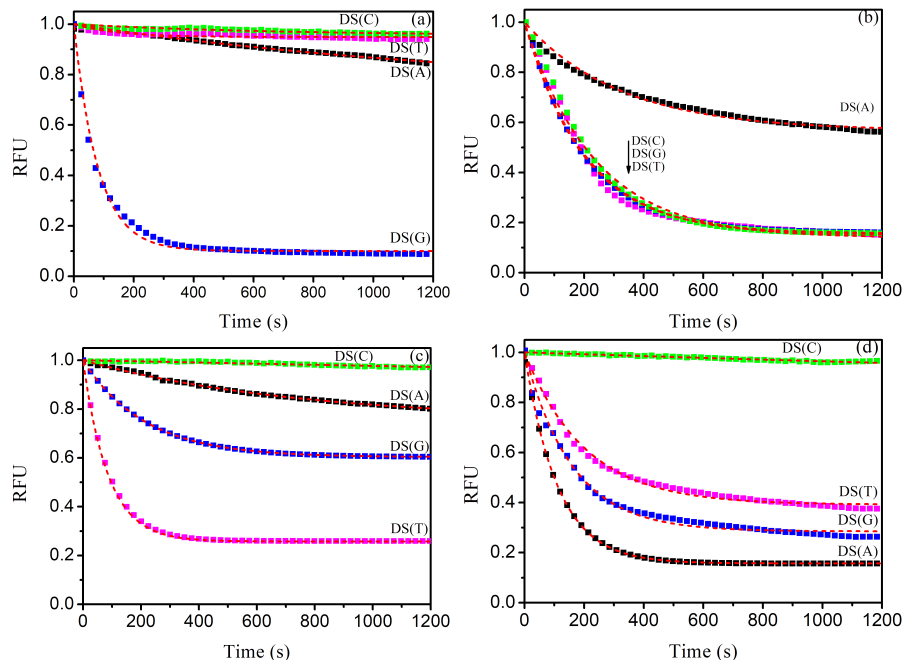


Figure 3.10: (a) TPP-C, (b) TPP-G, TPP-A and TPP-T (labelled with ATTO 647N) with DS(A) (black), DS(T) (pink), DS(G) (blue) and DS(C) (green) containing BHQ-1 and in the presence of ethidium bromide. Data plotted is an average of the results of 3 replicates. Every 20 data points was omitted for ease of viewing and the red dashed lines are the fits obtained using OriginPro 9 software.

Table 3.3 shows the k_{DS} as well as R_k values, calculated from the kinetic curves in Fig. 3.10. Table 3.2 also shows the data from the previous section to allow for comparison of the toehold-mediated strand displacement in the absence and presence of ethidium bromide.

3.3.3.1. TPP-C, labelled with ATTO 647N, toehold-mediated strand displacement in the presence of ethidium bromide

The displacement with DS(T) in the presence of ethidium bromide had a negligible decrease in fluorescence (Fig. 3.10 (a), pink), as opposed to without ethidium bromide where it reached below 0.8 RFU (Fig. 3.9 (a), pink).

Table 3.3: The displacement rate (kDS) and the kinetic discriminator ratio (R_K) of the toehold-mediated strand displacement reactions of all TPP (labelled with ATTO 647N) when treated with DS(T), DS(A), DS(C), or DS(G), in the absence and presence of ethidium bromide as determined from the kinetic curves presented in Fig. 3.9 and Fig. 3.10. Trimer sequences for TPP and the different DSs, where the underlined X is the SNP position and can be anyone of the nt (C, G, A and T). Included are the orders for the displacement rates

TPP	DS	Displacement rate, k_{DS} , ($M^{-1} s^{-1}$),	Kinetic Discriminator, R_K ,	Displacement rate, k_{DS} , ($M^{-1} s^{-1}$),	Kinetic Discriminator, R_K ,
$3' \implies 5'$	$5' \implies 3'$	no ethidium bromide	no ethidium bromide	with ethidium bromide	with ethidium bromide
TPP-C (C)	DS(T): <u>T</u>	1946 (± 424)	4.9	179 (± 42)	66.2
	DS(A): <u>A</u>	947 (± 9)	10.3	199 (± 24)	59.5
	DS(C): <u>C</u>	1209 (± 99)	7.9	157 (± 22)	75.4
	DS(G): <u>G</u>	9453 (± 114)	1.0 (complementary)	11853 (± 101)	1.0 (complementary)
Order of displacement rates:		DS(A) < DS(C) < DS(T) << DS(G)		DS(A) < DS(T) < DS(C) << DS(G)	
TPP-G (G)	DS(T): <u>T</u>	6511 (± 38)	1.9	7066 (± 33)	0.9
	DS(A): <u>A</u>	4222 (± 29)	1.3	3826 (± 23)	1.6
	DS(C): <u>C</u>	5551 (± 47)	1.0 (complementary)	6042 (± 52)	1.0 (complementary)
	DS(G): <u>G</u>	5986 (± 27)	1.1	6386 (± 24)	0.9
Order of displacement rates:		DS(A) < DS(G) < DS(C) < DS(T)		DS(A) < DS(C) < DS(G) < DS(T)	
TPP-A (A)	DS(T): <u>T</u>	6171 (± 136)	1.0 (complementary)	6282 (± 41)	1.0 (complementary)
	DS(A): <u>A</u>	2360 (± 18)	2.7	1548 (± 12)	4.0
	DS(C): <u>C</u>	1157 (± 18)	5.4	5.3 (± 0.1)	1164.3
	DS(G): <u>G</u>	4642 (± 42)	1.4	5480 (± 80)	1.1
Order of displacement rates:		DS(C) < DS(A) < DS(G) < DS(T)			
TPP-T (T)	DS(T): <u>T</u>	4861 (± 136)	1.7	6013 (± 5)	1.4
	DS(A): <u>A</u>	8069 (± 63)	1.0 (complementary)	8419 (± 51)	1.0 (complementary)
	DS(C): <u>C</u>	446 (± 38)	18.1	1.04 (± 0.1)	8095.2
	DS(G): <u>G</u>	7010 (± 41)	1.2	5897 (± 55)	1.4
Order of displacement rates:		DS(C) << DS(T) < DS(G) << DS(A)		DS(C) << DS(T) < DS(G) << DS(A)	

TPP–C (Table 3.3) displacement with DS(T), DS(A), DS(C) and DS(G) had rates of $k_{DS}(T) = 179 (\pm 42) \text{ M}^{-1} \text{ s}^{-1}$, $k_{DS}(A) = 199 (\pm 24) \text{ M}^{-1} \text{ s}^{-1}$, $k_{DS}(C) = 157 (\pm 22) \text{ M}^{-1} \text{ s}^{-1}$ and $k_{DS}(G) = 11853 (\pm 101) \text{ M}^{-1} \text{ s}^{-1}$, respectively. The k_{DS} followed the order of $DS(A) < DS(T) < DS(C) \ll DS(G)$.

The TPP–C with DS(G) was the most clearly distinguishable SNP in the complementary reaction from the non-complementary reactions. From Table 3.3 it can be seen that the R_k values increased considerably for displacement reactions with DS(T) and DS(C), increasing by an order of magnitude. However, the discrimination power of TPP–C was already the highest and so ethidium bromide seems to increase the destabilising ability of C mismatches. This may be because C mismatches impact on the DNA backbone, often stretching it open slightly,^{24,25} and providing more space for the intercalation of the ethidium bromide. This prevents the prevalence of the mismatches forming and so all the mismatches are slowed considerably.

The ANOVA results for TPP–C were calculated to be $F(1,10) = 7877$, $F_{\text{crit}} = 4.96$, $p = 8.7 \times 10^{-16}$. Similar to without the ethidium bromide, the ANOVA results shows that TPP–C displacement with all four DS has a high discrimination power, indicated by the high F value ($7877 > F_{\text{crit}} 4.96$) and the low p value.

3.3.3.2. TPP–G, labelled with ATTO 647N, toehold-mediated strand displacement in the presence of ethidium bromide

Once again, the displacement kinetic curves in the presence of ethidium bromide (Fig. 3.10 (b)) are similar to in the absence of ethidium bromide (Fig. 3.9 (b)), showing that it is still not possible to distinguish DS(C), DS(A) and DS(T). Ethidium bromide has the least effect on the displacement rate of TPP–G (Table 3.3) with DS(T), DS(A), DS(C) and DS(G), showing $k_{DS} = 7066 (\pm 33) \text{ M}^{-1} \text{ s}^{-1}$, $k_{DS} = 3826 (\pm 23) \text{ M}^{-1} \text{ s}^{-1}$, $k_{DS} = 6042 (\pm 52) \text{ M}^{-1} \text{ s}^{-1}$ and $k_{DS} = 6386 (\pm 24) \text{ M}^{-1} \text{ s}^{-1}$, respectively. The k_{DS} of the toehold-mediated strand displacement reaction of TPP–C in the presence of ethidium bromide follows the order of $DS(A) < DS(C) <$

DS(G) < DS(T).

There is however a general increase in displacement rates for DS(T), DS(C) and DS(G) with increases of $\Delta k_{DS} = 555 \text{ M}^{-1} \text{ s}^{-1}$, $\Delta k_{DS} = 491 \text{ M}^{-1} \text{ s}^{-1}$, and $\Delta k_{DS} = 1400 \text{ M}^{-1} \text{ s}^{-1}$. DS(A) showed the only decrease of $\Delta k_{DS} = -396 \text{ M}^{-1} \text{ s}^{-1}$. This is hypothesised to be due to the further stabilisation of the mismatch (and perfect match with DS(C)) from the ethidium bromide. Primarily due to the π stacking of the ethidium bromide with the G residue.

The ANOVA for TPP-G was calculated to be $F(1,10) = 0.102$, $F_{\text{crit}} = 4.96$, $p = 0.755$. Similar to without intercalated ethidium bromide in the TPP-G the ANOVA analysis showed that it is not possible to distinguish the TPP-G using the toehold-mediated strand displacement reaction as the F value is well below the F_{crit} .

3.3.3.3. TPP-A, labelled with ATTO 647N, toehold-mediated strand displacement in the presence of ethidium bromide

There is little change observed for TPP-A with all four DSs with and without ethidium bromide, Fig. 3.10 (c) and Fig. 3.9 (c), respectively. Notably, the displacement reaction with DS(G) did not go below 0.5 RFU ($\approx 50\%$ displacement of incumbent strands) in the presence of ethidium bromide unlike without ethidium bromide.

The TPP-A displacement with DS(T), DS(A), DS(C) and DS(G) gave displacement rates $k_{DS} = 6171 (\pm 136) \text{ M}^{-1} \text{ s}^{-1}$, $k_{DS} = 1548 (\pm 12) \text{ M}^{-1} \text{ s}^{-1}$, $k_{DS} = 5.3 (\pm 0.1) \text{ M}^{-1} \text{ s}^{-1}$ and $k_{DS} = 5480 (\pm 80) \text{ M}^{-1} \text{ s}^{-1}$. The k_{DS} of the toehold-mediated strand displacement reaction of TPP-C in the presence of ethidium bromide follows the order of DS(C) < DS(A) < DS(G) < DS(T).

In this case there appears to be no discernible change between the rate of the complementary reaction with DS(T), with ethidium bromide ($k_{DS} = 6171 (\pm 136) \text{ M}^{-1} \text{ s}^{-1}$) and without ethidium bromide ($k_{DS} = 6282 (\pm 41) \text{ M}^{-1} \text{ s}^{-1}$), indicating that the adenine-thymine

interaction is not stabilised, or remains unaffected, by the base stacking interactions of the ethidium bromide. There is however a decrease in the rate for the non-complementary DS(A) and DS(C) displacement (i.e., TAC/AAG and TAC/ACG mismatches, respectively) with ethidium bromide ($\Delta k_{DS} = -812 \text{ M}^{-1} \text{ s}^{-1}$) compared to without ethidium bromide ($\Delta k_{DS} = -1152 \text{ M}^{-1} \text{ s}^{-1}$). Both of these low reaction rate mismatches appear to be destabilised by the presence of ethidium bromide, thus further decreasing the rates of reaction. Interestingly, the DS(G) rates increased with the introduction of ethidium bromide, $\Delta k_{DS} = 838 \text{ M}^{-1} \text{ s}^{-1}$, indicating that this A residue to G residue (TAC/AGG) or purine/purine mismatch is stabilised by the intercalator.

Table 3.3 shows that the best discrimination from a non-complementary nt for the TPP-A was achieved when a C was present, $R_k = 1164.3$. This is substantially larger than without ethidium bromide ($R_k = 5.4$) indicating that ethidium bromide intercalation retards the rate of reaction.

The ANOVA results for TPP-A were calculated to be $F(1,10) = 6.88$, $F_{\text{crit}} = 4.96$, $p = 0.025$. The ANOVA analysis once again revealed that it was possible to distinguish TPP-A using toehold-mediated strand displacement reaction, with the F value being larger than the F_{crit} and the p value being below 0.05 and so within the 95

3.3.3.4. TPP-T, labelled with ATTO 647N, toehold-mediated strand displacement in the presence of ethidium bromide

Finally, the toehold mediated strand displacement reaction kinetic curves for TPP-T with all four DSs in the presence of ethidium bromide (Fig. 3.10 (d)) shows little change from the displacement in the absence of ethidium bromide (Fig 3.9(d)). The most noticeable change was the lag effect seen with DS(G), where it only reaches <0.3 RFU in 600 s with ethidium bromide (Fig 3.10 (d), blue) as opposed to 400 s without (Fig. 3.9 (d), blue)).

The displacement rates for TPP-T (Table 3.3) with DS(T), DS(A), DS(C) and DS(G) were $k_{DS} = 6013 (\pm 54) \text{ M}^{-1} \text{ s}^{-1}$, $k_{DS} = 8419 (\pm 51) \text{ M}^{-1} \text{ s}^{-1}$, $k_{DS} = 1.04 (\pm 0.01) \text{ M}^{-1} \text{ s}^{-1}$ and

$k_{DS} = 5897 (\pm 55) \text{ M}^{-1} \text{ s}^{-1}$. The k_{DS} of the toehold-mediated strand displacement reaction of TPP-C in the presence of ethidium bromide followed the order of $DS(C) < DS(T) < DS(G) < DS(A)$.

As expected the complementary DS(A) had the faster rate of displacement. The presence of ethidium bromide only slightly increased this reaction, $\Delta k_{DS} = 350 \text{ M}^{-1} \text{ s}^{-1}$. The rate of displacement of DS(T) in the presence of ethidium bromide was also increased, $\Delta k_{DS} = 1152 \text{ M}^{-1} \text{ s}^{-1}$. A decrease in the rate of displacement for DS(C) and DS(G) was observed with a $\Delta k_{DS} = -445 \text{ M}^{-1} \text{ s}^{-1}$ and $\Delta k_{DS} = -1113 \text{ M}^{-1} \text{ s}^{-1}$.

The ANOVA results for TPP-T were calculated to be $F(1,10) = 6.277$, $F_{\text{crit}} = 4.96$, $p = 0.031$. The ANOVA analysis once again revealed that it was possible to distinguish TPP-T, using toehold-mediated strand displacement reaction, with the F value being larger than the F_{crit} and the p value being below 0.05.

3.3.3.5. Effect of ethidium bromide on the toehold-mediated strand displacement reaction

In general, there was an increase, or negligible change, in the R_k values when ethidium bromide was introduced into the displacement reaction with only the R_k value between TPP-G and DS(G) decreasing. The R_k values are important for determining the kinetic discrimination power of the displacements and the effect of the ethidium bromide. The R_k values that contain the C mismatches, C•A, C•T and C•C (i.e., TPP-C and DS(C) with non-complementary displacements) were the largest values obtained. C mismatches were the weakest mismatch and therefore this mismatch was the more destabilising to the overall DNA structure and the reason for the high discriminatory power and R_k values.

The ethidium bromide appears to increase the discriminatory power of the C mismatches, with the largest increase being 447 orders of magnitude for TPP-T with DS(C) (i.e., ACG/TTC). There is also a decrease in the displacement rate for TPP-C with DS(T) (ATG/TCC) in the presence of ethidium bromide. It must be noted that when a C•T mismatch forms there is

a large gap that occurs due to the restraints from the DNA backbone preventing strong hydrogen bonds from forming. The reasoning for the decreased displacement rate here may be due to the fact that the intercalation of ethidium bromide allows the DNA to unwind adequately to prevent full hybridisation and therefore prevent the creation of the mismatch.

For A mismatches, A●A, A●G and A●C, an increasing trend was also observed. The intercalation of the ethidium bromide can potentially stabilise the A●A mismatch through base pair stacking as the mismatch has a high propensity for stacking. There is a slight increase with the A●G, comparing intercalated to not intercalated (Table 3.3), implying the ethidium bromide has small effect on the formation of this particular mismatch.

Overall it was found that the displacement rates for the TPPs with intercalated ethidium bromide, with the four DSs, followed the order of $TPP-G \leq TPP-A < TPP-T < TPP-C$ for their complementary displacing sequences. As with the previous complementary toehold-mediated strand displacement reactions it was found that the 80% displacement was reached in relatively the same time from when ethidium bromide was added. TPP-C was still the fastest of the TPPs to undergo toehold-mediated strand displacement. However, TPP-G saw an increase in the displacement rate allowing for displacement in ~ 250 s with ethidium bromide (Fig. 3.10), whilst taking ~ 400 s without (Fig. 3.9). This increased rate of displacement however did not increase the specificity of the reaction. Therefore, it can be concluded that the ethidium bromide had very little effect on the rate of displacement and specificity.

3.4. Concluding remarks

In this chapter, two fluorophores, ATTO 550 and ATTO 647N, were evaluated for use in the investigation of how ethidium bromide affects the toehold-mediated strand displacement reaction.

First, the effect of two different fluorophore labels on the SPP were examined to de-

termine the effect they had on the PCR amplification and toehold-mediated strand displacement process. Using primers labelled with ATTO 550 was found to result in the production of two SPPs. There was the desired ~ 80 bp SPP as well as a secondary non-specific SPP calculated to be around ~ 55 bp in length. It was determined that the ATTO 550 must stabilise non-specific hybridisation of the primer that resulted in the non-specific SPP. This was not seen using the primer labelled with ATTO 647N, which only produced the desired SPP of ~ 80 bp.

SPP, labelled with ATTO 550 and ATTO 647N were then used to fabricate TPP and perform a toehold-mediated strand displacement reaction. Using the TPP labelled with ATTO 550 resulted in uncharacteristic displacement kinetic curves that did not follow pseudo-first order kinetics. This was determined to be due to the production of the secondary non-specific SPP during the synthesis of the TPP interfering with the toehold-mediated strand displacement reactions.

In comparison, the toehold-mediated strand displacement reactions of TPP labelled with ATTO 647N were compatible with both PCR, TPP preparation and the toehold-mediated strand displacement reactions. ATTO 647N was able to increase the toehold-mediated strand displacement reaction, however it did not improve the discrimination power. Any mismatches that involved C were too unstable and hindered the displacement process. This meant that TPP-C had the highest discrimination power and was able to be easily distinguished when using all four DS.

Experiments involving the addition of ethidium bromide as an additive in the toehold-mediated strand displacement reaction showed that it was possible to increase the discrimination power of TPP-C, increasing the ability to distinguish when a C SNP was present. The addition of ethidium bromide also increased the discrimination power when the DS(C) was used to discriminate TPP-G. This is due to the destabilisation that occurs when the ethidium bromide intercalates. This is especially evident for the A•T mismatches which create large gaps that allow for the ethidium bromide to intercalate. This causes increased unwinding of

the DNA backbone (see Chapter 1, Section 1.3) which further strains the mismatch and subsequently preventing base pairing of the mismatch. It was found that mismatches that involved G residue, such as the G•T or G•A mismatch, were stabilised by the presence of the ethidium bromide, this could be due to increased base stacking that occurs allowing for a stable mismatch to form.

3.5. Chapter 3 References

- [1] Khodakov, D. A.; Khodakova, A. S.; Huang, D. M.; Linacre, A.; Ellis, A. V. Protected DNA strand displacement for enhanced single nucleotide discrimination in double-stranded DNA. *Sci Rep* **2015**, *5*, 8721.
- [2] Zhang, Q.; Jagannathan, L.; Subramanian, V. Label-free low-cost disposable DNA hybridization detection systems using organic TFTs. *Biosensors and Bioelectronics* **2010**, *25*, 972–977.
- [3] Stoneking, M. Hypervariable Sites in the mtDNA Control Region Are Mutational Hotspots. *The American Journal of Human Genetics* **2000**, *67*, 1029–1032.
- [4] Fridman, C.; Cardena, M. M. S. G.; Kanto, E. A.; Godinho, M. B. C.; Gonçalves, F. T. SNPs in mitochondrial DNA coding region used to discriminate common sequences in HV1-HV2-HV3 region. *Forensic Science International: Genetics Supplement Series* **2011**, *3*, 164–167.
- [5] Integrated DNA Technologies. 2006; <https://sg.idtdna.com/site/Catalog/Modifications/Product/1108>.
- [6] Winkle, S. A.; Rosenberg, L. S.; Krugh, T. R. On the cooperative and noncooperative binding of ethidium to DNA. *Nucleic Acids Research* **1982**, *10*, 8211–8223.
- [7] ATTO-TEC, ATTO-TEC GmbH - ATTO 550. https://www.attotec.com/attotecshop/product_info.php?language=en&info=p103_ATTO-550.html.
- [8] Technologies, L. B. Black Hole Quencher® Dyes — LGC Biosearch Technologies. <https://www.biosearchtech.com/support/education/fluorophores-and-quenchers/black-hole-quencher-dyes>.
- [9] Ganeshpandian, M.; Loganathan, R.; Suresh, E.; Riyasdeen, A.; Akbarsha, M. A.; Palaniandavar, M. New ruthenium(II) arene complexes of anthracenyl-appended diazacy-

cloalkanes: Effect of ligand intercalation and hydrophobicity on DNA and protein binding and cleavage and cytotoxicity. *Dalton Transactions* **2014**, *43*, 1203–1219.

- [10] Tikhomirova, A.; Beletskaya, I. V.; Chalikian, T. V. Stability of DNA duplexes containing GG, CC, AA, and TT mismatches. *Biochemistry* **2006**, *45*, 10563–10571.
- [11] Sipos, R.; Székely, A. J.; Palatinszky, M.; Révész, S.; Márialigeti, K.; Nikolausz, M. Effect of primer mismatch, annealing temperature and PCR cycle number on 16S rRNA genotyping bacterial community analysis. *FEMS Microbiology Ecology* **2007**, *60*, 341–350.
- [12] Broadwater, D. W.; Kim, H. D. The Effect of Basepair Mismatch on DNA Strand Displacement. *Biophysical Journal* **2016**, *110*, 1476–1484.
- [13] Allawi, H. T.; Santalucia, J. Thermodynamics and NMR of internal G.T mismatches in DNA. *Biochemistry* **1997**, *36*, 10581–10594.
- [14] Allawi, H. T.; SantaLucia, J. Nearest-neighbor thermodynamics of internal A.C mismatches in DNA: Sequence dependence and pH effects. *Biochemistry* **1998**, *37*, 9435–9444.

Chapter 4

Enhancement and characterisation of peroxidase-mimicking activity by screening G-quadruplexes using a genetic algorithm

4.1. Synopsis

This Chapter details a method for enhancing the catalytic activity of G-quadruplexes complexed with hemin (G4/hemin) aptamers that have peroxidase-mimicking activity, by utilising a genetic algorithm (GA) that mimics an evolutionary natural selection. This was achieved by a two-step process that was repeated multiple times. The first step was the generation of new DNA oligodeoxynucleotide (ODN) sequences, that are likely to form G4s, using an in-silico GA. The G4s were then folded and complexed with hemin, an iron containing porphyrin, to form a G4/hemin aptamer. The peroxidase-mimicking activity of each G4/hemin aptamer was tested using a 3,3',5,5'-tetramethylbenzidine (TMB) assay. Each G4/hemin aptamer within that generation of the GA was then ranked based on the initial rate of peroxidase-mimicking activity (V_0), which allowed for the identification of sequences with enhanced V_0 (used to form the G4/hemin aptamer) that led to the highest V_0 . Only the ODN sequences that formed G4/hemin

aptamers with the highest V_0 were used to create the next generation of ODN sequences for testing. Finally, the top 3 ranked G4/hemin aptamers were characterised using the Michaelis-Menten equation to determine catalytic rate (V_{max}), affinity (K_m) for the TMB substrate and catalytic activity (k_{cat}).

4.1.1. Introduction and purpose

G-quadruplexes (G4s) are unique DNA structures that are made up of multiple stacked guanine-tetrads (G-tetrads) (see Chapter 1, Section 1.5.3.4).¹⁻³ G4s are primarily comprised of guanine-rich (G-rich) DNA, with ≥ 2 subsequent guanines (G) residues forming guanine-tracts (G-tracts). These are able to hydrogen bond with three other G-tracts to form the stacking G-tetrads.

This chapter will primarily discuss unimolecular G4s referred to as intramolecular G4s. Intramolecular G4s commonly have the sequence: $5'—X_{t1}G_mX_{l1}G_mX_{l2}G_mX_{l3}G_mX_{t2}—3'$, where m is the number of G residues in the G-tracts that are able to form the G-tetrads that can then stack to form the G4. X_{t1} , X_{t2} , X_{l1} , X_{l2} , and X_{l3} can be any combination of nucleotide residues (adenine (A), thymine (T), cytosine (C) and (G)); $t1$ and $t2$ refer to the 5' and 3' terminal regions, respectively; and $l1$, $l2$ and $l3$ refer to the loop regions of the G4.

Fig. 4.1 shows an example of how this general oligodeoxynucleotide (ODN) sequence folds into a G4 structure (where $m = 3$ or 4), see Chapter 1, Section 1.5.3.4 for description of all the possible G4 structures.

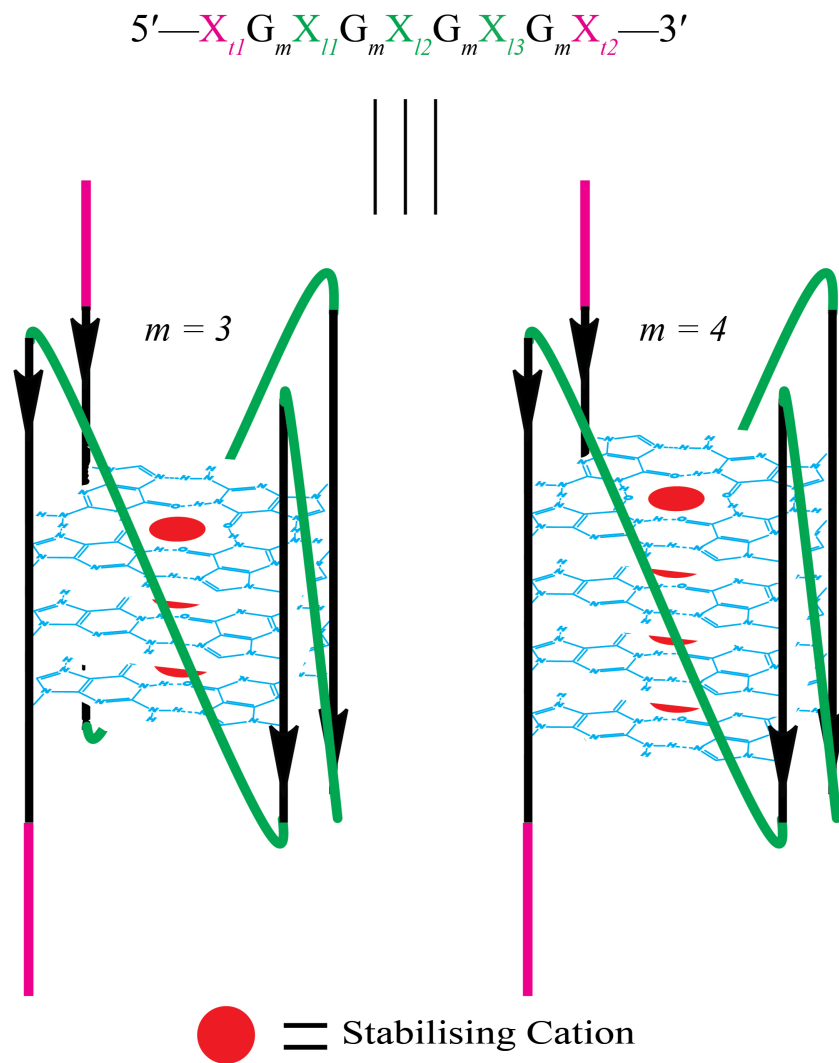


Figure 4.1: General structure of an intramolecular G4 made up of the oligodeoxynucleotide (ODN) sequence: $5' - X_{l1} G_m X_{l1} G_m X_{l2} G_m X_{l3} G_m X_{l2} - 3'$. Consisting of 3 (left, $m = 3$) or 4 (right, $m = 4$) stacked G-tetrads (blue) stabilised with a cation (red). The G4 is made up of 2 terminal regions (pink), 3 loop regions (green) and 4 G-tracts (black). Arrows indicate the direction of the backbone ($5'$ to $3'$).

G4s that recognise and complex with molecules are known as aptamers (see Chapter 1, Section 1.5.3.7) and these be used for several purposes; namely target recognition,⁴ enzyme inhibition¹ and DNAzymes.⁵ The aptamers of interest to this chapter are ones that are able to complex with hemin, an iron (III) containing protoporphyrin IX (see Fig. 4.2), to acquire peroxidase-mimicking activity. These aptamers are often referred to as G4/hemin aptamers.⁶ The peroxidase-mimicking activity refers the G4/hemin aptamers ability to mimic the activity of enzymes (such as horseradish peroxidase (HRP)) that oxidise various organic compounds in the presence of hydrogen peroxide species (see Chapter 1, Section 1.5.3.11).

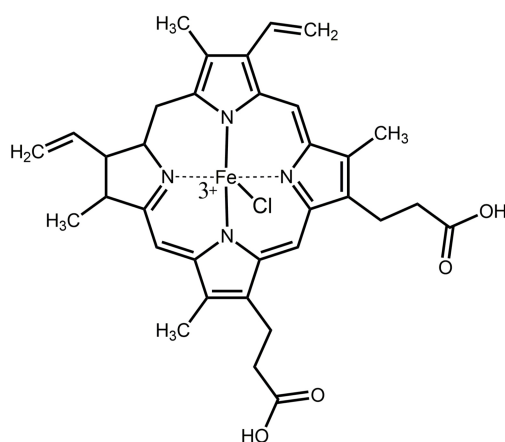


Figure 4.2: Chemical structure of hemin, an iron containing iron (III) protoporphyrin IX.

As mentioned in Chapter 1, Section 1.5.3.8, the discovery of nucleic acid (DNA and RNA) aptamers is often carried out through Systematic Evolution of Ligands by Exponential Enrichment (SELEX), which is a method designed to find aptamers that complex with high affinity to a target.⁷ However, high affinity does not necessarily equate to high peroxidase-mimicking activity in the case of G4/hemin aptamers. The reason for this will be discussed in detail in the next section. First, a method for discovering sequences that have high peroxidase-mimicking activity, called a GA, will be explained.

4.1.2. Evolution of G4 ODN sequences using a genetic algorithm

A GA is a set of rules that are followed in order to discover nucleic acid or peptide sequences that have desirable traits, such as high affinity, reactivity or inhibitory properties.¹ This is because the GA is designed to mimic evolutionary processes, whereby multiple generations of nucleic acid or peptide (amino acids) sequences are sequentially generated that retain and enhance desirable traits from the previous generation. Ikebukuro *et al.*^{1,8} have applied a GA to discover peptides and G4 aptamers with enhanced inhibition properties towards enzymes. By using a GA it is possible to test a large number G4 ODN sequences of G4 aptamers for activity and ensure that each generation has equal or greater activity than the previous one.

Fig. 4.3 shows the general schematic of the GA utilised in this thesis, and was performed using a simple program. i.e., Microsoft Excel (2015). In Fig. 4.3, Step 1 all the G4 ODN sequences in the n generation are divided into terminal regions (X_{t1} and X_{t2} , pink), loop regions (X_{l1} , X_{l2} and X_{l3} , green) and G-tract (G_m , black). The G-tracts are the only part of the sequence that will not be affected in the GA, as it is vital that a G4 is still able to form (see Fig. 4.3). In Fig. 4.3, Step 2 only the terminal and loop regions are shuffled within the respective groups. This is repeated multiple times to generate 10 new G4 ODN sequences that are able to form G4/hemin aptamers.

In Fig. 4.3, Step 3 each sequence is then mutated only once at any terminal or loop region. The mutations can be one of the following: substitution, deletion or insertion to produce generation $n + 1$.

Finally, in Fig. 4.3 (Step 4) the generation $n + 1$ of G4/hemin aptamers are tested using an assay (see Section 4.2.2 for more details). The sequences that are determined to have the highest peroxidase-mimicking activity using the assays are then used in the GA to produce another generation of 10 sequences.

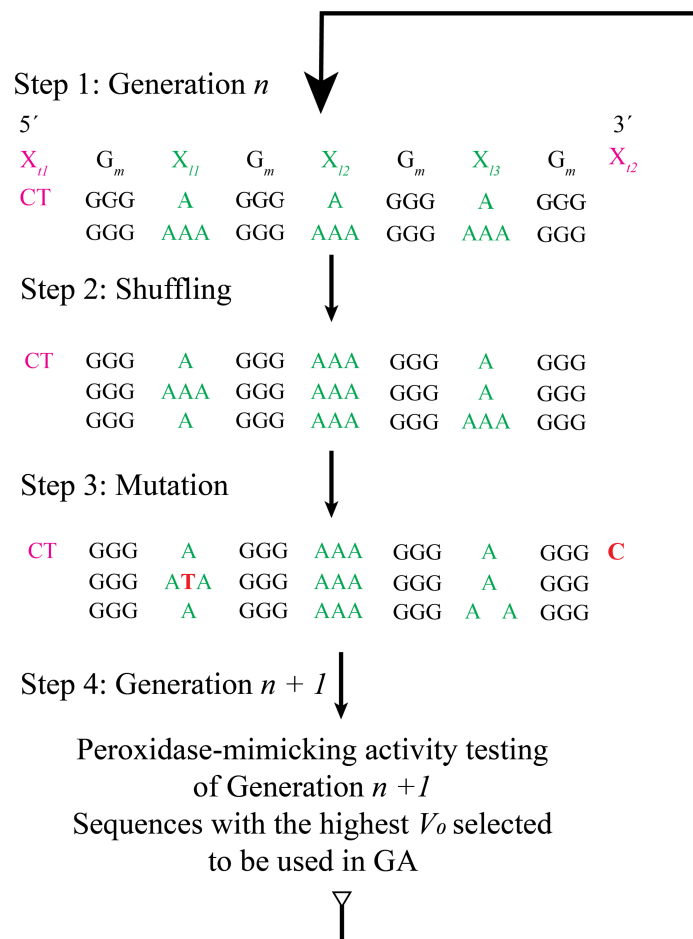


Figure 4.3: General schematic of how a GA was performed in this chapter. Step 1: The n generation is divided into terminal (X_{t1} and X_{t2} , pink), loop (X_{l1} , X_{l2} and X_{l3} , green) and G regions (G_m , black). Step 2: The terminal ends, and loops are shuffled within their respective groups. Step 3: A single base mutation, insertion (red) or deletion (blank space) to produce Generation $n + 1$. Step 4: Generation $n + 1$ is tested for peroxidase-mimicking activity (see Section 4.2.1) and the sequences with the highest peroxidase-mimicking activity are put back into the GA as Generation n .

4.1.2.1. Applications of G4/hemin aptamers with enhanced peroxidase-mimicking activity

Due to the lower cost of production and broader range of operating conditions (e.g., temperature,⁹ pH¹⁰ and reactants^{6,11}) there are an increasing number of studies that utilise G4/hemin aptamers to replace peroxidase enzymes.^{3,12} This allows for the development of new biosensors using already established assay methods, namely enzyme-linked immunosorbent assay (ELISA) (see Chapter 1, Section 1.5.3.11). These methods often depend on the oxidation of a reactant, which will be referred to as a 'substrate' henceforth, to produce a colorimetric or chemiluminescent readout. The advantage of these systems is the visual inspection of the results without the requirement of expensive equipment. Examples of these substrates include 3,3',5,5'-tetramethylbenzidine (TMB, absorbance max (λ_{max}) = 655 nm),¹³ 2,2'-azino-bis(3-ethylbenzothiazoline-6-sulfonic acid) diammonium salt (ABTS, λ_{max} = 414 nm)¹¹ and 3-aminophthalhydrazide (luminol, chemiluminescent).¹⁴

The proposed general mechanism for the oxidation of the substrates (e.g., TMB) by G4/hemin aptamers mediated by hydrogen peroxide is shown in Fig 4.4. Fig. 4.4 shows that the hemin (red) first complexes with the G4 (green) to form the G4/hemin aptamer. This aptamer then reacts with the hydrogen peroxide, essentially replacing the H₂O with H₂O₂, which can then result in the formation of two intermediate compounds. Compound I (heterolytic cleavage) is the π -cation radical G4/hemin aptamer and Compound II (homolytic cleavage) is the neutral G4/hemin aptamer.¹⁰ The heterolytic cleavage of the hydrogen peroxide occurs when two electrons are withdrawn from the hemin (with an Fe (III)) molecule to form a ferrylporphyrin radical (Fe (IV) = O^{•+}).⁶ These two electrons are withdrawn from the Fe(III) (forming the Fe(IV)) and one electron from the porphyrin itself. This active ferrylporphyrine is then able to withdraw electrons from a substrate, in this case the TMB, to generate an oxidised product (this will be discussed in more detail later).

G4/hemin aptamers have a broader range of substrates to react with in comparison to peroxidase enzymes, as there are less steric groups to prevent interaction with the substrate.⁶

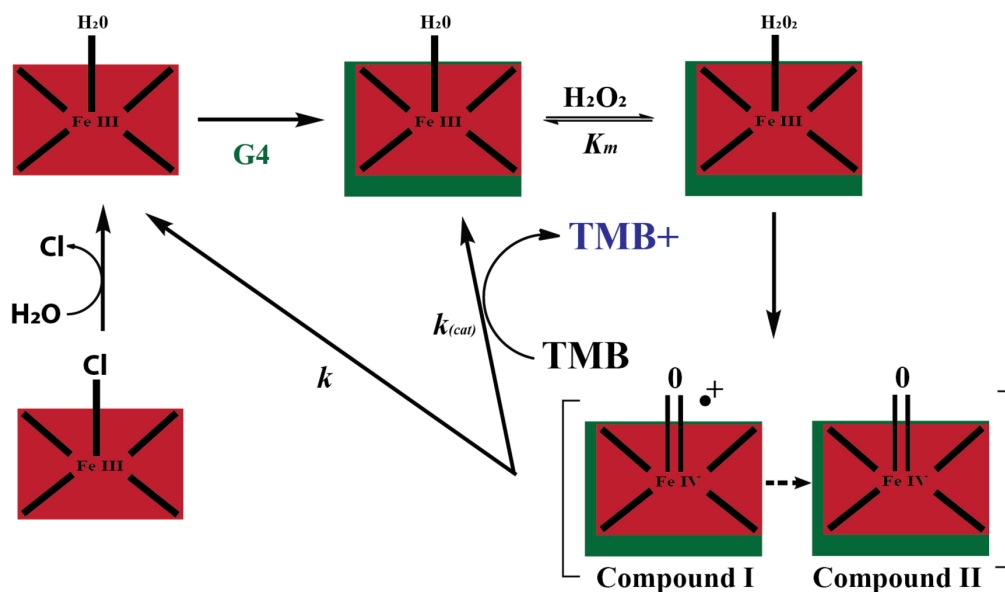


Figure 4.4: The proposed general mechanism for the catalytic cycle of G4/hemin with peroxidase-mimicking activity adapted from Chang *et al.*¹⁵ Initially, the hemin (red) replaces the Cl residue with a water residue. Then the hemin is able to complex with an already formed G4 (green). This complexation allows for the structure to acquire peroxidase-mimicking activity. The hemin reacts with a hydrogen peroxide, replacing the water with the hydrogen peroxide. Compound I and compound II are able to form depending on homocleavage or heterocleavage occurs, respectively. Compound I is the active component which is able to react with the substrate, TMB in this case and produces a blue coloured product. This reaction results in compound I becoming compound II. Compound II is able to be recycled back into the water containing hemin or G4/hemin.

Fig. 4.5 is a simulation of the G4/hemin aptamer, that shows the hemin is complexed on top of the G4 aptamer as opposed to being situated inside of the active site in the peroxidase.^{16,17}

In peroxidase enzymes the presence of a histidine residue influences the formation of heterolytic cleavage product (Compound I, Fig. 4.4)¹⁸ and in G4/hemin aptamers this role can be fulfilled by the presence of a nucleotide (nt), primarily an A or C residue.^{10,15,19} This is due to the histidine or the nt residue catalysing the heterolytic cleavage of the hydrogen peroxide that is bonded to the hemin (Fig. 4.4). The histidine (peroxidase) and nt are able to stabilise the intermediate through acid-base catalysis, donating or accepting protons as needed.^{20–22}

The proposed general mechanism for this heterolytic stabilisation involving a nt (in this case an A residue), is demonstrated in Fig.4.6. The effectiveness of the acid-base catalysis is dependent on the pH of the solution and therefore histidine (pKa ~7) is more effective at

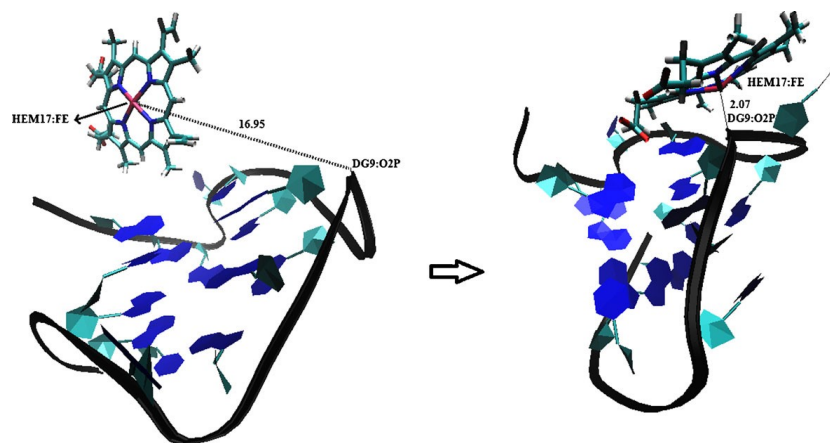


Figure 4.5: VMD snapshots of the G-quadruplex DNA-hemin complex for (left) initial and (right) final conformation resulting from MD simulation, adapted from Ghahremani Nasab *et al.*¹⁷

neutral pH while A and C residues (pKa \sim 4.1 and \sim 4.4, respectively) are more effective at lower pH.^{10,18,23} The nitrogens (N1 and N10) on the A nt allow for a hydrogen bond to form between the A nt residue and the coordinated hydrogen peroxide on the hemin. This stabilization encourages the formation of compound I and so the presence of A nt residues should enhance the peroxidase-mimicking activity of the G4 aptamer.¹⁹ A T nt residue is not expected to have the same effect on the G4/hemin aptamers. This is due to the T nt having a pKa of \sim 9.9.²⁴

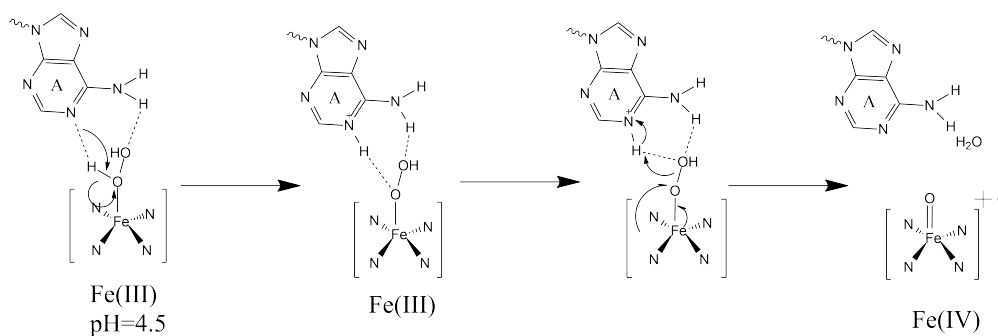


Figure 4.6: Proposed schematic for how an A nt plays a role in the heterolytic cleavage of hydrogen peroxide during peroxidase-mimicking of the G4/hemin aptamer, adapted from Li *et al.*¹⁰

4.2. G4/hemin aptamer enzyme kinetics

As G4/hemin aptamers have peroxidase-mimicking activity they are therefore considered a DNAzyme. It is possible to characterise them in a similar manner to enzymes, by utilising the Michaelis-Menten equation (Eq. 4.1).²⁵

$$V_0 = \frac{V_{max} \times S_0}{K_m + S_0} \quad (4.1)$$

Where V_0 is the initial velocity of the reaction, V_{max} is the maximum velocity of the reaction, K_m is the Michaelis constant and S_0 is the initial concentration of the substrate (TMB). Using the V_{max} it is possible to determine the catalytic rate ($k_{(cat)}$) of the G4/hemin aptamer using Eq. 4.2:

$$k_{(cat)} = \frac{V_{max}}{[E]} \quad (4.2)$$

The Michaelis-Menten equation is utilised to determine several crucial factors for the characterisation of the catalytic rate of the G4/hemin aptamers. These factors are the V_{max} , K_m and $k_{(cat)}$ of the G4/hemin aptamer. The V_{max} is the maximum rate of the enzyme when completely saturated with the substrate. The K_m is the inverse of the affinity of the substrate to the G4/hemin aptamer that is required to reach half its V_{max} ($\frac{1}{2}V$).²⁵ Therefore, K_m is an indication of the affinity of the substrate, the TMB in this case, to the G4/hemin aptamer.

A low K_m shows that the enzyme has a high affinity for the substrate, indicating that a low amount of the substrate is required to reach its $\frac{1}{2}V$. While a high K_m shows that the enzyme has a low affinity for the substrate and therefore require a higher concentration of substrate to reach its $\frac{1}{2}V$. The V_{max} can be used to determine the $k_{(cat)}$, which is the turnover or the number of times the G4/hemin aptamers are able to react with the substrate per second.

Although the reaction pathways of G4/hemin aptamers are similar to the peroxidase enzymes, they are still yet to reach the same sensitivity as the enzyme-based methods.²⁵ There are several factors that affect the peroxidase-mimicking activity of G4/hemin aptamers. The next section will therefore discuss how the TMB assay was optimised to ensure the highest peroxidase-mimicking activity could be achieved.

4.2.1. Optimisation of the first generation of G4/hemin aptamer's peroxidase-mimicking activity testing

To the best of the authors knowledge the sequence with the highest reported peroxidase-mimicking activity is CT(G₃A)3G₃ (denoted as EAD-2 henceforth) (Table 4.1).¹¹ It has been well established that the rate of the peroxidase-mimicking activity is dependent on the sequence and the structure of the G4.^{11,26} Therefore, it was hypothesised that the GA could be utilised to discover sequences with enhanced peroxidase-mimicking activity over the EAD-2. However, as the GA relies on multiple sequences being used during the shuffling step (Fig. 4.4, Step 2), the first generation had to be generated without the GA.

Therefore, the first generation was generated by purposefully mutating multiple residues to produce 10 sequences. This allowed for the investigation of the effects of the number of G residues in the G-tract, deletions and the substitution of A residues with T residues. This also allowed for the optimisation of parameters that would allow for enhanced peroxidase-mimicking activity. These included the folding step of the G4/hemin aptamer (see Chapter 2, Section 2.3.2.1) and the type of hemin used.

It was hypothesised that the way hemin was added to the G4 aptamer may also affect the overall peroxidase-mimicking activity. Therefore, post-addition and pre-addition of hemin were investigated in this Chapter. Another method that could possibly increase the peroxidase-mimicking activity of the G4 aptamers was to use hemin derivatives.

There currently does not exist research that tests the peroxidase-mimicking activity

of G4 aptamers complexed with hemin derivatives, such as the pegylated form polyethylene glycol-hemin (PEG-hemin, Fig. 4.7) and so this was trialled in this thesis. The PEG-hemin structures have been shown to have higher peroxidase activity as well as a longer half-life as compared to hemin.²⁷ PEG-hemin is also water soluble and so does not require the addition of dimethyl sulfoxide (DMSO) to become soluble in the buffer solution.

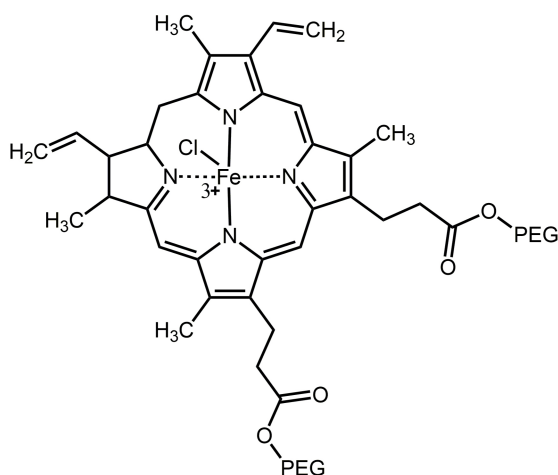


Figure 4.7: Chemical structure of polyethylene glycol-hemin (PEG-hemin).

This chapter will first discuss the optimisation parameters of enhancing the peroxidase-mimicking activity of the EAD-2 and first generation of G4/hemin aptamers towards the substrate TMB. The parameters that will be discussed are: (1) sequence modification, (2) pre-addition or post-addition of hemin during the folding step and (3) the use of PEG-hemin.

4.3. Results and discussion

4.3.1. Development of first generation of the G4/hemin aptamers and optimisation of TMB assay

This section will discuss how the first generation of the GA was developed and the optimisation of the parameters for the TMB assay.

4.3.1.1. Sequence modification: Investigation of additional G residues in the G-tracts affect on the G4 aptamer peroxidase-mimicking activity

Firstly, this section will discuss the modification of the sequence of G4/hemin aptamers to determine the effect of altering the number of G residues in the G-tract (Fig. 4.1, m) and the nt residues that make up the terminal and loop regions (Fig. 4.1, X_t and X_l). There is no research that has directly studied how the number of G residues in the G-tract effect the peroxidase-mimicking activity of G4/hemin aptamers. However, Tran *et al.*²⁸ determined that the number of G residues (Fig. 4.1, m) in the G-tract does not necessarily dictate the number of stacked G-tetrads. Therefore, if $m = 4$, it is still possible for a G4 with only 3 stacked G-tetrads to form (see Fig. 4.1, left). The remaining G residues make up part of the loop region, which can also play a role in the peroxidase-mimicking activity. Therefore, it was investigated how the addition of G residues affected the peroxidase-mimicking activity.

To investigate the optimum number of G residues in the G-tract the sequence EAD-2 was modified. Table 4.1 lists the EAD-2 sequence and modified G4 aptamer sequences. The samples were named after the generation and order in that generation (e.g., the first sequence in Generation 1 is named 1-01).

Table 4.1: Name and sequences used to investigate the effects of G residues on the peroxidase-mimicking activity of the EAD-2 sequence divided into separate terminal (X_{t1} and X_{t2}), loop (X_{l1} , X_{l2} , X_{l3}) and G (G_m) regions.

Sample	X_{t1}	G_m	X_{l1}	G_m	X_{l2}	G_m	X_{l3}	G_m	X_{t2}
EAD-2	CT	GGG	A	GGG	A	GGG	A	GGG	A
1-01*	CT	GGGG	A	GGG	A	GGGG	A	GGG	A
1-02*	CT	GGGG	A	GGGG	A	GGGG	A	GGG	A
1-03*	CT	GGGG	A	GGGG	A	GGGG	A	GGGG	A

*Red indicates changes from the EAD-2 sequence.

The G4 aptamers from Table 4.1 were tested using a TMB substrate solution, which will be referred to as a TMB assay for the remainder of this thesis. The TMB assay was performed following the procedure set out in Chapter 2, Section 2.3.2.3. In brief, the folded (in

the presence of cations) G4/hemin aptamers (5 μL) were placed into a 96-well microplate, and then TMB substrate (295 μL) at room temperature was added. The microplate was placed into a UV/vis plate reader that measured the absorbance at 595 nm over 15 min. The blanks referred to no aptamer only hemin in the assay.

All the G4 aptamer sequences from Table 4.1 were folded and tested. A plot of absorbance versus time resulted in a straight line. The resulting slope of the line was used to calculate the initial peroxidase-mimicking activity (V_0) using Eq. 4.3, adapted from Beer's Law:

$$V_0 = \frac{m}{\epsilon} \quad (4.3)$$

where m = slope and $\epsilon = 3.9 \times 10^4 \text{ M}^{-1} \text{ cm}^{-1}$ (molar extinction of TMB radical).¹³

The V_0 for each sequence is shown in Table 4.2.

Table 4.2: Peroxidase-mimicking activity (V_0) calculated for the G4 aptamer sequences from Table 4.1.

Sample	G4 aptamer sequence	Peroxidase-mimicking activity, $V_0, \mu\text{M s}^{-1\beta}$
EAD-2	CTG ₃ AG ₃ AG ₃ AG ₃ A	0.018
1-01	CTG ₄ AG ₃ AG ₄ AG ₃ A	0.012
1-02	CTG ₄ AG ₄ AG ₄ AG ₃ A	0.008
1-03	CTG ₄ AG ₄ AG ₄ AG ₄ A	0.009 \pm 0.006

^{β} Errors below 0.001 $\mu\text{M s}^{-1}$

Table 4.2 shows that the EAD-2 sequence has a peroxidase-mimicking activity at $V_0 = 0.018 \mu\text{M s}^{-1}$. Table 4.2 also shows that the 1-01, 1-02 and 1-03 sequence (containing extra G residues) have V_0 values of $0.012 \mu\text{M s}^{-1}$, $0.008 \mu\text{M s}^{-1}$ and $0.009 \pm 0.006 \mu\text{M s}^{-1}$, respectively. There is a change in the V_0 for all the sequences compared to EAD-2 of $\Delta V_0 = -0.006 \mu\text{M s}^{-1}$, $-0.010 \mu\text{M s}^{-1}$ and $-0.009 \mu\text{M s}^{-1}$, respectively. This data indicates that any addition of the G residues in the G-tracts decreases the V_0 of the EAD-2.

It appears that the more G-tracts that contain extra G residues the more the V_0 is reduced. For 1-03, the error is almost as large as the calculated V_0 , indicating that 4 Gs in the G-tract forms an unstable G4/hemin aptamer. Therefore, it was decided that the optimum number of G residues to use in the G-tracts was $m = 3$. This means that when performing the mutation step using the GA a G residue will not be added or substituted in a way that will form a G-tract with 4 G residues.

The next section will discuss how deletions and substitutions in the terminal and loop regions affect the peroxidase-mimicking activity of the G4/hemin aptamer.

4.3.1.2. Investigation of deletions and T residue substitutions affects on the G4 aptamer peroxidase-mimicking activity

In order to investigate the effects of deletions and T residue substitutions on the peroxidase-mimicking activity of the EAD-2 sequence, several new sequences were derived from EAD-2. Each sequence was derived from EAD-2 by selectively deleting, substituting an A residue for a T residue or both. These sequences are shown in Table 4.3, where the EAD-2 sequence has been sequentially altered to produce 7 new sequences (making 10 sequences in Generation 1 including those from Table 4.1). As A residues are considered to enhance the peroxidase-mimicking activity, the sequence $(G_3A_3)_3G_3$ (denoted as G_3A_3) was also tested for a more comprehensive comparison of how T residues affect the peroxidase-mimicking activity.

The G4/hemin aptamers from Table 4.4 were tested using a TMB assay. The resulting V_0 values are shown in Table 4.4 along with the ranking for each sequence based on the peroxidase-mimicking activity.

Table 4.4 shows that G_3A_3 (ranked 1st) and 1-10 (ranked 2nd) had peroxidase-mimicking activity at $V_0 = 0.032 \pm 0.001 \mu\text{M s}^{-1}$ and $0.026 \mu\text{M s}^{-1}$, respectively. These were the only two sequences to have increased V_0 when compared to the EAD-2 (ranked 3rd). The 4th highest V_0 was 1-04, with a rate of $0.016 \mu\text{M s}^{-1}$. The remaining sequences from Table 4.4 all had V_0

Table 4.3: Name and sequences used to investigate the effects of deletions and substitution of A residues with T residues on the peroxidase-mimicking activity of the Parent sequence divided into separate terminal (X_{t1} and X_{t2}), loop (X_{l1} , X_{l2} , X_{l3}) and G (G_m) regions.

Sample	X_{t1}	G_m	X_{l1}	G_m	X_{l2}	G_m	X_{l3}	G_m	X_{t2}
EAD-2	CT	GGG	A	GGG	A	GGG	A	GGG	A
1-04*	-	GGG	A	GGG	A	GGG	A	GGG	A
1-05*	-	GGG	A	GGG	A	GGG	A	GGG	-
1-06*	-	GGG	T	GGG	A	GGG	A	GGG	-
1-07*	-	GGG	A	GGG	T	GGG	A	GGG	-
1-08*	-	GGG	A	GGG	T	GGG	T	GGG	-
1-09*	-	GGG	A	GGG	T	GGG	T	GGG	A
1-10*	CT	GGG	A	GGG	T	GGG	T	GGG	A
$G_3G_3^*$	-	GGG	AAA	GGG	AAA	GGG	AAA	GGG	-

*Red indicates changes from the EAD-2 sequence.

Table 4.4: Peroxidase-mimicking activity (V_0) calculated for the G4 aptamer sequences in Table 4.3 With the ranking of each sequence based on V_0 and the top 4 sequences (highest V_0) are underlined.

Sample	G4 aptamer sequence	Peroxidase-mimicking activity, V_0 , $\mu\text{M s}^{-1} \beta$	Rank
EAD-2	CTG ₃ AG ₃ AG ₃ AG ₃ A	0.018	<u>3</u>
1-04	G ₃ AG ₃ AG ₃ AG ₃ A	0.016	<u>4</u>
1-05	G ₃ AG ₃ AG ₃ AG ₃ A	0.013	6
1-06	G ₃ AG ₃ AG ₃ AG ₃	0.007	7
1-07	G ₃ AG ₃ TG ₃ AG ₃	0.006	8
1-08	G ₃ AG ₃ TG ₃ TG ₃	0.004	9
1-09	G ₃ AG ₃ TG ₃ TG ₃ A	0.013	5
1-10	CTG ₃ AG ₃ TG ₃ TG ₃ A	0.026	<u>2</u>
G_3A_3	G ₃ A ₃ G ₃ A ₃ G ₃ A ₃ G ₃	0.032 ± 0.001	<u>1</u>
blank (no aptmaer)	N/A	0.001	0

β Errors below $0.001 \mu\text{M s}^{-1}$

values $\leq 0.013 \mu\text{M s}^{-1}$ and therefore were not considered for use with the GA to produce the next generation. However, this data does show that the sequence is vital for the peroxidase-mimicking activity.

In regards to the A residue substitutions with T residues, Table 4.4 shows a trend when comparing the V_0 of 1-05 (ranked 6th) with 1-06 (ranked 7th) and 1-07 (ranked 8th). If an A residue in the first or second loop were substituted with T residues the V_0 was decreased from 0.013 to $\mu\text{M s}^{-1}$, $0.007 \mu\text{M s}^{-1}$ and $0.006 \mu\text{M s}^{-1}$, respectively. When there is an T residue in the X_{l2} and X_{l3} , as in the case of 1-08 (Table 4.4), then the V_0 is reduced to $0.004 \mu\text{M s}^{-1}$. This shows that A residues can play an important role in the peroxidase-mimicking activity of

the G4/hemin aptamers.

G₃A₃ (Table 4.4, ranked 1st) having the highest peroxidase-mimicking activity was not unexpected as it is comprised of multiple A residues which are thought to promote the formation of the active Compound I (see Section 4.2, Fig. 4.4).^{10,19} A similar effect is shown by the comparison of 1-09 (Table 4.4, ranked 5th) and 1-08 (Table 4.4, ranked 9th). The rates differ by $\Delta V_0 = 0.009 \mu\text{M s}^{-1}$, however the only sequence difference is the deletion of an A residue from the 3' terminal region of 1-09 (Table 4.3, X₁₂). The same effect can be seen when comparing 1-04 (Table 4.4, ranked 4th) and 1-05 (Table 4.4, ranked 7th) to a lesser degree ($\Delta V_0 = 0.003 \mu\text{M s}^{-1}$). These results support the theory that A residues are able to enhance the peroxidase-mimicking activity of the G4/hemin aptamers.^{10,19}

Comparing 1-10 (Table 4.4, ranked 2nd) to 1-09 (Table 4.4, ranked 5th) shows that although the V_0 is halved, 1-10 contains a C and T residue at the 5' terminal position whereas 1-09 does not (Table 4.3, X₁₂). This supports the theory that the presence of a C residue can also increase the peroxidase-mimicking activity of the G4/hemin aptamer.¹⁵

Thus, A and C residue containing aptamers show enhanced activity when compared to those that contain an extra G in the G-tract (see 1-01 to 1-03, Table 4.1), deletion, or T residue substitution (1-04 to 1-10, Table 4.3). G₃A₃ was ranked 1st supporting this hypothesis.

The 10 sequences from Table 4.1 and 4.4 are regarded as Generation 1 and will be utilised in the next section to optimise the TMB conditions in order to obtain the highest possible peroxidase-mimicking activity. However, in order to produce the second generation the 4 sequences (G₃A₃, 1-10, EAD-2 and 1-04, in descending order) (Table 4.4) were used in the GA, discussed in Section 4.3.3.

The next section will discuss the optimisation of the addition of the hemin.

4.3.1.3. Optimisation of G4/hemin aptamer folding procedure

The second optimisation parameter investigated was the addition of the hemin before and after the folding of the G4/hemin aptamer (see Chapter 2, Section 2.3.2.1 for details). In order to achieve the optimal peroxidase-mimicking activity, it is vital for the hemin to complex with the G4 aptamer correctly. The two parameters that were investigated were the pre-addition or post-addition of the hemin during the folding step.

In order to fold the G4 aptamers, the G4 ODN (linear DNA) was placed into a buffer (containing K^+) and heated to 95 °C, then cooled to room temperature. For pre-addition the hemin was added to the G4 ODN before the heating step and will be referred to as pre-addition G4/hemin aptamers. The theory behind this was that the hemin would be able to complex with the G4 aptamer as it folded, and therefore form a more favourable conformation (i.e., parallel G4 structure, see Chapter 1, Section 1.5.3.4).

For post-addition the hemin was added after the folded G4 aptamer had cooled to room temperature and will be referred to as post-addition G4/hemin aptamers.).

The TMB assay was performed in the same manner as in previous sections. The G4/hemin aptamers from Table 4.1 and 4.3 were tested using a TMB assay. The calculated V_0 for pre-addition and post-addition are shown in Table 4.6. The V_0 post-addition G4/hemin aptamer data found in Table 4.6 is the same data found in Table 4.2 and Table 4.4 and simply added to allow for easier comparison to the pre-addition G4/hemin aptamers.

Table 4.5 shows that all the V_0 values for pre-addition resulted in a slower V_0 when compared to the corresponding post-addition sample. 1-10 pre-addition G4/hemin aptamer has the largest V_0 difference with a 77% decrease ($\Delta V_0 = 0.020 \mu\text{M s}^{-1}$) compared with the corresponding post-addition sample. G_3A_3 has the highest pre-addition V_0 at a $V_0 = 0.017 \mu\text{M s}^{-1}$, which is still a 53% decrease compared to the corresponding post-addition G4/hemin aptamer.

Table 4.5: Peroxidase-mimicking activity (V_0) calculated for the G4 aptamer sequence from Table 4.1 and 4.3 with post- and pre-addition of hemin during the folding procedure.

Sample	G4 aptamer sequence	Peroxidase-mimicking activity, V_0 , $\mu\text{M s}^{-1}$ $^{\beta}$	
		post-addition	pre-addition
EAD-2	CTG ₃ AG ₃ AG ₃ AG ₃ A	0.018	0.006
1-01	CTG ₄ AG ₃ AG ₄ AG ₃ A	0.012	0.004
1-02	CTG ₄ AG ₄ AG ₄ AG ₃ A	0.008	0.004
1-03	CTG ₄ AG ₄ AG ₄ AG ₄ A	0.009 ± 0.006	0.004
1-04	G ₃ AG ₃ AG ₃ AG ₃ A	0.016	0.008
1-05	G ₃ AG ₃ AG ₃ AG ₃	0.013	0.006
1-06	G ₃ TG ₃ AG ₃ AG ₃	0.007	0.003
1-07	G ₃ AG ₃ TG ₃ AG ₃	0.006	0.003
1-08	G ₃ AG ₃ TG ₃ TG ₃	0.004	0.002
1-09	G ₃ AG ₃ TG ₃ TG ₃ A	0.013	0.005
1-10	CTG ₃ AG ₃ TG ₃ TG ₃ A	0.026	0.006
G ₃ A ₃	G ₃ A ₃ G ₃ A ₃ G ₃ A ₃ G ₃	0.032 ± 0.001	0.017

$^{\beta}$ Errors below 0.001 $\mu\text{M s}^{-1}$

The reason for the decrease in V_0 was proposed to be due to degradation of hemin when being heated to 95 °C during the folding step of the G4/hemin aptamer. Therefore, all TMB assays in this thesis will use the post-addition of the hemin during the folding procedure. This ensures that the highest V_0 is achieved.

The next section will discuss using hemin derivatives to determine if it was possible to increase the peroxidase-mimicking activity of Generation 1.

4.3.2. Investigation of pegylated-hemin effect on the G4 aptamer peroxidase-mimicking activity

The pegylated form of hemin (PEG-hemin) (Fig. 4.7) was investigated to see if it enhanced the peroxidase-mimicking activity compared to pristine hemin (Fig. 4.2). PEG-hemin is the more soluble form of hemin, meaning that it does not require the addition of polar aprotic solvent such as DMSO to become miscible in an aqueous solutions.²⁷ This was hypothesised to allow for a better complexation of the hemin with the G4 aptamer due to increased solubility in the aqueous solution. Table 4.6 shows the calculated V_0 values using PEG-hemin in the TMB assay.

Table 4.6: Peroxidase-mimicking activity (V_0) calculated for the G4 aptamer sequence from Table 4.1 and 4.3 with PEG-hemin.

sample	G4 aptamer sequence	Peroxidase-mimicking activity, $V_0, \mu\text{M s}^{-1} \beta$
EAD-2	CTG ₃ AG ₃ AG ₃ AG ₃ A	0.008
1-01	CTG ₄ AG ₄ AG ₃ AG ₃ A	0.009
1-02	CTG ₄ AG ₃ AG ₄ AG ₄ A	0.007
1-03	CTG ₄ AG ₄ AG ₄ AG ₄ A	0.007
1-04	G ₃ AG ₃ AG ₃ AG ₃ A	0.003
1-05	G ₃ AG ₃ AG ₃ AG ₃	0.004
1-06	G ₃ TG ₃ AG ₃ AG ₃	0.005
1-07	G ₃ AG ₃ TG ₃ AG ₃	0.007
1-08	G ₃ AG ₃ TG ₃ TG ₃	0.006
1-09	G ₃ AG ₃ TG ₃ TG ₃ A	0.006
1-10	CTG ₃ AG ₃ TG ₃ TG ₃ A	0.009
G ₃ A ₃	G ₃ A ₃ G ₃ A ₃ G ₃ A ₃ G ₃	0.010
blank (no aptamer)	N/A	0.005

^{β} Errors below $0.001 \mu\text{s}^{-1}$

Table 4.6 shows that PEG-hemin blank (no aptamer) has a $V_0 = 0.005 \mu\text{M s}^{-1}$ and when compared with the hemin blank (Table 4.3), $V_0 = 0.001 \mu\text{M s}^{-1}$) shows that PEG-hemin has an increased peroxidase activity. Therefore, it was expected that this would allow for the G4/hemin aptamer sequences to have an increased V_0 . However, Table 4.6 shows that three G4/PEG-hemin aptamer sequences, 1-04 ($V_0 = 0.003 \mu\text{M s}^{-1}$), 1-06 ($V_0 = 0.004 \mu\text{M s}^{-1}$) and 1-07 ($V_0 = 0.005 \mu\text{M s}^{-1}$), had either a decrease or no increase in V_0 when compared to the blank (no aptamer). This indicates that those G4 aptamers either did not complex with the PEG-hemin, or once complexed with the G4 the peroxidase-mimicking activity was hindered.

Table 4.6 also shows that EAD-2, 1-01, 1-02, 1-07, 1-08, 1-09 and G₃A₃ were able to increase the peroxidase-mimicking activity of the PEG-hemin, however it should be noted that none were enhanced over any sequences found in Table 4.2 and Table 4.4. This could be attributed the interference due to the electrostatic interactions between the PEG-hemin and the G4 aptamer. Previous researchers have shown that PEG decrease the anion-cation electrostatic interaction between the positively charged hemin and the negatively charged backbone of the G4 (see Fig. 4.7).²⁹

Due to the low V_0 of the G4/PEG-hemin aptamers, PEG hemin was found to be

unsuitable for testing the G4/hemin aptamers produced by the GA. It was therefore, decided that the optimal conditions for investigating the peroxidase-mimicking activity of the G4/hemin aptamers generated by the GA were to use pristine hemin.

The next section will discuss the use of the GA to determine sequences that provided enhanced peroxidase-mimicking activity compared to the original EAD-2 G4/hemin aptamer.

4.3.3. Enhancement of peroxidase-mimicking activity using genetic algorithm

This section will discuss the utilisation of the GA starting with the top 4 sequences from generation 1 (Table 4.1 and Table 4.3). In brief, the sequences that were determined to have the highest peroxidase-mimicking activity by the TMB assay from each generation were used to generate the next generation of sequences using the GA (see Section 4.2.1, Fig. 4.3). This was repeated several times to produce sequences with enhanced peroxidase-mimicking activity.

The absorbance (TMB assay) was measured at 595 nm for 15 min and the resulting slope of the line was used to calculate V_0 using Eq. 4.3. In total this was performed 7 times, producing a total of 8 generations, and the V_0 values for all the sequences can be found in Appendix C.

Table 4.7 shows 20 sequences only, that were determined to have the highest peroxidase-mimicking activity along with each sequence ranking.

Table 4.7 shows that by using the GA it was possible to determine at least 20 sequences that had an enhanced peroxidase-mimicking activity when compared to the EAD-2 and G_3A_3 G4/hemin aptamers. It also shows that the top 2 sequences, 7-02 and 5-04 (Table 4.7), both had V_0 values of $0.099 \pm 0.001 \mu\text{M s}^{-1}$. The third highest sequence had a V_0 of $0.094 \pm 0.003 \mu\text{M s}^{-1}$. All three sequences have V_0 values at ~ 5 times higher than the original EAD-2 sequence and the G_3A_3 .

Table 4.7: Top 20 ranked G4 ODN sequences with the highest V_0 values after 8 generations (including generation 1) of the GA with EAD-2 and G_3A_3 .

Rank	Gen	G4 aptamer sequence	Peroxidase-mimicking activity, V_0 , $\mu\text{M s}^{-1}$ $^{\beta}$
1	7-02	$G_3A_3G_3CACG_3CG_3$	0.099 ± 0.001
2	5-04	$G_3A_3G_3A_2CG_3CG_3$	0.099 ± 0.001
3	7-01	$G_3TA_2G_3CACG_3TG_3$	0.094 ± 0.001
4	4-02	$G_3A_3G_3A_2CG_3TG_3$	0.082 ± 0.002
5	7-08	$G_3A_3G_3A_2CG_3CG_3$	0.079 ± 0.002
6	7-04	$G_3TA_2G_3CACG_3CG_3C$	0.078 ± 0.017
7	5-08	$TG_3TA_2G_3A_2CG_3TG_3$	0.076 ± 0.001
8	7-06	$G_3A_2TG_3CACG_3AG_3$	0.074 ± 0.015
9	6-08	$G_3TA_2G_3A_2CG_3CG_3$	0.071 ± 0.001
10	5-07	$G_3ACAG_3A_2CG_3TG$	0.065 ± 0.015
11	7-09	$G_3A_3G_3CACG_3AG_3$	0.064 ± 0.017
12	6-04	$G_3A_3G_3A_2CG_3AG_3$	0.062 ± 0.001
13	4-05	$G_3TA_2G_3A_2CG_3AG_3$	0.058 ± 0.001
14	5-05	$G_3A_3G_3A_2TG_3AG_3$	0.058 ± 0.002
15	5-06	$G_3A_3G_3A_2CG_3AG_3C$	0.058 ± 0.002
16	8-02	$G_3TACG_3CACG_3CG_3C$	0.053 ± 0.002
17	6-01	$G_3ATAG_3A_2TG_3CG_3$	0.052 ± 0.010
18	8-07	$G_3TA_2G_3CACG_3TG_4$	0.051 ± 0.001
19	3-02	$G_3A_3G_3TCAG_3TG_3$	0.047 ± 0.001
20	6-03	$G_3ATAG_3A_2TG_3TG_3$	0.047 ± 0.006
29	EAD-2	$CTG_3AG_3AG_3AG_3A$	0.018 ± 0.001
47	G_3A_3	$G_3A_3G_3A_3G_3A_3G_3$	0.032

$^{\beta}$ Errors below $0.001 \mu\text{ s}^{-1}$

After generation seven there are no sequences that had enhanced peroxidase-mimicking activity compared to the previous generation. Therefore, there were no subsequent generations generated and analysed as the GA was successful in determining sequences with considerably enhanced peroxidase-mimicking activity

In order to understand how the GA was able to discover sequences with enhanced peroxidase-mimicking activity Table 4.8 shows the most common loop sequences that occur in the top 20 sequences. The terminal regions were not analysed as only three sequences in Table 4.7, namely 7-04 (ranked 6), 5-06 (ranked 15) and 8-02 (ranked 16) contained a residue (a 3' C residue in all cases) in the terminal region.

Table 4.8 shows that there are several possible loop sequences that can enhance the peroxidase-mimicking activity for each loop region (X_{I1} , X_{I2} and X_{I3}). For X_{I1} region there are 6, X_{I2} there are 4 and X_{I3} there are 3 possible loop sequences.

Table 4.8: Number of times loop sequences (X_{I1} , X_{I2} and X_{I3}) are repeated in the top 20 G4 aptamers (with the highest V_0).

Loop sequence $5' \Rightarrow 3'$	X_{I1}	X_{I2}	X_{I3}
AAA	9	-	-
TAA	6	-	-
ATA	2	-	-
ACA	1	-	-
TAC	1	-	-
AAT	1	3	-
AAC	-	9	-
CAC	-	7	-
TCA	-	1	-
A	-	-	6
C	-	-	7
T	-	-	7
Total number of sequences	6	4	3

Further, Table 4.8 shows that there are two loop sequences that occur most prominently in the X_{I1} loop region and these are AAA (in 9 sequences) and TAA (in 6 sequences). The remainder of the sequences all contain at least one A residue, indicating that the presence of A residues in the X_{I1} region can enhance the peroxidase-mimicking activity. A similar phenomenon is observed in the X_{I2} loop region.

Table 4.8 also shows that for the X_{I2} loop region there are two loop sequences that occur most prominently in the top 20 sequences, these sequences are AAC (in 9 sequences) and CAC (in 7 sequences). However, once again all the remaining sequences also contain at least one A residue. Chen *et al.*¹⁹ had noted that the presence of A residues was able to enhance the peroxidase-mimicking activity by acting as an acid-base catalyst (see Section 4.1.2.1, Fig. 4.6) and so the data here corroborates their paper.

Finally, Table 4.8 shows that for the X_{I3} loop region there is no predominate sequence, as it can be comprised of any single nt residue (A, T, or C) that is not a G residue. This means that X_{I3} is the shortest of all the loop regions, and therefore the number of residues that formed the loop region (X_{I1} , X_{I2} and X_{I3} , Fig. 4.1) plays a larger role in the peroxidase-

mimicking activity. A short loop region length is known to affect the conformation that the G4/hemin aptamer is able to fold into (see Chapter 1, Section 1.5.3.4). The conformation and characterisation of the structures that formed the the fastest sequences will be discussed in the following section.

4.3.4. Characterisation of G4/hemin aptamer structures using polyacrylamide gel electrophoresis, circular dichroism and K⁺ dependence studies

In order to characterise the G4/hemin aptamer structures that the newly determined sequences form (from the GA), the sequences were analysed using polyacrylamide gel electrophoresis (PAGE), circular dichroism and their dependence on the presence of K⁺.

4.3.4.1. PAGE analysis of G4/hemin structures

PAGE was used to determine the structures of the following sequences: 7-01, 7-02, 5-04, 7-08, 4-02, 6-07, 7-04, 5-08, 7-06 and 6-08 (Table 4.7). PAGE was performed according to the procedure set out in Chapter 2, Section 2.4.3 using a premade PAGE (5-20% (w/v)) and visualised using a Safe Imager Blue-Light Transilluminator. Fig. 4.8 shows the PAGE (10-20% (v/v)) electrophoretogram of the G4 aptamer without and with added hemin.

Fig. 4.8 shows that all the G4 aptamers, without and with hemin, all occur below 40 nt (Fig. 4.8, 20 bp). G₃A₃ (Fig 4.8 (a)) has the highest molecular weight of 21 nt. However, the band for G₃A₃ appears at ~30 nt, which indicates the presence of a bimolecular G4 structure. This means that there are two single-strands of G4 ODN forming an intermolecular G4 structure (see Chapter 1, Section 1.5.3.4). The structure shows no change when hemin is added (Fig. 4.8 (b)).

This data does not agree with Vorlíčková *et al.*³⁰ who found that G₃A₃ forms an intramolecular G4 structure (consisting of a single ODN strand). However, they used a phosphate

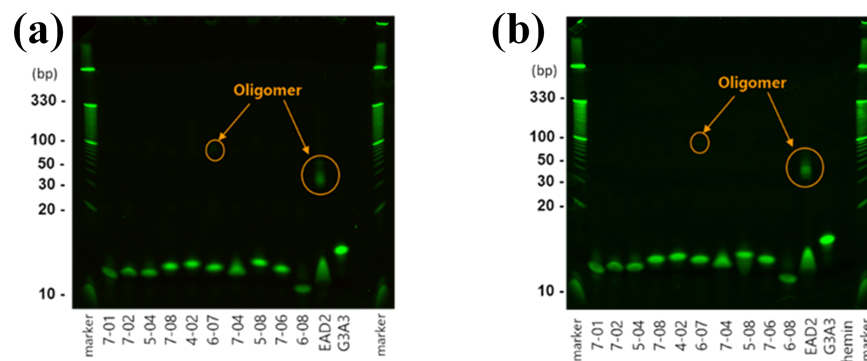


Figure 4.8: Native PAGE 10-20% (v/v) electrophoretogram, stained with 1x SYBR® gold and viewed using a Safe Imager Blue-Light Transilluminator, of 7-01, 7-02, 5-04, 7-08, 4-02, 6-07, 7-04, 5-08, 7-06 and 6-08, EAD-2 and G₃A₃ G4 aptamers (a) without hemin and (b) with hemin added. Both have Invitrogen 10 bp DNA Ladder DNA Ladder (L).

buffer with EDTA at pH 7.8, whereas the buffer used for these experiments was a TRIS-EDTA (TE) at pH 7.5 buffer. Therefore, it was hypothesised that the difference in buffers is the reason for seeing a differing structure.

For all the remaining G4 aptamers Fig. 4.8 (a) and (b) show that the remaining bands appear at 10 nt. This is an indication that intramolecular structures had been formed with no noticeable changes when hemin was added. This indicated that all the remaining G4 and G4/hemin aptamers were considered to be intramolecular. This also shows that the hemin does not have any effect on the intermolecular structure as there is no observable increase in nt length. EAD-2 and 6-07 appeared to have secondary bands as well which indicated that there was either an unknown secondary structure or intermolecular G4s and G4/hemin aptamers were formed.

Henceforth, only the top 3 sequences (7-02, 5-04 and 7-01) and the original EAD-2 and G₃A₃ were characterised to allow for simpler more in-depth discussion

4.3.4.2. Circular dichroism

Circular dichroism (CD) spectroscopy was used to determine whether the G4 aptamers were parallel or antiparallel (see Chapter 1, Section 1.5.3.4). This was performed according to the procedure set out in Chapter 2, Section 2.3.2.2.

Parallel G4 structures are identified by the positive maximum *ca.* 264 nm and negative minimum *ca.* 240 nm, while an antiparallel is identified by a maximum *ca.* 295 nm and minimum *ca.* 240 nm.¹¹ A mixture or hybrid of both parallel and antiparallel G4 aptamers have peaks present at 264 nm and 295 nm. For simplicity only the top 3 G4/hemin aptamers (7-01, 7-02 and 5-04) with the highest V_0 values, as well as EAD-2 and G_3A_3 (Table 4.3), were characterised using CD. These sequences were folded into G4 structures by following the procedure set out in Chapter 2, Section 2.3.2.1. The CD measurements of the G4 aptamers were carried out with and without hemin to understand the effect that hemin had on the final G4 aptamer structure.

Fig. 4.9 (a-c) shows the CD spectra for 7-01, 7-02 and 5-04 G4/hemin aptamers, respectively. All these spectra have maximum peaks at *ca.* 290 nm and 260 nm when no hemin was present (black). This indicated that a mixture of the parallel and antiparallel exist at the same time or that the G4 structures are hybrids. Upon the addition of hemin (Fig. 4.9 (a-c), red) there was a decrease in the maximum peak at 260 nm and a slight increase at 240 nm. This is indicative of a structural shift from mixture/hybrid towards parallel, however not a complete shift.³¹

Fig. 4.9 (d) shows that EAD-2 has a max and a min peak at *ca.* 260 nm and 240 nm, respectively, indicating a parallel structure. For G_3A_3 has a max and min peak at *ca.* 290 and 260 nm, respectively, indicative of a antiparallel G4 structure (Fig. 4.9 (e)). This is in agreement with the literature.^{19,30} The addition of hemin (Fig. 4.8 (d), red) has no effect on the EAD-2. However, there is a slight structural change seen for G_3A_3 upon the addition of hemin (Fig.

4.9 (e), red), with an increase occurring at between 240 and 260 nm. This structure is still considered an antiparallel G4 structure.

Cheng *et al.*¹¹ studied the peroxidase-mimicking activity of multiple G4/hemin aptamers and found that the parallel G4 structures had the highest peroxidase-mimicking activity when compared to antiparallel and mixed/hybrid structures. However, from Fig. 4.9 (a-c) and Table 4.7 it was deduced that the mixed/hybrid G4/hemin aptamers had the highest peroxidase-mimicking activity.

The next characterisation was to determine the dependence of the G4/hemin aptamers on the presence of K^+ .

4.3.5. Potassium ion dependence of G4/hemin aptamer

This section will discuss the dependence of the 7-01, 7-02 and 5-04 G4/hemin aptamer structure in the presence of K^+ . It is well understood that G4 structures require the presence of a cation in order to successfully stack the G-tetrads (see Chapter 1, Section 1.5.3.4). This was achieved by performing the TMB assay set out in Chapter 2, Section 2.3.2.3. Table 4.9 shows results for a TMB assay performed with the G4/hemin aptamers folded in Reaction buffer containing 50 mM K^+ and a TMB assay performed with G4/hemin aptamers folded in TE buffer with no K^+ ions.

Table 4.9: Effect of K^+ ions on G4/hemin peroxidase-mimicking (V_0) activity.

G4 aptamer	Peroxidase-mimicking activity, V_0 , ($\times 10^{-3}$) $\mu\text{M s}^{-1}$	
	without K^+	with 50 mM K^+
7-02	0.86 ± 0.02	98.72 ± 0.06
7-01	13.68 ± 0.03	93.59 ± 0.03
5-04	2.14 ± 0.05	98.72 ± 0.03
EAD-2	5.56 ± 0.01	20.94 ± 0.05
G ₃ A ₃	7.69 ± 0.47	32.48 ± 0.85
blank (no aptamer)	1.28 ± 0.02	1.28 ± 0.03

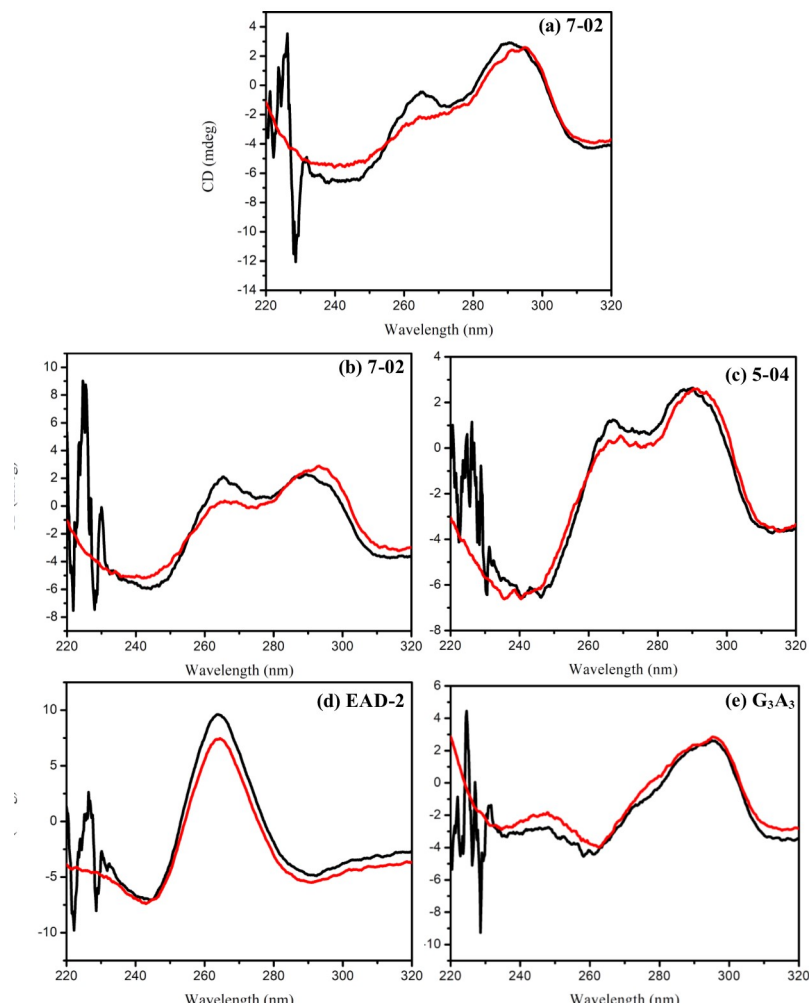


Figure 4.9: CD spectra of G4 aptamers: (a) 7-01, (b) 7-02, (c) 5-04, (e) EAD-2 and (d) G₃A₃ with (red) and without (black) hemin.

Table 4.9 shows that in the presence of 50 mM K⁺ ions 7-02 and 5-04 have an effective $V_0 = 98.72 \pm 0.06 \times 10^{-3} \mu\text{M s}^{-1}$ and $98.72 \pm 0.03 \times 10^{-3} \mu\text{M s}^{-1}$, respectively, and both decrease by 98% when no K⁺ is present ($V_0 = 13.68 \pm 2.14 \times 10^{-3} \mu\text{M s}^{-1}$ and $2.14 \pm 0.47 \times 10^{-3} \mu\text{M s}^{-1}$, respectively). Table 4.9 also shows that 7-01 was decreased by 85% in the absence of K⁺ with a decrease from $V_0 = 93.59 \pm 0.03 \times 10^{-3} \mu\text{M s}^{-1}$ to $V_0 = 13.68 \pm 2.14 \times 10^{-3} \mu\text{M s}^{-1}$.

Table 4.9 shows that both EAD-2 and G₃A₃ were reliant on the absence of K⁺ ions to achieve a $V_0 = 7.69 \pm 0.47 \mu\text{M s}^{-1}$ and $5.56 \pm 0.10 \mu\text{M s}^{-1}$, respectively. In the presence of K⁺, the V_0 is increased to $32.48 \pm 0.85 \mu\text{M s}^{-1}$ and $20.94 \pm 0.47 \mu\text{M s}^{-1}$, respectively. Table 4.9 shows that all the G4/hemin aptamers have a reduced V_0 when there are no K⁺ ions present. This gives an indication of how important the folded G-quadruplex is for the peroxidase-mimicking activity.

In the absence of the K⁺ ions the unfolded G4 has a lower V_0 compared to when in the presence of K⁺ ions, with decreases of between 63% and 98% in V_0 (Table 4.9). It should be noted that all G4/hemin aptamers, except for 7-02, samples with no K⁺ ions were still faster than the blank (no G4 aptamer) with and without K⁺ ions. This indicates that there must still be a small ratio of folded G4/hemin aptamers that still retain peroxidase-mimicking activity. This is hypothesised to be due to the hemin inducing a small degree of G4 folding. Thus, it would be more beneficial for a biosensor to use the 7-02 G4/hemin aptamer as there would be less possibility of a false-positive occurring.

4.3.6. Enzyme kinetics of G4 aptamers with peroxidase-mimicking activity

Finally, V_{max} , K_m and k_{cat} of the top 3 G4/hemin aptamers and the original EAD-2 and G₃A₃ were characterised using the Michaelis-Menten equation (see Section 4.2) In brief, this was achieved by measuring the V_0 of each G4/hemin aptamer (0.125 μM), using the TMB assay detailed above, with H₂O₂ (2 μM) with variable concentrations of TMB substrate: 0.0

mM, 0.2 mM, 0.4 mM, 0.8 mM. By plotting the V_0 of variable TMB concentrations it is possible to fit the Michaelis-Menten equation (Eq. 4.1).

This was done to elucidate the catalytic kinetic parameters of the G4/hemin aptamers (V_{max} and K_m) of the top 3 G4/hemin aptamers, EAD-2 and G_3A_3 once folded into the G4/hemin aptamers. All the Michaelis-Menten curves can be found in Fig. 4.10. Table 4.10 contains all the calculated rates using Michaelis-Menten Eq. 4.1.

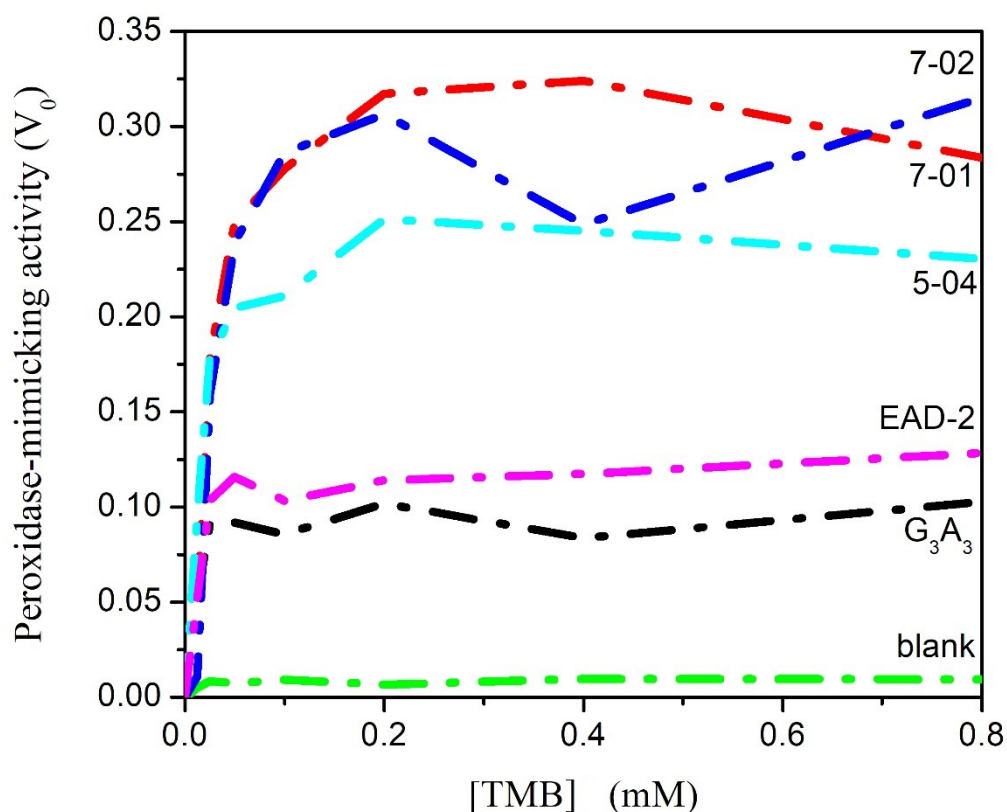


Figure 4.10: Michaelis-Menten curves for hemin base line (green), G_3A_3 (black), EAD-2 (pink), 7-01 (red), 7-02 (blue) and 5-04 (turquoise). Each line is an average of three curves and the red dotted line is the curve fit performed using OriginPro 9 applying software non-linear line fit function.

Table 4.10 shows the V_{max} and K_m derived from the Michaelis-Menten curves (Fig. 4.10) using Eq. 4.2. Table 4.10 also shows $k_{(cat)}$ that was calculated from the V_{max} using Eq. 4.2.

Table 4.10 shows that blank (no aptamer) has a V_{max} , K_m and $k_{(cat)}$ of 0.009 ± 0.001 $\mu\text{M s}^{-1}$, 0.006 mM and 0.072 s^{-1} , respectively. This indicates that hemin still has a small

Table 4.10: The calculated V_{max} , K_m , and $k_{(cat)}$ for the top 3 G4/hemin aptamers (with the highest V_0), the original EAD-2 and G₃A₃ derived from the Michaelis-Menten curves in Fig. 4.10

Name	$V_{max}, \mu\text{M s}^{-1}$	K_m, mM	$k_{(cat)}$
7-02	0.327 ± 0.035	0.031	2.616
7-01	0.336 ± 0.026	0.026	2.688
5-04	0.252 ± 0.009	0.014	2.016
EAD-2	0.124 ± 0.007	0.010	0.992
G ₃ A ₃	0.099 ± 0.006	0.007	0.792
blank (no aptamer)	0.009 ± 0.001	0.006	0.072

degree of peroxidase activity even without G4 aptamer being present.

EAD-2 has a V_{max} , K_m and $k_{(cat)}$ of $0.124 \pm 0.007 \mu\text{M s}^{-1}$, 0.010 mM and 0.992 s^{-1} , respectively (Table 4.10). G₃A₃ has a V_{max} , K_m and $k_{(cat)}$ of $0.099 \pm 0.006 \mu\text{M s}^{-1}$, 0.007 mM and 0.792 s^{-1} , respectively (Table 4.10). This shows that EAD-2 has a higher V_{max} , which is not expected based on the results from Table 4.7, where G₃A₃ was considered to have a higher V_0 . However, EAD-2 has a slightly lower affinity for the TMB substrate (based on the larger K_m value) and so at lower TMB concentrations the EAD-2 would have a slightly lower V_0 .

Table 4.10 also shows that 7-02 has a V_{max} , K_m and $k_{(cat)}$ of $0.327 \pm 0.035 \mu\text{M s}^{-1}$, 0.031 mM and 2.616 s^{-1} , respectively. 7-01 has a V_{max} , K_m and $k_{(cat)}$ of $0.336 \pm 0.026 \mu\text{M s}^{-1}$, 0.026 mM and 2.688 s^{-1} , respectively. Finally, 5-04 has a V_{max} , K_m and $k_{(cat)}$ of $0.252 \pm 0.009 \mu\text{M s}^{-1}$, 0.014 mM and 2.016 s^{-1} , respectively. This data shows that the G4 aptamer sequences, determined using the GA, have enhanced peroxidase-mimicking activity compared to the original EAD-2. However, the affinity for the TMB substrate has decreased considerably as the K_m values are much higher. Although the K_m values have increased it appears that the $k_{(cat)}$, which is the number of TMB molecules converted to TMB⁺ per second, has also increased.

This work shows that it is indeed possible to utilise a GA to discover G4/hemin aptamers that have enhanced peroxidase-mimicking activity. Thus, these G4/hemin aptamers are well suited for future biosensing applications. 7-02 however, is the only sequence out of the

top 3 that is completely reliant on the presence of K^+ (see Section 4.5.2.). This means that it is possible to have more control over the G4 structure of 7-02 and allow for more sensitive biosensors to be produced, especially for cation biosensors such as those developed by Sun *et al.* (see Chapter 1, Section 1.6).³¹

4.4. Concluding remarks

In this Chapter a GA was used to determine G4/hemin aptamers with enhanced peroxidase-mimicking activity. The top three sequences were characterised to determine the V_{max} , K_m and $k_{(cat)}$. The first generation of G4/hemin aptamers were designed to elucidate the effect of the addition of G-residues in the G-tracts, and deletions and T substitutions in the loop region. It was determined that additional G residues in the G-tract were detrimental to the peroxidase-mimicking activity of the G4/hemin aptamers. It was also found that A and C residues enhanced the peroxidase-mimicking activity, however T residues were found to decrease the peroxidase-mimicking activity. The four sequences with the highest peroxidase-mimicking activity in generation 1 were found to be the parent sequence (EAD-2), 1-08 ($G_3AG_3AG_3AG_3A$), 1-02 ($CTG_3AG_3TG_3TG_3A$) and G_3A_3 . These four G4/hemin aptamers were used to generate the next generation of G4 ODN sequences using a GA. This was repeated seven times to produce eight generations of G4 ODN sequences that had increasing peroxidase-mimicking activity. The GA was able to determine three sequences, 7-01 ($G_3TA_2G_3CACG_3TG_3$), 7-02 ($G_3A_3G_3CACG_3CG_3$) and 5-04 ($G_3A_3G_3A_2CG_3CG_3$) that were 5 times faster than the parent sequence. Analysis of the top 20 G4/hemin aptamer sequences showed that the presence of one A residue in the X_{11} and X_{12} loop region was crucial to enhancing the peroxidase-mimicking activity. The nt length of the X_{13} loop sequence was found to be more important than the nt residue. It was found that a single nt residue was favourable for enhanced peroxidase-mimicking activity.

The three G4/hemin aptamers were then characterised to determine the types of struc-

tures formed and the kinetic parameters. It was determined that the top sequences, determined by the GA, 7-01, 7-02 and 5-04, were intramolecular coexisting or mixed hybrid structures. All three of these sequences would be suitable for biosensing. 7-02 was determined to be the most suitable as it was more reliant on the presence of K^+ ions than the other two G4/hemin aptamers and thus allowed for stricter control over the G4/hemin aptamer structure.

4.5. Chapter 4 References

- [1] Ikebukuro, K.; Okumura, Y.; Sumikura, K.; Karube, I. A novel method of screening thrombin-inhibiting DNA aptamers using an evolution-mimicking algorithm. *Nucleic Acids Research* **2005**, *33*, 1–7.
- [2] Pfeiffer, F.; Tolle, F.; Rosenthal, M.; Brändle, G. M.; Ewers, J.; Mayer, G. Identification and characterization of nucleobase-modified aptamers by click-SELEX. *Nature Protocols* **2018**, *13*, 1153–1180.
- [3] Zhou, W.; Jimmy Huang, P. J.; Ding, J.; Liu, J. Aptamer-based biosensors for biomedical diagnostics. *Analyst* **2014**, *139*, 2627–2640.
- [4] Reuter, A.; Dittmer, W. U.; Simmel, F. C. Kinetics of protein-release by an aptamer-based DNA nanodevice. *European Physical Journal E* **2007**, *22*, 33–40.
- [5] Jiang, J.; He, Y.; Yu, X.; Zhao, J.; Cui, H. A homogeneous hemin/G-quadruplex DNAzyme based turn-on chemiluminescence aptasensor for interferon-gamma detection via in-situ assembly of luminol functionalized gold nanoparticles, deoxyribonucleic acid, interferon-gamma and hemin. *Analytica Chimica Acta* **2013**, *791*, 60–64.
- [6] Yang, X.; Fang, C.; Mei, H.; Chang, T.; Cao, Z.; Shangguan, D. Characterization of G-quadruplex/hemin peroxidase: Substrate specificity and inactivation kinetics. *Chemistry - A European Journal* **2011**, *17*, 14475–14484.
- [7] Darmostuk, M.; Rimpelova, S.; Gbelcova, H.; Ruml, T. Current approaches in SELEX: An update to aptamer selection technology. 2014.
- [8] Yokobayashi, Y.; Ikebukuro, K.; McNiven, S.; Karube, I. Directed evolution of trypsin inhibiting peptides using a genetic algorithm. *Journal of the Chemical Society - Perkin Transactions I* **1996**, *0*, 2435–2437.

- [9] Guo, Y.; Chen, J.; Cheng, M.; Monchaud, D.; Zhou, J.; Ju, H. A Thermophilic Tetramolecular G-Quadruplex/Hemin DNAzyme. *Angewandte Chemie - International Edition* **2017**, *56*, 16636–16640.
- [10] Li, W.; Li, Y.; Liu, Z.; Lin, B.; Yi, H.; Xu, F.; Nie, Z.; Yao, S. Insight into G-quadruplex-hemin DNAzyme/RNAzyme: Adjacent adenine as the intramolecular species for remarkable enhancement of enzymatic activity. *Nucleic Acids Research* **2016**, *44*, 7373–7384.
- [11] Cheng, X.; Liu, X.; Bing, T.; Cao, Z.; Shangguan, D. General peroxidase activity of G-quadruplex-hemin complexes and its application in ligand screening. *Biochemistry* **2009**, *48*, 7817–7823.
- [12] Loh, Q.; Lim, T. S. *Nucleic Acids - From Basic Aspects to Laboratory Tools*; 2016.
- [13] No, C. TMB , Soluble Suggested Procedure for Use of TMB in HRP-based ELISAs : **1800**, 1–2.
- [14] Jiang, Y. L.; Kwon, K.; Stivers, J. T. Turning On uracil-DNA glycosylase using a pyrene nucleotide switch. *The Journal of biological chemistry* **2001**, *276*, 42347–54.
- [15] Chang, T.; Gong, H.; Ding, P.; Liu, X.; Li, W.; Bing, T.; Cao, Z.; Shangguan, D. Activity Enhancement of G-Quadruplex/Hemin DNAzyme by Flanking d(CCC). *Chemistry - A European Journal* **2016**, *22*, 4015–4021.
- [16] Antipov, E.; Cho, A. E.; Wittrup, K. D.; Klibanov, A. M. Highly L and D enantioselective variants of horseradish peroxidase discovered by an ultrahigh-throughput selection method. *Proceedings of the National Academy of Sciences* **2008**, *105*, 17694–17699.
- [17] Ghahremani Nasab, M.; Hassani, L.; Mohammadi Nejad, S.; Norouzi, D. Interaction of hemin with quadruplex DNA. *Journal of Biological Physics* **2017**, *43*, 5–14.
- [18] Mazumdar, A.; Bandyopadhyay, D.; Bandyopadhyay, U.; Banerjee, R. K. *Probing the role of active site histidine residues in the catalytic activity of lacrimal gland peroxidase*; 2002; Vol. 237; pp 21–30.

- [19] Chen, J.; Guo, Y.; Zhou, J.; Ju, H. The Effect of Adenine Repeats on G-quadruplex/hemin Peroxidase Mimicking DNAzyme Activity. *Chemistry - A European Journal* **2017**, *23*, 4210–4215.
- [20] Mayfield, J. A.; Blanc, B.; Rodgers, K. R.; Lukat-Rodgers, G. S.; Dubois, J. L. Peroxidase-type reactions suggest a heterolytic/nucleophilic o-o joining mechanism in the heme-dependent chlorite dismutase. *Biochemistry* **2013**, *52*, 6982–6994.
- [21] Traylor, T. G.; Kim, C.; Fann, W. P.; Perrin, C. L. Reactions of hydroperoxides with iron(III) porphyrins: Heterolytic cleavage followed by hydroperoxide oxidation. *Tetrahedron* **1998**, *54*, 7977–7986.
- [22] Rowe, G. T.; Rybak-Akimova, E. V.; Caradonna, J. P. Heterolytic cleavage of peroxide by a diferrous compound generates metal-based intermediates identical to those observed with reactions utilizing oxygen-atom-donor molecules. *Chemistry - A European Journal* **2008**, *14*, 8303–8311.
- [23] Verdolino, V.; Cammi, R.; Munk, B. H.; Schlegel, H. B. Calculation of pKa values of nucleobases and the guanine oxidation products guanidinohydantoin and spiroiminodihydantoin using density functional theory and a polarizable continuum model. *Journal of Physical Chemistry B* **2008**, *112*, 16860–16873.
- [24] Ganguly, S.; Kundu, K. K. Protonation/deprotonation energetics of uracil, thymine, and cytosine in water from e.m.f./spectrophotometric measurements. *Can. J. Chem* **1994**, *72*, 1120–1126.
- [25] Sheiner, L. B.; Beal, S. L. Evaluation of methods for estimating population pharmacokinetic parameters. III. Monoexponential model: Routine clinical pharmacokinetic data. *Journal of Pharmacokinetics and Biopharmaceutics* **1983**, *11*, 303–319.
- [26] Kosman, J.; Juskowiak, B. Peroxidase-mimicking DNAzymes for biosensing applications: A review. *Analytica Chimica Acta* **2011**, *707*, 7–17.

- [27] Fang, J.; Qin, H.; Seki, T.; Nakamura, H.; Tsukigawa, K.; Shin, T.; Maeda, H. Therapeutic Potential of Pegylated Hemin for Reactive Oxygen Species-Related Diseases via Induction of Heme Oxygenase-1: Results from a Rat Hepatic Ischemia/Reperfusion Injury Model. *Journal of Pharmacology and Experimental Therapeutics* **2011**, *339*, 779–789.
- [28] Tran, P. L. T.; Mergny, J. L.; Alberti, P. Stability of telomeric G-quadruplexes. *Nucleic Acids Research* **2011**, *39*, 3282–3294.
- [29] Miller, D. D.; Chuang, S. S. The Effect of Electron-Donating Groups and Hydrogen Bonding on H₂S Capture over Polyethylene Glycol/Amine Sites. *Journal of Physical Chemistry C* **2016**, *120*, 1147–1162.
- [30] Vorlíčková, M.; Bednářová, K.; Kejnovská, I.; Kypr, J. Intramolecular and intermolecular guanine quadruplexes of DNA in aqueous salt and ethanol solutions. *Biopolymers* **2007**, *86*, 1–10.
- [31] Kong, D. M.; Yang, W.; Wu, J.; Li, C. X.; Shen, H. X. Structure-function study of peroxidase-like G-quadruplex-hemin complexes. *Analyst* **2010**, *135*, 321–326.

Chapter 5

Immobilisation of G-quadruplexes onto 2D and 3D surfaces and T7 endonuclease I digestion for biosensing applications

5.1. Synopsis

This chapter will discuss the use of surface immobilised DNA for biosensing of single nucleotide polymorphism (SNPs). To achieve this G-quadruplexes (G4) aptamers, with a capture region containing a G SNP, were immobilised onto Corning® DNA-Bind 96-well microplates (2D surface) or BcMagTM magnetic silica iron core beads (3D surface). The capture regions were then exposed to two target strands containing either a perfect match (PM, C residue at SNP location) or single mismatch (SM, T residue at the SNP location). A T7 endonuclease I (enzyme that cleaves non-canonical bonds) was then added to cleave the mismatched bonds, releasing the G4 aptamer from the surface. The G4 aptamers were then detected both on surface (indicative of a PM) and in solution (indicative of a SM).

First the G4 aptamers were tested for resistance to T7 endonuclease digestion as well as optimisation of digestion parameters. This was done by exposing G4 aptamers with captured

target strands to the T7 endonuclease at varying times.

Following this, the G4 aptamers (with pendant capture region) were immobilised onto 2D surfaces. To test for successful attachment, a TMB assay (using 3,3',5,5'-tetramethylbenzidine substrate) was performed to test for the presence of peroxidase-mimicking activity. It was found that it was not possible to detect immobilised G4 aptamers on 2D surfaces. To improve detection a 3 polyethylene glycol (PEG) rate accelerator solutions, PEG 6000 5% (v/v), PEG 6000 10% (v/v) and PEG 8000 5% (v/v), were used to increase the reactivity of the substrate to the G4 aptamers.

Next it was determined if it was possible to detect cleaved G4 aptamers from the 2D surface (after the T7 endonuclease digestion) by using a TMB assay. It was found that although possible to detect the cleaved G4 aptamers, there was random cleavage and no way to distinguish PM immobilised aptamers from SM immobilised aptamers.

Finally to increase the surface area of immobilised G4 aptamers, G4 aptamers were immobilised onto microbeads (3D surfaces) and digested with T7 endonuclease I. Then the peroxidase-mimicking activity was measured using the TMB assay.

5.2. Introduction and purpose

G-quadruplex (G4) aptameric biosensors present a myriad of potential applications such as detectors of metal ions in solutions, and DNA genotyping. These biosensors have detected a range of different target molecules, ranging from salts (K^+ , Na^+) to biomolecules (thrombin).¹⁻⁴ G4 aptamers have also been used to detect DNA sequences for genotyping of single nucleotide polymorphisms (SNPs).⁵ These G4 aptameric biosensors are useful as they produce a colorimetric or chemiluminescent readout that can be observed visually with the naked eye, with substrates such as 3-aminophthalhydrazide (luminol),⁶ 2,2'-azino-bis(3-ethylbenzthiazoline-6-sulfonic acid) (ABTS)⁷ and 3,3',5,5'-tetramethylbenzidine (TMB).⁸ Therefore, when utilising these substrates there is no requirement for expensive detection equipment for successful detection.

Although many researchers have immobilised G4 aptamers onto various surfaces (e.g., silica or gold^{9,10}) there is yet a method that has been developed to allow for detection of SNPs within surface immobilised G4 aptamers (to the best of the authors' knowledge). By immobilising G4 oligodeoxynucleotide (ODN) sequences with capture regions for SNP genotyping, it may be possible to develop a method that allows for point-of-care biosensors.

As discussed in Chapter 1, Section 1.5.3.7 G4 aptameric biosensors are often used in conjunction with other methods (DNAzymes, see Chapter 1, Section 1.5.3.11 for details) to allow for the colorimetric,² fluorometric,¹¹ and/or electrochemical¹² detection of whether the reaction or other methods have been successful. Many of the G4 biosensors used in literature rely on the production of a G4 structure after a reaction has taken place (i.e., cleavage of a target DNA strand or hybridisation to a target), which acts as a reporter molecule that reacts with substrates (Luminol, ABTS or TMB) to produce a visually detectable readout.^{2,3,6} This has the potential for the fabrication of point-of-care biosensors that do not require expensive equipment, such as fluorometers, for detection.

In this Chapter, surface immobilised G4 aptamers were investigated as a possible SNP detection reporter system. The hypothesis for this was that perfect match (PM) and single-mismatch (SM) DNA can be detected with the aid of a T7 endonuclease I enzyme. The T7 endonuclease I is able to detect and cleave SM dsDNA to release the G4 aptamer into solution to be analysed. The proposed mechanism of the biosensor is depicted in Fig. 5.1.

In Fig. 5.1, Step1: amine-functionalised ssDNA containing a capture region with SNP (G) and a G-rich (for G4 formation) region is immobilised onto a surface through an NHS coupling reaction (Fig. 5.1, Step 1). The surfaces used were either NHS-functionalised Corning® DNA-Bind 96-well microplates (2D surface) or BcMag™ magnetic silica iron core beads (3D surface) (see Chapter 2, Section 2.3.3.2 and 2.3.4.3 for experimental details) (Fig. 5.1, yellow). The advantage of utilising immobilised ODN on surfaces is that it is possible to wash away any non-immobilised ODN from the surface as well as making it possible to replace buffers without loss of immobilised ODN.

In Fig.5.1 Step 2: The complementary target sequences were added to form either a PM (G-C, blue) or SM (G-T, purple) dsDNA with the target region on the G4 ODN.

In Fig. 5.1 Step 3: The addition of the T7 endonuclease enzyme (multi-coloured) in a buffer solution at 37 °C, that can recognise and cleave any SM dsDNA. This will release the G-rich part of the ODN sequence into solution and can be extracted for testing.

In Fig.5.1 Step 4: The G-rich ODNs, in solution or on the surface, are then folded with the addition of 50 mM K⁺ ions and finally in Step 5: A TMB assay was performed in the presence of hemin to produce a colorimetric readout.

Thus, if the ODN on the surface was not cleaved it can be determined that a PM was present (G-C) and any cleaved ODN would be SM (G-T, A or G). As with most other genotyping techniques, as long as the SNP in the capture ODN on the surface is known it is possible to determine what SNPs may be present in the target strand and *vice versa*.

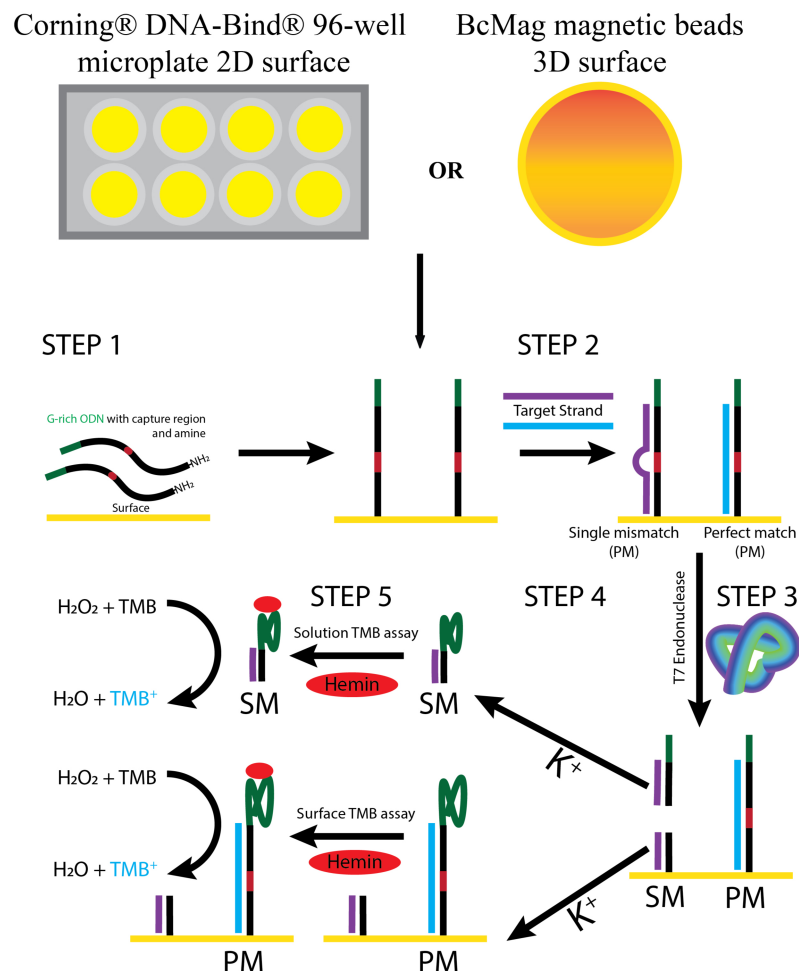


Figure 5.1: Proposed mechanism for the SNP biosensor that utilises an enzymatic digestion step and a G-quadruplex (G4) aptamer for single nucleotide polymorphism (SNP) detection. Step 1: Immobilisation of ODN that contains a G-rich (green), SNP (red) and capture region (black), onto the surface (yellow) of either a 2D or 3D surface. Step 2: Target ODN is captured to the surface immobilised capture region, forming either a perfect match (PM, blue) or single mismatch (SM, purple). Step 3: T7 endonuclease enzyme (multicoloured) is added to cleave the any mismatched DNA and release the G-rich ODN into solution. Step 4: The G-rich ODN in solution is removed and then both G-rich ODN in solution and on the surface are folded with the addition of 50 mM K^+ to form G4 aptamers. Step 5: Hemin is added and a TMB assay is performed to determine the presence of G4 aptamers in solution and those remaining on the surface.

5.3. Results and discussion

5.3.1. Optimisation of T7 endonuclease I digestion

T7 endonuclease I is an enzyme that has a range of applications, such as cleavage of: homoduplexed (perfect matched, $>40\text{ }^{\circ}\text{C}$) and heteroduplexed (mismatched, $<40\text{ }^{\circ}\text{C}$) dsDNA.^{13 14 15} T7 endonuclease I is used in this thesis to recognise mismatches and cleave the dsDNA at the first, second or third phosphodiester on the 5' bond of the mismatch.¹⁵ However, the issue faced when using the T7 endonuclease I in the presence of a G4 aptamer is that there is a possibility the G4 structure will be recognised as a mismatch and be cleaved. As mentioned in Chapter 1, Section 1.5.3.9, G4 aptamers are known to prevent recognition of certain enzymes such as telomerase (telomere extension enzyme).¹⁶ It has also been seen that G4 aptamers are resistant to nucleases, acting as a 'knot' that prevents recognition and cleavage.¹⁷ However, this may not apply to the T7 endonuclease I, which is specifically designed to cleave mismatched dsDNA and this was tested in this thesis.

In order to determine if it was viable to use surface immobilised G4 aptamers for the proposed biosensor presented in Fig. 5.1, the T7 endonuclease I digestion step must first be investigated. This is due to two key reasons. The first reason is to ensure that the G4 aptamer is not digested by T7 endonuclease I, as successful detection using the biosensor relies on the presence of the G4 aptamer (in the TMB assay). The second reason is to optimise the digestion conditions so that only SM dsDNA is digested, and not PM dsDNA, as otherwise it will not be possible to discriminate the SNP.

5.3.2. G4 resistance to T7 endonuclease I digestion

The procedure set out in Chapter 2, Section 2.3.3.1 was performed in solution to determine if the G4 aptamers were resistant to the T7 endonuclease I cleavage. This section will look at the G4 aptamer consisting of ODN G4(G) 001 that contains a G-rich sequence and

a target region that is complementary to G4(C) 002 and partially complementary to G4(T) 003 (where the letter in brackets indicates the nt at the SNP position). The dsDNA schematic is shown in Fig. 5.2, showing the resulting PM and SM dsDNA products.

(a) Perfect Match (PM)



(b) Single-mismatch (SM)



Figure 5.2: Schematic of (a) perfect match (G4(G) 001 + G4(C) 002) and (b) single-mismatch (G4(G) 001 + G4(T) 003), showing the G-rich (green), SNP (red, underlined) and captured target strands (PM blue, SM purple).

Fig. 5.3 shows a polyacrylamide gel electrophoresis (PAGE) 10-20% (v/v) electrophoretogram of the dsDNA products formed between G4(G) 001 + G4(C) 002 (PM) and G4(G) 001 + G4(T) 003 (SM).

Fig. 5.3 shows the lanes with PM and SM each present as a single bright band at ~60 bp (dotted line), indicating a high concentration of DNA. There is a faint second band at ~25 bp (dotted line). The bp length was determined using the calibration curve produced using the ladder. Fig. 5.3 shows the predominant structures have a bp length of ~60 bp and ~25 bp. In order to calculate the likely structure that is formed Eq. 5.1 was used.

$$\text{bp} = n \frac{x+y}{2} \tag{5.1}$$

Where bp = calculated bp length from PAGE, x = nt in G4 aptamer (45 nt) and y = nt

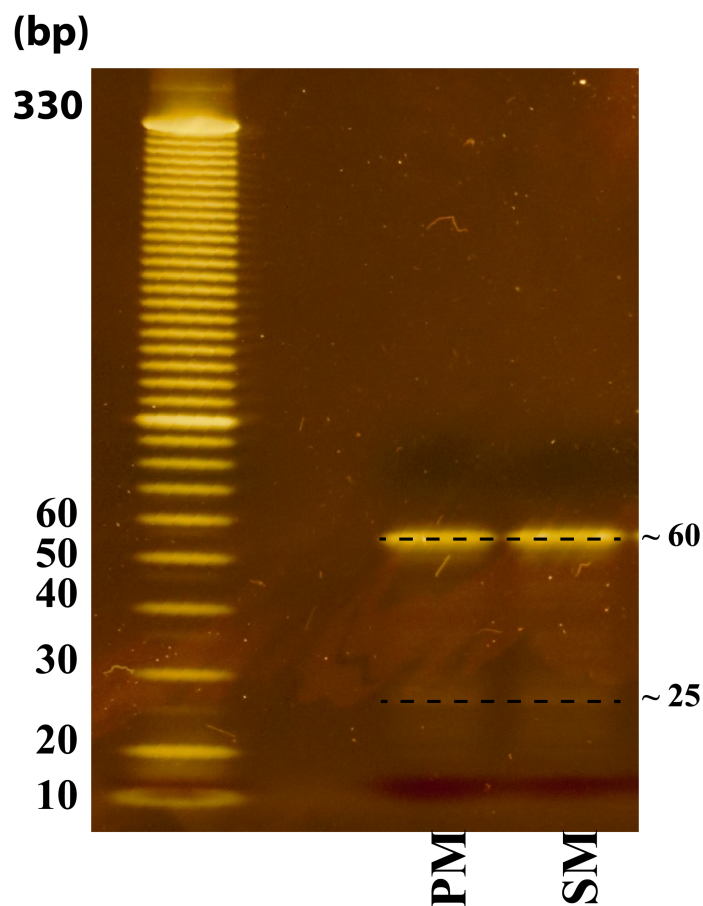


Figure 5.3: PAGE ePage 10-20% (v/v) electrophoretogram, stained with 1x SYBR® gold and viewed using a Safe Imager Blue-Light Transilluminator, of G4(G) 001 with G4(C) 002 (perfect match (PM)) and G4(G) 001 with G4(T) 003 (single-mismatch (SM)) solutions after formation of the G4 aptamers with respective target strands. A DNA Ladder (Invitrogen 10 bp DNA ladder) was used as the reference. Dotted lines are to guide the eye to the bands of interest.

in target strand (15 nt). n is used to determine the number of strands that are within the G4 and can therefore be used to determine if the structure is intramolecular ($n = 1$) or intermolecular ($n \geq 2$).

For the ~ 60 bp, Eq. 5.1 was rearranged and n was determined to equal 2 ssDNA in the G4 aptamer. This is indicative of an intermolecular G4 structure, consisting of two strands.

For the second band of interest observed at ~ 25 bp in Fig. 5.3 was $n = 1$. This is then classified as an intramolecular G4 structure. As discussed in Chapter 4, Section 4.3.4.1, G4 structures appear to move faster through PAGE and hence the band appears at ~ 25 bp as

opposed to the expected 30 bp. This shows that although both intramolecular and intermolecular G4 aptamers are formed in the PM and SM solutions, the intermolecular G4 structure is the preferred product. Fig. 5.3 also confirms that the PM and SM were successfully formed and will hereon be referred to as the PM and SM solutions, respectively.

The next step was to digest the PM and SM solutions with the T7 endonuclease I enzyme, which is proposed to cleave the SM but not the PM or G4 structure at 37 °C. This was achieved by following the manufacturer's instructions which can be found in Chapter 2 Section 2.3.3.1. In brief, the PM and SM solutions were made up to 20 μ L in 1X NEB 2 buffer. Then 2.5 U of T7 endonuclease I enzyme was added and the mixtures were incubated at 37 °C for 15 min. The resulting digestions were then visualised on a PAGE 10-20% (v/v) (Fig. 5.4).

Initial experiments showed that with fresh enzyme all DNA was digested (data not shown). Therefore, the following protocol was used for the enzyme preparation. A single freeze-thaw cycle was first performed on the T7 endonuclease I. This was then added to a frozen sample of the G4 aptamer with captured target strand. Then, while still frozen the G4 aptamer and T7 endonuclease I mixture were placed into a thermocycler set at 37 °C. The theory behind this was that by slightly denaturing the enzyme it was slightly less effective at digesting the PM DNA.

Fig. 5.4 shows that although both the PM and SM solutions were incubated with the T7 endonuclease I according to the manufacturer's instructions, it was observed that the cleavage of the SM mixture did not occur. It was hypothesised that this was due to the short length of the dsDNA target region, as well as the short digestion time. Therefore, it was determined that following the manufacturer's instructions did not result in the digestion of the PM or SM solutions (see Appendix D). This may be due to three factors.

The first factor was that although G4(G) 001 is 45 nt in length, the captured target is only 15 bp in length, which may be too small for the T7 endonuclease I to effectively bind and digest within 15 min. This kit has previously been used by Vouillot *et al.*¹⁸ and Wu *et al.*¹⁹

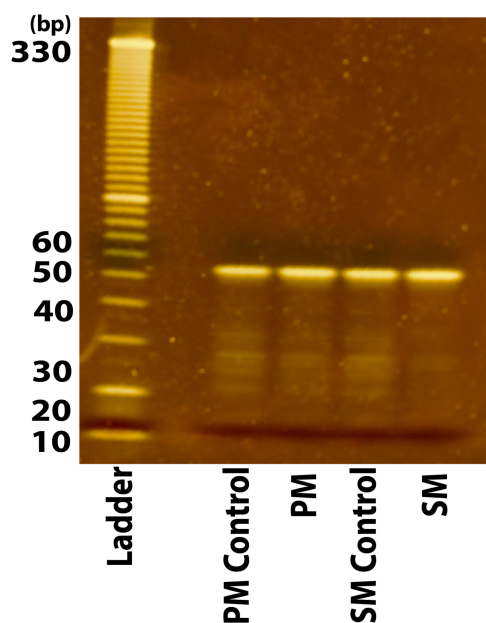


Figure 5.4: PAGE ePagel 10-20% (v/v) electrophoretogram, stained with 1x SYBR® gold and viewed using a Safe Imager Blue-Light Transilluminator, of perfect match (PM) and single mismatch (SM) solutions after incubation with T7 endonuclease for 15 min. A DNA Ladder (Invitrogen 10 bp DNA ladder) was used as the reference.

which digested longer dsDNA targets (>100 bp) when compared to these experiments (15 bp). Thus, it is not unreasonable for shorter DNA to behave differently. The second factor could be the possible steric hinderance from the G4, which is in close proximity to the capture region on the G4(G) 001 (Fig. 5.2, green). A third factor may be the type of mismatch formed (G to T). As discussed in Chapter 3, Section 3.3.1.1 G mismatches (G to T and G to A) are just as stable as perfectly matched A to T. This may make it more difficult for the T7 endonuclease I to recognise and cleave the SM.

The optimisation of the T7 endonuclease I digestion of the PM and SM mixtures will be discussed in Section 5.3.3

5.3.3. Optimisation of T7 endonuclease I of PM and SM solutions

The G4 aptamers were determined to be resistant to digestion by T7 endonuclease I, therefore the investigation moved to optimise conditions to allow selective digestion of the SM

solution over the PM solution. As following the manufacturer's instructions did not digest the PM or SM structures occurred.

In order to favour cleavage of the SM DNA using T7 endonuclease I, the time of digestion was optimised. It was not viable to change the temperature at which the mixtures and T7 endonuclease I were incubated. This is because the manufacturer states that incubation in temperatures above 40 °C will result in random cleavage of the DNA, which is undesirable for the proposed biosensor.¹⁵ The times investigated were 15, 30, 45, 60, 120, and 240 min. These results can be found in Appendix E; however, no digestion of the PM or SM was observed at any of the times investigated.

The digestion time was then increased to 16 h. Although this ran the risk of complete digestion (including PM DNA). Appendix E shows an electropherogram of the overnight T7 endonuclease I incubation with the PM and SM solutions. The absence of bands after the 16 h incubation of the T7 endonuclease with PM and SM solutions indicates a complete degradation of all DNA. Thus, a 16 h digestion was attempted with a lower concentration of the T7 endonuclease I, of 1 U as compared to the 2.5 U previously.

Fig. 5.5 shows the PAGE electropherogram 10-20% (v/v) of the 16 h incubation of T7 endonuclease I (1 U) with the PM and SM solutions.

From Fig. 5.5 shows that the PM and SM solution controls are not digested with T7 endonuclease I (band at ~60 bp). This is to be expected from previous experiments (see Section 5.3.2). The PM solution still presents a band ~60 bp, however it is fainter than the corresponding control indicating slight digestion of the G4 ODN. From the absence of a bright band at ~60 bp in the SM solution it was deduced that the SM was digested successfully to below the limits of detection. However, it was not able to completely digest the intramolecular G4 structure of the SM at ~25 bp (Fig. 5.5).

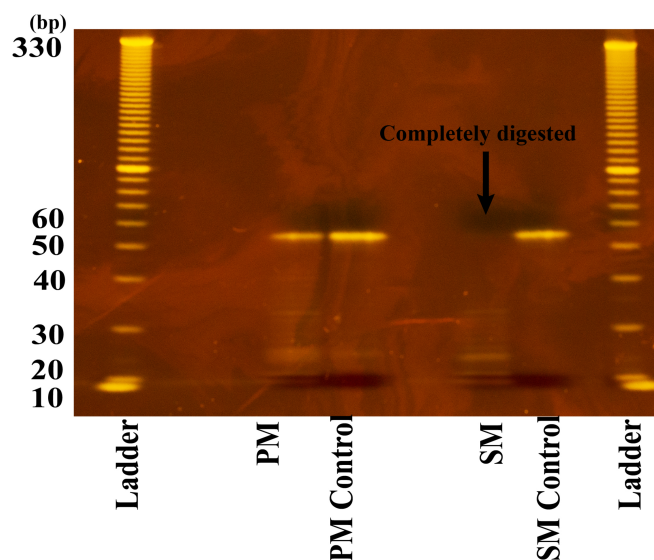


Figure 5.5: PAGE ePage 10-20% (v/v) electrophoretogram, stained with 1x SYBR® gold and viewed using a Safe Imager Blue-Light Transilluminator, of 16 h digestion with T7 endonuclease I (1 U) incubation with the PM and SM solutions with undigested controls. A DNA Ladder (L) (Invitrogen 10 bp DNA ladder) was used as the reference.

5.3.4. Investigation of G4 aptamer immobilised on 2D surfaces

This section will discuss how G4 aptamers were immobilised and detected on the surface of Corning® DNA-Bind® 96-well microplates. This was achieved following the manufacturer’s instructions outlined in Chapter 2, Section 2.3.3.2. First, a G4(G)T 001 (1 μ L, 100 μ M), where T is a T₂₀ tail after the G4(G) 001 ODN (see Table 2.6). Then 100 μ L was placed into a well of a Corning® DNA-Bind® 96-well microplate, ensuring that the bottom of the well was completely submerged in buffer. After incubating the ODN on the surface of the well for 2 h at room temperature (following the manufacturer’s instructions) the immobilisation buffer was removed, leaving behind only immobilised G4 aptamers. The well was washed with a wash buffer (see Chapter 2, Section 2.3.3.2) to remove any physisorbed DNA. The next step was to detect the presence of the immobilised G4 aptamers on the surface.

In order to determine if there was sufficient immobilisation of G4 aptamers on the surface of the Corning® DNA-Bind® 96-well microplates a TMB assay was performed (see Fig. 5.1, Step 4). This involved folding the G4 on the surface of the Corning® DNA-Bind® 96-

well microplate in Reaction buffer (containing 50 mM K⁺), heated to 70 °C (this was to ensure that a high enough temperature to denature all ODN present but not damage the polystyrene 96-well plates) and cooled to room temperature on a bench. Then a hemin 10% (v/v) solution was added into each well to allow for the formation of the G4/hemin aptamer on the surface of the Corning® DNA-Bind® 96-well microplates (Fig. 5.1).

The blank (no G4 aptamer) refers to a TMB assay that was performed in wells that did not have immobilised G4 aptamers. This was done to obtain the peroxidase-mimicking activity (V_0) of hemin in the absence of the G4 aptamers. As hemin has an inherent V_0 and the G4 aptamers V_0 will be compared to the blank. An increase in the V_0 will indicate the presence of the G4 aptamers.

5.3.4.1. Comparison of three detection systems of G4 aptamer testing on 2D surfaces

Three different assays using different substrates were used to test for the presence of G4 aptamers on the Corning® DNA-Bind® 96-well microplates. The substrates tested were luminol, ABTS and TMB. Luminol and ABTS are considered to undergo quicker oxidation reactions than TMB and thus were thought to be more suitable for the detection of low concentration G4 aptamers, such as on the surface of the 2D surface.^{7,8,11} These substrates were tested following the procedure set out in Chapter 2, Section 2.3.4.2 and 2.3.4.1.

Luminol was detected using a plate reader set up to detect chemiluminescent signatures and ABTS was detected by measuring the change in absorbance at 430 nm (25 °C). The results of each can be found in Appendix F (with ANOVA results) and Appendix G, respectively. Neither reaction could be detected above the hemin signature and therefore G4 aptamer detection focused on the use of TMB as a substrate.

Section 5.3.5 will discuss the application of the TMB assay showing absorbance (a.u) versus time (min) used to calculate the V_0 using Eq. 4.3.

5.3.5. TMB assay of the G4 aptamers immobilised on the 2D surface

Fig 5.6 shows the UV/vis spectra of the change in absorbance (a.u) versus time (min) of the TMB assays used to detect the immobilised G4 aptamers on the surface of the Corning® DNA-Bind® 96-well microplates.

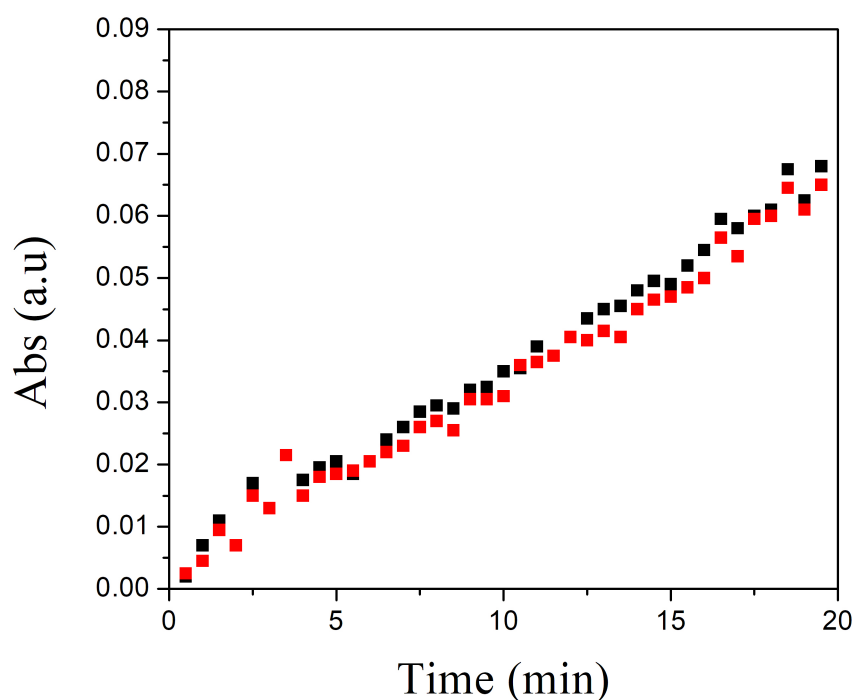


Figure 5.6: Average of 3 UV/vis spectra (absorbance (a.u) vs time (min)) of TMB assay for blank (no G4 aptamer, red) and immobilised G4 aptamer (black) on the surface of Corning® DNA-Bind® 96-well microplates. Averages were performed using OriginPro 9 average curve function.

Table 5.1 shows the calculated V_0 (Eq. 4.3) using the slopes from the blank (red) and immobilised G4 aptamer (black) data in Fig. 5.6.

Table 5.1: Peroxidase-mimicking activity (V_0) of G4 immobilised on the surface of the Corning® DNA-Bind® 96-well microplates compared to the blank (no G4 aptamer) calculated from Fig. 5.6.

Sample	Peroxidase-mimicking activity $V_0, \mu\text{M s}^{-1}, (\times 10^{-3})$		p = 0.05 (95% CI)
	No aptamer	G4 aptamer	
Corning® DNA-Bind® 96-well microplates	1.27 ± 0.01	1.36 ± 0.03	$p < 0.05, s$

s = Significant

Table 5.1 shows the calculated V_0 (from Fig. 5.6 of the blank (no aptamer) with a $V_0 = 1.27 \pm 0.01 \times 10^{-1} \mu\text{M s}^{-1}$ and the immobilised G4 aptamers on the surface of the Corning® DNA-Bind® 96-well microplates with a $V_0 = 1.36 \pm 0.03 \times 10^{-1} \mu\text{M s}^{-1}$ ($p < 0.05$). Although this difference is statistically significant, it is not possible to distinguish between wells that have G4 aptamers immobilised and wells that do not. This indicates that the dominant reaction in this case would be the hemin oxidation of the TMB substrate in the bulk solution.

The dominant hemin oxidation reaction is attributed to the localisation of the G4 aptamers on the surface of the wells. whereby the TMB substrate must first diffuse through the bulk solution to reach the surface of the Corning® DNA-Bind® 96-well microplates to undergo a reaction.²⁰ Unlike a solution base TMB assay, whereby the G4 aptamers are free in solution, the TMB substrate must diffuse via mass transfer to the surface of the wells in order for the reaction to occur. The peroxidase-mimicking activity for a surface based immobilised enzymatic reaction can be calculated with the following Eq. 5.2:²¹

$$V_0 = k_l A ([S_0] - [S]) \quad (5.2)$$

Where V_0 is the peroxidase-mimicking activity, k_l is the mass transfer coefficient, A is the total surface area, S_0 is the initial concentration of the substrate, S is the concentration of the substrate. The k_l can be calculated using Eq. 5.3:²¹

$$k_l = \frac{D_S}{\delta} \quad (5.3)$$

Where D_S is the substrates diffusivity and δ is the effective thickness that the substrate must diffuse through. This equation assumes that all the surface area is equally accessible to the substrate.

Eq. 5.2 shows that as the substrate is depleted ($[S_0] \rightarrow 0$) the slower the rate of the V_0

will become. A larger K_I indicates that the substrate will diffuse through the solution faster and increase the V_0 . If δ is large and D_S is small, then the overall K_I will be low and therefore the reaction will proceed slower (Eq. 5.3). Adding to this issue may be a low density or efficiency of surface coupling of the G4 aptamers on the surface as well as the orientation of the strands on the surface due to non-specific interactions (lying flat instead of sticking up into solution). In that case, the rate accelerators should still be able to increase the overall V_0 of the immobilised G4 aptamers.

To overcome the mass transfer issues, rate accelerators such as polyethylene glycol (PEG) can be used to increase the peroxidase-mimicking activity on the surface microplates. Section 5.3.5.1 will discuss the use of PEG rate accelerators (such as PEG 6000 and PEG 8000) to achieve the increased peroxidase-mimicking activity.

5.3.5.1. Increasing the sensitivity of the TMB assay with PEG rate accelerators

The addition of PEG rate accelerators was investigated to determine if it was possible to increase the peroxidase-mimicking activity of the immobilised G4 aptamers. Aumiller Jr. *et al.*⁸ have shown that TMB activity towards horseradish peroxidase (HRP) was increased in the presence of PEG 8000 30% (w/v). They show that the TMB's D_S decreased from $7.18 \pm 0.07 \times 10^{-10} \text{ m}^2 \text{ s}^{-1}$ to $1.83 \pm 0.07 \times 10^{-10} \text{ m}^2 \text{ s}^{-1}$ due to the increased viscosity of the PEG 8000 solution, whereby it was more difficult for the TMB to diffuse away from the HRP. Therefore, the TMB was always in closer proximity to the HRP and would be able to increase the local reactivity. Thus, it would be reasonable to trial PEG 6000 and PEG 8000 in order to increase the reactivity of the TMB substrate in the presence of surface immobilised G4 aptamers with hemin.

PEG rate accelerators of PEG 6000 5% (w/v), PEG 6000 10% (w/v) and PEG 8000 5% were tested. These tests were performed using the immobilised G4 aptamers in the presence of hemin on the surface of the Corning® DNA-Bind® 96-well microplates. Fig. 5.7 shows the

UV/vis spectra of the change in absorbance (a.u) versus time (min) of the TMB assay used to detect the immobilised G4 aptamers in the presence of hemin with (a) no PEG control, (b) PEG 6000 5% (w/v) (c) PEG 6000 10% (w/v) and (d) PEG 8000 5% (w/v). Fig. 5.7 (a) "no PEG control" is the same data from Fig. 5.6 and 5.1 and simply relabelled here for clear comparison.

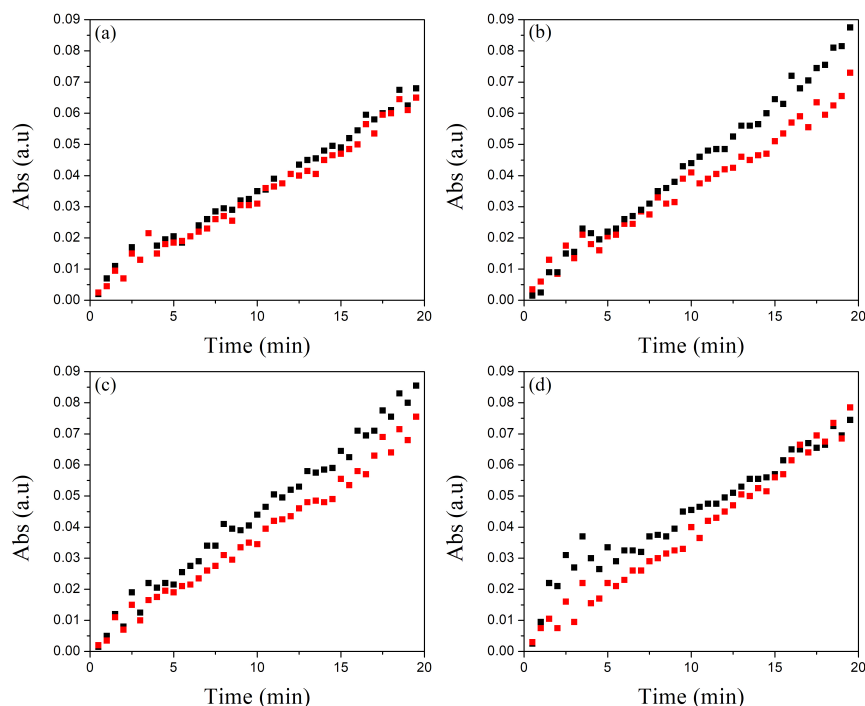


Figure 5.7: Average of 3 UV/vis spectra (absorbance versus time (min)) of TMB assay for no aptamer blank (red) and immobilised G4 aptamer (black) on the surface of Corning® DNA-Bind® 96-well microplates with (a) no PEG control, (b) PEG 6000 5% (w/v), (c) PEG 6000 10% (w/v) and (d) PEG 8000 5% (w/v), determined using a TMB assay. Averages were performed using OriginPro 9 average curve function.

Table 5.2 shows the V_0 calculated using 4.3 from the slopes of the absorbance (a.u) versus time (min) from the blank (red) and immobilised G4 aptamers (black) calculated from the data in 5.7.

Table 5.2 shows the calculated V_0 of the no PEG control, no PEG control, PEG 6000 5% (w/v), PEG 6000 10% (w/v) and PEG 8000 5% (w/v) with corresponding blanks. The no PEG control, no G4 aptamer and G4 aptamer, had a baseline V_0 of $1.27 \pm 0.01 \times 10^{-3} \mu\text{M s}^{-1}$ and $1.36 \pm 0.03 \times 10^{-3} \mu\text{M s}^{-1}$, respectively.

Table 5.2 shows that when the TMB assay was performed in solution with no ap-

Table 5.2: Peroxidase-mimicking activity (V_0) of immobilised G4 aptamers in the presence of no PEG control, PEG 6000 5% (w/v), PEG 6000 10% (w/v) and PEG 8000 5% (w/v) calculated from the data in Fig. 5.7.

Sample	Peroxidase-mimicking activity $V_0, \mu\text{M s}^{-1}, (\times 10^{-3})$		p = 0.05 (95% CI)
	No aptamer	G4 aptamer	
no PEG control*	1.27 ± 0.01	1.36 ± 0.03	$p < 0.05, s$
PEG 6000 5% (w/v)	1.38 ± 0.03	1.76 ± 0.06	$p < 0.05, s$
PEG 6000 10% (w/v)	1.57 ± 0.10	1.77 ± 0.06	$p < 0.05, s$
PEG 8000 5% (w/v)	1.33 ± 0.15	1.53 ± 0.01	$p < 0.05, s$

s = Significant

*Data from Table 5.1

tamers present, both the PEG 6000 5% (w/v) and PEG 6000 10% (w/v) increased the V_0 to $1.38 \pm 0.03 \times 10^{-3} \mu\text{M s}^{-1}$ and $1.57 \pm 0.10 \times 10^{-3} \mu\text{M s}^{-1}$, respectively. However, the PEG 8000 5% was not able to increase the V_0 in the blank solution. This may be due to the higher molecular weight of the PEG 8000 which decreases the mobility of the TMB in the solution and thus the activity.

Table 5.2 also shows that the TMB assays performed with aptamers present show that all PEG rate accelerators were able to increase the V_0 when compared to the no PEG control (with G4 aptamers). PEG 6000 5% (w/v) and PEG 6000 10% (w/v) were able to increase the V_0 the most, from $1.36 \pm 0.03 \times 10^{-3} \mu\text{M s}^{-1}$ (no PEG control) to $1.76 \pm 0.06 \times 10^{-3} \mu\text{M s}^{-1}$ and $1.77 \pm 0.06 \times 10^{-3} \mu\text{M s}^{-1}$, respectively. An increase of $\Delta V_0 = \sim 0.40 \times 10^{-3} \mu\text{M s}^{-1}$. Where as PEG 8000 5% (w/v) only increased the V_0 to $1.53 \pm 0.01 \times 10^{-3} \mu\text{M s}^{-1}$, a difference of $\Delta V_0 = 0.17 \times 10^{-3} \mu\text{M s}^{-1}$.

From this data it was concluded that the addition of the PEG rate accelerators was able to increase the V_0 of the immobilised G4 aptamers on the surface of the Corning® DNA-Bind® 96-well microplates. With PEG 6000 5% (w/v) and PEG 6000 10% (w/v) showing the largest increase in V_0 . Although when comparing the no G4 aptamer blanks to the corresponding PEG rate accelerator with G4 aptamer it Table 5.2 shows that PEG 6000 5% (w/v) has the largest difference, with a $\Delta V_0 = 0.38 \times 10^{-3} \mu\text{M s}^{-1}$. Compared with PEG 6000 10% (w/v) and PEG 8000 5% (w/v), both having a $\Delta V_0 = 0.20 \times 10^{-3} \mu\text{M s}^{-1}$. Therefore, it was concluded

that PEG 6000 5% would be the best PEG rate accelerator for studying surface immobilised G4 aptamers (see Section 5.3.6).

Although all the PEG rate accelerators were able to increase the V_0 of the surface immobilised G4 aptamers, the increase was considered too low to be useful for the proposed biosensor. This is due to the possibility of false positives being high, as there is a small difference between the no G4 aptamer wells and the wells that had immobilised G4 aptamers.

5.3.5.2. Solution-based detection of cleaved G4 aptamers containing a PM or SM from 2D surfaces

This section will discuss the detection of the T7 endonuclease I cleaved G4 aptamers in solution. In order for the solution-based detection to be useful there must be sufficient cleavage of the SM G4 aptamers. As this is solution-based detection, the PEG rate accelerators were not required.

This was achieved by first forming PM G4 aptamer (G4(G)T 001 + G4(C) 002) and SM (G4(G)T 001 + G4(T) 003) on the surface of the Corning® DNA-Bind® 96-well microplates, by adding the corresponding target sequence. The microplates were heated to 70 °C and cooled to room temperature. The microplates were washed according to Chapter 2, Section 5.3.4 and then dried by extracting all the Milli-Q water. T7 endonuclease I (1 U) in NEB 2 buffer (20 μ L) was added to each well and incubated for 16 h at 37 °C. The resulting solution was then extracted, made up to 50 μ L with Reaction buffer (see Chapter 2, Section 2.1, Table 2.3) and the G4 aptamers formed as previously outlined in Chapter 2, Section 2.3.2.1. Solutions extracted will be referred to as PM and SM solutions henceforth.

A TMB assay was performed (see Chapter 2, Section 2.3.2.3) to detect the presence of any G4 aptamers for both the PM and SM solutions after digestion with the T7 endonuclease I. Fig. 5.8 shows the results for the TMB assay (absorbance (a.u) versus time (min)) performed on the PM and SM solutions.

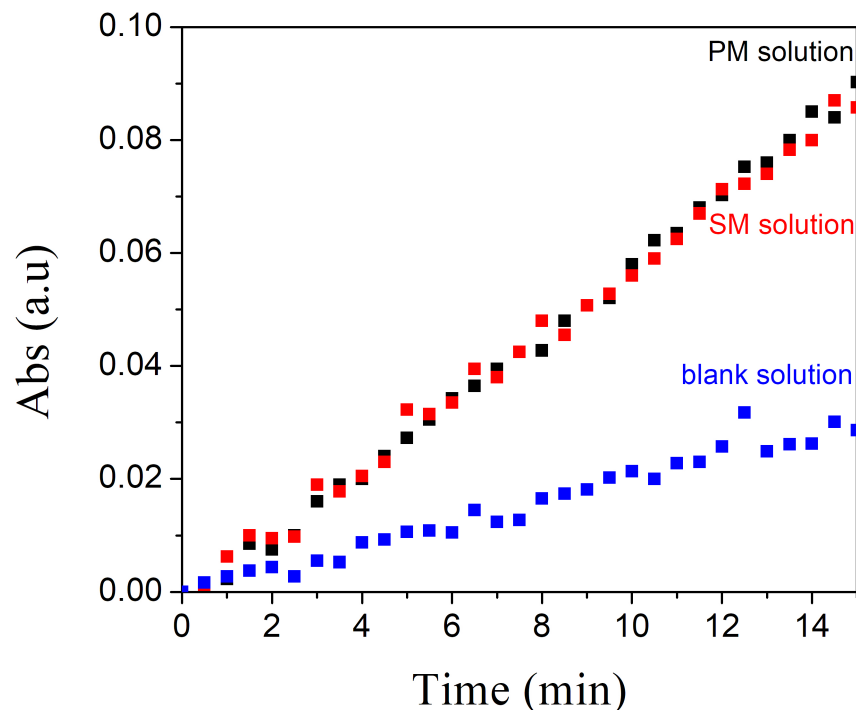


Figure 5.8: Average of 3 peroxidase-mimicking activity measurements of PM and SM G4 aptamers released into solution after 16 h digestion at 37 °C with T7 endonuclease I. Showing blank (no aptamer) (blue), perfect match (PM, red) and single mismatch (SM, black) after digestion. Averages were performed using OriginPro 9 average curve function.

Table 5.3 shows the V_0 calculated using Eq. 4.3 from the slopes of the absorbance (a.u) versus time (min) from the blank (no G4 aptamer) (blue), PM solution (red) and SM solution (black) after digestion, calculated from Fig. 5.8.

Table 5.3: Peroxidase-mimicking activity (V_0) of blank (no aptamer), PM and SM after digestion calculated from Fig. 5.8.

Sample	Peroxidase-mimicking activity, V_0 , $\mu\text{M s}^{-1}$, ($\times 10^{-3}$)	$p = 0.05$ (95% CI), compared to blank
blank(no G4 aptamer)	1.71 ± 0.38	-
PM solution	2.69 ± 0.25	$p < 0.05$, s
SM solution	2.60 ± 0.18	$p < 0.05$, s

s = Significant

Table 5.3 shows that compared to the blank ($V_0 = 1.71 \pm 0.38 \times 10^{-3} \mu\text{M s}^{-1}$) both the digested PM and SM solutions have an increased V_0 at $2.69 \pm 0.25 \times 10^{-3} \mu\text{M s}^{-1}$ and 2.60

$\pm 0.18 \times 10^{-3} \mu\text{M s}^{-1}$, respectively. This indicates that it is possible to detect the presence of cleaved G4 aptamers from the 2D surface in solution. This data shows that it was not possible to distinguish PM and SM solutions and that the T7 endonuclease I had non-specific cleavage activity towards the surface immobilised G4 aptamers on the surface of the microplates.

Therefore, a new approach was taken that is described in Section 5.3.6. The following section will discuss the immobilisation of the same G4 aptamers (PM and SM) onto BcMagTM silica coated iron oxide magnetic beads (3D surface).

5.3.6. Investigation of PM and SM immobilised on 3D surfaces

The issue with utilising flat 2D surfaces of the Corning® DNA-Bind® 96-well microplates is the low surface area and slow substrate diffusion to the surface. Even with the added PEG rate accelerators the peroxidase-mimicking activity of the G4 aptamers immobilised on the 2D surfaces was found to be too low to be useful (see Section 5.3.4). This is a common problem that is often encountered when biological catalysts (e.g., enzymes and DNAszymes) are immobilised on surfaces.²² In this section these were investigated by using the 3D surface of BcMagTM silica coated iron oxide magnetic beads (1 μm in diameter) to overcome low surface area and substrate diffusion. The beads not only offer increased surface area, the concentration of the beads can be increased to introduce more G4 aptamers into a single solution. The disadvantage is that due to the use of UV/vis spectroscopy for the TMB assay, the concentration must not be too high as to interfere with the measurements.

In this work PEG 6000 5% was used as it showed to be effective at increasing the peroxidase-mimicking activity of the immobilised G4 aptamers on the 2D surface (see Section 5.3.5.1).

The immobilisation of the amine-functionalised G4(G)T 001 ODN to the surface of the beads was performed following the manufacturer's instructions set out in Chapter 2, Section 2.3.4.3. PM and SM G4 aptamers were formed following the method set out in Section 5.3.2

and will be referred to as PM beads and SM beads, respectively, henceforth. Beads with no immobilised G4 aptamers were used as a blank (no G4 aptamer) for comparison with the PM and SM beads. In this section the term dried beads simply refers to beads (PM and SM) that have had the buffer solution removed allowing for a new buffer to be added with minimal dilution.

Dried beads (PM and SM) were then placed into a 1X NEB 2 buffer containing 1 U of T7 endonuclease I and incubated for 16 h at 37 °C. The digested beads will henceforth be referred to as digested PM and SM beads. Beads that were not digested will be referred to as undigested and will be used as a comparison to reveal any affect that the T7 endonuclease I had on the PM and SM beads.

The dried beads were then washed according to the wash procedure set out in Chapter 2, Section 2.3.4.3 to remove all the G4 aptamers that were not immobilised onto the surface of the beads. After digestion the dried beads were placed into a 1X Reaction buffer with peg 6000 5% and a TMB assay was performed according to the procedure set out in Chapter 2, Section 2.3.4.4.

Fig. 5.9 shows the resulting absorbance versus time (min) spectra for the undigested and digested PM and SM beads.

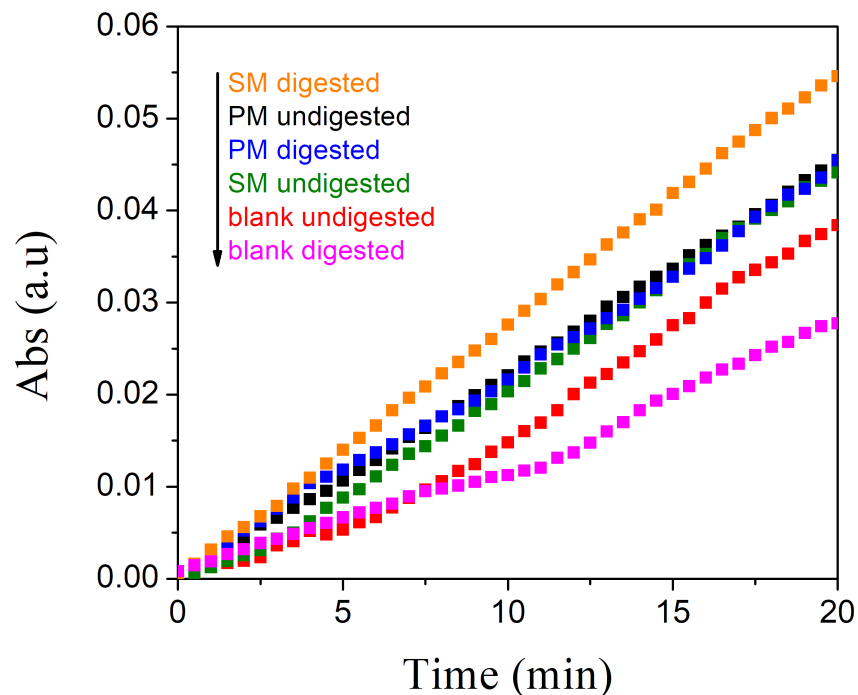


Figure 5.9: Average of 3 peroxidase-mimicking activity measurements of G4 aptamers immobilised onto BcMag® silica iron core microbeads: blank (no G4 aptamer) undigested (red), blank (no G4 aptamer) digested (pink), PM undigested (black), PM digested (blue), SM undigested (green), and SM digested (orange). Averages were performed using OriginPro 9 average curve function.

Table 5.4 shows the V_0 calculated using 4.3 from the slopes of the absorbance (a.u) versus time (min) from the undigested and digested blank (no aptamer), PM beads and SM beads calculated from the data in 5.9.

Table 5.4 shows that the undigested blank (no G4 aptamer), PM and SM beads have a V_0 of $1.4 \pm 0.2 \times 10^{-3} \mu\text{M s}^{-1}$, $1.5 \pm 0.1 \times 10^{-3} \mu\text{M s}^{-1}$ and $1.4 \pm 0.2 \times 10^{-3} \mu\text{M s}^{-1}$, respectively. From this it was deduced that it was not possible to detect the G4 aptamers immobilised on the surface of either the PM or SM beads despite the addition of PEG 6000 5% (w/v).

Table 5.4: Peroxidase-mimicking activity (V_0) of undigested and digested PM and SM beads calculated using Eq. 5.4 from Fig. 5.9

Sample	Peroxidase-mimicking activity $V_0, \mu\text{M s}^{-1}, (\times 10^{-3})$		p = 0.05 (95% CI)
	undigested	digested	
blank (no G4 aptamer)	1.4 ± 0.2	1.2 ± 0.2	$p > 0.05$, ns
PM beads	1.5 ± 0.1	1.5 ± 0.5	$p > 0.05$, ns
SM beads	1.4 ± 0.2	1.6 ± 0.3	$p > 0.05$, ns

ns =Not significant

Table 5.4 shows that the digested blank (no G4 aptamer), PM and SM beads have a V_0 of $1.2 \pm 0.2 \times 10^{-3} \mu\text{M s}^{-1}$, $1.5 \pm 0.5 \times 10^{-3} \mu\text{M s}^{-1}$ and $1.6 \pm 0.3 \times 10^{-3} \mu\text{M s}^{-1}$, respectively. This indicates that after digestion has occurred it is still not possible to detect the presence of the G4 aptamers on the surface of the PM and SM beads. The large errors associated with these measurements is thought to be due to the difficulty of maintaining consistent concentration of beads and therefore G4 aptamers across multiple runs. As initial pipetting may not result in the same number of beads being extracted from the bulk solution and multiple washing procedures can result in a loss of beads. It was therefore concluded that the BcMagTM silica oxide magnetic beads were not suitable for the proposed biosensor.

Strategies for improving this method could include the use of different enzymes such as Endonuclease MS, Endonuclease V or T4 endonuclease VII.^{23,24} Toehold-mediated strand displacement techniques could also be employed to help release the G4 aptamer from the surface of the wells or plates, however this has had limited success in literature.²⁵

5.4. Concluding remarks

In this chapter G4 aptamers were immobilised onto the 2D and 3D surfaces and were investigated for the development of a SNP genotyping biosensor.

G4 aptamers with a capture region, containing a SNP, were duplexed with a target strand. Complementary and partially-complementary target strands were used to form a perfect match (PM) and single mismatch (SM) G4 aptamer, respectively. They were then digested with

T7 endonuclease I to cleave the SM G4 aptamer with minimal cleavage of the PM G4 aptamer. Due to the short length of the ODN and possible steric hindrance from the G4 structure a 16 h incubation was required. It was found that the G4 aptameric structures were not recognised by the T7 endonuclease I, making it potentially viable for SNP genotyping.

Next the PM and SM G4 aptamers were immobilised on the surface of Corning® DNA-Bind® 96-well microplates (2D surface) and tested with a TMB assay. It was determined that it was not possible to detect the the G4 aptamers on the surface. PEG rate accelerators were utilised to increase the peroxidase-mimicking activity of the immobilised G4 aptamers. The PEG rate accelerators effectively decrease the volume that the TMB substrate would have to diffuse through. PEG 6000 5% (w/v) and PEG 6000 10% (w/v) were found to increase the peroxidase-mimicking activity as compared to the blank (no aptamer). However, it was still not sufficient enough to be considered useful for the proposed biosensor.

The immobilised PM and SM aptamers were then digested with the T7 endonuclease I. The resulting solution was tested to determine if there was any release of the G4 aptamers into solution. It was found that it was possible to detect the G4 aptamers that were released into solution, despite no added PEG rate accelerator. However, it was determined that the T7 endonuclease I was cleaving PM and SM G4 aptamers from the surface.

Finally, the same approach was taken with BcMag™ silica coated iron oxide magnetic beads (3D surface). The G4 aptamers were first immobilised onto the surface of the microbeads. It was determined that it was not possible to detect the G4 aptamers on the surface of the microbeads, even after digesting with the T7 endonuclease I. This indicated that it was not possible to use the BcMag™ silica coated iron core oxide magnetic beads for the proposed biosensor.

Further work is required to increase the limits of detection on the both the 2D and 3D surfaces to allow for sufficient detection of immobilised G4 aptamers. The use of G4 aptamers with increased peroxidase-mimicking activity as well as the addition of more effective

polymeric rate accelerators may be able to increase the sensitivity of the proposed biosensor. Finally, a new strategy for cleaving the SM may need to be employed to overcome the non-specific cleavage seen with the T7 endonuclease I.

5.5. Chapter 5 References

- [1] Hud, N. V.; Smith, F. W.; Anet, F. A.; Feigon, J. The selectivity for K⁺ versus Na⁺ in DNA quadruplexes is dominated by relative free energies of hydration: A thermodynamic analysis by ¹H NMR. *Biochemistry* **1996**, *35*, 15383–15390.
- [2] Loh, Q.; Lim, T. S. *Nucleic Acids - From Basic Aspects to Laboratory Tools*; 2016.
- [3] Zhou, W.; Jimmy Huang, P. J.; Ding, J.; Liu, J. Aptamer-based biosensors for biomedical diagnostics. *Analyst* **2014**, *139*, 2627–2640.
- [4] Hu, Y.; Xu, X.; Liu, Q.; Wang, L.; Lin, Z.; Chen, G. Ultrasensitive electrochemical biosensor for detection of DNA from *Bacillus subtilis* by coupling target-induced strand displacement and nicking endonuclease signal amplification. *Analytical Chemistry* **2014**, *86*, 8785–8790.
- [5] Wenzel, J. J.; Rossmann, H.; Fottner, C.; Neuwirth, S.; Neukirch, C.; Lohse, P.; Bickmann, J. K.; Minnemann, T.; Musholt, T. J.; Schneider-Rätzke, B.; Weber, M. M.; Lackner, K. J. Identification and prevention of genotyping errors caused by G-quadruplex- and i-motif-like sequences. *Clinical Chemistry* **2009**, *55*, 1361–1371.
- [6] Zou, P.; Liu, Y.; Wang, H.; Wu, J.; Zhu, F.; Wu, H. G-quadruplex DNAzyme-based chemiluminescence biosensing platform based on dual signal amplification for label-free and sensitive detection of protein. *Biosensors and Bioelectronics* **2016**, *79*, 29–33.
- [7] Kong, D. M.; Yang, W.; Wu, J.; Li, C. X.; Shen, H. X. Structure-function study of peroxidase-like G-quadruplex-hemin complexes. *Analyst* **2010**, *135*, 321–326.
- [8] Aumiller, W. M.; Davis, B. W.; Hatzakis, E.; Keating, C. D. Interactions of macromolecular crowding agents and cosolutes with small-molecule substrates: Effect on horseradish

- peroxidase activity with two different substrates. *Journal of Physical Chemistry B* **2014**, *118*, 10624–10632.
- [9] Wu, S. H.; Zeng, Y. F.; Chen, L.; Tang, Y.; Xu, Q. L.; Sun, J. J. Amplified electrochemical DNA sensor based on hemin/G-quadruplex DNzyme as electrocatalyst at gold particles modified heated gold disk electrode. *Sensors and Actuators, B: Chemical* **2016**, *225*, 228–232.
- [10] Lam, E. Y. N.; Beraldi, D.; Tannahill, D.; Balasubramanian, S. G-quadruplex structures are stable and detectable in human genomic DNA. *Nature Communications* **2013**, *4*, 1796.
- [11] Jiang, J.; He, Y.; Yu, X.; Zhao, J.; Cui, H. A homogeneous hemin/G-quadruplex DNzyme based turn-on chemiluminescence aptasensor for interferon-gamma detection via in-situ assembly of luminol functionalized gold nanoparticles, deoxyribonucleic acid, interferon-gamma and hemin. *Analytica Chimica Acta* **2013**, *791*, 60–64.
- [12] Yin, B. C.; Guan, Y. M.; Ye, B. C. An ultrasensitive electrochemical DNA sensor based on the ssDNA-assisted cascade of hybridization reaction. *Chemical Communications* **2012**, *48*, 4208–4210.
- [13] Babon, J. J.; McKenzie, M.; Cotton, R. G. H. The use of resolvases T4 endonuclease VII and T7 endonuclease I in mutation detection. *Molecular biotechnology* **2003**, *23*, 73–81.
- [14] Sadowski, P. D. Bacteriophage T7 Endonuclease I. *J. Biol. Chem.* **1971**, *246*, 209–216.
- [15] Biolabs, N. E. Reagents For the Life Sciences Industry — NEB. <https://www.neb.com/>.
- [16] Zahler, A. M.; Williamson, J. R.; Cech, T. R.; Prescott, D. M. Inhibition of telomerase by G-quartet DMA structures. *Nature* **1991**, *350*, 718–720.
- [17] Cao, Z.; Huang, C. C.; Tan, W. Nuclease resistance of telomere-like oligonucleotides monitored in live cells by fluorescence anisotropy imaging. *Analytical Chemistry* **2006**, *78*, 1478–1484.

- [18] Vouillot, L.; Thélie, A.; Pollet, N. Comparison of T7E1 and Surveyor Mismatch Cleavage Assays to Detect Mutations Triggered by Engineered Nucleases. *G3: Genes—Genomes—Genetics* **2015**, *5*, 407–415.
- [19] Wu, Z.-K.; Zhou, D.-M.; Wu, Z.; Chu, X.; Yu, R.-Q.; Jiang, J.-H. Single-base mismatch discrimination by T7 exonuclease with target cyclic amplification detection. *Chem. Commun.* **2015**, *51*, 2954–2956.
- [20] Peterson, A. W.; Heaton, R. J.; Georgiadis, R. M. The effect of surface probe density on DNA hybridization. *Nucleic Acids Research* **2001**, *29*, 5163–5168.
- [21] Oppermann, R. *Journal of the Franklin Institute*; Cambridge University Press, 1944; Vol. 237; pp 498–499.
- [22] Dunn, K. E.; Trefzer, M. A.; Johnson, S.; Tyrrell, A. M. Investigating the dynamics of surface-immobilized DNA nanomachines. *Scientific Reports* **2016**, *6*, 29581.
- [23] Fuhrmann, M.; Oertel, W.; Berthold, P.; Hegemann, P. Removal of mismatched bases from synthetic genes by enzymatic mismatch cleavage. *Nucleic acids research* **2005**, *33*, e58.
- [24] Ishino, S.; Nishi, Y.; Oda, S.; Uemori, T.; Sagara, T.; Takatsu, N.; Yamagami, T.; Shirai, T.; Ishino, Y. Identification of a mismatch-specific endonuclease in hyperthermophilic Archaea. *Nucleic acids research* **2016**, *44*, 2977–86.
- [25] Fenati, R.; Khodakov, D.; Ellis, A. Optimisation of DNA hybridisation and toehold strand displacement from magnetic bead surfaces. *International Journal of Nanotechnology* **2017**, *14*.

Chapter 6

Chapter 6: Investigation of G-quadruplex aptamers as possible antimicrobial agents against S. aureus and S. epidermidis

6.1. Synopsis

This chapter presents the synthesis and utilisation of G-quadruplex (G4) aptamers as an antimicrobial agent to eradicate microbes present in biofilms. This would rely on G4 aptamers coupled with and without antibiotics penetrating the biofilm and undergoing peroxidase-mimicking activity to eradicate bacterial cells present inside of the biofilm.

Initial experiments involved the coupling of an antibiotic, with carboxyl group, to a 5' amine-functionalised G4 oligodeoxynucleotide (ODN), labelled with a 5' CY3.5 fluorophore, through a carbodiimide coupling reaction. The two antibiotics used were fluoroquinolonic acid and oxacillin (a methacillin β -lactum antibiotic). The antibiotic coupled G4 ODNs were purified and concentrated using an ethanol precipitation method, however only oxacillin coupled G4 (OXG4) aptamers were successfully purified. fluoroquinolonic acid was not able to be successfully recovered to a concentration that was viable for use in experiments. OXG4 was then

tested for peroxidase-mimicking activity and antibiotic activity towards *Staphylococcus aureus* (*S. aureus*).

OxG4 was then utilised to treat bacteria, such as *S. aureus* and *Staphylococcus epidermidis* (*S. epidermidis*), protected by a biofilm. After determining that there was not enough endogenous peroxide species, *G4* aptamers (no coupled antibiotic) were tested for antimicrobial activity with added 0.5% hydrogen peroxide (v/v).

6.2. Introduction and purpose

Biofilms (containing sessile bacteria) present challenges to the health sector, as biofilms have been linked to chronic illnesses and the rise in antimicrobial resistance of bacteria (see Chapter 1, Section 1.7.2).^{1,2} This resistance attributed to the existence of ‘persister cells’ (metabolically dormant cells) that are resistant to antimicrobial treatments.³ Treatment of biofilms with the successful eradication of the persister cells has required new strategies, including: high-dose topical treatments,⁴ combined or sequential treatments,⁵ and antibiotic adjuvants.⁶ However, these approaches have become less effective at treating microbes over time. The World Health Organisation (WHO) has shown that *Escherichia coli* (*E. coli*), *Staphylococcus aureus* (*S. aureus*) and *Staphylococcus pneumoniae* (*S. pneumoniae*) most commonly reported to have some degree of antibiotic resistance.⁷ New and more effective treatments are required to combat the rising number of antibiotic resistant bacterial.

Nanoparticles and antiseptics have demonstrated little success in the elimination of biofilms and persister cells (see Chapter 1, Section 1.7.5.1).^{8–11} Additionally, these treatments can be toxic to human cells at high concentrations, which hinders the implementation of high-dose antimicrobials.¹² Development of new drugs with low toxicity (towards humans) are required to eradicate biofilms to prevent the rising antibiotic resistant bacterial strains. A new strategy being investigated is hydrogen peroxide based systems that destroy the bacteria effectively and do not rely on antibiotic pathways.

Peroxidase enzymes are an emerging technology for bacterial eradication.¹³⁻¹⁶ Due to the fact that peroxidases do not inherently have antimicrobial activity, often an oxidisable substrate is added that will be able to eliminate the bacteria (see Chapter 1, Section 1.7.5.1).^{16?} However, enzymes are difficult to isolate, concentrate and cheaply implement with current technologies.¹⁷ This has led to the development of enzyme-free systems utilising substrates that are readily oxidised by hydrogen peroxide, such as iodide and thiocyanate compounds.¹³ However, these compounds can have adverse side effects on humans, namely disruption of thyroid function.¹⁸ Thus, it is imperative that safer and cheaper alternatives to enzymes and thiocyanate methods be developed.

In this chapter G4 aptamers were investigated as possible antimicrobials in the presence and absence of hydrogen peroxide. Table 6.1 details two G4 oligodeoxynucleotide (ODN) sequences were utilised in this chapter. Both G4 ODNs contain the G4 forming sequence (Table 6.1, red) with the highest peroxidase-mimicking activity as determined in Chapter 4, Section 4.10.

Table 6.1: Sample names and Sequences of G4 ODNs utilised throughout this chapter.

Sample name	ODN sequence 5' \implies 3'
G4 aptamer	G₃A₃G₃CACG₃CG₃
NH ₂ -G4	NH ₂ —ATGA ₂ T ₂ C ₂ G₃A₃G₃CACG₃CG₃ CACAC ₂ A—CY3.5

Red nucleotides indicate the G4 forming sequence and black nucleotides are the spacer sequences to prevent interaction between the folded G4 aptamer, and either the fluorophore (CY3.5) or coupled antibiotic (replacing the NH₂ after the coupling reaction).

It was proposed that the G4 aptamers with complexed hemin act as an antimicrobial by reacting with the cell walls of the bacteria, which has been observed in humans to a lesser degree.¹⁹ This occurs due to hemin inducing the formation of oxygen radical species that go on to oxidise and damage lipids, proteins and DNA.^{19,20} G4 aptamers are hypothesised to increase the formation of the oxygen radical species.

The first issue to be considered is if the G4 aptamers are able to penetrate and diffuse

through a biofilm. Chapter 1, Section 1.7.5.1 describes how antibiotics can penetrate biofilms. So in this chapter antibiotic coupled G4 aptamers were utilised to determine if the antibiotic could be used to increase diffusion across the biofilm.

A carbodiimide reaction was used to couple an amine-functionalised G4 ODN with an antibiotic that contain a carboxylic acid. Both antibiotics were chosen for the presence of carboxylic acid that was not involved in the pharmacophore, allowing for attachment without inhibiting the antimicrobial properties. FQ was chosen as it has been shown to be able to be superior at crossing into the biofilm.²¹ OX was chosen due to being effective against *S. aureus* but less effective against the *S. epidermidis*.^{22,23}

The following section will discuss the coupling and purification of the G4 aptamer with the antibiotic. The resulting product will be an antibiotic coupled G4 aptamer that will be used for subsequent experiments.

6.3. Results and discussion

6.3.1. Coupling and purification of antibiotic coupled G4 aptamers

A carbodiimide reaction was first used to couple the antibiotic (FQ or OX) to the G4 aptamer then purified using the method set out in Chapter 2, Section 6.3.1 and 2.3.5.2. Fig. 6.1 shows the antibiotics considered were fluoroquinolonic acid (FQ, Fig. 6.1 (a)) and oxacillin (OX, Fig. 6.1 (b)) with the carboxylic acid functional groups (Fig. 6.1 red).

The carbodiimide coupling reaction followed is detailed in Chapter 2, Section 2.3.5.1. Fig. 6.2 shows the general scheme for the carbodiimide coupling reaction that was utilised to couple the antibiotic carboxyl acid group (AB-COOH, red) to the NH₂-G4 aptamer (NH₂-G4).

Firstly, the carboxylic acid moiety on the AB-COOH reacts with 1-ethyl-3-(3-dimethylaminopropyl) carbodiimide hydrochloride (EDC) to form an intermediate. The resulting inter-

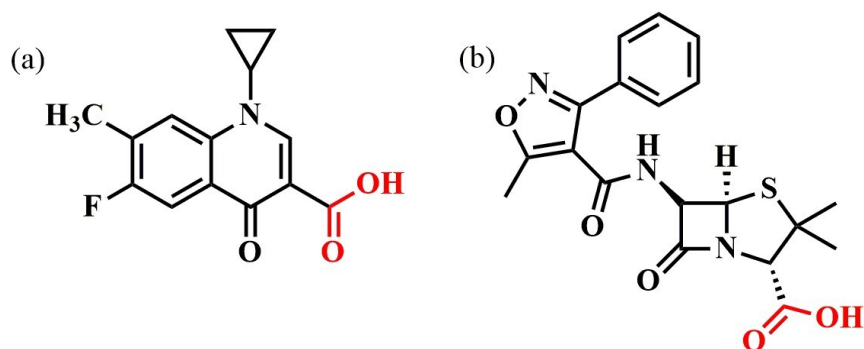


Figure 6.1: The chemical structure of (a) fluoroquinolonic acid and (b) oxacillin. The carboxylic acid functional groups used for coupling with the G4 ODN are highlighted in red.

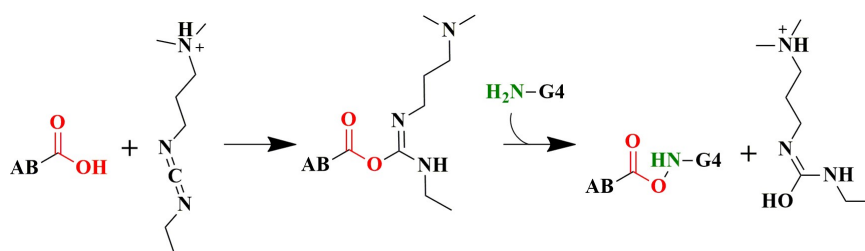


Figure 6.2: General scheme for the carbodiimide coupling reaction. The antibiotic with carboxylic acid functional group (red) reacts with 1-ethyl-3-(3-dimethylaminopropyl) carbodiimide hydrochloride (EDC) to form an intermediate that reacts with the amine-functionalised G4 aptamer (amine-functionalised, green).

mediate is then able to react with the amine group on the aptamer resulting in an amide-linkage the formation of a final product, antibiotic coupled G4 ODN (Fig. 6.2) and hydroxylated-EDC. The resulting antibiotic coupled G4 ODN, which is able to form a G4 aptamer, synthesised in this thesis will be referred to as FQG4 aptamer and OXG4 aptamer.

6.3.1.1. Purification of antibiotic coupled G4 aptamers

The resulting FQG4 aptamer and OXG4 aptamers were then purified using ethanol precipitation (Chapter 2, Section 2.3.5.2). This was done to remove excess antibiotic that did not couple to the G4 aptamer. The antibiotic G4 aptamer must be purified to ensure that the antibiotic does not interfere with subsequent experiments that involve bacteria. The concentration of the precipitated antibiotic coupled G4 aptamer was determined using a Roto Gene 6-plex

real-time PCR device. A orange channel (Table 2.9) was utilised to detect antibiotic coupled G4 ODN, as the G4 ODN contains a 3' CY3.5 fluorophore (excitation wavelength (ϵ_{max}) = 579 nm and emission wavelength (λ_{max}) = 589 nm). It was determined that 50-80% of OXG4 was purified and 10-20% of FQG4 was purified by ethanol precipitation. The low yield of the FQG4 aptamer was attributed to the increase in hydrophobicity after coupling of the fluoroquinolonic acid. Thus, the product prefers to remain in the ethanol fraction rather than precipitate out. Due to the reasonable recovery of the OXG4 aptamer was used for antimicrobial studies.

Agarose gel electrophoresis and polyacrylamide gel electrophoresis were used to determine if purification of the OXG4 was successful (see Appendix H). The gel electrophoresis could also be used to determine if there were any significant structural changes that was caused by the coupling of the antibiotic to the G4 aptamer. However, due to the small weight difference it is not possible to determine if successful antibiotic coupling occurred. It should be noted that the NH₂G4 and G4 ODNs both form intramolecular and intermolecular G4 structures, in a similar manner to the G4 ODNs from Chapter 5, Section 5.3.2 (G4(G) 001 + G(C) 002 and G4(G) 001 + G4(T) 003). Therefore it is vital to test if the OXG4 aptamer retained peroxidase-mimicking activity. The following section will discuss the characterisation of the OXG4 aptamer by testing its peroxidase-mimicking activity and antimicrobial activity.

6.3.2. Testing of the peroxidase-mimicking activity and antimicrobial activity of OXG4 aptamers

As mentioned in Chapter 4, Section 4.3.3, the DNA sequence can affect the peroxidase-mimicking activity of G4 aptamers. Therefore, the OXG4 aptamer was tested for peroxidase-mimicking activity (V_0) and antimicrobial activity to determine if it was viable for use in antimicrobial experiments.

6.3.2.1. TMB assay testing of OXG4 aptamer

The peroxidase-mimicking activity of the OXG4 aptamer was tested using the TMB assay (see Chapter 2, Section 2.3.2.3). Figure 6.3 shows the resulting absorbance (a.u) versus time (min) spectra for blank (no G4 aptamer), G4 aptamer, NH₂-G4 aptamer, OXG4 aptamer and OX (no G4 aptamer).

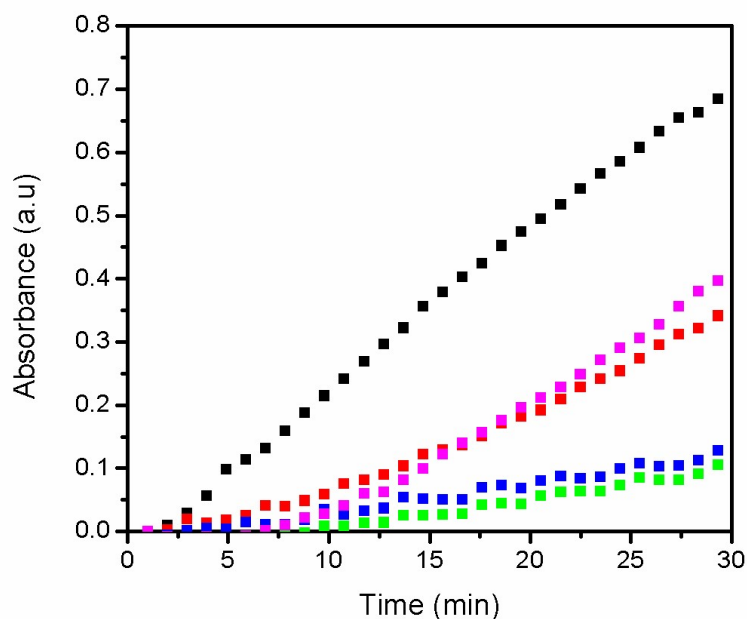


Figure 6.3: Average of 3 UV/vis spectra (absorbance versus time (min)) of TMB assay for blank (no G4 aptamer, green), G4 aptamer (black), NH₂-G4 aptamer (pink), OXG4 aptamer (red) and OX (no G4 aptamer, blue). Averages were performed using OriginPro 9 average curve function.

Fig 6.3 was used to calculate the V_0 by first calculating the slope of the line for each sample and then using Eq. 4.3 (see Chapter 4, Section 4.3.3). Table 6.2 shows the calculated V_0 using Eq. 4.3 from the slopes in Fig. 6.3 The V_0 OXG4 aptamer was compared to the V_0 of G4 aptamer, NH₂-G4 aptamer and OX to determine the effects of the coupled OX.

Table 6.2 show that the blank and OX (no aptamer) have the lowest peroxidase-mimicking activity with at $V_0 = 0.001 \mu\text{M s}^{-1}$. The G4 aptamer has the highest peroxidase-

Table 6.2: Peroxidase-mimicking activity (V_0) of TMB assay for blank (no G4 aptamer, green), G4 aptamer (black), NH₂-G4 aptamer (pink), OXG4 aptamer (red) and OX (no G4 aptamer, blue) calculated from Fig. 6.3

Sample	Peroxidase-mimicking activity, V_0 , $\mu\text{M s}^{-1}$, (Error = $\leq 1\%$)
Blank (no G4 aptamer)	0.001
G4 aptamer	0.204
NH ₂ -G4 aptamer	0.130
OXG4 aptamer	0.170
OX (no aptamer)	0.001

mimicking activity at $V_0 = 0.204 \mu\text{M s}^{-1}$. The NH₂-G4 aptamer appears to have a decreased peroxidase-mimicking activity at $V_0 = 0.130 \mu\text{M s}^{-1}$ when compared to the G4 aptamer. This inhibition of the NH₂-G4 aptamer is likely due the addition functionalities that restrict it from forming the correct structure for enhancement of peroxidase-mimicking activity.

A slight decrease in the peroxidase-mimicking activity of the OXG4 aptamer was observed in comparison to the G4 aptamer at $V_0 = 0.170 \mu\text{M s}^{-1}$. This indicates that the coupling of the OX to the G4 aptamer has not restricted its peroxidase-mimicking activity. Thus, the G4 structure is still able to fold despite substantial modifications. The OXG4 aptamers has slightly increased the V_0 compared to the NH₂-G4 aptamer. This was proposed to be due to the amine being the causal affect of the lower V_0 , as once the amine group has been reacted the V_0 increases once again. However, further experiments would be required in order to determine as to how the amine group interferes with the G4 aptamer V_0 , this is outside the scope of this project.

The next section will discuss the testing of the antimicrobial activity of the OXG4 aptamer by determining the minimum inhibitory concentration (MIC).

6.3.2.2. Minimum inhibitory concentration

In order to determine if the OX was coupled to G4 aptamer and still able to interact with bacteria, the MIC of the OXG4 and OX were determined. MIC is a method that is used to determine what is the lowest concentration required in order to inhibit the visible growth of bacteria after an overnight incubation. The method was performed to the Clinical and Laboratory Standards Institute (CLSI) guidelines using the cation adjusted Mueller-Hinton broth (MHB) dilution method set out in Chapter 2, Section 2.3.5.4. The only modification of the CLSI standard procedure that was used in this work was the use of flat bottomed 96-well plates as opposed to round bottom. This has been previously published as an acceptable modification.²⁴ The bacterial used for this MIC determination was *S. aureus* ATCC 25923 (Table 2.8 non-biofilm forming), which is susceptible to methicillin antibiotics such as OX.

In brief, a stock solution of OX was made up to 1000 $\mu\text{g mL}^{-1}$. Serial dilutions of the stock solutions of 8.000, 4.000, 2.000, 1.000, 0.500, 0.250 and 0.125 $\mu\text{g mL}^{-1}$ were made up, following CLSI guidelines. In order to calculate the concentrations required for the study of OXG4 aptamer, it was calculated that 2.5 μM of OXG4 aptamer was equivalent to 1 $\mu\text{g mL}^{-1}$ attached OX and so this solution was diluted to 2.000, 1.000, 0.500, 0.250 and 0.125 $\mu\text{g mL}^{-1}$ for the MIC studies. Identical solutions were obtained for NH_2 -G4 aptamer. A cell suspension *S. aureus* cells were inoculated into 20 μL of MHB in a 96-well plate. 20 μL of each solution mentioned above was added to separate wells in triplicate (avoiding the first row and column). The 96-well plates were incubated for 20 h at 35 °C. After the incubation the plates were observed visually to determine if there was any cell population growth. Cell population growth was determined by any discolouration of the MHB or film on the surface of the 96-wells.

For NH_2 there was no antimicrobial activity visually observed, as all the wells showed signs of cell growth. It was found that both the OX and OXG4 aptamer both had a MIC of 0.5 $\mu\text{g mL}^{-1}$ (or 1.25 μM OXG4 aptamer). This indicates that the OX is indeed coupled with the NH_2 -G4 aptamer and that it retains antimicrobial activity.

Therefore, it was decided that $1 \mu\text{g mL}^{-1}$ of OX and $2.5 \mu\text{M}$ OXG4 would be used to study the effects on biofilms. This was decided to ensure that the concentration was high enough to eradicate the bacteria, while limiting the amount of OXG4 aptamer required for each experiment. Sign *et al.*²² determined that $1 \mu\text{g mL}^{-1}$ was not enough to eradicate bacteria inside of biofilm, and so any antimicrobial effects seen with the OXG4/hemin aptamer would be attributed to the peroxidase-mimicking activity. The next section 6.3.3 will discuss how the impact of the G4 aptamer, OXG4 aptamer and OX on bacterial biofilms.

6.3.3. Impact of G4 aptamer, OXG4 and OX on biofilms

As described in Chapter 1, Section 1.7.5.1 natural peroxidase enzyme systems have been utilised to treat bacteria, however these systems have drawbacks (toxic substances) and have never been utilised to treat bacteria present inside of a biofilm. The issue with these systems is the inhibition of the antimicrobial activity due to reaction with components present in the matrix that the cells exist in.²⁵ This is due to the wide range of reactants that the active thiocyanate is able to react with. Peroxidase enzymes on the other hand have a very narrow range of reactants and so cannot be used in isolation. G4/hemin aptamers have been shown to have a wider range of possible reactants than the peroxidase enzymes, but a narrower range of reactants than thiocyanate.²⁰ Therefore it was reasonable to use G4 aptamers and OXG4 aptamers as a possible method for eradication of biofilm bacteria.

For the remainder of this thesis the G4 aptamer refers to the G4 aptamer ODN from Table 6.1, the G4/hemin aptamer refers to the same sequence with added hemin. OXG4 aptamer refers to the synthesised OXG4 aptamer from Section 6.3.1 and OXG4/hemin aptamer (which refers to the same sequence with added hemin).

As determined in previous sections the OXG4 aptamers retain both peroxidase-mimicking activity (in the presence of hemin) and antimicrobial activity. The coupled antibiotic was hypothesised to help the OXG4/hemin aptamer to penetrate into the biofilm.²² Once the OXG4/hemin

aptamer has penetrated into the biofilm the OXG4/hemin aptamers would begin to react with the cell walls of the bacteria present in the bacteria through the same reaction pathway set out in Chapter 4, Section 4.4.

Thus, in this section the peroxidase-mimicking activity of G4 aptamer, OXG4 aptamer, hemin and OX effect on the biofilms was investigated. The bacteria strains used for this study were *S. aureus* ATCC 29213 and *S. epidermidis* RP62A, which are known to produce biofilms (see Table 2.8).

In order to investigate the effects of G4 aptamers, OXG4 aptamers complexed with hemin, compared to the OX alone was examined using the procedure set out in Chapter 2, Section 2.3.5.5 was followed. These studies rely on bacteria being able to produce endogenous peroxide species. Due to this system relying on the presence of hydrogen peroxide or peroxide species it is hypothesised that the eradication of the bacteria inside of the biofilm will only be successful if those components are present.

First, it was determined if it was possible to successfully grow biofilms using the bacterial strain found in Chapter 2, Section 2.8. In brief, *S. aureus* and *S. epidermidis* bacterial biofilms were grown in 96-well plates and on silicone coupons for 20 h and 24 h, respectively, in MHB. The wells and coupons were washed with phosphate buffer to remove bacteria not inside the biofilm. The number of cells present in the biofilms was determined using the drop method (see Chapter 2, Section 2.3.5.7) to calculate the number of colony forming units (CFU) present in the biofilm after the addition of the samples. This gives an indication of how many cells were still present in the biofilm.

The CFU showed that the number of viable *S. aureus* and *S. epidermidis* cells present after 48 h was $5.95 \pm 0.18 \log \text{CFU mL}^{-1}$ and $7.30 \pm 0.04 \log \text{CFU mL}^{-1}$, respectively. Crystal violet staining (see Chapter 2, Section 2.3.5.8) was utilised on the 96-well plates to determine if a biofilm had formed. It was found that *S. aureus* had a CV value of $3.17 \pm 0.43 \text{ D}_{600}$ and *S. epidermidis* had a CV value of $3.30 \pm 0.06 \text{ OD}_{600}$. Finally the silicone coupons with

biofilm growth (see Chapter 2, Section 2.3.5.5) were stained with LIVE/DEAD™ BacLight™ Bacterial Viability Kit and analysed using fluorescence confocal scanning microscopy (CFSM).

The resulting CFSM images for *S. aureus* and *S. epidermidis* is shown in Fig. 6.4 showing the presence of stained biofilms. These results indicated that both *S. aureus* and *S. epidermidis* biofilms were successfully produced. The FCSM images and the CV data confirm the presence of the biofilms and the CFU was determined that the cells inside of the biofilm were still viable even after up to 48 h. This shows that any reduction of cells after a 48 h growth will be due to the samples that were added and not due to the incubation step.

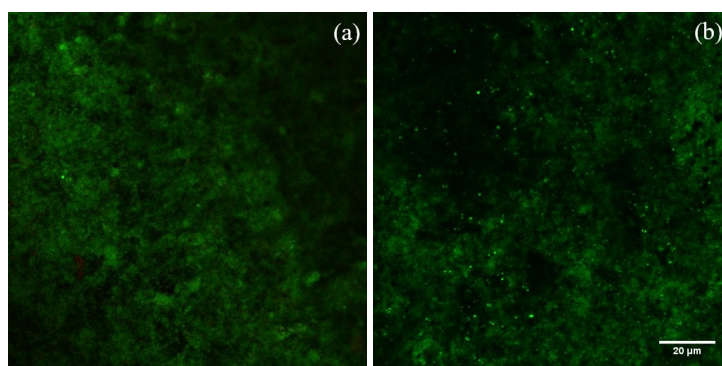


Figure 6.4: Fluorescence confocal scanning microscope image of (a) *S. aureus* and (b) *S. epidermidis* biofilms grown on silicone coupons for 20 h and 24 h, respectively. Stained with LIVE/DEAD™ BacLight™ Bacterial Viability Kit.

Using newly grown biofilms in 96-well plates, the samples shown in Table 6.3 were evaluated for antimicrobial activity. MHB was used as a blank. The G4 aptamer, G4/hemin aptamer, OXG4 aptamer and OXG4/hemin aptamer were folded according to the procedure set out in Chapter 2, Section 2.3.2.1 and then each sample was added on top of the biofilm and incubated for 2 h. Then 50 µL of MHB was added to each well and the 96-well plates were incubated once again for 24 h. The resulting CFU (calculated using the drop plate method as mentioned above) is shown in Fig. 6.5.

Fig. 6.5 shows that the CFU *S. aureus* and *S. epidermidis* still had $\sim 10^6$ – 10^7 CFU mL⁻¹ present in the biofilms after 48 h of growth without any sample additives. In order to de-

Table 6.3: List of samples incubated with biofilm for 2 h, showing concentration of G4 aptamer, hemin and OX in each sample.

Samples	[G4 aptamer], μM	[hemin], μM	[OX], $\mu\text{g mL}$
G4 aptamer	50	-	-
G4/hemin aptamer	50	8	-
OXG4 aptamer	2.5	-	Equivalent to 1
OXG4/hemin aptamer	2.5	8	Equivalent to 1
hemin	-	8	-
OX	-	-	1
Blank (MHB)	-	-	-

termine how effective each samples was at reducing the number of cells present in the biofilm for both *S. aureus* and *S. epidermidis*, the $\Delta\log_{10}$ CFU mL^{-1} was calculated. This was achieved by subtracting the \log_{10} CFU mL^{-1} for each additive from the blank (MHB). The $\Delta\log_{10}$ CFU mL^{-1} *S. aureus* and *S. epidermidis* can be found in Table 6.4 and Table 6.5, respectively.

Table 6.4: The $\Delta\log_{10}$ CFU mL^{-1} and percentage reduction of number of viable *S. aureus* cells, compared to the blank (MHB), after treatment with additives: G4 aptamer, G4/hemin aptamer, OXG4 aptamer, OXG4/hemin aptamer, hemin and OX. Also shown is confidence intervals.

Sample	Reduction of viable cells compared to blank (MHB), $\Delta\log_{10}$ CFU mL^{-1}	Percentage of reduction compared to blank (MHB), %	p = 0.05 (CI of 95%)
G4 aptamer	1.36 ± 0.01	19.15 ± 0.36	s (p < 0.05)
G4/hemin aptamer	1.21 ± 0.05	17.73 ± 0.80	s (p < 0.05)
OXG4 aptamer	2.10 ± 0.01	28.76 ± 0.51	s (p < 0.05)
OXG4/hemin aptamer	1.89 ± 0.08	25.82 ± 1.18	s (p < 0.05)
hemin	1.49 ± 0.06	20.81 ± 0.92	s (p < 0.05)
OX	0.95 ± 0.01	11.81 ± 2.32	s (p < 0.05)

s = statistically significant, ns = not statistically significant.

Table 6.4 shows that the addition of G4 and G4/hemin aptamer only had an effect once a concentration was 10 times that of the OXG4 aptamer with a decrease of viable *S. aureus* cells by 19.15% (1.36 ± 0.01 $\Delta\log_{10}$ CFU mL^{-1}) and 17.73% (1.21 ± 0.05 $\Delta\log_{10}$ CFU mL^{-1}), respectively. This could simply be due to over saturation of the biofilm with G4 aptamer, however would require further investigation as to what is the effect may be. The

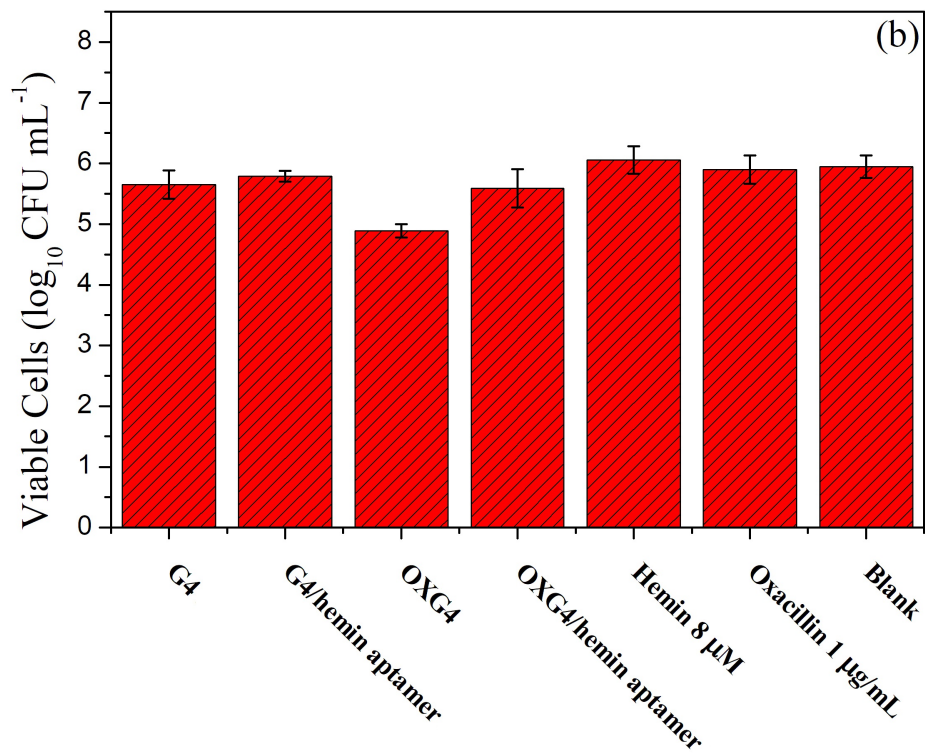
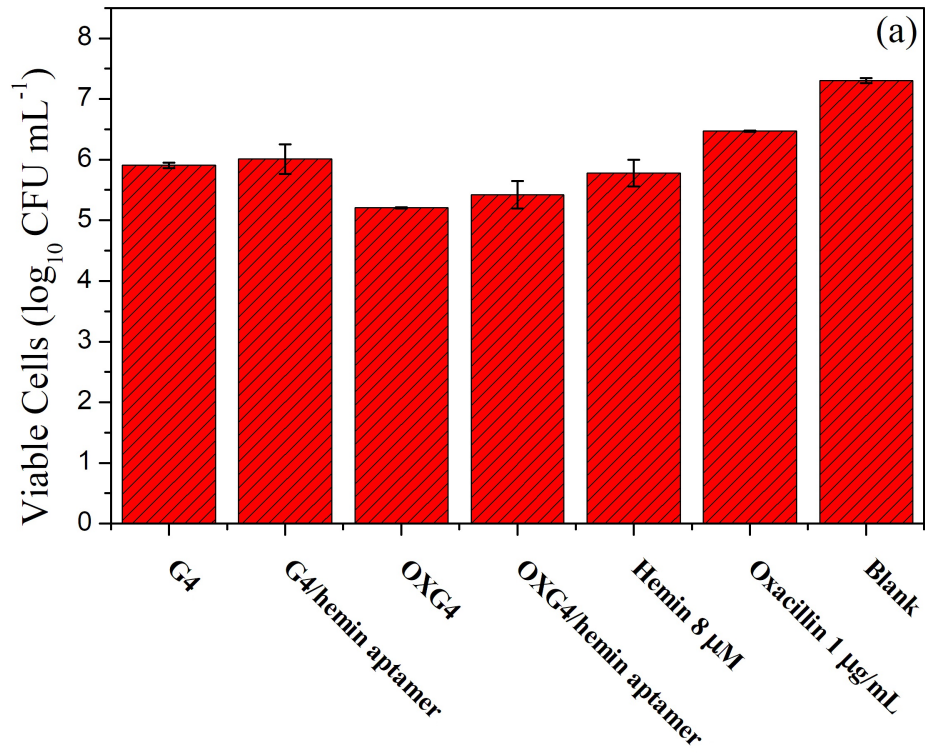


Figure 6.5: Graph comparing the number of viable (a) *S. aureus* and (b) *S. epidermidis* cells (\log_{10} CFU mL^{-1}) after treatment with additives: blank (MHB only), G4 aptamer, G4/hemin aptamer, OXG4, OXG4/hemin aptamer, hemin and oxacillin (see Table 6.3).

G4/hemin aptamer had a smaller effect on the number of viable cells compared to the G4 aptamer alone. This could be due to the stacking of the G4/hemin aptamers, the reason for this will be discussed later in relation to hemin.

Table 6.4 shows that the OXG4 aptamer and OXG4/hemin aptamer had the largest effect in regards to the reduction in the number of viable *S. aureus* cells, with a reduction of 28.76% ($2.10 \pm 0.01 \Delta\log_{10}$ CFU mL⁻¹) and 25.82% ($1.89 \pm 0.08 \Delta\log_{10}$ CFU mL⁻¹), respectively. This indicates that the effect of the reduction in cells is due to the OX and not the G4/hemin aptamer. This is hypothesised to be due to the lack of endogenous peroxide species in the MHB and biofilm.

Hemin (Table 6.4) had a slight effect as well, with a decrease of 20.81% ($1.49 \pm 0.06 \Delta\log_{10}$ CFU mL⁻¹). This could be attributed to the growth-inhibition nature of bacteria when grown in the presence of hemin, which although is well below the effective concentration (5 mM), still has a prominent effect on the *S. aureus*. Comparing G4 aptamer and hemin with the G4/hemin aptamer shows that both the former are more effective alone than combined. This may be due to a stacking effect whereby every hemin molecule complexes with two G4 aptamers, forming a so-called G-wire. Effectively reducing the G4/hemin aptamer concentration. Fig. 6.6 shows an example of how this might occur.

Finally, Table 6.5 shows that OX had the lowest reduction of viable cells by 11.43% ($0.95 \pm 0.01 \Delta\log_{10}$ CFU mL⁻¹), indicating that the OX is not able to readily cross the biofilm. This does support the findings of Singh *et al.*²² who found that 1 $\mu\text{g mL}^{-1}$ of OX was not able to penetrate through *S. aureus* biofilms easily. Although it was first hypothesised that the coupled antibiotic would help to increase the diffusion of the G4/hemin aptamer across the biofilm, this work shows that by coupling the OX to a G4 aptamer increases the movement of the antibiotic across the *S. aureus* biofilm.

Table 6.5 shows that there was no noticeable affect when performing the same studies

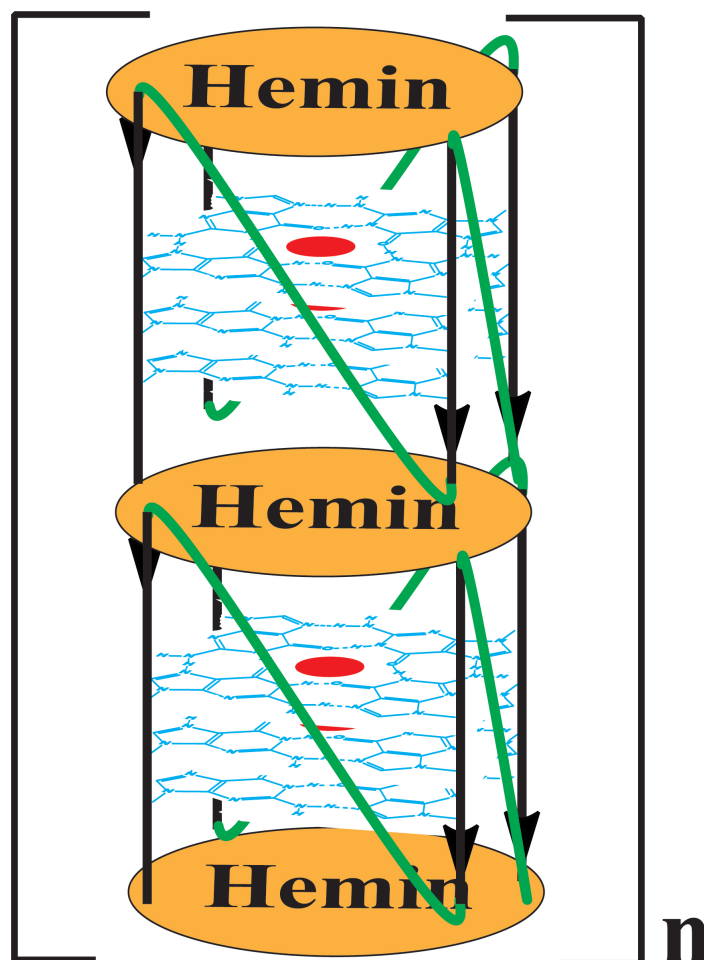


Figure 6.6: Example of a possible G-wire structure that can form between one hemin and two G4 aptamers.

using *S. epidermidis*. *S. epidermidis* was chosen as it is not susceptible to methicillin antibiotics and so any effects of the G4/hemin aptamers would be more prominent. However, as with the *S. aureus* there was no affect noticed from the G4/hemin aptamers peroxidase-mimicking activity.

Due to the low level of antimicrobial activity seen from all the samples in Table 6.3 it was concluded that there was not enough endogenous peroxide or peroxide species in the MHB, *S. aureus* or *S. epidermidis* biofilms. Therefore, in Section 6.3.4 the use of H₂O₂ 0.5% (v/v) with increasing concentrations of the G4/hemin aptamer on its own will be discussed. Only G4/hemin aptamer was tested with *S. aureus* due to time constraints as well as issues with equipment for measuring the concentration of the purified OXG4 aptamer.

Table 6.5: The $\Delta\log_{10}$ CFU mL⁻¹ and percentage reduction of number of viable *S. epidermidis* cells, compared to the blank (MHB), after treatment with additives: G4 aptamer, G4/hemin aptamer, OXG4 aptamer, OXG4/hemin aptamer, hemin and OX. Also shown is confidence intervals.

Sample	Reduction of viable cells compared to blank (MHB), $\Delta\log_{10}$ CFU mL ⁻¹	Percentage of reduction compared to blank (MHB), %	p = 0.05 (CI of 95%)
G4 aptamer	0.74 ± 0.48	4.93 ± 4.98	ns (p > 0.05)
G4/hemin aptamer	0.15 ± 0.44	2.60 ± 3.44	ns (p > 0.05)
OXG4 aptamer	0.74 ± 0.37	12.43 ± 6.29	ns (p > 0.05)
OXG4/hemin aptamer	0.55 ± 9.29	5.98 ± 6.10	ns (p > 0.05)
hemin	-0.12 ± 0.29	-1.88 ± 4.90	ns (p > 0.05)
OX	0.05 ± 0.30	1.00 ± 5.00	ns (p > 0.05)

s = statistically significant, ns = not statistically significant.

6.3.4. Impact of G4 aptamer and OX on biofilms with added hydrogen peroxide (0.5%)

The OXG4 aptamers and OXG4/hemin aptamers, had a limited effect on the biofilms for the *S. aureus* and *S. epidermidis*, therefore one final attempt was made with the G4/hemin aptamer and added hydrogen peroxide. Hydrogen peroxide at high concentrations (1-5% (v/v)) is able to eradicate bacteria inside of a biofilm, whereas it has no affect at 0.5% (v/v).²⁰ 3% (v/v) hydrogen peroxide or lower has been found to not affect human cells and therefore it 0.5% (v/v) was chosen to see if it was possible to increase the antimicrobial effect of low concentration hydrogen peroxide to be able to kill bacteria in biofilms without harming human cells.²⁶ Biofilms were grown as in the previous section, with *S. aureus*. For this section only 2 μ M, 3 μ M, 4 μ M, 5 μ M G4/hemin aptamer, hemin (8 μ M) and oxacillin (1 μ g mL⁻¹) was added. After incubation the MHB with 0.5% hydrogen peroxide was added and the biofilms incubated for 20 h. The drop tests, as in the previous section, was used to determine the CFU of all the samples. Table 6.6 shows the results of the reduction log₁₀ of the CFU and the biofilms.

Fig. 6.7 shows that the blank sample with 0.5% (v/v) had a CFU of $\sim 10^7$ CFU mL⁻¹ present in the biofilms after 48 h of growth. Therefore, there is still the same amount of cells present as the previous experiments (see Fig. 6.5, $\sim 7 \log_{10}$ mL⁻¹ c.f. $\sim 8 \log_{10}$ mL⁻¹).

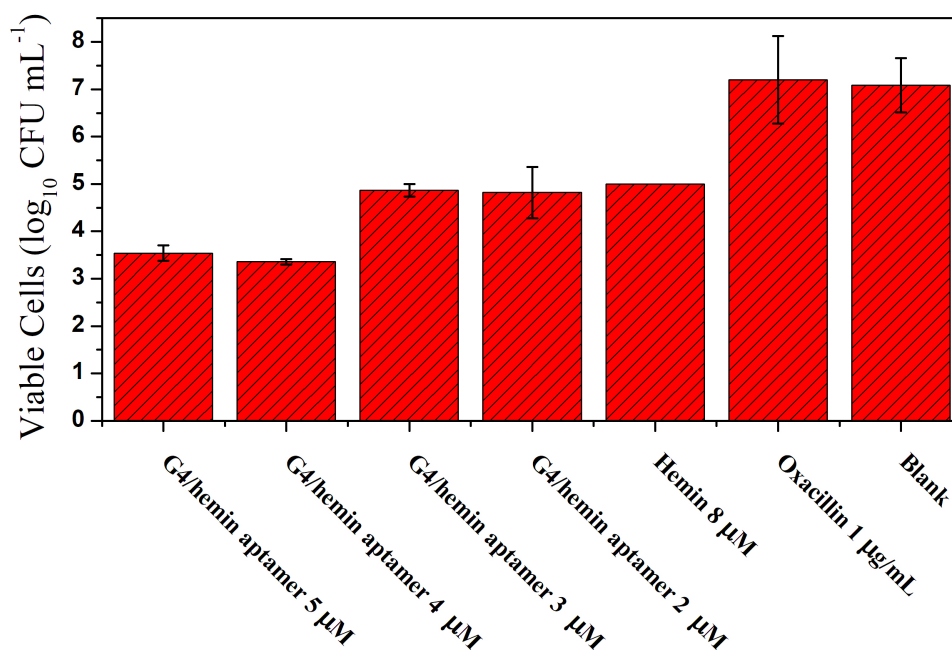


Figure 6.7: Bar graph comparing the 3 averages of viable *S. aureus* cells (\log_{10} CFU mL⁻¹) after treatment with additives: blank (broth only), G4/hemin aptamer 2 μ M, 3 μ M, 4 μ M and 5 μ M (with hemin 8 μ M), hemin (8 μ M) and oxacillin (1 μ g mL⁻¹) in the presence of 0.5% hydrogen peroxide (v/v).

In order to determine how effective each sample was at reducing the number of cells present in the biofilm for *S. aureus* in the presence of H₂O₂ 0.5% (v/v), the $\Delta\log_{10}$ CFU mL⁻¹ was calculated. This was achieved by subtracting the \log_{10} CFU mL⁻¹ for each additive from the blank (MHB). The $\Delta\log_{10}$ CFU mL⁻¹ *S. aureus* can be found in Table 6.6.

Table 6.6 shows that the OX has a negligible effect on the cells. The OX is unable to cross or diffuses too slow to have any affect. This is in line with previous experiments (see Section 6.3.3). Hemin at 8 μ M with 0.5% H₂O₂ (v/v) appeared to have an increased effective antimicrobial activity on the cells inside of the biofilm (*c.f.* to Section 6.3.3), with a reduction of $29.43 \pm 2.39\%$ ($2.12 \pm 0.05 \Delta\log_{10}$ CFU mL⁻¹) of viable cells. This was not expected as hemin is thought to have low peroxidase-mimicking activity. This implies that the addition of H₂O₂ 0.5% may be able to enhance the antimicrobial activity of the hemin.

There was no change in the reduction in viable cells for 2 μ M and 3 μ M. However, once the concentration of the G4/hemin aptamer reaches 4 μ M and 5 μ M the effectiveness to

Table 6.6: The $\Delta\log_{10}$ CFU mL⁻¹ and percentage reduction of number of viable cells, compared to the control, after treatment with 0.5% H₂O₂ (v/v) additives: G4/hemin aptamer 2 μ M, 3 μ M, 4 μ M and 5 μ M (with hemin 8 μ M), hemin (8 μ M) and oxacillin (1 μ g mL⁻¹). Included are confidence intervals.

Sample	Reduction of viable cells compared to blank (MHB), $\Delta\log_{10}$ CFU mL ⁻¹	Percentage of reduction compared to blank (MHB), %	p = 0.05 (CI of 95%)
G4/hemin aptamer 5 μ M	3.58 \pm 0.56	50.02 \pm 4.64	s (p < 0.05)
G4/hemin aptamer 4 μ M	3.76 \pm 0.54	52.58 \pm 4.36	s (p < 0.05)
G4/hemin aptamer 3 μ M	2.26 \pm 0.56	31.30 \pm 2.68	s (p < 0.05)
G4/hemin aptamer 2 μ M	2.30 \pm 0.76	31.97 \pm 4.43	s (p < 0.05)
hemin	2.12 \pm 0.05	29.43 \pm 2.39	s (p < 0.05)
OX	-0.08 \pm 1.07	-1.61 \pm 0.24	s (p < 0.05)

s = statistically significant, ns = not statistically significant.

reduce the number of viable *S. aureus* cells in the biofilm is doubled to 50.02 \pm 4.64% (3.58 \pm 0.56 $\Delta\log_{10}$ CFU mL⁻¹) and 52.58 \pm 4.36 % (52.58 \pm 4.36 $\Delta\log_{10}$ CFU mL⁻¹), respectively.

This shows that although the hemin has an antimicrobial affect, it is further increased by the presence of the G4/hemin aptamer. This can be attributed to both the G4 and the hemin being able to diffuse across the biofilm. Typical peroxidase enzymes do not exert antimicrobial affect but are often able to produce substrates with antimicrobial affects. However, it is known that G4/hemin complexes are able to react with cell components (e.g., cell wall) and damage cells.¹⁹ The G4/hemin complexes, and the hemin to a certain degree, is able to increase the effect of the 0.5% H₂O₂ (v/v), which is thought to have no effect on its own to bacteria within the biofilm.

Yang *et al.*²⁰ investigated the effect that G4/hemin aptamers had on amino acids commonly found in proteins: tyrosine and tryptophan, as well as vitamins such as sodium ascorbate. They determined that G4/hemin aptamers were able to oxidise more readily than the enzyme horseradish peroxidase (HRP). HRP, like most enzymes, has high specificity for substrates and so is not able to oxidise a broad range of substrates. However, the G4/hemin aptamer has a much broader range of substrates it can react with than the HRP. Therefore, it is

hypothesised that the G4/hemin aptamers are more targeted towards the bacterial cells inside of the biofilm.

6.4. Concluding remarks

The utilisation as G4/hemin aptamers coupled with and without antibiotics was investigated as a novel antimicrobial system. This was achieved by coupling a G4 aptamer with the antibiotic OX, purifying and quantifying the concentration of the antibiotic coupled G4. Then it was investigated if the OX coupled G4 aptamer (OXG4 aptamer) retained both peroxidase-mimicking activity and antimicrobial effectiveness. Finally, G4/hemin aptamers and OXG4/hemin aptamers were exposed to biofilms to determine the effect on the number of viable cells still present in the biofilm.

Initial experiments involved coupling the antibiotics FQ and OX to the G4 ODN through a carbodiimide coupling method. It was found that it was only possible to recover and purify the OXG4 (oxacillin coupled G4 ODN), with 50-80% yield, utilising the ethanol precipitation procedure. The FQG4 (fluoroquinolonic acid coupled G4 ODN) was found to only have <20% recovery rate using all three techniques.

Next it was determined if the OXG4 was able to retain the peroxidase-mimicking activity of the OXG4/hemin aptamer by testing with a TMB assay. It was found that the OXG4/hemin had an enhanced peroxidase-mimicking activity over the G4/hemin aptamer. Then it was determined if the MIC of the OXG4 was still as effective as the OX antibiotic alone. The OXG4 was found to have the same MIC as the antibiotic alone.

Finally, it was investigated how the G4 aptamer, G4/hemin aptamer, OXG4 aptamer and OXG4/hemin aptamer in the absence of hydrogen peroxide affected sessile *S. aureus* and *S. epidermidis* biofilms. It was found that 5 μM OXG4 aptamer and OXG4/hemin aptamer were able to decrease the CFU of *S. aureus* by $2.10 \pm 0.01 \log_{10} \text{CFU mL}^{-1}$ and $1.89 \pm 0.08 \log_{10}$

CFU mL⁻¹ respectively, which was twice as effective as the oxacillin alone ($0.95 \pm 0.01 \log_{10}$ CFU mL⁻¹). 50 μ M G4 and G4/hemin aptamer decreased the CFU by 1.36 ± 0.01 and $1.21 \pm 0.05 \log_{10}$ CFU mL⁻¹, respectively. It was found that there was no affect from any additives on *S. epidermidis*.

Hemin, G4 and G4/hemin aptamers were tested to determine the effect on sessile *S. aureus* in the presence of hydrogen peroxide. It was determined that 4 μ M and 5 μ M were able to increase the antimicrobial effect of the hemin alone from $2.12 \pm 0.54 \Delta \log$ CFU mL⁻¹ to $3.76 \pm 0.54 \Delta \log$ CFU mL⁻¹ and $3.58 \pm 0.56 \Delta \log$ CFU mL⁻¹, respectively.

This chapter developed a new antimicrobial system for combating *S. aureus* bacteria protected by biofilms. However, in order to be used for therapeutic purposes it would have to be made more effective at reducing the bacterial cells present inside of the biofilm. This could be done by using different sequences, developed by the Genetic Algorithm from Chapter 4. Once developed to be more effective this antimicrobial system could possibly replace similar peroxidase systems such as those mentioned in Chapter 1, Section 1.7.5.1.²⁷

6.5. Chapter 6 References

- [1] Høiby, N.; Bjarnsholt, T.; Givskov, M.; Molin, S.; Ciofu, O. Antibiotic resistance of bacterial biofilms. *International Journal of Antimicrobial Agents* **2010**, *35*, 322–332.
- [2] Wolcott, R. D.; Ehrlich, G. D. Biofilms and chronic infections. *JAMA - Journal of the American Medical Association* **2008**, *299*, 2682–2684.
- [3] Lewis, K. Persister cells, dormancy and infectious disease. *Nature Reviews Microbiology* **2007**, *5*, 48–56.
- [4] Sukumaran, V.; Senanayake, S. Bacterial skin and soft tissue infections. *Australian Prescriber* **2016**, *39*, 159–163.
- [5] Read, T. R. H.; Fairley, C. K.; Murray, G. L.; Jensen, J. S.; Danielewski, J.; Worthington, K.; Doyle, M.; Mokany, E.; Tan, L.; Chow, E. P. F.; Garland, S. M.; Bradshaw, C. S. Outcomes of Resistance-guided Sequential Treatment of Mycoplasma genitalium Infections: A Prospective Evaluation. *Clinical Infectious Diseases* **2018**,
- [6] Ciofu, O.; Rojo-Molinero, E.; Macià, M. D.; Oliver, A. Antibiotic treatment of biofilm infections. *Apmis* **2017**, *125*, 304–319.
- [7] WHO - World Health Organization, High levels of antibiotic resistance found worldwide, new data shows. *Media centre* **2018**, 1–7.
- [8] Ikuma, K.; Decho, A. W.; Lau, B. L. T. When nanoparticles meet biofilms-interactions guiding the environmental fate and accumulation of nanoparticles. *Frontiers in microbiology* **2015**, *6*, 591.
- [9] Kalishwaralal, K.; BarathManiKanth, S.; Pandian, S. R. K.; Deepak, V.; Gurunathan, S. Silver nanoparticles impede the biofilm formation by Pseudomonas aeruginosa and Staphylococcus epidermidis. *Colloids and Surfaces B: Biointerfaces* **2010**, *79*, 340–344.

- [10] Silver, S. Bacterial silver resistance: Molecular biology and uses and misuses of silver compounds. *FEMS Microbiology Reviews* **2003**, *27*, 341–353.
- [11] Cheow, W. S.; Hadinoto, K. Antibiotic polymeric nanoparticles for biofilm-associated infection therapy. *Methods in Molecular Biology* **2014**, *1147*, 227–238.
- [12] Martínková, N.; Nová, P.; Sablina, O. V.; Graphodatsky, A. S.; Zima, J. Karyotypic relationships of the Tatra vole (*Microtus tatricus*). *Folia Zoologica* **2004**, *53*, 279–284.
- [13] Tonoyan, L.; Fleming, G. T.; Mc Cay, P. H.; Friel, R.; O’Flaherty, V. Antibacterial potential of an antimicrobial agent inspired by peroxidase-catalyzed systems. *Frontiers in Microbiology* **2017**, *8*, 680.
- [14] Klebanoff, S. J.; Clem, W. H.; Luebke, R. G. The peroxidase-thiocyanate-hydrogen peroxide antimicrobial system. *BBA - General Subjects* **1966**, *117*, 63–72.
- [15] Carter, J. D.; LaBean, T. H. Coupling strategies for the synthesis of peptide-oligonucleotide conjugates for patterned synthetic biomineralization. *Journal of Nucleic Acids* **2011**, *2011*, 926595.
- [16] Chandler, J. D.; Day, B. J. Thiocyanate: A potentially useful therapeutic agent with host defense and antioxidant properties. *Biochemical Pharmacology* **2012**, *84*, 1381–1387.
- [17] Pidot, S. J. et al. Increasing tolerance of hospital *Enterococcus faecium* to handwash alcohols. *Science Translational Medicine* **2018**, *10*, eaar6115.
- [18] Amar K, C. Iodine, Thiocyanate and the Thyroid. *Biochemistry & Pharmacology: Open Access* **2015**, *04*, 1–6.
- [19] Cheng, X.; Liu, X.; Bing, T.; Cao, Z.; Shangguan, D. General peroxidase activity of G-quadruplex-hemin complexes and its application in ligand screening. *Biochemistry* **2009**, *48*, 7817–7823.

- [20] Yang, X.; Fang, C.; Mei, H.; Chang, T.; Cao, Z.; Shangguan, D. Characterization of G-quadruplex/hemin peroxidase: Substrate specificity and inactivation kinetics. *Chemistry - A European Journal* **2011**, *17*, 14475–14484.
- [21] SHARMA, P. C.; JAIN, A.; JAIN, S. Fluoroquinolone Antibacterials: A Review on Chemistry Microbiology and Therapeutic Prospects. *Acta Poloniae Pharmaceutica-Drug Research* **2009**, *66*, 587–604.
- [22] Singh, R.; Ray, P.; Das, A.; Sharma, M. Penetration of antibiotics through *Staphylococcus aureus* and *Staphylococcus epidermidis* biofilms. *Journal of Antimicrobial Chemotherapy* **2010**, *65*, 1955–1958.
- [23] Dickinson, T. M.; Archer, G. L. Phenotypic expression of oxacillin resistance in *Staphylococcus epidermidis*: roles of *mecA* transcriptional regulation and resistant-subpopulation selection. *Antimicrobial agents and chemotherapy* **2000**, *44*, 1616–23.
- [24] Qu, Y.; Istivan, T. S.; Daley, A. J.; Rouch, D. A.; Deighton, M. A. Comparison of various antimicrobial agents as catheter lock solutions: Preference for ethanol in eradication of coagulase-negative staphylococcal biofilms. *Journal of Medical Microbiology* **2009**, *58*, 442–450.
- [25] HØiby, N.; Olling, S. *Pseudomonas aeruginosa* infection in cystic fibrosis. *APMIS* **1977**, *85*, 107–114.
- [26] Presterl, E.; Suchomel, M.; Eder, M.; Reichmann, S.; Lassnigg, A.; Graninger, W.; Rottler, M. Effects of alcohols, povidone-iodine and hydrogen peroxide on biofilms of *Staphylococcus epidermidis*. *Journal of Antimicrobial Chemotherapy* **2007**, *60*, 417–420.
- [27] Aikpokpodion Paul, E.; Atewolara-Odule, O. C.; Osobamiro, T.; Odunwale, O. O.; Ademola, S. M. A survey of copper, lead, cadmium and zinc residues in cocoa beans obtained from selected plantations in Nigeria. 2013; <http://www.ncbi.nlm.nih.gov/pubmed/11730017>
<http://www.pubmedcentral.nih.gov/articlerender.fcgi?artid=PMC1941713>.

Chapter 7

Conclusion

7.1. Synopsis

The aim of this thesis was to investigate the methods that allowed for optimal dynamic and static DNA applications. These applications included SNP genotyping, biosensing and possible antimicrobial.

In Chapter 3 a toehold-mediated strand displacement reaction was performed with a ATTO 647N fluorophore to allow for the study of the effects of ethidium bromide. Next in Chapter 4 a G4 aptamer with enhanced peroxidase-mimicking activity was discovered using a genetic algorithm to evolve G4 aptamer with already established activity. Chapter 5 used G4 aptamers that were immobilised onto 2D and 3D surfaces to determine if it was possible to fabricate a SNP biosensor. Finally, in Chapter 6, G4 aptamers were utilised as a possible antimicrobial.

7.2. Concluding remarks and future work

In Chapter 1 it was discussed how DNA, both static and dynamic, has been used to develop new techniques and biosensors. Here in this thesis it was attempted to build upon these developments to allow for more accurate genotyping and biosensing. Toehold-mediated strand displacement is fast becoming recognised as a tool for accurate, robust and reliable DNA genotyping. Whereas, G-quadruplexes (G4) are being integrated into sensitive biosensors with a myriad of applications.

In Chapter 3 the toehold-mediated strand displacement process, for single nucleotide polymorphism (SNP) genotyping, was investigated to determine the effects of added ethidium bromide. First it was determined that ATTO 647N, a fluorophore, was compatible with the polymerase chain reaction (PCR) and toehold-mediated strand displacement process. ATTO 647N labelled primers were then used to produce toehold-PCR products (TPP) for all the possible SNPs (C, guanine (G), adenine (A) and thymine (T)). In the absence of ethidium bromide it was found that the displacement rates for the TPPs with their complementary displacing sequence (DSs) follows the order of $TPP-G \leq TPP-A < TPP-T < TPP-C$. With ethidium bromide added it was found that the displacement rates for the TPPs, with the four DSs, followed the order of $TPP-G \leq TPP-A < TPP-T < TPP-C$. This indicates that when the SNP on the TPP is either a C residue or a T residue (a pyrimidine) the rate of displacement is higher than when the SNP on the TPP is an A residue or a G residue (a purine). It was also found that G mismatches were stable and had low discrimination power. However, C mismatches were the most unstable and therefore had the highest discrimination power. Although TPP-G had the slowest displacement rate, the displacement was decreased from ~ 400 s to ~ 250 s. The addition of the ethidium bromide was found to further destabilise the C mismatches and so the discrimination power was increased.

The addition of ethidium bromide to the toehold-mediated strand displacement procedure was not able to successfully increase the discrimination power of all the TPPs. Therefore

in order to be useful for genotyping intercalator or metallo-intercalator that could potentially be further destabilising should be investigated.^{1,2} An example of metallo-intercalators could be [Pt(2,2',2''-terpyridine)(Cl)]⁺ or ruthenium complexes such as ([Ru(DIP)₃]²⁺) and Ru(2,2'-bipyridine)₂dipyrido[3,2-a:2',3'-c]phenazine⁺².^{2,3-6} Intercalators that are bulkier than ethidium bromide might destabilise mismatches enough to increase the discrimination power of the toehold-mediated strand displacement process.

In Chapter 4 a Genetic Algorithm (GA) was utilised to enhance the peroxidase-mimicking activity of already published G4 aptamers sequences. The GA was performed for 8 generations, when it was determined that it was no longer possible to enhance the peroxidase-mimicking activity. Analyses of the top 20 sequences with the highest peroxidase-mimicking activity found that enhancements occurred when an A residue was present in the first (X_{I1}) and second (X_{I2}) loop region of the G4 aptamer sequence (see Fig. 4.1). A single nucleotide residue in the third (X_{I3}) loop region of the G4 aptamer also showed favourable enhancement of the peroxidase-mimicking activity. It took 7 generations to obtain three sequences with a peroxidase-mimicking activity ~5 times that of the original EAD-2 sequence. These sequences were 7-01, 7-02 and 5-04 and were characterised using the Michaelis-Menten equation (Eq. 4.1). All three sequences were found suitable for biosensing.

This work showed that it was possible to discover new G4 aptameric ODN sequences that had increased peroxidase-mimicking activity. Ways to further improve the peroxidase-mimicking activity would be to test sequences that contain more than 3 nucleotide residues in the loop regions (Fig. 4.1, X_{I1} , X_{I2} and X_{I3}). The GA could also be used with a variety of different substrates such as luminol and 2,2'-azinobis(3-ethylbenzothiazoline)-6-sulfonic acid diammonium salt (ABTS). This would allow for the fabrication of more sensitive and robust biosensors. These sequences could potentially decrease the limits of detection for the currently existing biosensors due to the much higher V_{max} . Using the data from this Chapter found in Table 4.8 it might be possible to design G4 aptamers with peroxidase-mimicking activity faster than those found in this thesis.

For Chapter 5, a G4 aptameric biosensor was developed for SNP genotyping. First it was determined that the G4 aptamers were resistant to T7 endonuclease I enzyme digestion. Then the G4 aptamers were immobilised onto NHS-functionalised Corning® DNA-Bind 96-well microplates (2D surface) or BcMag™ magnetic silica iron core beads (3D surface). Complementary and partially complementary ssDNA was used to form a perfect match (PM) and a single mismatch (SM) at the SNP position on the G4 aptamer. It was determined that it was not possible to detect the G4 aptamers immobilised on the 2D surfaces. PEG 6000 5% (v/v) was used to increase the peroxidase-mimicking activity of the immobilised G4 aptamers and allowed for successful detection of the immobilised G4 aptamers. It was also tested to see if it was possible to detect the digestion of the G4 aptamers from the 2D surfaces. However this was deemed too low to be used for a biosensor, so the cleaved G4 aptamers in the solution were detected using the TMB assay. It was found that although possible to detect cleaved G4 aptamers from the 2D surfaces, it was not possible to distinguish between PM and SM G4 aptamers. It was not possible to detect the G4 aptamers immobilised on the 3D surfaces despite the addition of PEG6000 5% (w/v).

Further work is required to increase the limits of detection on the both the 2D and 3D surfaces to allow for sufficient detection of immobilised G4 aptamers. The use of G4 aptamers with increased peroxidase-mimicking activity as well as the addition of more effective polymeric rate accelerators may be able to increase the sensitivity of the proposed biosensor. Also a new strategy for cleaving the SM may need to be employed to overcome the non-specific cleavage seen with the T7 endonuclease I. Further work could include determination of the concentration of G4 aptamers immobilised on the surface of the wells and microbeads. Possible ways to do this would be to use N-methyl mesoporphyrin IX and Crystal Violet, which have been shown to quantitatively measure G4 folding propensity and conformation specificity in both ss- and dsDNA.⁷

Finally, in Chapter 6 it was investigated if the G4 aptamers with enhanced peroxidase-mimicking activity, 7-02 from Chapter 4, could be utilised as possible antimicrobials. The the-

ory being that the high peroxidase-mimicking activity would deplete the food source for the bacterial cells or damage the cells enough to prevent proliferation. The antibiotic oxacillin (OX) was coupled with an amine-functionalised derivative of the 7-02 sequence (referred to as OXG4). OXG4 aptamers and OXG4/hemin aptamers were investigated for antimicrobial activity towards *Staphylococcus aureus* (*S. aureus*) or *Staphylococcus epidermidis* (*S. epidermidis*) in biofilms. It was found that OXG4 aptamers and OXG4/hemin aptamers had limited effect on the *S. aureus* cells with a reduction of $2.10 \pm 0.01 \log_{10} \text{CFU mL}^{-1}$ and $1.89 \pm 0.08 \log_{10} \text{CFU mL}^{-1}$, respectively. This was found to be twice as effective as the oxacillin on its own ($0.95 \pm 0.01 \log_{10} \text{CFU mL}^{-1}$). It was then decided to use a range of G4 aptamer concentrations (without antibiotic) in the presence of 0.5% peroxide (v/v) to try eradicate biofilm protected bacteria. It was found that 4 μM and 5 μM of G4 aptamer with 0.5% (v/v) were able to eradicate up to 50% of the bacteria inside of the biofilm.

A viable path increasing the antimicrobial activity of the G4 aptamers could be to use different sequences that might have a higher affinity for the bacterial cell components inside of the biofilm. Another improvement could be changing the antibiotics used, to antibiotics that bacteria are more susceptible to or able to penetrate biofilms better. Antibiotics such as such as aqueous soluble fluoroquinolone drugs, cefotaxime or amikacin.⁸ These drugs could allow for more recovery of the antibiotic coupled G4 aptamers during the precipitation process as well as allow for more antibiotic coupled G4 aptamers to enter the cells. This may in turn further increase the killing antimicrobial activity in the presence of the 0.5% peroxide (v/v). Further work could also include investigating the effect on other bacterial strains to determine if this technique can be viable for therapeutic applications.

7.3. Chapter 7 References

- [1] Ganeshpandian, M.; Loganathan, R.; Suresh, E.; Riyasdeen, A.; Akbarsha, M. A.; Palaniandavar, M. New ruthenium(II) arene complexes of anthracenyl-appended diazacycloalkanes: Effect of ligand intercalation and hydrophobicity on DNA and protein binding and cleavage and cytotoxicity. *Dalton Transactions* **2014**, *43*, 1203–1219.
- [2] Garbay-Jaureguiberry, C.; Laugâa, P.; Delepierre, M.; Laalami, S.; Muzard, G.; Le Pecq, J. B.; Roques, B. P. DNA bis-intercalators as new anti-tumour agents: modulation of the anti-tumour activity by the linking chain rigidity in the ditercalinium series. *Anti-cancer drug design* **1987**, *1*, 323–35.
- [3] Wheate, N. J.; Brodie, C. R.; Collins, J. G.; Kemp, S.; Aldrich-Wright, J. R. DNA intercalators in cancer therapy: organic and inorganic drugs and their spectroscopic tools of analysis. *Mini reviews in medicinal chemistry* **2007**, *7*, 627–48.
- [4] Luedtke, N. W.; Hwang, J. S.; Nava, E.; Gut, D.; Kol, M.; Tor, Y. The DNA and RNA specificity of eilatin Ru(II) complexes as compared to eilatin and ethidium bromide. *Nucleic Acids Research* **2003**, *31*, 5732–5740.
- [5] Bond, P. J.; Langridge, R.; Jennette, K. W.; Lippard, S. J. X-ray fiber diffraction evidence for neighbor exclusion binding of a platinum metallointercalation reagent to DNA. *Proceedings of the National Academy of Sciences of the United States of America* **1975**, *72*, 4825–4829.
- [6] McCoubrey, A.; Latham, H. C.; Cook, P. R.; Rodger, A.; Lowe, G. 4-Picoline-2,2':6',2''-terpyridine-platinum(II)- a potent intercalator of DNA Angela. *FEBS Letters* **1996**, *380*, 73–78.
- [7] Kreig, A.; Calvert, J.; Sanoica, J.; Cullum, E.; Tipanna, R.; Myong, S. G-quadruplex forma-

tion in double strand DNA probed by NMM and CV fluorescence. *Nucleic Acids Research* **2015**, *43*, 7961–7970.

- [8] Singh, R.; Ray, P.; Das, A.; Sharma, M. Penetration of antibiotics through *Staphylococcus aureus* and *Staphylococcus epidermidis* biofilms. *Journal of Antimicrobial Chemotherapy* **2010**, *65*, 1955–1958.

Chapter 8

Appendix

A. Additional possible SPP

Example 1

```
5'          ATGCTTACAAGCAAGTACAGCAAT
           :      ||||| : :
3' TACGAATGTTTCGTTTCATGTCGTTAGTTGGGAGTTGATAGTGTGATGTTGACGTTGAGGTTTCGGTGGGGAGUGGGUGATC
```

Example 2

```
5'  ATGCTTACAAGCAAGTACAGCAAT
     :      |||||
3'   TACGAATGTTTCGTTTCATGTCGTTAGTTGGGAGTTGATAGTGTGATGTTGACGTTGAGGTTTCGGTGGGGAGUGGGUGATC
```

Example 3

```
5'                                     ATGCTTACAAGCAAGTACAGCAAT
                                       : : : : : |||||
3' TACGAATGTTTCGTTTCATGTCGTTAGTTGGGAGTTGATAGTGTGATGTTGACGTTGAGGTTTCGGTGGGGAGUGGGUGATC
```

Figure A.1: Examples of three other possible non-specific primer hybridisation with the target strand. Showing that although there are other possible non-specific targets, there is no possible way for the GoTaq® Flexi polymerase to extend the primer during the PCR process

B. Displacement curves for TPP-C

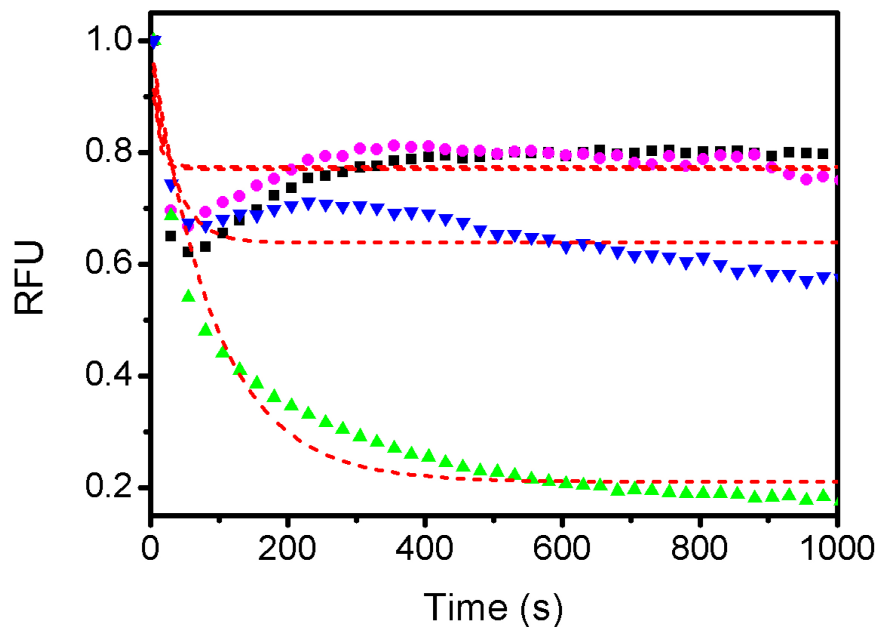


Figure B.2: Toehold-mediated strand displacement kinetic curves (relative fluorescence unit (RFU) versus time) of the displacement reactions of the incumbent strand of the TPP-C, labelled with ATTO 550, with DS(A)(black), DS(T)(pink), DS(G)(blue) and DS(C) (green). Each set of data is an average of 3 replicates. Every 20 data points was omitted for ease of viewing and the red dashed lines are the fits obtained using OriginPro 9 software.

C. Genetic algorithm generations with G4 ODN sequences and peroxidase-mimicking activity

Table C.1: Generations (Gen) generated utilising the genetic algorithm with peroxidase-mimicking activity (V_0). Including the original EAD-2 and G_3A_3 sequences.

Gen	Sample	ODN sequence 5' \implies 3'	Peroxidase-mimicking activity, V_0 , $\mu\text{M s}^{-1}$
1 st	EAD-2	CTG ₃ AG ₃ AG ₃ AG ₃ A	0.018
	G_3A_3	$G_3A_3G_3A_3G_3A_3G_3$	0.032
	1-01	CTG ₄ AG ₃ AG ₄ AG ₃ A	0.008
	1-02	CTG ₄ AG ₄ AG ₄ AG ₃ A	0.012
	1-03	CTG ₄ AG ₄ AG ₄ AG ₄ A	0.009
	1-04	$G_3AG_3AG_3AG_3A$	0.017
	1-05	$G_3AG_3AG_3AG_3$	0.013
	1-06	$G_3TG_3AG_3AG_3$	0.007
	1-07	$G_3AG_3TG_3AG_3$	0.006
	1-08	$G_3AG_3TG_3TG_3$	0.004
1-09	$G_3AG_3TG_3TG_3A$	0.014	
1-10	CTG ₃ AG ₃ TG ₃ TG ₃ A	0.026	
2 nd	2-01	CTG ₃ A ₃ G ₃ A ₃ G ₃ A ₃ G ₃ A	0.006
	2-02	CTG ₃ A ₃ G ₃ A ₃ G ₃ A ₃ G ₃	0.009
	2-03	CTG ₃ A ₃ G ₃ A ₃ G ₃ A ₃ G ₃ A	0.007
	2-04	CTG ₃ A ₃ G ₃ T ₃ G ₃ A ₃ G ₃ A	0.010
	2-05	$G_3A_2G_3A_2G_3A_2G_3$	0.012
	2-06	CTG ₃ A ₂ G ₃ A ₂ G ₃ A ₂ G ₃	0.006
	2-07	CTG ₃ A ₂ G ₃ A ₂ G ₂ A ₂ G ₃	0.008
	2-08	CTG ₃ A ₃ G ₃ TG ₃ A ₃ G ₃ A	0.010
	2-09	CTG ₃ A ₃ G ₃ TA ₂ G ₃ TG ₃ A	0.019
	2-10	CTG ₃ A ₃ G ₃ TG ₃ TG ₃ A	0.015

Dashed lines separate generations.

Table C.1: Generations (Gen) generated utilising the genetic algorithm with peroxidase-mimicking activity (V_0). Including the original EAD-2 and G_3A_3 sequences continued.

Gen	Sample	ODN sequence 5' \implies 3'	Peroxidase-mimicking activity, V_0 , $\mu\text{M s}^{-1}$
3 rd	3-01	CTG ₃ TG ₃ TG ₃ TG ₃	0.017
	3-02	G ₃ A ₃ G ₃ TCAG ₃ TG ₃	0.047
	3-03	G ₃ A ₃ G ₃ AG ₃ A ₃ G ₃	0.011
	3-04	G ₃ AG ₃ TG ₃ TA ₂ G ₃ A	0.012
	3-05	G ₃ AG ₃ TG ₃ CG ₃	0.003
	3-06	CTG ₃ AG ₃ A ₂ G ₃ AG ₃	0.009
	3-07	T ₂ G ₃ A ₃ G ₃ AG ₃ AG ₃ A	0.014
	3-08	C ₃ G ₃ A ₃ G ₃ TG ₃ A ₃ G ₃	0.011
	3-09	CTG ₃ A ₃ G ₃ A ₂ CG ₃ TG ₃ A	0.045
	3-10	CTG ₃ TA ₂ G ₃ TA ₂ G ₃ A ₃ G ₃ 3	0.023
4 th	4-01	CTG ₃ A ₃ G ₃ TCAG ₃ TG ₃ A	0.006
	4-02	G ₃ A ₃ G ₃ A ₂ CG ₃ TG ₃	0.081
	4-03	G ₃ A ₃ G ₃ TA ₂ G ₃ A ₃ G ₃ T	0.006
	4-04	G ₃ T ₂ G ₃ TA ₂ G ₃ TG ₃	0.012
	4-05	G ₃ TA ₂ G ₃ A ₂ CG ₃ AG ₃	0.059
	4-06	TG ₃ A ₃ G ₃ TA ₂ G ₃ A ₃ G ₃ A	0.029
	4-07	AG ₃ TA ₂ G ₃ TA ₂ G ₃ A ₃ G ₃	0.023
	4-08	CTG ₃ AGAG ₃ TA ₂ G ₃ A ₃ G ₃	0.015
	4-09	T ₂ G ₃ TA ₂ G ₂ TCAG ₃ A ₃ G ₃ A	0.030
	4-10	CTG ₃ TA ₂ G ₃ TGAG ₃ A ₃ G ₃	0.024
5 th	5-01	G ₃ A ₃ G ₃ TCAG ₃ AG ₃	0.028
	5-02	AG ₃ TA ₂ G ₃ TCAG ₃ TG ₃	0.023
	5-03	G ₃ A ₂ G ₃ A ₂ CG ₃ AG ₃	0.020
	5-04	G ₃ A ₃ G ₃ A ₂ CG ₃ CG ₃	0.079
	5-05	G ₃ A ₃ G ₃ A ₂ TG ₃ AG ₃	0.058
	5-06	G ₃ A ₃ G ₃ A ₂ CG ₃ AG ₃ C	0.058
	5-07	G ₃ ACAG ₃ A ₂ CG ₃ TG ₃	0.065
	5-08	TG ₃ TA ₂ G ₃ A ₂ CG ₃ TG ₃	0.076
	5-09	G ₃ A ₂ G ₃ TCAG ₃ AG ₃	0.019
	5-10	G ₃ TA ₂ G ₃ TA ₂ G ₃ AG ₃	0.021

Dashed lines separate generations.

Table C.1: Generations (Gen) generated utilising the genetic algorithm with peroxidase-mimicking activity (V_0). Including the original EAD-2 and G_3A_3 sequences continued.

Gen	Sample	ODN sequence 5' \implies 3'	Peroxidase-mimicking activity, V_0 , $\mu\text{M s}^{-1}$
6 th	6-01	$G_3ATAG_3A_2TG_3CG_3$	0.052
	6-02	$G_3ACAG_3ACG_3CG_3$	0.011
	6-03	$G_3ATAG_3A_2TG_3TG_3$	0.047
	6-04	$G_3A_3G_3A_2CG_3AG_3$	0.062
	6-05	$G_3AGAG_3A_2TG_3CG_3$	0.025
	6-06	$G_3ACTG_3A_2TG_3TG_3$	0.39
	6-07	$G_3TA_2G_3CACG_3AG_3$	0.061
	6-08	$G_3TA_2G_3A_2CG_3CG_3$	0.71
	6-09	$G_3A_2G_3A_2CG_3CG_3$	0.15
	6-10	$G_3ATAG_3A_3G_3CG_3$	0.025
7 th	7-01	$G_3TA_2G_3CACG_3TG_3$	0.088
	7-02	$G_2A_3G_3CACG_3CG_3$	0.104
	7-03	$AG_3A_3G_3A_2CG_3CG_3$	0.035
	7-04	$G_3TA_2G_3CACG_3CG_3C$	0.078
	7-05	$CG_3A_3G_3A_3CG_3AG_3$	0.046
	7-06	$G_3A_2TG_3CACG_3AG_3$	0.074
	7-07	$G_3TA_2G_3ACG_3CG_3$	0.041
	7-08	$G_3A_3G_3CACG_3AG_3$	0.085
	7-09	$G_3A_3G_3CACG_3AG_3$	0.65
	7-10	$G_3TA_2G_3CCG_3CG_3$	0.018
8 th	8-01	$AG_3TA_2G_3CACG_3TG_3$	0.029
	8-02	$G_3TACG_3CACG_3CG_3C$	0.053
	8-03	$G_3ACAG_3CACG_3TG_4$	0.024
	8-04	$G_3A_3G_3CACG_3TG_4$	0.044
	8-05	$TG_3TA_2G_3ACG_4CG_4$	0.011
	8-06	$CG_3A_3G_3ACG_4CG_3$	0.012
	8-07	$G_3TA_2G_3CACG_3TG_4$	0.051
	8-08	$G_3A_3G_3ACG_3AG_3T$	0.018
	8-09	$G_3A_3G_3CTCG_3AG_3$	0.012
	8-10	$G_3A_3G_3ACG_4TG_3$	0.023

Dashed lines separate generations.

D. Digestion of G4 aptamers with T7 endonuclease I (2.5 U)

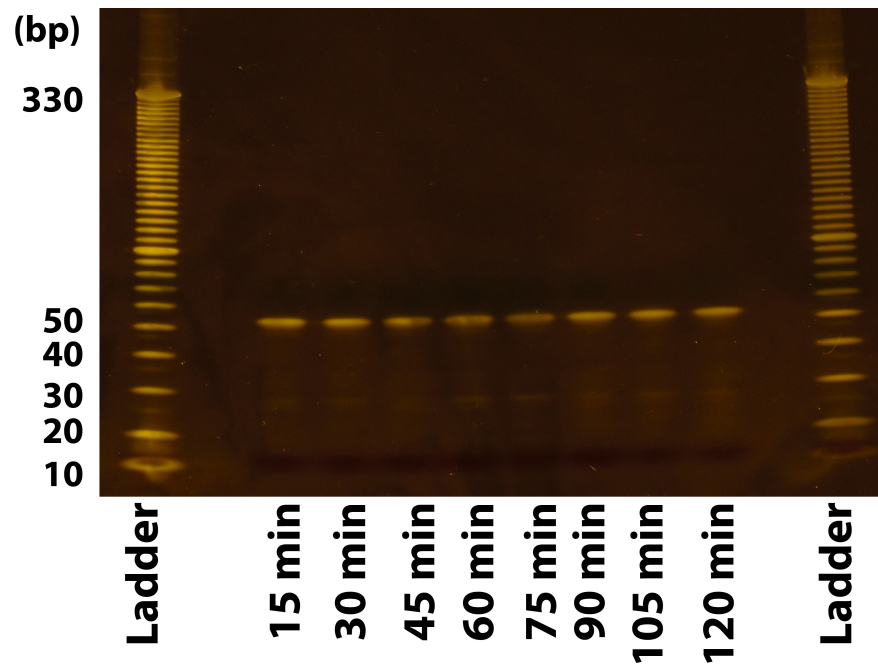


Figure D.1: PAGE ePage1 10-20% (w/v) electrophoretogram, stained with 1x SYBR® gold and viewed using a Safe Imager Blue-Light Transilluminator, of 15, 30, 45, 75, 90, 105 and 120 min digestion with T7 endonuclease I (2.5 U) incubation with the PM and SM solutions. A DNA Ladder (L) (Invitrogen 10 bp DNA ladder) was used as the reference.

E. 16 h digestion of G4 aptamers with T7 endonuclease I (2.5 U)

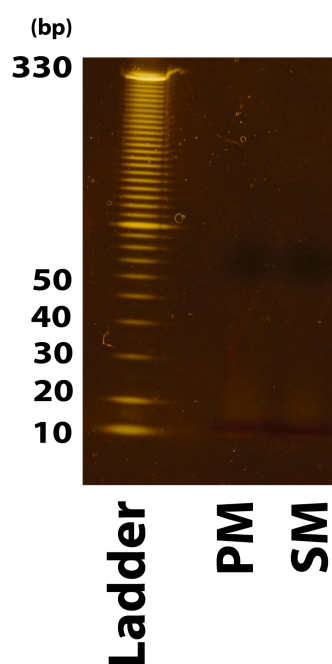


Figure E.1: PAGE ePagel 10-20% (w/v) electrophoretogram, stained with 1x SYBR® gold and viewed using a Safe Imager Blue-Light Transilluminator, of 16 h digestion with T7 endonuclease I (2.5 U) incubation with the PM and SM solutions. A DNA Ladder (L) (Invitrogen 10 bp DNA ladder) was used as the reference.

F. Detection of surface immobilised G4 aptamers using luminol assay

Table F.1: Chemiluminescent signatures of blank (no G4 aptamer) and immobilised G4 aptamer wells.

Sample	Chemiluminescent signature, a.u
blank (no G4 aptamer)	323821.8 ± 73074.4
G4 aptamers	319763.8 ± 86489.1

Anova results: $F(1,14) = 0.009$, $F_{\text{crit}} = 4.600$ $p = 0.926$.

G. Detection of surface immobilised G4 aptamers using ABTS assay

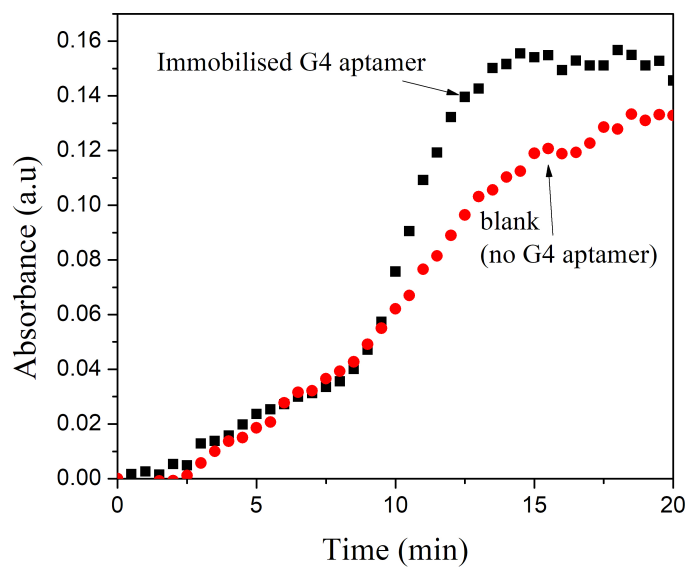


Figure G.1: Average of 3 UV/vis spectra (absorbance (a.u) versus time (min)) of ABTS assay for blank (no G4 aptamer) (red) and immobilised G4 aptamer (black).

H. OXG4 and NH₂G4 gel electrophoresis results

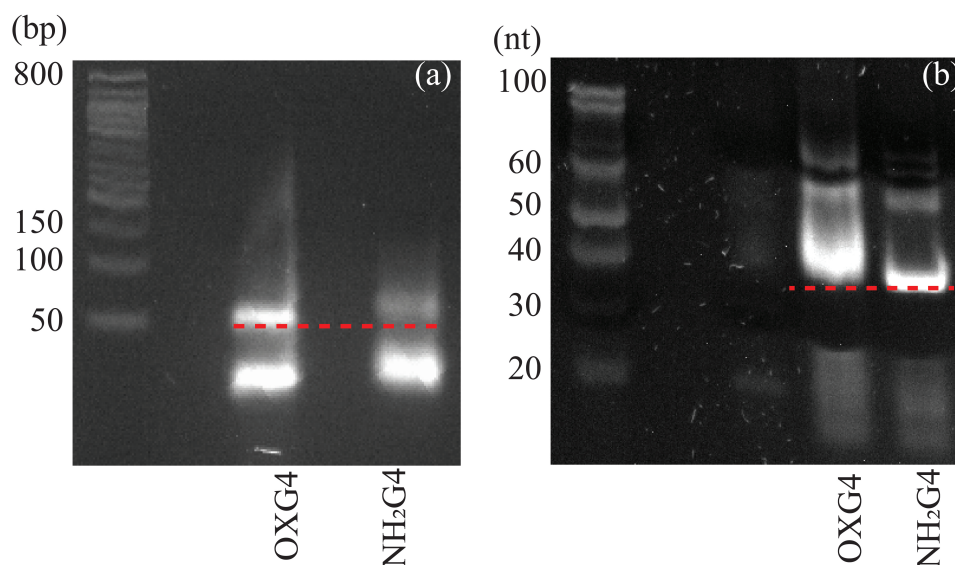


Figure H.1: Left: Agarose 4% (w/v, made according to Chapter 2, Section 2.4.3) electrophoretogram, stained with 1X SYBR® Green I and viewed using a Gel Doc, of NH₂G4 aptamer and OXG4 aptamer. A DNA a Ladder (Quick-Load® Purple 50 bp DNA ladder) was used for reference. Right: PAGE 12% (v/v, made according to Chapter 2, Section 2.4.3) electrophoretogram, stained with 1X SYBR® Green I and viewed using a Gel Doc, of NH₂G4 aptamer and OXG4 aptamer. A DNA a Ladder (20/100 Ladder Oligo length standards) was used for reference. Red dotted line is to guide the eye to the intermolecular structures.